Design and development of novel irreversible GSK-3β inhibitors to address Alzheimer's disease

by

Anton Ruben Hamann

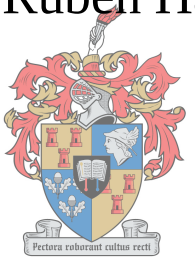

Thesis presented in partial fulfilment of the requirements for the degree

Doctor of Philosophy in Chemistry at the University of Stellenbosch

Supervisor: Dr. M.A.L. Blackie

Co-supervisor: Prof. W.A.L. van Otterlo

Department of Chemistry and Polymer Science

Faculty of Natural Science

March 2018

Declaration

By submitting this thesis/dissertation electronically, I declare that the entirety of the work contained therein is my own, original work, that I am the sole author thereof (save to the extent explicitly otherwise stated), that reproduction and publication thereof by Stellenbosch University will not infringe any third party rights and that I have not previously in its entirety or in part submitted it for obtaining any qualification.

November 2017

Abstract

Molecular modelling on the GSK-3β protein was carried out to identify a library of suitable electrophilic warhead containing ligands that have the necessary interactions with the binding site. Several series of novel irreversible inhibitors for GSK-3β with potential anti-Alzheimer's disease activities were then synthesised. In total, eleven compounds were successfully synthesised. The compounds have been fully characterised using standard spectroscopic and analytical techniques.

The scaffold, 5-{4-[(4-methylpiperazin-1-yl)sulfonyl]phenyl}pyrazin-2-amine, was equipped with an α,β-enone Michael acceptor, that allowed for the coupling of various side chains using substitution chemistry. A library of two different series with an internal Michael acceptor was synthesised. The synthesis of the third series that consisted of a terminal Michael acceptor or a halomethylketone was attempted but proved futile.

Suzuki-Miyaura chemistry has been thoroughly explored to find the best conditions to offer the products in acceptable yields. $Pd(dppf)Cl_2$ as a catalyst, in a solvent system of toluene:ethanol:water, was found to be the best candidate for the Suzuki-Miyaura reactions to synthesise the aforementioned scaffold.

The compounds were tested against the human recombinant GSK-3β and were found to have weak to good activity (GSK-3β IC_{50} range: 0.12 - >10 μM). The most active compound (GSK-3β IC_{50}: 0.12 μM) consisted of a pyridine ring and the carbonyl of the Michael acceptor is situated directly next to the aminopyrazine core. The results showed that the libraries have the potential to be expanded into a second generation of new compounds.

Opsomming

Deur gebruik te maak van molekulêre modellering was verskeie nuwe reekse onomkeerbare inhibitore vir GSK-3β gesintetiseer wat potensiële aktiwiteit bevat vir die bestryding van Alzheimer se siekte. Elf molekules was suksesvol gesintetiseerd en volledig gekarakteriseerd met behulp van spetroskopiese en analitiese tegnieke.

Die raamwerk, 5-{4-[(4-metielpiperasien-1-iel)sulfoniel]feniel}pyrasien-2-amien, was verbind aan ‘n elektrofiliese “lokval”. Verskeie syketting was dan gekoppel deur gebruik te maak van S_N2 substitusie. Twee reekse molekules met ‘n interne α, β-enoon Michael ontvanger is gesintetiseer. Die sintese van die derde reeks wat ‘n terminale Michael ontvanger of ‘n halometielketoon bevat, het probleme opgelewer en was nie suksesvol nie.

Die Suzuki-Miyaura chemie was deeglik ondersoek om die beste kondisies te vind wat die produkte in aanvaarbare opbrengste sal lewer. $Pd(dppf)Cl_2$ as katalis in ‘n oplosmiddel sisteem van tolueen:etanol:water was bepaal as die beste kandidaat vir die Suzuki-Miyaura reaksies om die bogenoemde raamwerk te sintetiseer.

Die molekules was getoets op die menslike rekombinante GSK-3β en die aktiwiteite was bepaal as matig tot goed (GSK-3β IC_{50} reeks: 0.12 - >10 μM). Die mees aktiefste molekuul (GSK-3β IC_{50}: 0.12 μM) bevat ‘n piridien ring en die karboniel van die Michael ontvanger is direk gekoppeld aan die aminopiperasien kern. Die resultate het ook gewys dat die molekules die potensiaal het om onomkeerbaar te bind aan GSK-3β. Gebaseerd op die positiewe resultate, het die reekse ook die potensiaal om verder uitgebrei te kan word.

Acknowledgements

I want to express my heartfelt gratitude to my supervisors, Dr. Margaret Blackie and Prof. Willem van Otterlo, for their enthusiasm and extensive knowledge of organic chemistry, as well their patience and guidance. I also want to thank them for giving me the ability to express my own ideas, to evolve into a better person and as a researcher. And then to Dr. Gareth Arnott for his advice and the discussions about synthetic methods and mechanisms.

Many thanks go out to all the members of the Group of Medicinal and Organic Chemistry, past and present, who were always there when there was a problem in the lab or the office. A special thanks to one of my greatest mentors, Dewald Kleinhans, for his tremendous wealth of knowledge and advice. Jonathan 'Jonny' Hay and Monica Clements, you guys have made this project more bearable with your friendship. I don't think I would have made it through some days if not for all the gatherings in the De Beers and outside, where we could all laugh and talk, discuss problems and talk about chemistry. To my lab mates Luke 'Lukas' 'Gemmerkatjie' Hodson, Jana Botha, Leandi 'Leandieee' van der Westhuizen, Alet 'Aletta' van der Westhuyzen, Tienie Botes, Phillip 'Jean-Phillip' Potgieter, Dominic Castell, Lonwabo 'Lobster' Ngodwana, Lana 'Petronella' Wessels, Siobhan 'Siob' Briggs, Christopher Jurisch, Tim 'Timmie' Kotze, Ashlyn Bhana, Kevin 'Visagie' Visagie, Mari 'Marie beskuit' Janse van Rensburg, Asslly 'Mafaune' Mafaune, Babak 'BBQ' Eghbali, Riyad Domingo, Leanne Barnard, Tanya Mabank, Leon Jacobs, Nicole Pribut, Christoff Albertyn and Hannes 'Skillie' Lerm for their advice, support, conversations and lighter moments in the lab and outside the lab.

Theresa Neumann, you gave me the best experience one could ask for in Germany. Thank you so much for your kindness and support during my time in Darmstadt. Those were one of my most memorable times! Dennis Bensinger and Johannes Pilakowski, many thanks for your advice, support, beer and the Fußballspiel at SV Darmstadt. And to the other Deutsche Freunde, vielen dank! Lastly, Die Lilien ist da!!!!

To all my friends outside the lab, I want to say thank you for your support and interest in my work, although you have no idea what I'm doing and think that I'm making drugs!

To my parents, Willie and Annelie, for being the greatest ever; your undying love and support brought me where I am now. To my brothers and sister, Martin, André and Melanie, for being the best siblings one can ask for. To my in-laws, Johan, Yolanda and Jolene, for their support.

Additional acknowledgements

Stellenbosch University, for providing me with the opportunity to study at this institution.

The technical staff, Raymond Willemse, Mary Johnson and Mr. de Jongh, without whom this research could never have been accomplished.

Prof. Boris Schmidt, for providing me with an incredible opportunity to work in his lab at the Technische Universität Darmstadt, Germany.

Elsa Malherbe and Dr. Jaco Brand for their advice and assistance with my NMR spectroscopic work.

Monica Clements for processing my crystallography data.

Central Analytical Facility for processing my mass spectrometry data.

Prof. Ana Martinéz for the GSK-3β biological testing.

Prof. Peter Smith, Dr. Dale Taylor and Carmen de Kock for the malaria biological testing.

The NRF and DAAD for funding this project.

Someone is sitting in the shade today because someone planted a tree a long time ago

Warren Buffett

Table of Contents

List of technical abbreviations

NMR	Nuclear Magnetic Resonance
TLC	Thin Layer Chromatography
rt	room temperature
IR	Infra-Red
DCM	dichloromethane
MeOH	methanol
EtOAc	ethyl acetate
Hex	hexane
Et_3N	triethylamine
THF	tetrahydrofuran
n-Buli	*n*-butyllithium
Mp	melting point
R_f	ratio of movement of solute to solvent on TLC
HRMS	High Resolution Mass Spectrometry

Chapter 1

Introduction

1.1 Overview

This chapter is concerned with the roles of various hypotheses in Alzheimer's disease (AD) and to introduce key findings on drug development to address AD. In addition, key aspects of the biology and biochemistry associated with the role of Aβ and tau in AD are also summarised. Lastly, several clinical trials on promising anti-AD drug candidates are discussed in this chapter. (This chapter is a minor adaptation of a review paper currently in peer review.)

1.2 Background

Most people seek to live as long as possible, staving off death with medical treatments. Life expectancies have improved dramatically since the beginning of the 20th century in most industrialised countries.[1] The increase in longevity has been made possible by the enormous advancement within scientific and medical domains. The gain in years of life does not always mean that there is good quality of life throughout, as the increase in life span is not without complications. The prevalence of degenerative diseases such as dementia, Parkinson's disease and AD have been increasing with increasing life expectancy. Millions of people around the world suffer from these diseases. Degenerative diseases are currently costing the caregivers over $200 billion annually to provide the necessary aid and treatment for those suffering from these illnesses.[1] With the increasingly aged population and no viable cure or treatment for the degenerative diseases, the cost in both financial and human terms looks set to increase dramatically in coming decades.

The principal risk factor for AD is age. The accumulation of misfolded proteins in the aging brain results in oxidative and inflammatory damage, which in turn leads to synaptic dysfunction and eventually death.[2] In 2012, the worldwide number of AD cases stood around 36 million and is expected to triple by 2050.[3] Furthermore, AD is one of the diseases that cannot yet be prevented, cured or slowed down and one out of three individuals older than 60 years dies of

AD.[1] The average period of survival is approximately eight years after initial diagnosis.[4] Most cases occur later in life (>65 years old), although around 5% of cases occur in patients under 60 years old.[5] These cases are termed early-onset familial Alzheimer's disease (FAD) and are the result of the inheritance of gene mutations on chromosome 14 and 21. The most defined mutations are located on the β-amyloid precursor protein gene (APP) and presenelin genes.[6, 7] The rest of the cases are termed late-onset sporadic Alzheimer's disease (SAD) and have one important risk factor, namely the carriage of the ε4 allele of the apolipoprotein (APOE).[8] Inheritance of a single ε4 allele increases the likelihood of developing AD by 2–5-fold and two ε4 alleles may increase risk by 10-fold or more.[9, 10]

AD is characterised by progressive loss of multiple higher cortical functions including thinking, memory, orientation and language skills.[6, 11] Furthermore, a loss in brain weight is observed that appears to be due to shrinkage and loss of neuronal processes.[12] It has been suggested that AD does not destroy neuronal networks, but rather disrupts the neuronal activity that might interfere with delicate processes underlying cognitive functions.[3] Experiments carried out on plaque-bearing mice with AD have shown that memory formation at synapses are impaired. The aged mice, containing a mutant APP gene that generates amyloid beta (Aβ) plaques, showed profound neuritic dystrophy and extensive activation of microglial cells compared to control aged mice. In addition, the maximum synaptic field potentials in the aged transgenic mice were much smaller (55%).[13] Subsequent to these findings, signalling molecules critical to memory, are inhibited due to the disrupted release of presynaptic neurotransmitters.[14, 15] Due to the activities of the abnormal neuronal network, some AD patients experience non-convulsive epileptic episodes.[16]

There are several hypotheses as to what causes AD and this will be explained in this chapter, along with the current treatments. Because of the vast number of papers on AD, this chapter focuses on key papers and recent works that illustrate the main features of the subject in the following sections.

The aforementioned mutations and risk factors are associated with abnormal production or clearance of Aβ, a 39- to 43-residue peptide that eventually forms senile plaques. The discovery of Aβ in senile plaques,[17, 18] mutations in APP[19] and presenilin genes[20, 21] that leads to the accumulation of Aβ, has resulted in the formulation of the "Amyloid Cascade Hypothesis".[22, 23]

1.3 The amyloid precursor protein (APP) and the amyloid β-peptide (Aβ)

Aβ is a 39- to 43-residue peptide that is cleaved from a much larger peptide, the amyloid precursor protein (APP), and is found in the membrane of cells and organelles such as mitochondria.[24, 25] The function of APP is still unclear, but it has been suggested that it could play a role in regulating metal ion transport and homeostasis.[26] Recently, a report has demonstrated that APP facilitates the efflux of iron and increases the stability of ferroportin on the cell surface.[27] It is also thought that APP plays a role in synaptic formation and repair, signalling and cell adhesion.[28]

The cleavage of the APP by proteases is done in two different pathways, namely, the non-amyloidogenic- and amyloidogenic pathways. In the non-amyloidogenic pathway, the APP is cleaved by α-secretase between residues K687 and L688 of the protein to form a large soluble fragment (sAPPα). In the amyloidogenic pathway, the APP is cleaved by β-secretase (BACE1) between residues M671 and D672 to form another soluble fragment (sAPPβ). The remaining membrane-bound fragments of the APP of the two pathways are then further cleaved by the γ-secretase (GS) to produce monomeric Aβ peptides of varying lengths. From the amyloidogenic pathway, the cleaved $A\beta_{1\text{-}42}$, with the length of 42 amino acids, is not very soluble and tends to aggregate and form the fibrils that are characteristic of AD.[25, 26] These fibrils are also known as senile plaques and are deposited extracellularly in the brain.[29]

1.4 Inhibitors of Aβ aggregation

Aβ aggregation can be inhibited in two ways: either through binding to Aβ monomers and prevent oligomerisation or by reacting with Aβ oligomers to promote clearance. Tramiprosate, **1** (Fig. 1.1), has been showed to maintain Aβ in the nonfibrillar state and increase cognitive ability in mild AD. However, Phase III clinical trials have been inconclusive due to variability in drug studies, low CNS bioavailability and, consequently, further studies were terminated.[30-32] Scyllo-inositol, **2** (Fig. 1.1), an orally-administered stereoisomer of inositol that can cross the blood-brain barrier (BBB), binds to Aβ and modulates its misfolding. The aggregation of Aβ is thereby inhibited and dissociation of aggregates is stimulated. Studies carried out on animals have shown that scyllo-inositol **2** reduces the concentration of soluble and insoluble Aβ, plaque

burden and synaptic loss while improving spatial memory function.[32] Results of Phase I clinical trials suggested that the compound is well tolerated, but in Phase II trials there were serious adverse events among patients in the high dose groups (1000 mg and 2000 mg) that included nine deaths. Therefore, further trials were restricted to lower dose groups (250 mg and 500 mg). Unfortunately, no viable cognitive or functional improvements were observed at 500 mg/day doses and the trials were subsequently aborted.[32, 33]

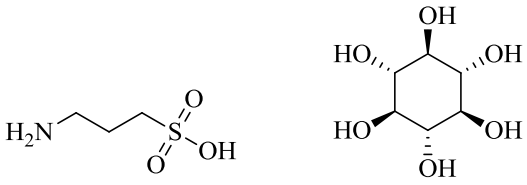

1 **2**

Figure 1.1. Aβ aggregation inhibitors: Tramiprosate **1** and scyllo-inositol **2**

Curcumin, **3** (Fig. 1.2), is a well-known ingredient found in turmeric. This polyphenol has the ability to cross the BBB, inhibits the formation of Aβ oligomers and binds to already existing plaques.[34, 35] For optimal activity, structure-activity relationship (SAR) studies suggested two phenyl groups containing polar substituents on one side for hydrogen bonding and a spacer of 8–16 Å containing less than two sp^3-hybridised carbons.[36] Owing to these attractive findings, a large database of curcumin derivatives have been developed over the years. Longvida, a curcumin dietary supplement, is currently being evaluated in a Phase II trial (NCT01001637).[37] Recently, a promising curcumin derivative, **4** (Fig. 1.2), has been reported to significantly bind Aβ aggregates with reduced cell toxicity. Furthermore, it has been suggested that a substituent on the spacer could improve the efficacy of the compound.[38] In addition, the poor aqueous solubility of curcumin (<0.1 mg/ml), was overcome by substituting the methoxy functional groups with dimethylamine, affording **5** (Fig. 1.2). This allows the derivative to be converted into a hydrochloride salt, where the aqueous solubility improved to 16.7 mg/ml. Not only was the solubility improved, but also the half-life of the derivative and the potential to inhibit Aβ aggregation.[39] Unfortunately, new studies have shown that curcumin is a notorious false positive compound for inhibiting Aβ aggregation. It was suggested that the activity was due in large part to compound-mediated fluorescence interference in assays.[40]

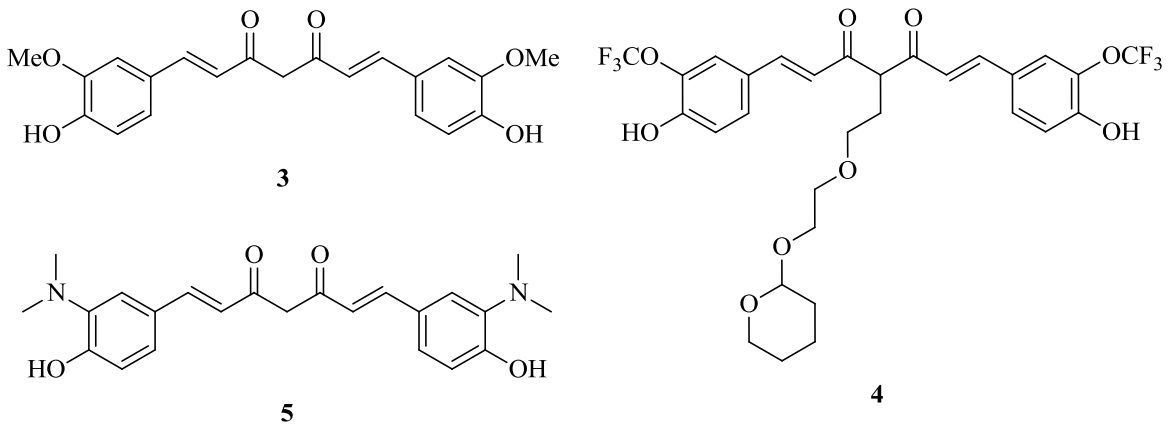

Figure 1.2. Optimisations of curcumin **3** that led to derivatives **4** and **5** with enhanced water solubility and activity

The first rational design of non-peptidic, small molecule Aβ aggregation inhibitors was derived from the KLVFF peptide, an $A\beta_{16-20}$ fragment.[41] In this work, Tjerenberg *et al.* reported that the KLVFF peptide was able to bind to full length $A\beta_{1-42}$ and arrest the aggregation of Aβ to toxic fibrils.[42] Using the KLVFF peptide as the starting point, a pharmacophore was developed that comprised the side-chains of Leu, Val and Phe residues. Two small non-peptidic inhibitors, **6** and **7** (Fig. 1.3), were designed and reported to diminish the formation of large oligomers and fibrils of $A\beta_{1-42}$. In addition, by using the thioflavin-T (ThT) dye assay, the aggregation inhibitory activity of inhibitors **6** and **7**, at a concentration of 50 μM each, were measured as 71% and 47% against $A\beta_{1-42}$ (10 μM), respectively.[43]

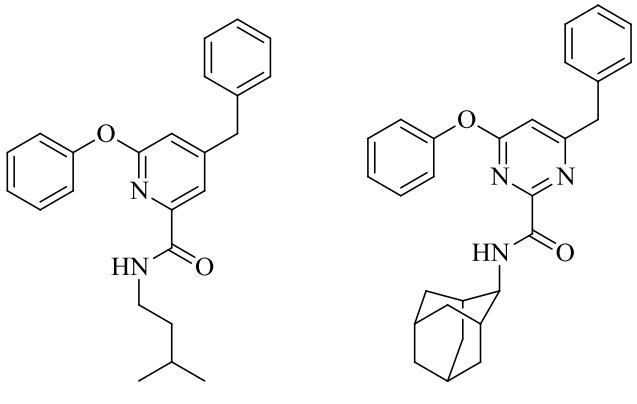

Figure 1.3. The first non-peptidic inhibitors developed by Tjerenberg *et al*.[42]

1.5 Designing secretase inhibitors

Although the APP cleavage enzymes, beta secretase (BACE1) and gamma secretase (GS), has been known for a long time, it has been a challenging task to develop secretase inhibitors that penetrate the BBB and specifically inhibit the cleavage of APP. In addition, the inhibitors should not affect the cleavage of Notch signalling pathway and voltage-gated sodium channel subunits.[3, 44-46] It has been found that a variety of GS inhibitors have the potential to inhibit the cleavage of Notch which could have an adverse effect on the regulation of cellular signalling.[47, 48] Non-selective inhibition of the GS developed adverse side effects that included hematological and gastrointestinal toxicity, skin reactions and hair colour changes.[32] In addition, presenilin-1 (PS1) and presenilin-2 (PS2) are directly involved in the GS cleavage event and it has been suggested that PS is the catalytic core of GS.[47]

Whereas in BACE1, the large active site and the fact that it is less hydrophobic than other aspartyl proteases, makes it extremely difficult to develop small molecule inhibitors that have the ability to cross the BBB.[45, 49, 50]

1.5.1 Beta secretase (BACE1)

Since the discovery of BACE1, small peptide-based mimetics of the APP cleavage site, such as statine, **8** (Fig. 1.4) were developed in the 2000s.[45] (*S*)-Statine inhibited the activity of BACE1 with an IC_{50} of ~40 μM. Modification of the (*S*)-statine through acetylation or replacement of the (*S*)- with the (*R*)-statine enantiomer resulted in diminished activity.[51] One of the first potent BACE1 inhibitors, OM99-2, **9** (Fig. 1.4), was created based upon an octapeptide BACE1 substrate, where the scissile peptide bond had been replaced by a Leu-Ala hydroxyethylene transition-state isostere.[52] The K_i value for OM99-2 on recombinant BACE1 was reported to be 1.6 nM.[52] An example of another potent BACE1 inhibitor is the cell permeable statine-derived BACE1 inhibitor, **10** (Fig. 1.4), that displayed effective inhibition against the BACE1 (IC_{50} = 0.12 μM) and Aβ formation (EC_{50} = 4.0 μM) in transfected human embryonic kidney (HEK-293) cells. The absolute configuration of the active diastereomer was not determined.[53] Optimisation of the statine-derived scaffold, by inserting oxygen, led to the development of new

phenyloxy- and benzyloxy residues. As an example, the benzyloxy statine-derived compound, **11** (Fig. 1.4), inhibited BACE1 with an IC_{50} of 13 nM.[54]

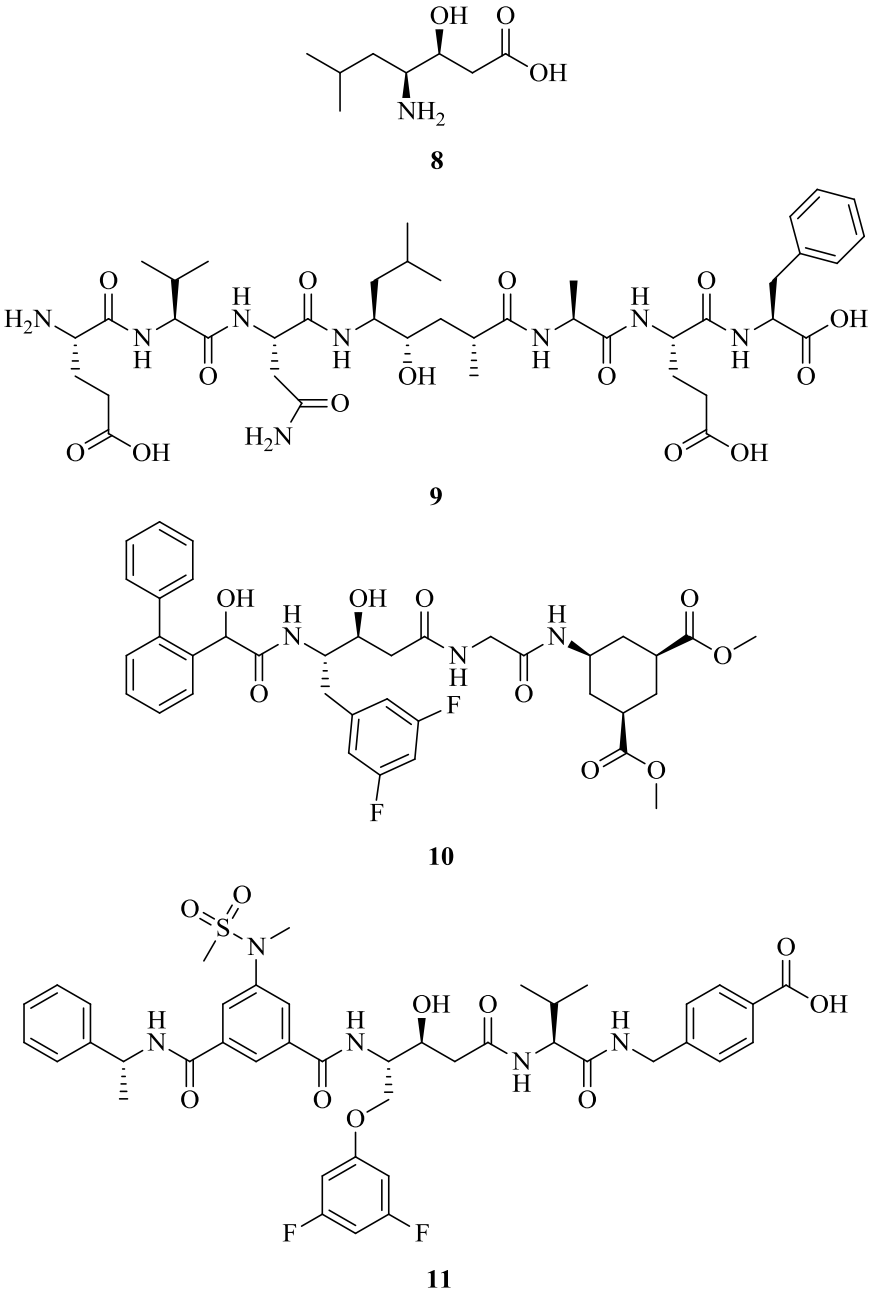

Figure 1.4. Statine, **8,** and statine-derived peptide-based mimetic inhibitors

Other peptidomimetic inhibitors, based on piperazinone and imidazolidinone scaffolds, were developed through molecular modelling and X-ray crystallography. In particular, piperazinones were determined to be tolerant to a wide diversity of modifications. Compound **12** (Fig. 1.5)

induced potent inhibition of BACE1 (IC_{50} = 3 nM), but modest reduction of $A\beta_{1-40}$ (cell IC_{50} = 300 nM). The imidazolidinone-based compound, **13** (Fig. 1.5), displayed similar results (BACE1 IC_{50} = 5 nM, cell IC_{50} = 1100 nM). It was suggested that the introduction of the carbonyl in the scaffold improved the potency of the compounds and this was confirmed by an X-ray crystal structure that showed a hydrogen bond between the carbonyl moiety and Thr72 NH.[55]

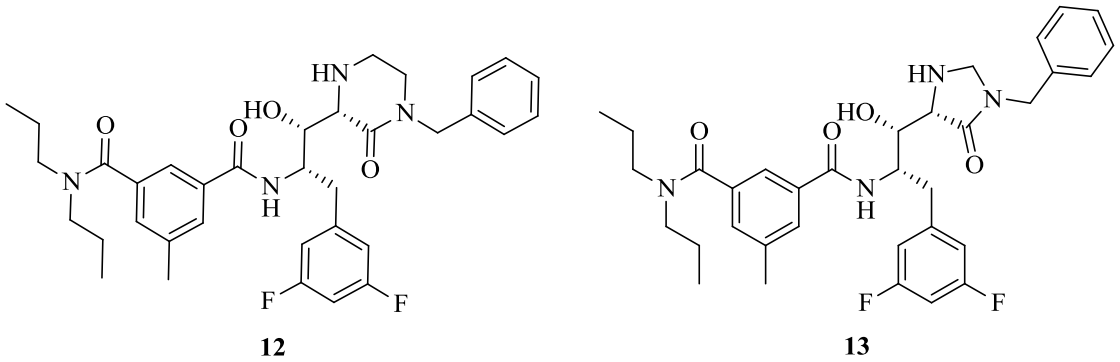

Figure 1.5. Peptidomimetic inhibitors based on piperazinone and imidazolidinone scaffolds

One of the major challenges in the design of protease inhibitors is the transition from peptidomimetics to small molecules. This task has proven to be quite challenging in the case of BACE1. The large size of the active site and the need for efficient brain penetration created additional challenges for the design of small non-peptidic inhibitors.[50] Nonetheless, a wide variety of novel small molecule non-peptidomimetic BACE1 inhibitors have been developed through fragment-based discovery. BACE1 fragment screening methods have been distributed among nuclear magnetic resonance (NMR) spectroscopy,[56-59] X-ray crystallography,[59-62] surface plasmon resonance (SPR),[59, 63] *in situ* chemistry and biochemical enzyme assays.[59, 64] Several groups have reported the identification of fragment hits using NMR methods such as HSQC,[56] waterLOGSY[58] and ^{19}F NMR spectroscopy.[65] Using these techniques, three major structural classes, isothiourea **14**, 2-aminopyrimidinone **15** and aminoquinoline **16** (Fig. 1.6), were discovered as BACE1 fragment hits. Over 200 isothiourea analogues were selected for a focused screen in a BACE1 HTRF assay. The most potent analogue in this series, compound **17** (Fig. 1.6), dose-dependently inhibited BACE1 with an IC_{50} of 210 μM in the BACE1 HTRF assay. An X-ray crystal structure of the complex between the isothiourea **17** and BACE1 showed hydrogen

bonds between the NH groups of the isothiourea moiety and two catalytic aspartates (Asp32 and Asp228) in the active site.[56] Folmer and co-workers focused on optimising the aminopyrimidinone fragment hit through BIAcore assay format after a NMR spectroscopy screen on a 2000-compound general fragment library. The best BACE1 inhibitor, compound **18** (Fig. 1.6), had a modest affinity for BACE1 (K_d = 0.66 mM), but bound efficiently to BACE1 and was therefore deemed a suitable starting point for chemical optimisations.[58]

In another NMR spectroscopy approach, a library of 1200 fluorine-containing fragments was screened by ^{19}F NMR.[65] One of the hits, an aminoquinoline fragment **16**, was investigated with different hydrophobic substituents at the 6-position. The fluorine moiety resulted in better K_d values (SPR K_d = 1.2 mM) in comparison to the -CF_3 group (SPR K_d = 3.9 mM), which was likely due to the reduced hydrophobic effects and/or the significant decrease in the van der Waal's (VDW) volume. Further hydrophobic substitutions at the 6-position of aminoquinoline **16** led to potencies in the low micromolar range. Compound **19** (Fig. 1.6), a trifluorinated aryl-aminoquinoline, with a SPR K_d value of 200 μM was mixed with ^{19}F-containing compounds to identify potential candidates for fragment linking. ^{19}F-^{19}F {^{1}H decoupled}-NOESY NMR spectroscopy experiments suggested that compounds **19** and **20** (Fig. 1.6) bind close in space and may be successfully combined which provided the inspiration to synthesise compound **21** (Fig. 1.6). This compound had a greater than 100-fold increase in potency when compared to the original fragment **19**.[65]

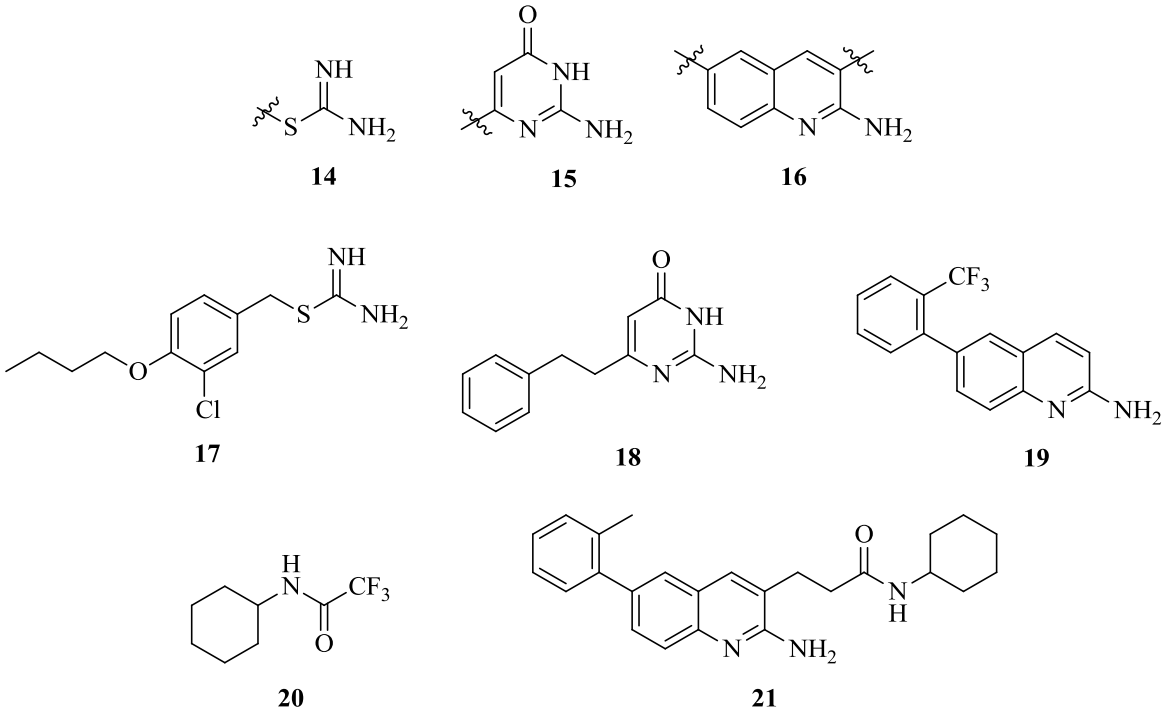

Figure 1.6. Development of inhibitors after fragment-based screening

In 2014, novel tetrahydropyran (THP) chromene inhibitors, armed with spirocyclic motifs, were developed that overcame the aforementioned BACE1 challenges. Guided by the SAR studies, 8-THP chroman, **22** (Fig. 1.7), equipped with the aminooxazoline motif, showed great potential in terms of inhibiting BACE1 (IC_{50} = 45 nM) and had a 1300-fold selectivity over cathepsin D (CatD), which possesses a similar active site. Furthermore, compound **22** showed sufficient cell permeability in the apical to basolateral direction (P_{app} AB = 19 10^{-6} cm/s), but demonstrated a moderate efflux ratio in LLC-PK1 cells transfected with human MDR1 (P-gp). In addition, pharmacodynamic studies carried out on rats with compound **22** demonstrated a 69% reduction of $A\beta_{1\text{-}40}$ in cerebrospinal fluid (CSF).[66]

Eli Lilly identified isothiourea hits with potential in a fragment-based screening assay of approximately 8000 fragments. Modification of the amino-benzothiazine scaffold to include a sp^3 carbon led to the development of the chiral compound **23** (Fig. 1.7). The fluorine atoms were added to enhance the metabolic stability of the compound.[67] The BACE1 inhibitor showed promising results (IC_{50} = 240 nM with high cell permeability) and was the first of the amidine class to reach Phase I clinical trials. In healthy volunteers, the inhibitor demonstrated long-

lasting Aβ reductions in lumbar CSF after oral dosing of 30 and 90 mg. Unfortunately, further clinical trials were discontinued as a result of the development of off-target retinal pathologies.[61, 68, 69]

AstraZeneca evaluated a series of bicyclic aminoimidazoles as potent BACE1 inhibitors to fine-tune the properties of the amidine moiety by introducing substituents on the bicyclic ring. The basicity of the aminoimidazole group (p*K*a >8) was lowered by introducing fluorinated substituents to improve blood-brain permeability. Aminoimidazole **24** (Fig. 1.7), with fluorine-propyl ether and difluoromethoxy substituents on the bicyclic rings, showed good membrane permeability (Caco-2 cells, 8×10^{-6} cm/s). Furthermore, compound **24** showed low nanomolar potency against BACE1 with an IC_{50} of 7.5 nM and reduced brain- and plasma $A\beta_{1\text{-}40}$ levels with 17% and 76%, respectively in wild-type mice when co-administered with efflux inhibitor GF120918.[70]

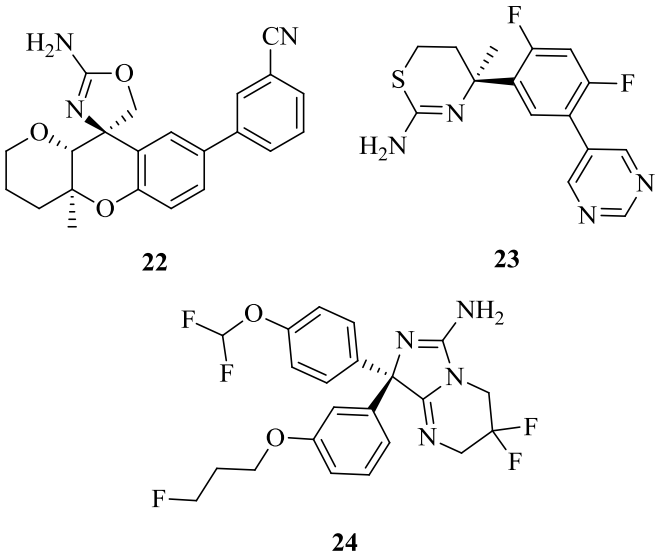

Figure 1.7. A series of the amidine inhibitors developed through fragment-based screenings

In another attempt to improve selectivity for BACE1 over CatD without affecting CNS penetration, compound **23** was redesigned. As shown in Figure 1.8, a thorough analysis of the structure of BACE1 and CatD resulted in subtle differences being observed that could potentially be exploited to design compounds to improve selectivity for BACE1. The flap loop conformation represented by BACE1 Tyr71 and Trp76 is similar to that in CatD (region III), but the substitution of Trp76 by Leu (CatD) in the flap loop prevents hydrogen bond formation to Tyr78

(by Trp). Instead, Tyr78 engages Trp40, which is not within the flap loop, likely creating greater rigidity in this region in CatD. Using this strategy, the pyrimidine side chain of compound **23** was removed and the amidine scaffold **25** (Fig. 1.9) was expanded to fill the space of S2′. Compound **26** (Fig. 1.9), with a tetrahydropyran (THP) ring fused to the amidine scaffold, was developed with the fluoromethyl moiety occupying the S2′ pocket. Selectivity over CatD increased significantly (76-fold) with similar potency (BACE1 whole cell assay (WCA) IC_{50} = 61 nM) when compared to compound **23** (BACE1 WCA IC_{50} = 50 nM). Furthermore, the fused THP compound **26** exhibited good brain penetration and, in rat toxicology assessment, no signs of autofluorescent material accumulation in retinal pigment epithelium at two doses (75 and 25 mg/kg) were observed.[71]

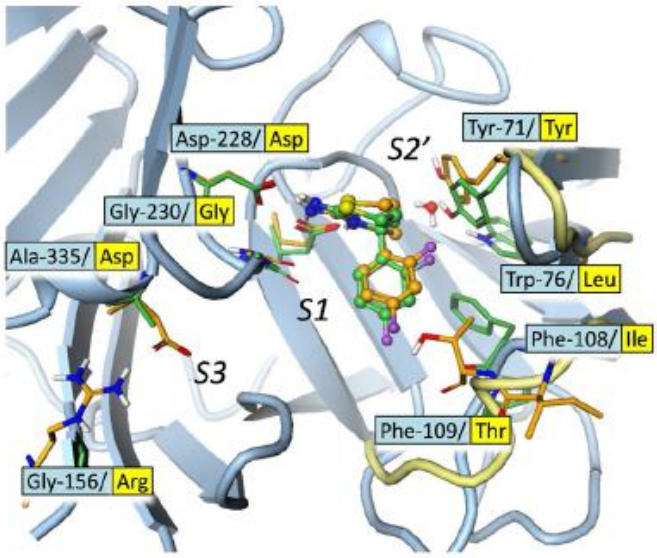

Figure 1.8. X-ray crystal structure of the amidine scaffold **25** (green ball and stick) with BACE1 (light blue ribbon) with a model of **25** (orange ball and stick) in cathepsin D (yellow ribbon). Residues in the areas of interest are labelled with BACE1 residue names and numbers (light blue) following by the corresponding CatD residue names (yellow)[71]

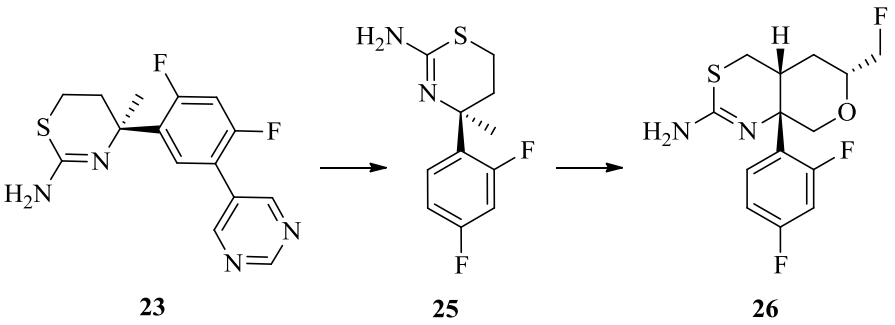

Figure 1.9. Attachment of a fused THP ring on the amidine scaffold **25** to improve the selectivity towards BACE1 over catD

1.5.2 Gamma secretase (GS)

DAPT, **27**, (Fig. 1.10) was the first peptidomimetic compound with GS inhibitory activity when tested *in vivo*.[72, 73] This compound inhibited Aβ production in cells, with an IC_{50} of 115 nM, but high doses (100 mg/kg) were needed to lower Aβ in the brain of young APP transgenic mice.[72, 74] Unfortunately, DAPT was found to be an inhibitor of the Notch signalling pathway, and pharmacokinetic (PK) profiling revealed potential acid instability of the *t*-butyl ester group.[73, 75] Using a SAR strategy, the acid-labile *t*-butyl ester group was replaced with a more robust imidazole side chain **28** (Fig. 1.10). For this compound, cellular potency was greatly increased (WCA IC_{50} = 0.4 nM) with significant reductions of brain, plasma, and CSF Aβ in guinea pigs after an acute dose.[75]

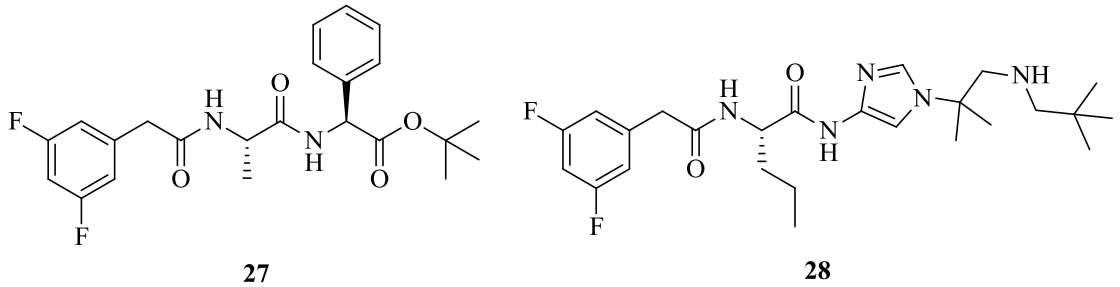

Figure 1.10. The first peptidomimetic GS inhibitor **27** and the optimisation of the acid-labile side chain that led to the development of **28**.

Eli Lilly developed a non-selective GS inhibitor, semagacestat, **29** (Fig. 1.11), that inhibits APP and Notch cleavage (APP IC_{50} = 15 nM and Notch EC_{50} = 49 nM).[76] In Phase I human trials, the drug showed a maximum inhibition of plasma $A\beta_{1\text{-}40}$ (73% reduction) at six hours after the administration of the 140 mg dose. A rebound effect on plasma $A\beta_{1\text{-}40}$ levels was observed 8-12 hours after administration.[76] Unfortunately, in Phase III human trials, semagacestat, **29**, did not improve cognitive status and was associated with adverse events, including skin cancers and infections. In comparison to the placebo, patients receiving higher doses (140 mg) had significant worsening of functional ability and the trial was terminated before completion.[77]

Inspired by the semagacestat series, the Hoffman-La Roche group developed a potent, metabolically-labile malonamide GS inhibitor, **30** (Fig. 1.11), that inhibited $A\beta_{1\text{-}40}$ with an IC_{50} of 22 nM in a cell-free GS assay derived from human embryonic kidney (HEK) cells.[78] Replacement of the metabolically-labile difluorobenzyl group with the pentafluoropropyl group, in addition to changing the malonamide into its carbamate analogue, afforded **31** (Fig. 1.11), which demonstrated improved solubility and stability. However, compound **31** potently inhibited Notch processing (Notch-1 IC_{50} = 1.7 nM) in an HEK cellular assay.[78, 79]

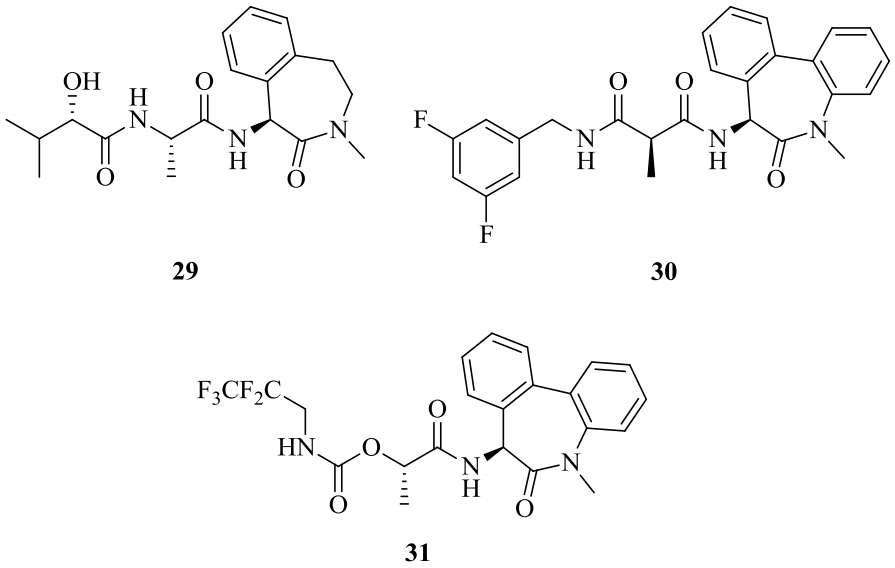

Figure 1.11. Semagacestat **29** and associated Hoffman-La Roche inhibitors

Using high throughput screening (HTS) in a whole cell assay (SHSY5Y cells), a Merck group identified the benzodiazepine lead, **32** ($A\beta_{1\text{-}40}$ IC_{50} = 33 nM) (Fig. 1.12) as a GS inhibitor.[80]

Modification to the benzodiazepine substituent and the hydrocinnamate side chain, in an attempt to improve membrane permeability and potency, offered analogues such as **33** ($A\beta_{1\text{-}40}$ IC_{50} = 4 nM) (Fig. 1.12).[76] A QSAR analysis of this series of GS inhibitors revealed that inhibitory activity increased in parallel with increasing lipophilicity.[81] Further optimisation of this series led to the potent GS inhibitor **34** with picomolar activity ($A\beta_{1\text{-}40}$ IC_{50} = 60 pM) (Fig. 1.12). Unfortunately, no Notch-sparing selectivity data for **34** were reported.[82]

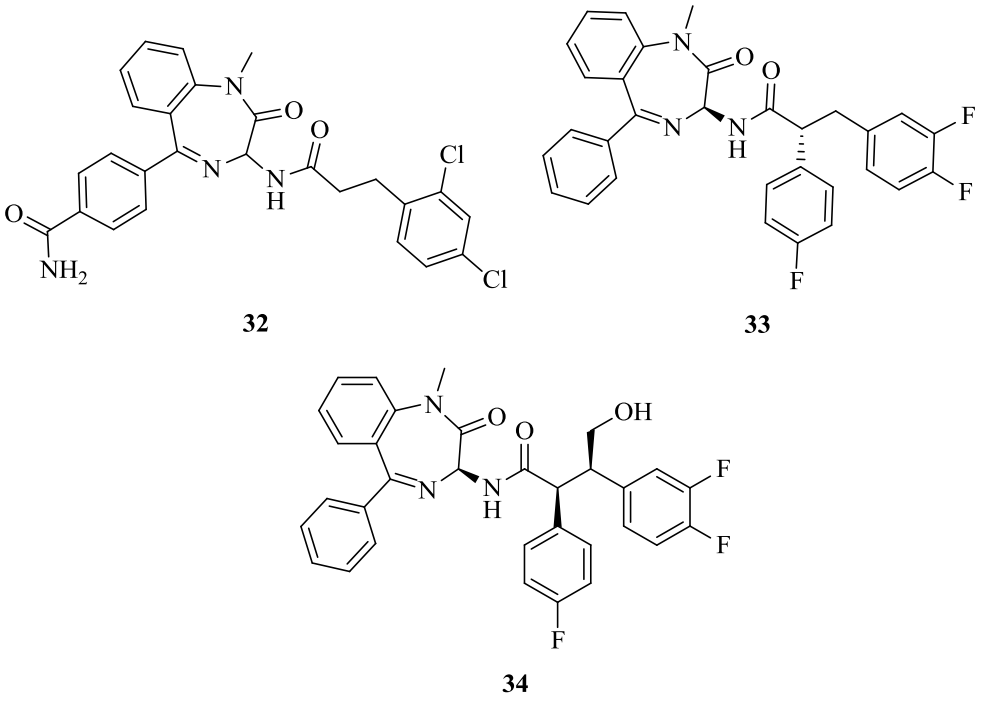

Figure 1.12. Merck's benzodiazepine-based GS inhibitors

In 2007, Bristol-Myers Squibb identified lead GS-inhibiting arylsulfonamides from an HTS campaign.[83] In this campaign, which employed a cellular assay ($hAPP_{swe}H4$ cells), compound **35** (Fig. 1.13) was identified to be a modest inhibitor of GS (IC_{50} = 850 nM). A significant increase in potency (~ 10 fold) was observed when compounds were branched with an α-methyl group at the point of attachment to the sulfonamide nitrogen, as observed in the case of the cyclohexyl derivatives **36** ($A\beta_{1\text{-}40}$ IC_{50} = 1000 nM and **37** ($A\beta_{1\text{-}40}$ IC_{50} = 190 nM) (Fig. 1.13). Further SAR studies led to the potent 4-chlorophenyl analogue, **38** ($A\beta_{1\text{-}40}$ IC_{50} = 5 nM) (Fig. 1.13). Three hours after oral administration of a single 500 μmol/kg dose of **38** to Tg2576 βAPP-Swedish

transgenic mice, tests showed a 25% reduction in brain Aβ. Furthermore, this compound had a low brain Aβ level of 5.2 μM and a plasma level of 1.6 μM.

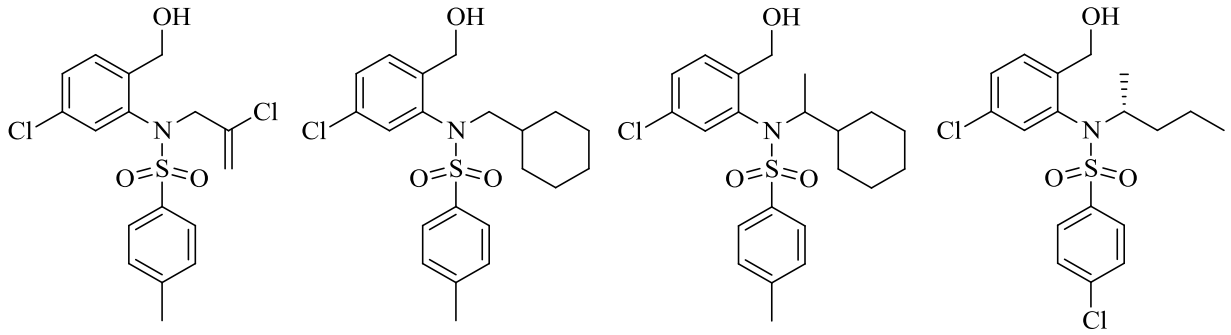

35 **36** **37** **38**

Figure 1.13. Bristol-Myers Squibb's first generation of arylsulfonamides GS inhibitors

To improve the *in vivo* efficacy, various nitrogen-appended analogues of **38** were next synthesised.[84] Methanesulfonamide **39** (Fig 1.14) proved to be one of the most potent inhibitors in this series ($A\beta_{1\text{-}40}$ IC_{50} = 320 pM in $hAPP_{swe}H4$ cells). When this compound was orally administered to Tg2576 mice at 200 μmol/kg, a 27% reduction in brain Aβ was observed. This represents a similar reduction in brain Aβ, but at less than half the dose of **38**. However, the brain/plasma ratio of sulfonamide **39** was relatively poor (0.06) with respect to that of **38** (3.25). Replacement of the methylsulfonamide functional group with a tetrazole group afforded analogue **40** (Fig. 1.14) with similar potency ($A\beta_{1\text{-}40}$ IC_{50} = 510 pm in $hAPP_{swe}H4$ cells), but with improved efficacy (41% reduction in brain Aβ in Tg2576 mice at 200 μmol/kg) and a better brain/plasma ratio of 0.21.

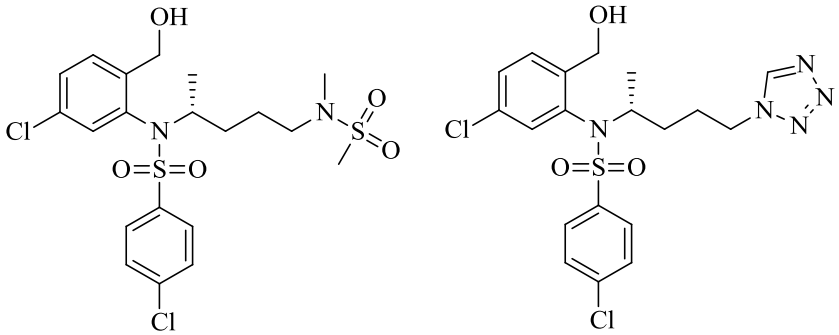

39 **40**

Figure 1.14. Bristol-Myers Squibb's second generation of arylsulfonamide GS inhibitors

Wyeth and ArQule employed HTS screening on their compound collections in a cellular assay (hAPPCHO cells) with respect to Aβ production, to furnish two lead GS inhibitors, **41** ($A\beta_{1\text{-}40}$ IC_{50} = 5449 nM) and **42** ($A\beta_{1\text{-}40}$ IC_{50} = 2214 nM) (Fig. 1.15).[85] Furthermore, both leads had moderate Notch-sparing selectivity of 3.7-fold and 9-fold, respectively. Replacing the butyl chain of **41** with a 3-pentyl group afforded **43** (Fig 1.15), a structural modification that greatly improved the potency ($A\beta_{1\text{-}40}$ IC_{50} = 294 nM) and Notch-sparing selectivity (14-fold). A further increase in potency ($A\beta_{1\text{-}40}$ IC_{50} = 25 nM) was observed for **44** (Fig 1.15), in which the 4-chlorophenyl moiety had been replaced with the 5-chlorothiophene group. Not only was **44** a potent GS inhibitor, it also had promising Notch-sparing selectivity (10-fold). Compound **44**, *in vivo*, reduced brain $A\beta_{1\text{-}40}$ and $A\beta_{1\text{-}42}$ by ~25% when administered at 100 mg/kg to TG2576 mice. Furthermore, compound **44** had good solubility (6.7 mg/mL) and exhibited high membrane permeability (Caco2 assay: (A-B), P_{app} = 50 x 10^6 cm/s; (B-A), P_{app} = 42 x 10^6 cm/s) and good brain/plasma ratio (2.0). Unfortunately, the metabolic stability of **44** was low [$t_{1/2}$ = 1 min (rat), $t_{1/2}$ = 2 min (mouse), 8 min (human)]. The primary sites of metabolism were found to be the oxidation of the terminal methyl group of the 3-pentyl group and glucuronidation of the primary hydroxyl group. To improve the metabolic stability, the side chain was shortened and the labile methyl groups were replaced with trifluoromethyl groups to afford begacestat, **45** (Fig 1.15), which has high potency ($A\beta_{1\text{-}40}$ IC_{50} = 15 nM) and Notch-sparing selectivity (14-fold). Increased metabolic stability for begacestat was observed in mice and human microsomes [$t_{1/2}$ = 3 min (rat); $t_{1/2}$ = 48 min (mouse); $t_{1/2}$ = >90 min (human). Begacestat has shown promising results in preclinical trials and is currently under clinical evaluation for AD treatment.[86]

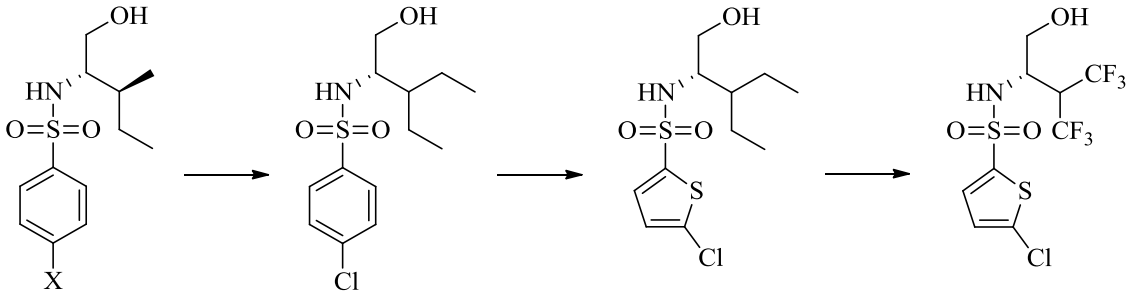

Figure 1.15. The development of begacestat **45**

Further improvement of the pharmacokinetic properties through HTS and SAR exploration on the aryl sulfonamide series led to the development of avagacestat (BMS-708163) **46** (Fig 1.16).[87] For this compound, brain penetration and metabolic stability improved significantly through the incorporation of the bioisosteric oxadiazole and the trifluoromethyl group.[87] In a Phase I clinical trial, avagacestat reduced cerebrospinal fluid concentrations of $A\beta_{1-38}$, $A\beta_{1-40}$ and $A\beta_{1-42}$ at daily doses of >50 mg/day for 28 days without any sign of potential Notch toxicity.[88] After the promising results of the Phase I clinical trial, avagacestat was subjected to Phase II clinical trials. Unfortunately, the results were disappointing as cognitive performances at daily doses of 25 and 50 mg were comparable to the placebo over 24 weeks. In addition, higher doses (100 and 125 mg) of avagacestat led to adverse GI and dermatological effects.[89]

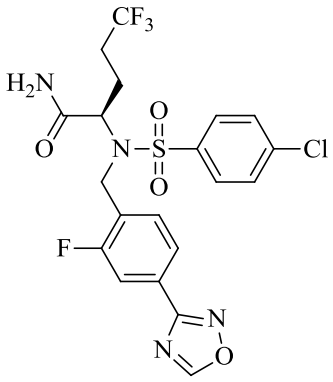

46

Figure 1.16. Avagacestat

In 2006, Merck developed a series of 4-substituted cyclohexyl sulfones which inhibited GS *in vivo* in the low nanomolar range. Investigation of substitution at the 4-position of the cyclohexane moiety led to the development of a potent sulfone, **47** (Fig. 1.17), that demonstrated a robust decrease of brain $A\beta_{1-40}$ levels in APP-YAC mice 4 hours after oral dosing of 1 mg/kg.[90] Sulfone **47** was also found to have significantly higher inhibition (37-fold) of the isoform of GS composed of PS1 than that of PS2.[91] In addition, chronic dosing with sulfone **47** in mice did not cause Notch-mediated side effects as reported with other GS inhibitors.[92] The good safety profile of sulfone **47** made it an attractive starting point for further optimisation.

Through conformational analysis, the sulfone series was expanded to include tricyclic compounds.[93] Preliminary results of tricyclic sulfones showed a much improved *in vitro* potency and *in vivo* CRND8 mouse PK profile. An example is the tricyclic triflate, **48** (Fig. 1.17), which inhibited membrane $A\beta_{1\text{-}40}$ with an IC_{50} of 27.1 nM and inhibited cortex $A\beta_{1\text{-}40}$ by 42% three hours after a single oral dose of 30 mg/kg.[93] Furthermore, this series had lower Notch-related side effects in comparison to other GS inhibitors.

Based on these results, Merck went on to develop the next generation of tricyclic sulfones with improved SAR.[94] By shifting the sulfonamide group to position 7 of the tricyclic core structure, alkyl sulfonamide **49** (Fig. 1.17) showed improved bioactivity by inhibiting membrane $A\beta_{1\text{-}40}$ with an IC_{50} of 13 nM and this compound involved 69% inhibition of $A\beta_{1\text{-}40}$ in the brain, three hours after a single oral dose of 10 mg/kg.[94]

In 2015, Merck developed a spirocyclic series based on the SAR data of the aforementioned sulfone GS inhibitors.[95] To improve the stability of the chair conformation, the sulfonamide group was replaced with a spirocycle. For example, cyclic phosphonate **50** (Fig. 1.17) inhibited the membrane $A\beta_{1\text{-}40}$ with an IC_{50} of 9.5 nM and had 33-fold selectivity for presenilin-1 over presenilin-2. Also, phosphonate **50** demonstrated improved pharmacokinetic properties when compared to sulfone **47** and the phosphonate cycle appeared stable *in vivo*. The improved stability of the phosphonate **50** and high selectivity for PS1 paves the way for safer GS inhibitors in the future.[95]

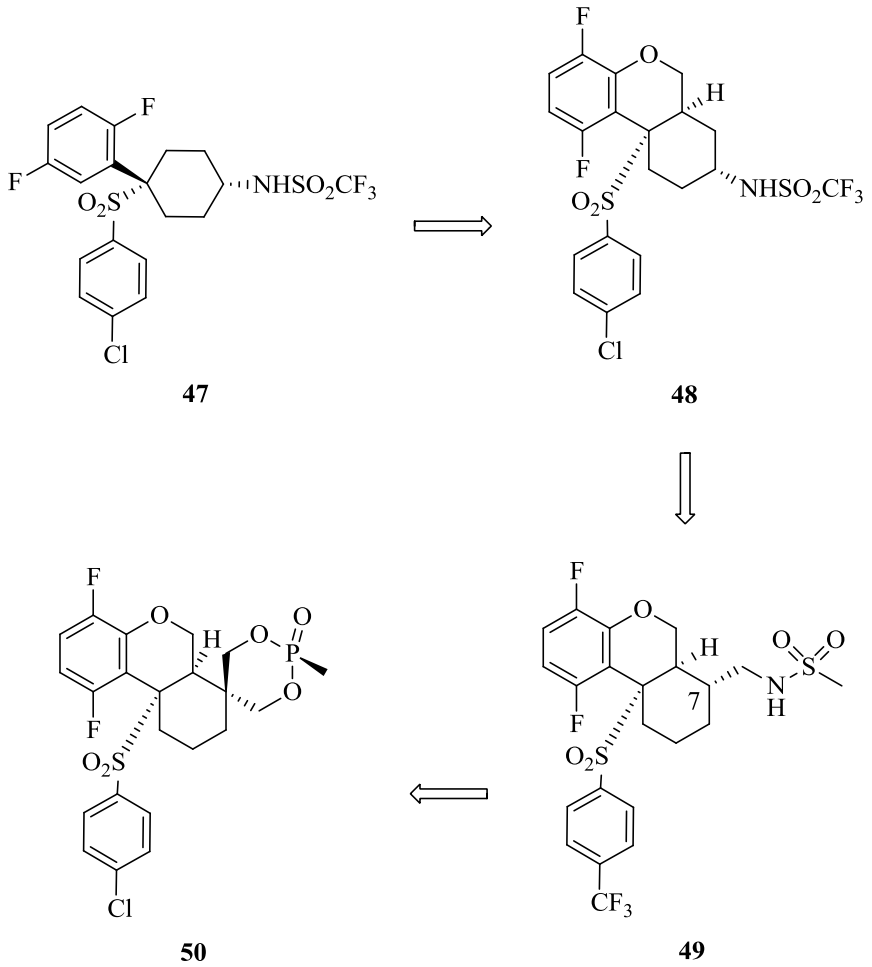

Figure 1.17. Merck's rational design strategy resulted in spirocyclic phosphonate GS inhibitor **50**

The discovery that nonsteroidal anti-inflammatory drugs (NSAIDs) such as (*R*)-ibuprofen **51**, indomethacin **52**, sulindac sulfide **53** and (*R*)-flurbiprofen **54** (Fig. 1.18) selectively lower the $A\beta_{1\text{-}42}$ formation in favour of $A\beta_{1\text{-}38}$, without inhibiting Notch cleavage, has encouraged the development of NSAIDs-like GS inhibitors.[96, 97] However, their weak *in vitro* potencies ($A\beta_{1\text{-}42}$ IC_{50} >10 μM) have limited their development. Nonetheless, (*R*)-flurbiprofen **54** was advanced into clinical studies and was moderately successful in Phase II clinical trials.[97, 98] Unfortunately, during Phase III clinical trials, (*R*)-flurbiprofen **54** failed to slow down cognitive decline or loss of ability to carry out daily activities in patients with mild AD.[99] Nevertheless, these results encouraged further research into how NSAIDs inhibit GS. An example would be the confirmation that sulindac sulfide **53** noncompetitively inhibits GS at a concentration of

10–30 μM.[100] (*R*)-Flurbiprofen **54** has also been shown to inhibit GS noncompetitively (IC_{50} = 307 μM).[101]

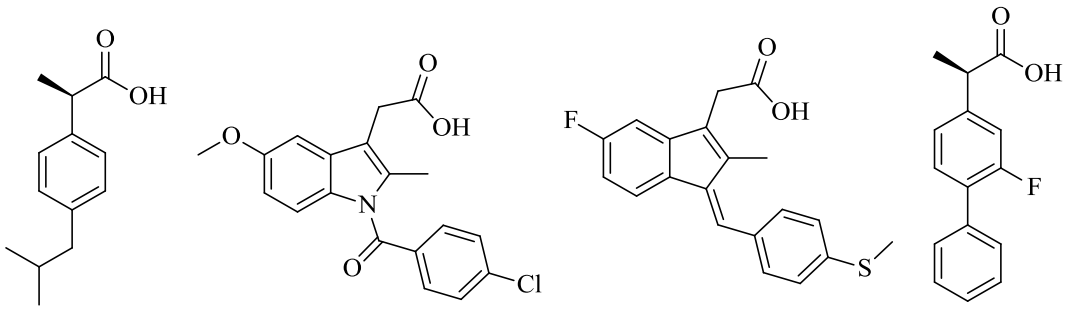

51 **52** **53** **54**

Figure 1.18. Structures of NSAIDs that decrease the formation of $A\beta_{1-42}$

These findings have prompted the development of a second generation of NSAID derivatives with improved potency while removing the cyclooxygenase (COX) inhibition that is associated with NSAIDs. The company, Chiesi, used (*R*)-flurbiprofen **54** as starting point and replaced the methyl substituent with a cyclopropyl group and added substituents on the terminal phenyl group to yield compound **55** ($A\beta_{1-42}$ IC_{50} = 41 μM) (Fig. 1.19), which was found to be 7-fold more potent than (*R*)-flurbiprofen **54** ($A\beta_{1-42}$ IC_{50} = 305 μM).[102, 103] However, brain penetration for compound **55** was found to be poor, with a brain/plasma ratio of about 5% in mice after 100 or 300 (mg/kg)/day for 4-5 days.[103]

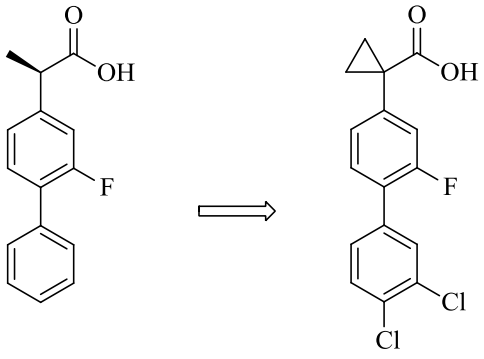

54 **55**

Figure 1.19. Chiesi's second generation NSAID derived GS modulator

A Japanese-based company, Eisai, developed a series of NSAID-piperidine derivatives with the aim to improve brain penetration. Replacement of the aryl ring with piperidine led to the development of isoamyl derivative **56** (Fig. 1.20) that demonstrated good penetration of the CNS (brain concentration = 4.2 μM at a 5 mg/kg oral dose after 2 h). In addition, **56** inhibited $A\beta_{1\text{-}42}$ at a pIC_{50} of 6.5. It was suggested that lipophilicity plays a crucial part in terms of the compound's potency and brain penetration.[104] To improve the pharmacokinetic properties of the piperidine acetic acid series, researchers at Merck incorporated fluorine onto the piperidine ring. The resultant 3,3-difluoropiperidine **57** (Fig. 1.20) demonstrated good *in vitro* activity against $A\beta_{1\text{-}42}$ with a selective inhibition (IC_{50} = 230 nM) relative to $A\beta_{1\text{-}40}$ (IC_{50} = >10 000 nM).[105] The shift of the carboxylic acid to the 3- position led to the development of 4,4-difluoropiperidine **58** (Fig. 1.20) that showed similar activity ($A\beta_{1\text{-}42}$ IC_{50} = 600 nM, $A\beta_{1\text{-}40}$ IC_{50} = >10 000 nM). When the APP-YAC transgenic mice were dosed with **57** and **58** (10 mg/kg, oral, 7 h), both compounds showed potent $A\beta_{1\text{-}42}$ reduction (of 84% and 64% respectively).[105]

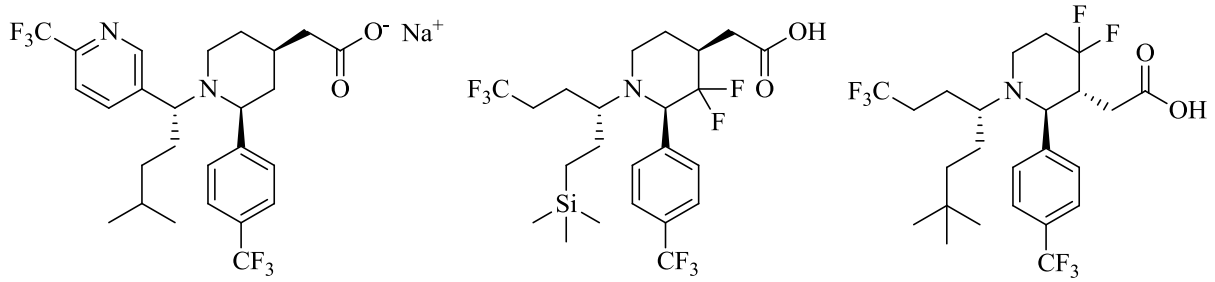

56 **57** **58**

Figure 1.20. NSAID-piperidine derived GS modulators

Around 2006, researchers at Eisai worked on a non-NSAID-derived GS modulator, called the cinnamide series.[106-109] This work culminated in the development of E-2012, **59** (Fig. 1.21), and a number of patent applications involving salts,[110] processes[111, 112] and prodrugs[113] have been found in the patent literature. In terms of activity, E2012 **59** inhibits $A\beta_{1\text{-}42}$ with an IC_{50} of 92 nM and $A\beta_{1\text{-}40}$ with an IC_{50} of 330 nM. In rat CSF, E2012 **59** significantly decreased $A\beta_{1\text{-}42}$ levels by 17% and 47% at doses of 10 and 30 mg/kg, respectively. Furthermore, the reduction of $A\beta_{1\text{-}42}$ levels in rat brain at doses of 10 and 30 mg/kg were 17% and 43%, respectively. In addition, no evidence of adverse effects on Notch were seen *in vitro* up to 3 μM.[114] Based on these promising results, modifications on the scaffold core emerged. Replacing the cinnamide olefin, which is a

potential Michael acceptor, and lowering the lipophilicity, Pfizer came up with a dihydrobenzofuran amide core.[115] From this group of compounds, benzofuran **60** (Fig. 1.21) demonstrated improved CNS physicochemical properties (*c*log*P* = 3.96, Topological Polar Surface Area (TPSA) = 78, Lipophilic Efficiency (LipE) = 4.18, Central Nervous System Multiparameter Optimization (CNS MPO) = 4.8) in comparison to E2012 **59** (*c*log*P* = 4.8, TPSA = 47, LipE = 2.19, CNS MPO = 3.7). In addition, benzofuran, **60**, achieved good *in vitro* potency ($A\beta_{1\text{-}42}$ IC_{50} = 188 nM) and was found to be inactive against Notch (IC_{50} >50 μM).[115] The rat PK profile of benzofuran **60** showed good oral bioavailability and moderate clearance with moderate liability for CYP inhibition (CYP3A4 and CYP2D6 IC_{50} >30 μM). Benzofuran, **60**, reduced $A\beta_{1\text{-}40}$ and $A\beta_{1\text{-}42}$ significantly *in vivo* in guinea pigs with 16% and 36% respectively (100 mg/kg, oral dose, 4 hours).[115] Based on these results, Pfizer went on to improve membrane permeability and brain penetration. A conformational lock on the molecule was introduced and the number of rotatable bonds, as well the number of hydrogen bond donors, were reduced.[116] Replacing the amide with a lactone gave rise to two possible regioisomers, shown by **61** and **62** (Fig. 1.21). Complete loss of activity was observed for **62** ($A\beta_{1\text{-}42}$ IC_{50} = >16 μM), whereas **61** preserved some $A\beta_{1\text{-}42}$ activity ($A\beta_{1\text{-}42}$ IC_{50} = 3.4 μM). This finding provided valuable insight into the pharmacophore, as it suggested that the two polar functional groups need to be situated on opposite sides of the scaffold. The scaffold was then converted into pyridopyrazine-1,6-dione to afford the desired polar functional groups. Compounds **63** and **64** (Fig. 1.21) showed substantially improved activity ($A\beta_{1\text{-}42}$ IC_{50} = 252 nM and 101 nM, respectively) over **61** and **62**. Furthermore, **63** had 100% oral bioavailability in rats and showed excellent membrane permeability (Ralph Russ Canine Kidney (RRCK) $P_{app,A\text{-}B}$ = 17.7 × 10^{-6} cm/s and Multidrug Resistance $(MDR)_{A\text{-}B}$ = 13.1 × 10^{-6} cm/s). Both compounds were less lipophilic with respect to E-2012 **59** and demonstrated good CNS physicochemical properties. Compound **64** was able to reduce 68% of $A\beta_{1\text{-}42}$ *in vivo* in guinea pigs in oral doses of 90 mg/kg after 4 hours.[116] Further optimisation on the right side of the pyridopyrazine-1,6-dione core, to improve the ADME profile, led to the development of compound **65**. This compound exhibited potent *in vitro* inhibition ($A\beta_{1\text{-}42}$ IC_{50} = 6 nM), good rodent brain penetration (brain to plasma ratio of 0.8 and an unbound brain to unbound plasma ratio of 0.4) and as well robust *in vivo* $A\beta_{1\text{-}42}$ lowering in guinea pigs (42% reduction after 3 h for 60 mg/kg oral dose).[117]

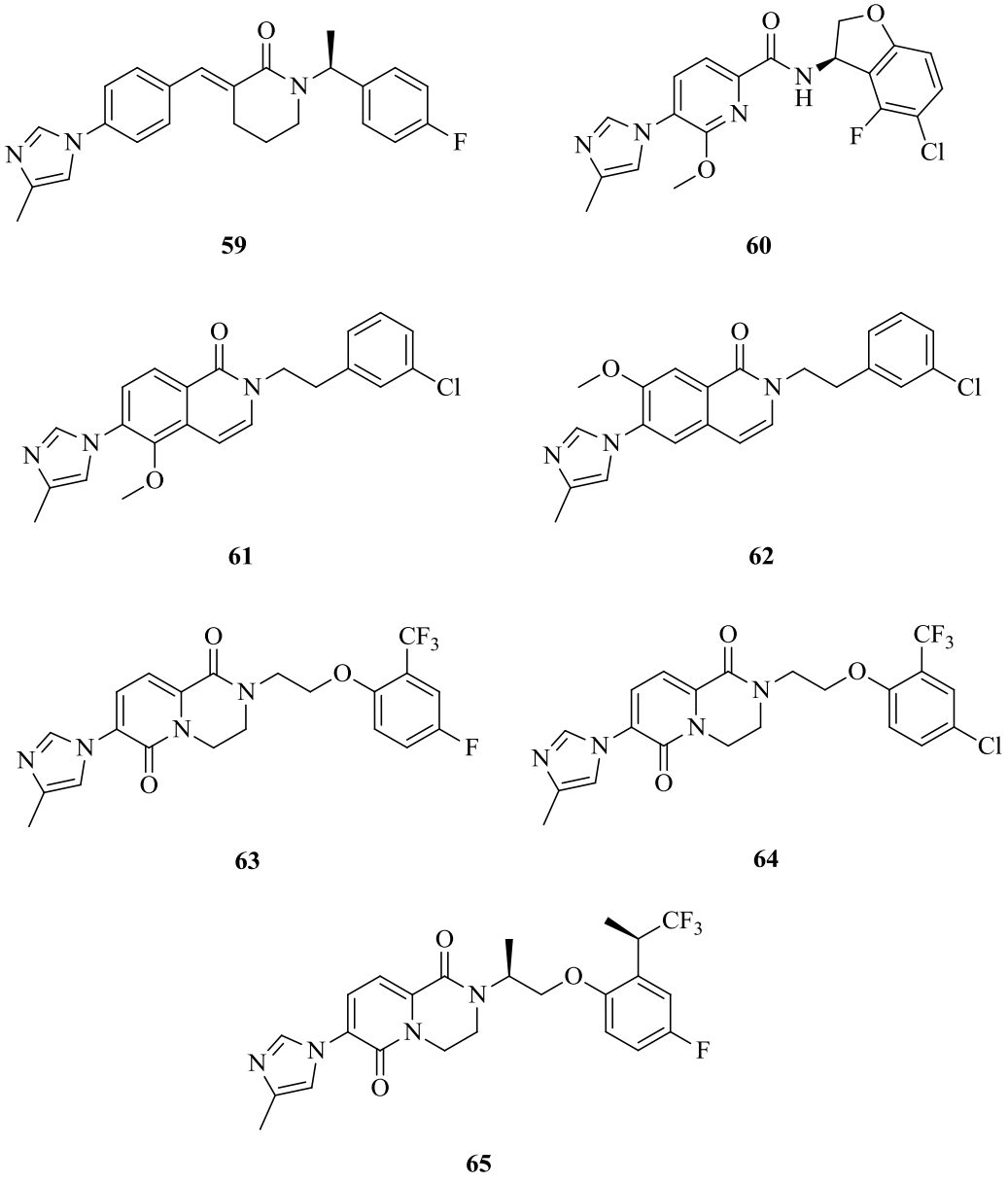

Figure 1.21. Optimised pyridone analogues

There has been an enormous effort by scientists to identify potent secretase inhibitors that do not possess adverse side effects. Various pharmacophores have been identified with varying degrees of success. Several compounds have advanced into clinical trials, but no sign of a successful drug has emerged yet. However, there is still ongoing activity in the development of safe and potent secretase inhibitors.

The next section of this chapter will discuss the hypothesis of metal dyshomeostasis and oxidative stress. This section will also discuss the development of metal chelators and antioxidants to address AD.

1.6. Metal dyshomeostasis and oxidative stress

The lack of clinical success of antiamyloid drugs has led to the modification of the amyloid cascade hypothesis or to the development of a new hypothesis.[32, 118, 119] Approximately 20 – 40% of cognitively normal elderly people have enough Aβ plaque deposit to cause AD based on the autopsy studies that have been carried out. This finding suggests that the presence of Aβ plaque deposit alone, even in large quantities, is not sufficient to produce AD-related abnormalities.[120] Furthermore, the toxic mode of Aβ has not been found to be a direct cause of AD.[121] Early research has indicated that transition metals are abnormally distributed in AD and that elevated levels of zinc, iron and copper are found in senile plaques.[122, 123] It has been confirmed that metal ions bind to Aβ and influence Aβ toxicity through multiple mechanisms that include Aβ aggregation accelerator, Fenton-like reactions and the generation of reactive oxygen species (ROS). Aβ could then damage biomolecules or overwhelm antioxidant mechanisms leading to increased oxidative stress and inflammation.[124] In the diseased state of the organism, the natural antioxidant defence mechanisms may malfunction, leading to ROS accumulation and oxidative stress.[125]

The loss of mitochondrial function that is prevalent in the early events of AD, associated with the accumulation of ROS, plays an important role in synaptic dysfunction.[126, 127] There is evidence that suggests that the oxidation of mitochondrial DNA renders it more susceptible to somatic mutation.[128] These mutations may lead to the formation of pathological Aβ.[129]

It has also been suggested that in AD, metal ions are likely mislocalised from the intracellular to extracellular environment around the synapses and that the free metal ions bind to the Aβ fibrils due to its affinity for copper and zinc.[130] The above findings and later observations[131-134] formed the basis of the metal dyshomeostasis hypothesis, which showed that AD correlated with the dyshomeostasis of metal ions.

Metals such as copper, iron and zinc have defined physiological functions in living organisms that maintain normal cellular processes.[135] Many key enzymes such as ceruloplasmin, dopamine β-hydroxylase and carbonic anhydrase rely on metals for their catalytic activity.[136-138] Metals

also play key roles in gene expression, single electron transfer, regulation of synaptic functions and many more important functions.[139-141]

Transition metals, though crucial to many biochemical neuronal processes are abnormally regulated in AD.[142, 143] The levels of Aβ are controlled by metal ions at both the APP and Aβ processing levels.[24, 144] Dysfunctional levels of metal ions in the brain have been shown to promote the precipitation of Aβ and the induction of Aβ aggregation in senile plaques.[145] Furthermore, iron levels are much higher in AD neuropils with respect to healthy neuropils (the region between neurons where synaptic connections form) and iron is abnormally concentrated in amyloid plaques.[24] Deregulated levels of copper have been shown to interfere with the processing of APP and reduce the clearance rate of Aβ, which leads to the precipitation of Aβ plaques.[146]

Aβ has also been determined to be redox active, and since metal ions such as Cu^{2+} and Fe^{3+} are enriched in AD neuropil and plaque deposits, they undergo reduction to Cu^{+} and Fe^{2+} respectively. Hydrogen peroxide, a freely permeable molecule, is then produced through the subsequent reduction of molecular oxygen as Cu^{2+} and Fe^{3+} reform.[147] It has been suggested that Aβ deposition could act as a sink for trapping potentially harmful transitional metal ions that would otherwise catalyse the oxidation of biomolecules. The formation of amyloid plaques could thus be considered as a compensatory mechanism to reduce oxidative stress.[148] Copper and zinc have been found to play key roles in regulating synaptic function by modulating receptors of the glutamatergic system. Copper and zinc released into the synapse are weakly coordinated and readily exchangeable. Aβ has also been reported to interact with receptors of the glutamatergic system, in a manner which interrupts processes regulating cognition and memory. Therefore, the synaptic space is an ideal location for metal-Aβ interactions that may lead to neuron apoptosis.[123, 149, 150]

The role of calcium dyshomeostasis in AD has been determined via mutants in presenilin genes[151] and increased intraneuronal [Ca^{2+}] is correlated with Aβ-plaque formation, APP mutations and tau hyperphosphorylation.[152] Impaired calcium homeostasis reduces synaptic plasticity and memory deficits in AD and may also contribute to the synaptic loss and reduction of dendritic spine density in pyramidal neurons.[153, 154] Furthermore, caspases that mediate cell apoptosis directly depend on calcium homeostasis and are found to be activated in aging people.[155, 156] In patients with AD, an enhanced capacity for the transport of calcium from the

endoplasmic reticulum (ER) to the mitochondria is observed. This may lead to mitochondrial calcium overload and a collapse of the mitochondrial membrane potential. This results in the potential collapse of the proton gradient, which in turn suppresses ATP synthesis and triggers apoptosis.[154]

Finally, it has also been suggested that the sequestration of zinc by Aβ deposits leads to reduced intra-neuronal zinc levels, or in some cases, excess zinc in neighbouring neurons. The abnormal levels of zinc destabilise microtubules, leading to neurofibrillary tangles (NFT) and cognitive impairment.[157]

1.6.1 Metal homeostatic therapy

The brain requires metal ions for a number of cellular processes. For that reason, the brain contains a high concentration of several transition metals such as iron, copper and zinc. These transition metals are involved in the neuronal activity within the synapses and also in various metalloproteins. Therefore, cells have developed a sophisticated mechanism for controlling metal-ion homeostasis. In the case of a breakdown of these mechanisms, or absorption of metals with no known biological function, the ionic balance is altered and can result in a disease state such as AD.[158]

Although metal dyshomeostasis is not the only cause of AD, therapeutic interventions aimed at restoring metal homeostasis is a viable strategy for the treatment of AD. The development of metal chelators as sequestering agents for metal overload is well known.[134, 159] The chelator drug must have certain properties such as low molecular weight, able to cross the BBB, stable, low toxicity and target a specific metal.[158] Furthermore, the chelator drug should be able to coordinate a metal ion with two or more points of attachment. This chelation effect provides the necessary stability to the corresponding metal complexes. For the metal chelate complex to remove metal ions in overload situations, the complex should thus have a high thermodynamic stability and also not depend on dilution effects.[159]

1.6.1.1 Metal overload chelation therapy

Desferrioxamine **66** (Fig. 1.22) was one of the first compounds used to treat iron and aluminium overload in AD patients. A clinical trial of two year intramuscular injections showed that

desferrioxamine slowed down the clinical progression of AD. Unfortunately, many patients suffered side effects such as anemia and weight loss.[160]

Several other chelating agents have been investigated for their ability to sequester copper and zinc. For example, the *in vitro* treatment of extracted Aβ deposits in a phosphate-buffered saline medium with three different chelating agents, bathocuproine **67**, EGTA **68** and TPEN **69** (Fig. 1.22) at concentrations from 4 μM, found that they were able to redissolve Aβ deposits.[161]

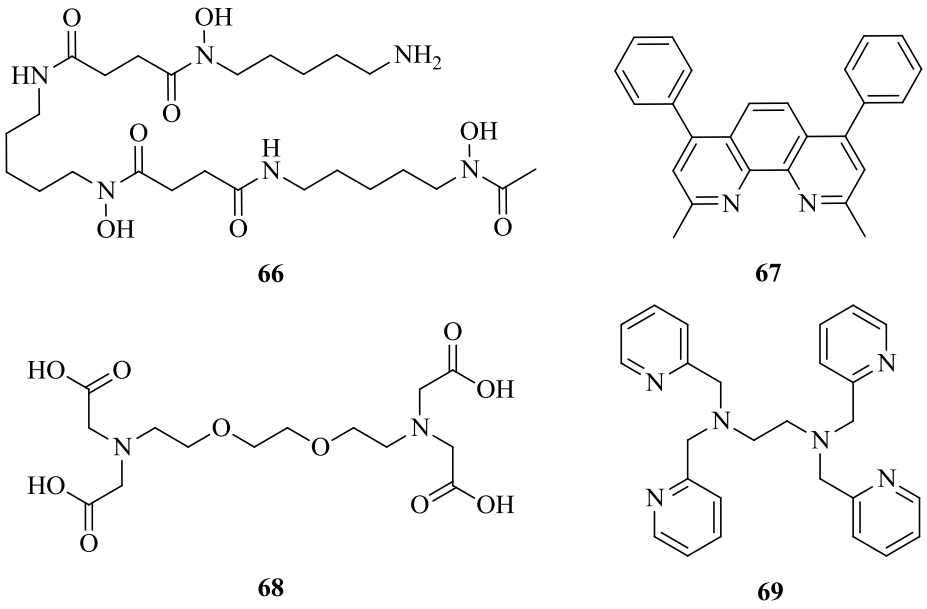

Figure 1.22. Early metal chelators used to treat metal overload

1.6.1.2 Rare metal complex chelators

The three His residues near the N-terminus of the Aβ sequence (His-6, His-13 and His-14) form a high affinity metal binding site for copper, zinc and iron. These metal interactions affect peptide aggregation and toxicity.[162] Therefore a different strategy was examined with rare metal complexes as metal chelators. Pt(II) complexes have been determined to be stable and redox inert when present in biological systems. The association of slow kinetics with substitution reactions at the Pt(II) centre makes it difficult to displace the Pt(II) metal when bound to a target.[163] Targeting the imidazole side chains of the His residues of Aβ with Pt(II) complexes was suggested.[163] Three platinum phenanthroline derivatives, Pt(1,10-phenanthroline)Cl_2 **70**, Pt(4,7-diphenyl-1,10-phenanthroline)Cl_2 **71** and Pt(4,7-diphenyl-1,10-phenanthroline disulfonate)Cl_2 **72** (Fig. 1.23) were evaluated for their ability to inhibit the metal-dependent

biochemical and cellular actions of Aβ. The binding of the platinum complexes with $A\beta_{1-42}$ were confirmed with SELDI-TOF mass spectrometry and NMR spectroscopic experiments showed strong interactions between the platinum complexes and the imidazole side chains of the His-6, -13 and -14 residues. With the confirmation that the platinum complexes bind to Aβ peptides, primary mouse cortical neuronal cell cultures were treated with 10 μM $A\beta_{1-42}$ for four days and resulted in a 35% cell viability reduction. Treatment of the affected cultures with the platinum complexes **70**, **71** and **72** at a concentration of 5 μM restored neuronal viability with 20 to 35% improvement.[163] These data suggest that the interaction between the platinum complex and Aβ, mediated by the His residues, blocks copper, zinc and iron binding to Aβ and consequently prevents metal-mediated phenomena such as ROS. It was suggested that the coordination of the Pt(II) complexes to Aβ inhibited the aggregation of the peptide and leads to precipitation of amorphous aggregates rather than toxic amyloid fibrils.[162]

In 2010, ruthenium complexes were proposed as a better alternative to platinum complexes for selective inhibition of Aβ-histidines. Ruthenium has a stronger tendency to coordinate with imidazole nitrogen atoms and ruthenium compounds are typically accompanied by a more favourable toxicity profile compared to platinum compounds.[164] In this research, spectroscopic analysis of *fac*-$[Ru(CO)_3Cl_2(N_1\text{-thz})]$ **73** (Fig. 1.23) showed strong binding of the ruthenium complex, $\{Ru(CO)_3\}^{2+}$, to the His residues of the $A\beta_{1-28}$ model, after the release of chloride and thiazole ligands. However, no *in vitro* results were published regarding Aβ inhibition.[164]

Murphy and co-workers have suggested that ruthenium complexes of the 2,3-*bis*(2-pyridyl)benzoquinoxaline bridging ligand interact with DNA via intercalation of the ligand.[165] Studies have also shown that DNA binding capabilities of the Pt(II) complexes could be increased by incorporating another metal moiety through bridging ligands.[166-168] These observations resulted in the idea of developing a complex with a bridging ligand that interact with Aβ.[166] Rangachari and co-workers[166] have thus developed a heterobimetallic complex, containing Pt(II) and Ru(II) metal centres, that is based on Pt(II) complex **72**. The introduction of a Ru(II) metal centre with a hydrophobic bipyridyl (bpy) ligand to Pt(II) complex **72** led to the development of the binuclear complex $[Ru(bpy)_2(dpp)_2PtCl_2]_2$ **74** (Fig. 1.23). The hydrophobic surface of the bipyridyl ligands may enhance the ability of the complex to interact with similar surfaces present in Aβ peptide. Furthermore, two molecules of complex **74** were determined to bind to $A\beta_{1-42}$, suggesting the presence of more than one binding site. Therefore, it was

concluded that **74** may alter the random coil conformation of $A\beta_{1-42}$ to a more compactly folded form and thereby inhibit the formation of amyloid fibrils.[166]

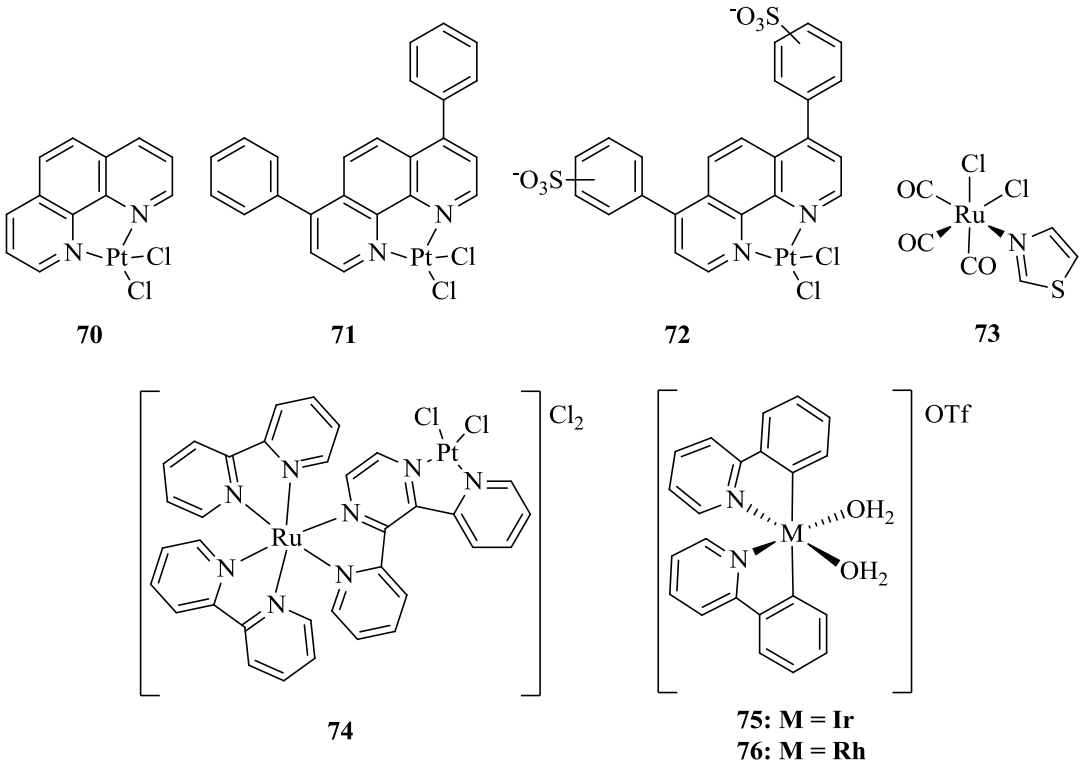

Figure 1.23. Metal complexes as chelators to inhibit amyloid fibrillation

Metal complexes containing Group 9 metals such as iridium and ruthenium have also been shown to bind to histidine-rich proteins, and have been applied to luminescent protein staining.[169] Two Group 9 metal-based inhibitors were thus developed to target the His-residues of $A\beta_{1-40}$. Iridium **75** and rhodium **76** complexes (Fig. 1.23) possess labile co-ligands (H_2O), which can be displaced by the imidazole *N*-donor moiety of the His-residues of $A\beta_{1-40}$. Both complexes were able to inhibit $A\beta_{1-40}$ at 5 μM and prevent misfolding of the Aβ peptide. Rhodium complex **76** was determined to be the most active with an IC_{50} of 25 – 50 μM on the neuroblastoma cell line (SH-SY5Y). Both complexes demonstrated significant enhancement in emission intensity in the presence of $A\beta_{1-40}$ peptide. It was suggested that the coordinative bond formation between the group 9 metal centre and the His-residues of the $A\beta_{1-40}$ peptide produced this phenomena.[170]

Unfortunately, most of the Pt(II) complexes tend to have poor bioavailability and BBB penetration that make the likelihood of their clinical development questionable.[171, 172] The orally bio-available Pt(IV) complex cancer drug, satraplatin[173] **77** (Fig. 1.24), has inspired the development of Pt(IV) complexes for Aβ inhibition. Pt(IV) complexes undergo slow substitution in a biological system, are stable in the acidic environment of the stomach and are able to cross the gut membranes intact. The prodrug, [Pt(IV)(*N*,*N*-dimethyl-2-[2-(quinolin-8-yl)-1*H*-benzimidazol-1-yl]ethanamine)Cl_4] **78** (Fig. 1.24), was found to be reduced *in vivo* by natural reductants such as glutathione, to the active Pt(II) complex. Treatment of Tg2576 mice with the Pt(IV) complex **78** for 18 weeks at a dose of 15 mg/kg/day by oral gavage reduced Aβ plaque by 29%. Also, high levels of Pt were found in the blood plasma (1.7 ± 0.8 μmol) and in the brain tissue (0.006 ± 0.002 μg/g of body weight). These data suggested a high bioavailability for the Pt(IV) prodrug **78**.[172]

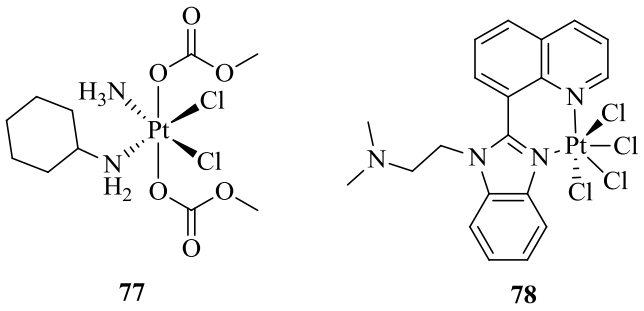

Figure 1.24. Pt(IV) complexes with improved bioavailability

1.6.1.3 8-Hydroxyquinoline-based chelators

Clioquinol (CQ) **79** (Fig. 1.25) was used in the 1960s as an oral anti-parasitic agent for the treatment and prevention of intestinal amebiasis, but was later withdrawn from the market due to reports of neurotoxicity. However, CQ **79** has re-emerged as a potential therapy for AD.[174] The hydrophobic CQ **79** selectively binds to zinc and copper with greater affinity when compared to calcium and magnesium [K_1(Zn) = 7.0; K_1(Cu) = 8.9; K_1(Ca) = 4.9; K_1(Mg) = 5.0] and can cross the BBB freely. Tg2576 mice that were treated with CQ **79** at 20 mg/kg by gavage for 12 weeks showed a 65% decrease in sedimental Aβ. At a higher dose of 30 mg/kg/day for 9 weeks, the older 21-month-old mice experienced a 41% decrease in levels of Aβ in the brain pellet.[175, 176] In a small Phase II clinical trial, oral administrations of CQ, in moderately severe AD patients, for

36 weeks slowed the rate of cognitive decline and reduced plasma $A\beta_{1-42}$ levels when compared to the placebo controls.[121] CQ **79** has a nanomolar affinity for Cu^{2+} and Zn^{2+}, which facilitates the dissociation of these metal ions from the low affinity metal binding sites of Aβ.[121] These results are promising and suggest a possible unique approach for the treatment of Aβ plaques.

Prana Biotechnology Ltd. developed PBT2 **80** (Fig. 1.25), a second generation 8-hydroxyquinoline (8HQ) derivative of CQ **79**, with a greater BBB penetration and Aβ plaque reduction. Transgenic AD mice that was treated with PBT2 **80**, showed improved performance.[121] Unfortunately, a Phase II clinical trial failed to show significant improvement in cognitive functions.[177]

It should be noted that the 8HQ scaffold has inspired scientists to make further modifications, all with the aim of making more bioactive compounds. Most of the modifications have been done around the phenolic ring.[159]

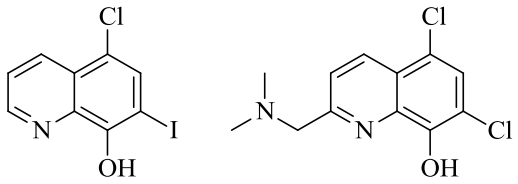

79 **80**

Figure 1.25. The first 8HQ metal chelators

Recently, Schiff-base derivatives have been reported as antioxidants and modulators of copper-mediated Aβ peptide aggregation. Hydrazinecarbothioamide **81** and hydrazinecarboxamide **82** (Fig. 1.26) were found to form stable complexes of 1:1 and 1:2 metal-to-ligand ratios with copper under physiological conditions. In the Trolox Equivalent Antioxidant Capacity (TEAC) test, both compounds demonstrated roughly a 3-fold improvement in quenching the 2,2′-azinobis(3-ethylbenzothiazoline-6-sulfonic acid) radical cation ($ABTS^{\bullet+}$) when compared to CQ **79**. It was suggested that the potent antioxidant properties observed for the Schiff bases are due to the negative inductive effect of the Cl and I ring substituents in CQ **79**, which decrease the stability of the hydroxyl radical. Furthermore, the extended conjugation in the Schiff bases increases the stability of the hydroxyl radical. In the turbidity assay, both compounds induced a significant decrease in aggregation of $A\beta_{1-40}$ in the presence of Cu(II),

thereby indicating that these Schiff bases could limit oligomer formation by sequestering Cu(II).[178]

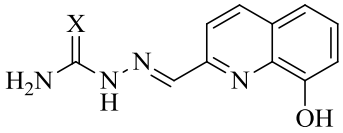

81: X = S
82: X = O

Figure 1.26. Schiff bases as metal chelators

Cyclodextrins (CycD) are a family of sugars well known for their ability to alleviate undesirable properties of drug molecules by forming inclusion complexes. Furthermore CycD can bind to the surface membrane of the cells, which may improve drug absorption across biological barriers.[179] CycD also has the ability to quench hydroxyl radicals, which suggests that it has antioxidant properties.[180] The coupling of the CycD moiety with the 8HQ scaffold was explored to improve the aqueous solubility, antioxidant activity and pharmacokinetic properties of the hybrid compounds. Three CycD conjugates, **83 - 85** (Fig. 1.27), were reported to exhibit strong ability to scavenge the free radical $ABTS^{\bullet+}$ in the TEAC experiment. The activities were also found to be higher than the known antioxidant, Trolox. Furthermore, all three CycD compounds possessed the ability to quench the radical in presence of Cu(II). On five different cell lines, the CycD compounds demonstrated IC_{50} values of greater than 100 μM, even in the presence or absence of Cu(II). This indicates that high concentrations could be used without the anticipated toxicity on healthy tissues.[181]

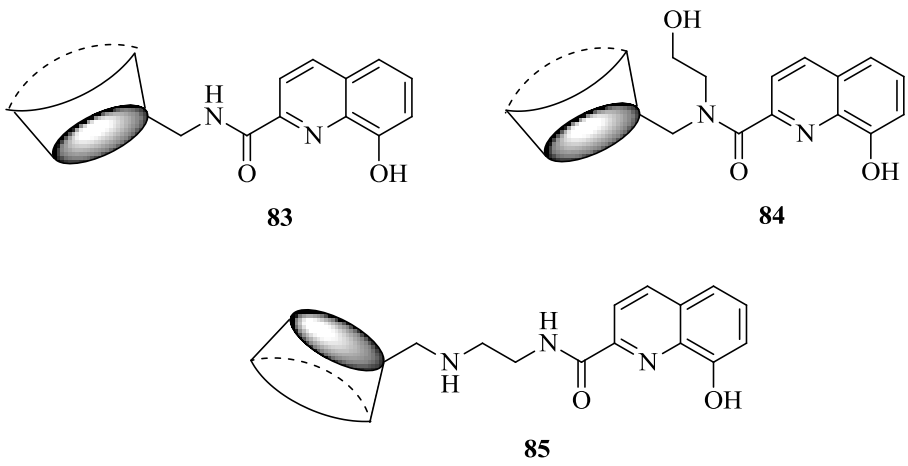

Figure 1.27. Cyclodextrin-8HQ conjugates as metal chelators

Conjugation of sugar moieties such as trehalose with 8HQ showed similar results as observed with the CycD conjugates.[182] Trehalose is known to protect proteins and cells against environmental stresses and oxidative damage. In addition, trehalose has been reported to disrupt amyloid fibril formation and reduce cytotoxicity, thereby increasing cell viability in presence of Aβ aggregates.[182] In the TEAC studies, trehalose-8HQ conjugates **86** and **87** (Fig. 1.28) showed significant ability to quench the ABTS•$^{+}$ radical in the presence of Cu(II) and Zn(II). Both compounds were more active than CQ and Trolox. The free radical scavenging ability of the trehalose compounds could be attributed to the high reactivities of the hydroxyl substituents. In the turbidimetric measurement studies of $A\beta_{1\text{-}40}$ with Cu(II), trehalose **86** and **87** were able to inhibit Aβ aggregation [Abs (405 nm): <0.025]. The disaccharide moiety alone failed to inhibit Aβ aggregation, suggesting that it plays no role in metal chelation. In addition, with Zn(II), both trehalose compounds significantly inhibited $A\beta_{1\text{-}40}$ aggregation [Abs (405 nm): <0.015]. These results suggest that glycoconjugation is a valid option to allow the quinoline moiety to exert its metal-binding capability in aqueous solution.[182]

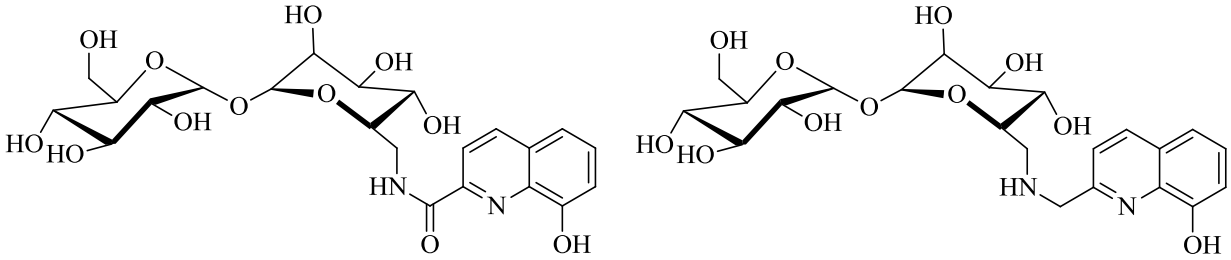

86 **87**

Figure 1.28. Trehalose-8HQ conjugates as metal chelators

It has been determined that an increase in oxidative stress is correlated with a decrease in levels of the antioxidant glutathione (GSH), which suggests that the presence of GSH offers neurological protection. In fact, the addition of GSH precursor to Aβ protein reduced oxidation in neuronal cells. The presence of Aβ has also been shown to lead to GSH depletion in various *in vitro* cell models. These findings suggest that glutathione plays a critical role in AD pathogenesis.[183]

Therefore, the use of a GSH-based substrate with the 8HQ scaffold is potentially a viable option in developing an antioxidant chelator with neuroprotective activity. GSH can also be used as a BBB shuttle for the delivery of the metal chelator drug. In this respect, GSH-8HQ **88** (Fig. 1.29) has a very high water solubility (12 g/mL) and is stable in acid (pH <5). Based on the hydrolysis studies in 80% human plasma, compound **88** may also be stable enough to arrive at the BBB intact. Lastly, compound **88** was found to have the potential to remove both Cu(II) and Zn(II) from the Aβ-peptide without causing any copper or zinc depletion *in vivo*.[184]

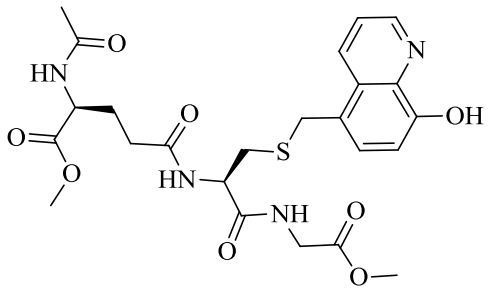

88

Figure 1.29. Glutathione-8HQ conjugate as metal chelators

1.6.2 Natural metal chelators and antioxidants

A wide variety of natural compounds are known to have antioxidant and metal-chelating properties. Many of such compounds can be found in nature or can be obtained as part of a diet.[185]

Gingko biloba has been the subject of much attention for its medicinal and antioxidant properties. Its clinical effects in dementia have been studied and it has been suggested that the extract offers neuroprotection.[186-188] It should be noted that mixed results have been reported about the use of Gingko biloba as treatment for AD. A Cochrane review[189] claimed this extract offered improvement in cognition and activities of daily living, but no significant differences between Gingko biloba and placebo were determined in short clinical trials.[190]

The consumption of curry is associated with improved cognitive function and a lower prevalence of AD in some populations, putatively due to the curcumin **3** (Fig 1.2) found in curry. It has also been suggested that **3** has antioxidant properties. The enol structure with the intramolecular hydrogen bond is suggested to be involved with the free radical scavenging activity. Furthermore, **3** has been observed *in vitro* and *in vivo* to have the ability to complex with metal ions via the diketone and pairs of phenol and methoxy groups.[191, 192]

Epidemiological studies have shown that moderate consumption of alcohol is associated with lowered risk of AD.[185] Red wine contains antioxidants such as resveratrol **89** (Fig. 1.30), a flavonoid, that scavenges ROS and up-regulates cellular antioxidants including GSH. In rat studies, **89** was observed to protect astrocytes in hippocampal slices from H_2O_2-induced oxidative stress by increasing GSH levels. Piceatannol **90** (Fig. 1.30), a metabolite of **89**, occurs in many resveratrol-containing solutions, but at lower concentrations. It is a more efficient scavenger of ROS than **89** due to the additional phenol group and has also been considered for application as treatment in neurodegenerative diseases.[185, 191]

Green tea leaves contain polyphenolic compounds, with catechins as the major constituents. Catechins are well known for their antioxidant, ROS scavenger and metal ion-chelating abilities.[191] Epigallocatechin gallate (EGCG) **91** (Fig. 1.30) is the main catechin of green tea and contains several sites for the bidentate coordination of metal ions via the phenol groups. EGCG is BBB-penetrable and binds effectively to Fe(II), Cu(II) and Zn(II).[24]

Melatonin **92** (Fig. 1.30), a natural hormone, is a BBB-penetrable compound involved in maintaining the circadian rhythm and memory formation in the hippocampus. Lower levels of

melatonin are found in older people, which results in numerous biological changes that includes the generation of ROS.[193, 194] Transgenic mice that were treated with melatonin for ~5 months were protected from cognitive impairment. Furthermore, significant reduction of brain Aβ deposit and elevated levels of soluble Aβ in blood were observed.[195]

Ginsenoside Rg1 **93** (Fig. 1.30), a natural product extracted from *Panax ginseng*, has been reported to exert neuroprotective activities. Rg1 **93** reduced the cytotoxicity induced by 400 μM of H_2O_2 in PC12 cells at a concentration of 0.1 – 10 μM. It was suggested that **93** could protect the cells from oxidative stress, but further research on this topic is needed.[196] In a different study on PC12 cells that were treated with $A\beta_{25\text{-}35}$ for 48h, **93** reduced the ROS production by 17% and 28% at a concentration of 0.1 μM and 10 μM respectively. This study also showed that **93** prevented the increased concentration of Ca(II) in PC12 cells that were treated with 50 μM of $A\beta_{25\text{-}35}$.[197]

Sesame glucosides (SG), found in sesame seeds, have also been shown to inhibit endogenous lipid peroxidation, as well as oxidative DNA damage in rat liver and kidney cells.[198] *In vitro* experiments have also showed that SG exhibited the ability to scavenge peroxyradicals.[198] Mice that were fed on a diet of 0.5% weight SG showed a complete blockage of oxidative DNA damage in $A\beta_{25\text{-}35}$ induced brain tissue.[199] Lastly, the generated ROS of 50 μM $A\beta_{25\text{-}35}$-induced PC12 cells was completely reduced with 50 μg/mL of SG. These data suggests that SG could have a protective effect on Aβ-induced neuronal cell death via its antioxidant properties.[198]

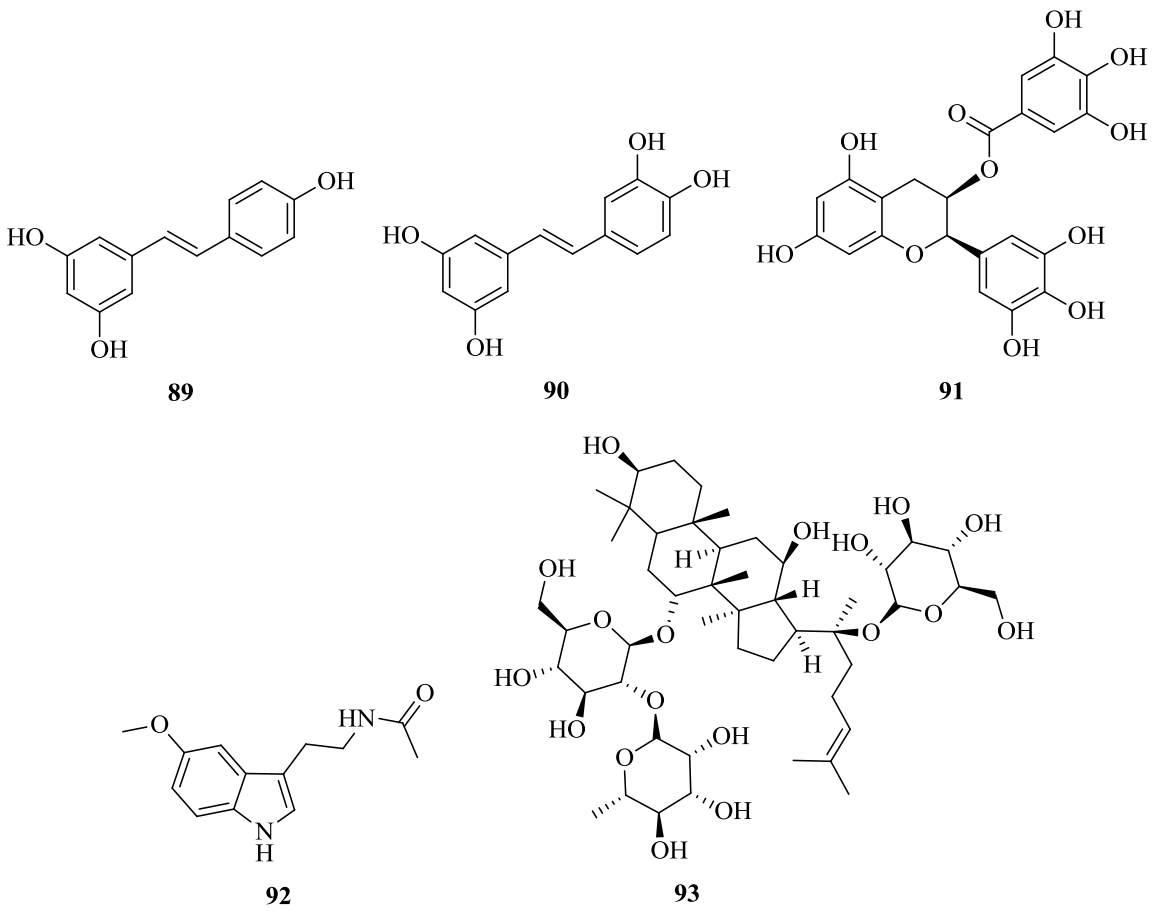

Figure 1.30. Natural metal chelators and antioxidants

Disturbances in the distribution of metals are central to the aggregation pathology of Aβ associated with AD. In addition, elevated levels of metals at the sites of Aβ oligomer formation could promote the generation of hydrogen peroxide that leads to oxidative stress. Several compounds have been identified that could reduce the Aβ pathology, improve memory and cognition. Clinical trials have shown some positive results, however, further research is required to determine whether the reduction of metal levels could provide relief against AD.

The next section of this chapter describes the hypothesis of how the formation of neurofibrillary tangles (NFT) could promote AD. Different strategies have been developed to counteract the formation of NFT and will be discussed next in more detail.

1.7. Tauopathy

(For the purposes of this dissertation – the focus of the design and synthesis of molecules described herein, falls under this category)

Two types of aggregates are found in AD: extracellular amyloid plaques that were discussed earlier and intracellular NFT.[200] The microtubule-associated protein tau was identified as the main component of NFT that accumulates inside neurons and their processes in AD brains.[201, 202] In AD patients, the protein tau is abnormally hyperphosphorylated and in this modified state, forms the NFT.[203] NFTs are aggregations of paired helical filaments, which are made up of abnormally phosphorylated tau.[204] Studies have shown that normal tau contains approximately two moles of phosphate per mole of the protein but in the AD-affected brain, tau is hyperphosphorylated roughly three times more.[205]

Partially phosphorylated tau protein plays a role in maintaining neuronal integrity and stabilisation of microtubules to ensure their function as tracks for axonal transport and as cytoskeletal elements.[206-208] In the case of hyperphosphorylated tau, the protein destabilises the microtubules and consequently interferes with tubulin binding.[207] The density and length of the microtubules in AD neurons are greatly reduced and declines with aging in normal individuals.[209] Only a small part of tau is involved in the abnormal aggregation process. One or two “hexapeptide motifs", which consists of approximately 31 imperfectly repeated amino acids, may be absent owing to alternative splicing.[29] It should be noted that the complete loss of tau function does not lead to cytoskeletal collapse in transgenic mice but, a decrease in cytoskeletal function.[210]

The phosphorylation of a protein is one of the main activities of protein kinases and phosphatases acting on it. Hyperphosphorylated tau can be dephosphorylated by phosphatases, but in AD brains the activities of phosphatases are reduced. Therefore, the decline of activity in phosphatases could be one of the causes of abnormal tau phosphorylation in AD.[211]

However, the removal of tau in mice does not induce neurological deficits or cell death, but instead, makes the tau knockout more resistant to seizures, suggesting that the neuronal dysfunction is not due solely to a loss of tau function. Even though the mechanism by which neuronal cell death is caused by tau aggregates is unknown, there is a large body of evidence showing that aggregated tau acquires a toxic function in which tau oligomers are the

culprit.[212, 213] Mutations of tau can influence tau either at the mRNA level, changing the alternative splicing of tau, or at the protein level, by changing the binding characteristics of tau with microtubules.[214]

There are two major approaches that can be employed for the inhibition of tau aggregation. The first approach is the search for inhibitors of kinases that phosphorylate tau, based on the assumption that abnormally phosphorylated tau aggregates more readily.[215, 216] The second approach is the development of inhibitors that disrupt the tau aggregation process.[29]

1.7.1 Glycogen synthase kinase (GSK-3)

Glycogen synthase kinase-3 (GSK-3) was first discovered approximately three decades ago as a glycogen synthase responsible for phosphorylating activity in rabbit skeletal muscle.[217] GSK-3 is the last enzyme in the glycogen biosynthesis pathway that phosphorylates and inactivates glycogen synthase.[218] Nowadays, GSK-3 is known to be involved in other biological functions such as cell division, stem cell renewal, insulin action and transcription. Furthermore, GSK-3 is believed to play a role in many diseases and disorders such as cancer, AD, diabetes, immune disorders, metabolic disorders, bipolar disorder, mood disorders, Parkinson's disease and heart disease.[219, 220] There are two GSK-3 genes, GSK-3α and GSK-3β, which account for all GSK-3 activity in mammals. Both kinases have distinct roles, but are highly conserved and share 98% identity within their catalytic domains.[220] GSK-3 is active under resting conditions and is rapidly inhibited by diverse stimuli and signalling pathways.[219, 220] Many of its cellular targets are held in an inactive state through inhibitory phosphorylation.[220]

Over activity of GSK-3 results in hyperphosphorylation of substrates that give rise to many diseases as mentioned earlier. Studies have shown that signal transduction plays a critical role in controlling the activity of GSK-3. Wingless-type MMTV integration site family member (Wnt) and insulin signalling are related to GSK-3 and increases its activity, which results in substrate hyperphosphorylation.[221] Since the insulin signalling levels are decreased in AD brain, AD was suggested to be regarded as diabetes type III.[222] This may be the reason behind the hyperphosphorylation of tau, one of the GSK-3 substrates, which eventually lead to the formation of NFT.[221] In addition, increased GSK-3 activity may induce increased Aβ formation through its action on GS and thereby give rise to the senile plaque formation in AD.[223] Furthermore, studies have shown that GSK-3β interacts with presenilin, a critical molecule for

GS activity. Therefore, the inhibition of GSK-3β may alter the γ-cleavage of APP and subsequently inhibit the hyperphosphorylation of tau.[224] Several studies have demonstrated that the inhibition of GSK-3 leads to decreased Aβ production and a reduction in tau hyperphosphorylation.[225]

1.7.1.1 Designing GSK-3β inhibitors

GSK-3β is highly enriched in the brain and several publications have reported that GSK-3β is responsible for the hyperphosphorylation of tau.[226-228] Under normal conditions, GSK-3β is negatively regulated, but in the diseased state, GSK-3β is activated by the elimination of inactivation signals, leading to neurodegeneration. Based on this assumption, the development of a GSK-3β inhibitor as a therapeutic drug against AD is an attractive option.[229]

The homology of the ATP-binding pocket in GSK-3α and GSK-3β presents a challenge for the development of isoform selective inhibitors.[207, 230] In addition, the GSK-3 also has a co-factor Mg^{2+} binding site.[231, 232] Inhibitors have to be designed in such a way that it interacts with Lys85, Glu97 and Asp200, the amino acids that are required for ATP recognition. Furthermore, establishing hydrogen bonds with the backbone atoms of Asp133 and Val135 in the hinge region, greatly improves the selectivity for GSK-3β.[207, 230] The majority of the designed GSK-3β inhibitors are ATP competitive, have low molecular weight (<600 g/mol), contain heterocycles and are reasonably planar.[221] The non-ATP competitive inhibitors do not compete with the high intracellular ATP concentration and could offer distinct pharmacological advantages since complete inhibition of GSK-3β will result in adverse events.[207] It should also be noted that over 500 kinases have been identified so far and that the GSK-3β inhibitor should be selective and not affect the other kinases.[233]

1.7.1.2 Metal cation inhibitors

Lithium chloride (LiCl) was the first inhibitor discovered that selectively inhibits GSK-3. *In vitro* experiments showed that at a concentration of 1-2 mM, LiCl caused a reversible dose-dependent inhibition of GSK-3β. Intact cells that were treated with LiCl were shown to possess GSK-3β with a reduced ability to phosphorylate tau.[234, 235] One of the hypotheses was that lithium (Li^+) acts as a competitive inhibitor of GSK-3 with respect to magnesium (Mg^{2+}).[236] The other suggested that Li^+ inhibits GSK-3 under low potassium (K^+) conditions.[237] Some clinical trials

have shown that continuous treatment with lithium improved cognition and memory scores in patients with dementia.[238] However, there have been other trials involving patient treatment with lithium in which no such improvement of cognition or reduce tau phosphorylation in AD patients was reported. Finally, lithium has been found to have toxic side effects in some elderly patients. This has essentially put an end to further exploration of the use of lithium chemotherapy in AD treatment.[238]

Beryllium (Be^{2+}) has been found to be a more potent GSK-3β inhibitor than Li^{+} and competes for both Mg^{2+} and ATP. In addition, results suggested that GSK-3 has two magnesium-binding sites based on the experiments where two inhibitors (Be^{2+} and Li^{+}) were used. One binding site was found to be Li^{+} sensitive, the other Li^{+} insensitive and interacting with the Mg:ATP binding site.[239]

Zinc (Zn^{2+}) is also a more potent (IC_{50}: ~15 μM) GSK-3β inhibitor than lithium and elevates cellular β-catenin levels.[240] It is noteworthy that abnormal zinc levels are linked with major depression and mental functions. Patients that were treated with dietary supplements of zinc showed improved mood behaviour. Therefore it is tempting to speculate that the improvement in mood behaviour and cognitive functions is mediated by zinc's ability to inhibit GSK-3β. However, it is important to remember that zinc is a co-factor of many enzymes and may initiate many cellular effects independently of GSK-3.[238]

Remarkably, sodium tungstate (Na_2WO_4) has also been reported to inhibit GSK-3β in neural cells (neuroblastoma cell line SH-SY5Y) and consequently decreases tau phosphorylation. Experiments have demonstrated that tungsten inhibits the GSK-3-dependent phosphorylation sites of tau.[241] Sodium tungstate has a low toxicity profile, but only one human clinical trial (as an anti-obesity agent) has been performed to date.[242]

1.7.1.3 Purine, pyrimidine, pyrazolo and pyrazine derivatives

Purine derivatives, developed by Chiron, were one of the first synthetic molecules reported as GSK-3 inhibitors. Purine derivative **94** (Fig. 1.31) showed a 63% inhibition of GSK-3 activity at 1 μM.[243] Chiron went further to develop a series of pyrimidine analogues: CHIR98014 **95**, CHIR98023 **96** and CHIR99021 **97** (Fig. 1.31) that inhibit GSK-3 within the nanomolar range. Pyrimidine derivatives **95** and **97** exhibited 500- to 10 000 -fold selectivity for GSK-3 versus 20 other kinases tested.[244, 245] It should be noted that the majority of the studies have been tested in

diabetic models. Nevertheless, these inhibitors showed potential to reduce tau phosphorylation in cultured neurons and the rat brain.[246]

A high-throughput phenotypic cell-based screen of kinase-directed combinatorial libraries led to the discovery of a pyrrolopyrimidine, TWS119 **98** (Fig. 1.31), that can bind to GSK-3β and modulates its activity. In addition, the inhibition of GSK-3β with TWS119 **98** at 10 μM resulted in an 11-fold increase of β-catenin activation.[247]

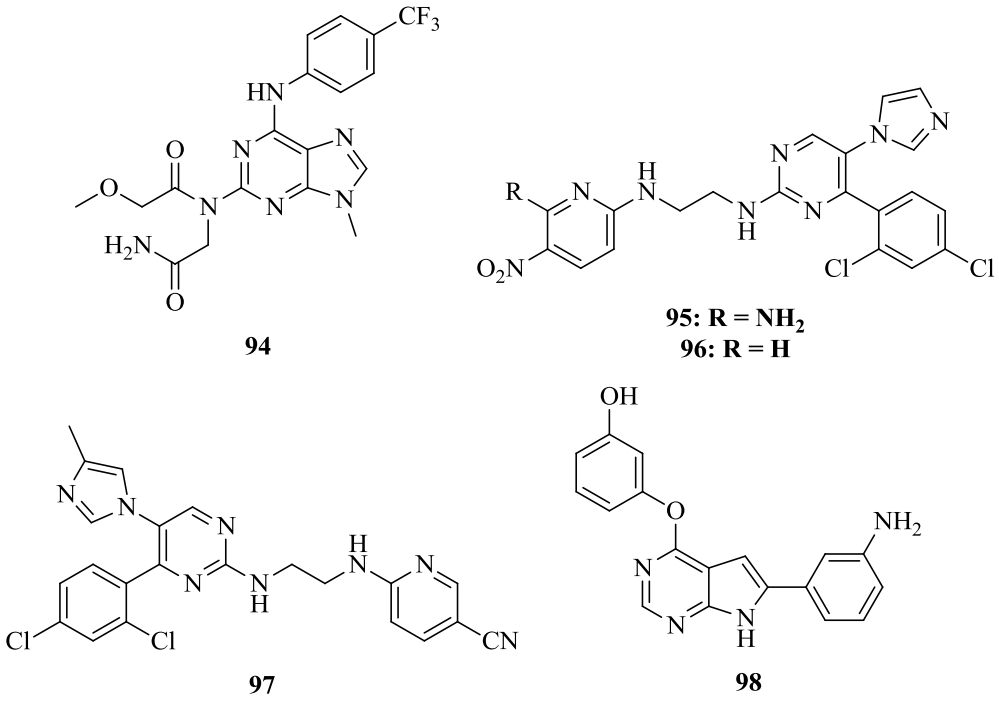

Figure 1.31. Some of the early purine and pyrimidine inhibitors

A search in the publicly available protein data bank for GSK-3β structures that interact with Lys85 resulted in the development of methoxy pyrimidine **99** (Fig. 1.32). *In vitro* studies showed that **99** possesses potent GSK-3β inhibitory activity (IC_{50} 5.9 nM). The pyrimidine N lone pair was thought to allow greater freedom for the two rings to maintain co-planarity, which is required for effective occupation of the binding site. X-ray crystallography studies also showed the favourable interaction of Lys85 with the carbonyl oxygen of the amide. Further modification to replace the methoxy group with an isopropyl derivative subsequently yielded a more potent inhibitor, **100** (IC_{50} = 0.83 nM) (Fig. 1.32).[248]

Wang and co-workers started with purinone **101** (Fig. 1.32) that had been identified from the screening of a kinase compound collection. The *in vitro* GSK-3β inhibitory activity was determined to be moderate (IC_{50} = 2.4 μM). Several modifications on the purinone core and phenyl rings failed to provide significant gains in potency. From the same screening process, a different core, nitropyrimidine **102** (Fig. 1.32) was determined to be more active (GSK-3β IC_{50} = 0.15 μM). Replacement of the phenyl group with an adamantyl group resulted in a potent inhibitor, **103** (GSK-3β IC_{50} = 3 nM) (Fig. 1.32).[249] However, studies have shown that aryl nitro moieties pose a potential risk for the *in vivo* generation of toxic metabolites.[250-253] Therefore, alternative groups were substituted for the nitro functionality, but all failed to show acceptable potency. A different strategy was then employed with the electron-poor diazonium moiety to form a 5,6-fused ring system. Azapurine **104** (Fig. 1.32) displayed poorer potency (GSK-3β IC_{50} = 628 nM) than the nitropyrimidine series even in the absence of the carboxylic acid group. A further search involving other fused pyrimidine ring systems to improve the potency of the pyrimidine series then led to the development of pyrazolopyrimidine **105** (Fig. 1.32). The fused pyrimidine ring with a halogen functionality inhibited GSK-3β with an IC_{50} of 180 nM. Lastly, a further investigation with the adamantyl moiety resulted in the development of **106** (Fig. 1.32). The replacement of the nitro group with trifluoromethyl group showed that a nitro group was not essential for potency (GSK-3β IC_{50} = 41 nM). Based on these results, it was suggested that the potency rank order correlated inversely to the electron density of the pyrimidine core.[249]

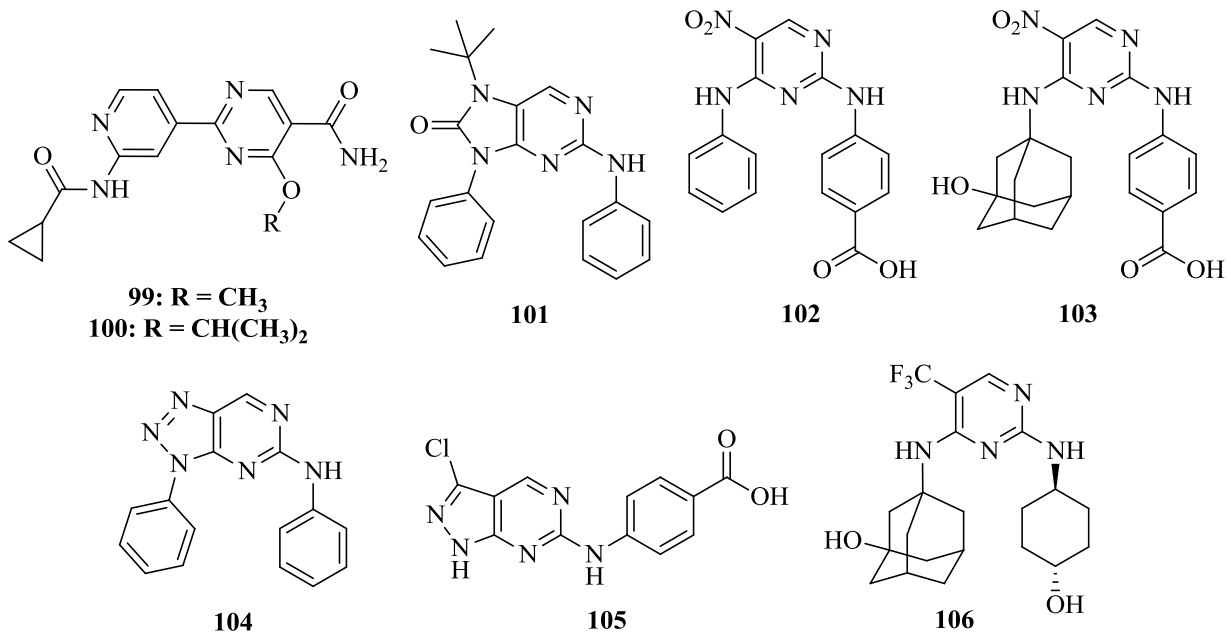

Figure 1.32. Pyrimidine-based derivatives as GSK-3β inhibitors

GlaxoSmithKline identified a novel class of pyrazolopyrimidine derivatives from HTS that inhibits GSK-3. The original screening hit, **107** (Fig. 1.33), was determined to be an ATP-competitive inhibitor for GSK-3β (IC_{50} = 100 nM). The *in silico* docking showed that the hydrazone hydrogen interacts with the carbonyl of Val135 in the hinge region and that the pyrimidine nitrogen interacts with NH of Val135. In addition, the hydrophilic phenol group is exposed to the solvent front and that the phenyl group on the pyrazole core is buried deep inside the binding pocket towards Lys85. Based on these findings, the SAR of the aromatic groups were explored. For example, the hydrophilic aromatic moieties demonstrated better potency compared to hydrophobic aromatic moieties. From the SAR studies, compound **108** (Fig. 1.33) was found to be one of the most active GSK-3β inhibitors (GSK-3β IC_{50} = 6.2 nM).[254] A second generation of GSK-3β inhibitors was then developed using compound **108** as springboard. The second generation required a co-planar arrangement between the pyrazole core and the aromatic ring. Replacing the methoxy-phenyl group with a benzimidazole group resulted in compound **109** (Fig. 1.33) that showed improved potency (GSK-3β IC_{50} = 4 nM). It was suggested that the NH of the benzimidazole could interact with Lys85. Furthermore, **109** showed better cellular permeability in a MDCK cell line (212 nM/s) compared to compound **107** (127 nM/s).[255] Further modifications of the pyrimidine scaffold led to the development of pyrrolopyrimidine **110**

(GSK-3β IC_{50} = 5 nM) and pyrazolopyrimidine **111** (GSK-3β IC = 5 nM) (Fig. 1.33). *Ab initio* calculations suggested that the *S-cis* hydrazone conformation is preferred due to an intramolecular hydrogen bond.[256]

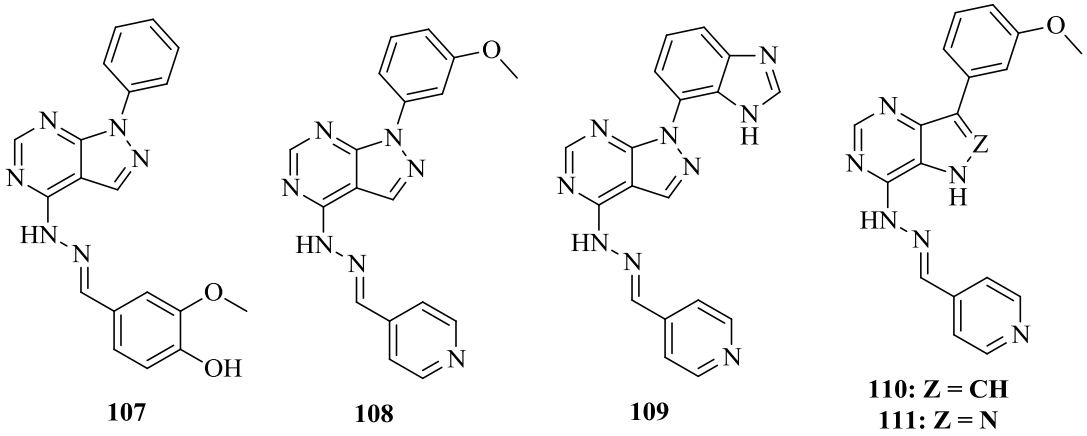

Figure 1.33. Pyrimidine derivatives developed by GlaxoSmithKline

Furopyrimidine **112** (Fig. 1.34) was identified by GlaxoSmithKline as a GSK-3β inhibitor having an IC_{50} value of 81 nM. Molecular modelling studies suggested that the aminopyrimidine core interacts with the hinge region of the ATP binding site. To improve the affinity for GSK-3β, a series of acylated furopyrimidines was developed. From this initiative, compound **113** (Fig. 1.34) was found to inhibit GSK-3β with an IC_{50} of 32 nM. Based on further molecular modelling studies, the cyclopentyl group was found to have a unique binding interaction with Pro136 in the hydrophobic pocket. In addition, the methoxyphenyl group was located close to Lys85 and exposed to the solvent system. Replacing the methoxyphenyl group with a pyridine resulted in a more potent inhibitor **114** (GSK-3β IC_{50} = 5 nM) (Fig. 1.34). Compound **114** displayed excellent selectivity against 25 kinases including CDK-2, which was inhibited with an IC_{50} of 457 nM. The high selectivity over CDK-2/Cyclin A can be prescribed to the steric clash between the cyclopentyl group and its interacting site in CDK-2. Lastly, compound **114** was examined in a glycogen accumulation assay in L6 cells and displayed excellent induction of glycogen accumulation (EC_{50} = 390 nM).[257] The furopyrimidine series was then expanded to include amide and sulfonamide moieties. Based on molecular docking studies, it was suggested that **112** could be "flipped" to fit better inside the ATP binding-pocket of GSK-3β. To achieve that, an amide side chain was attached to the 5 position of the furopyrimidine core. Amide **115**

(Fig. 1.34) showed moderate potency (GSK-3β IC_{50} = 1.6 μM) and the sulfonamide **116** (Fig. 1.34) displayed potent GSK-3β inhibitory activity (IC_{50} = 30 nM). The docking of **116** into the ATP binding site of GSK-3β showed that one nitrogen and the NH_2 of the aminopyrimidine are anchored to the carbonyl moiety and NH of Val135 via hydrogen-bonding interactions, respectively. In addition, the 3-pyridine moiety is located close to Lys85 of the conserved salt bridge (Lys85/Glu97). Sulfonamide **116** displayed good selectivity against CDK-2 and eight other kinases.[258]

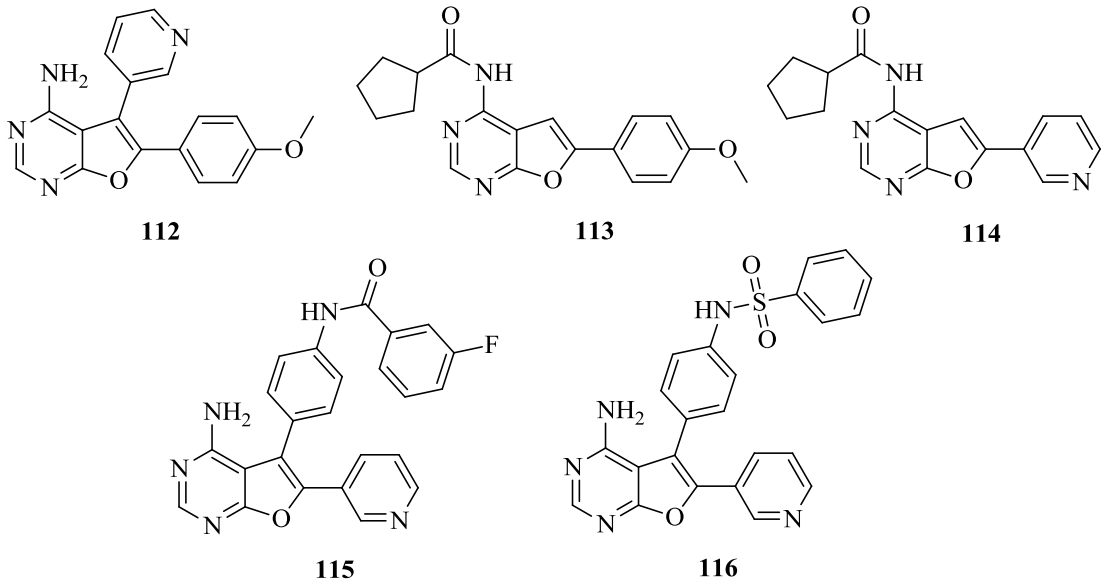

Figure 1.34. Furopyrimidine derivatives developed by GlaxoSmithKline

A library of 8-arylated purine derivatives bearing an alkyl moiety at position 6 displayed good GSK-3β inhibitory activity, with good selectivity over ten kinases. The three purine derivatives, **117**, **118** and **119** (Fig. 1.35), showed moderate potency of 26%, 49% and 43% enzyme inhibition, respectively on human GSK-3 cells. Naphthalene **120** (Fig. 1.35) was the most active of the set (91% enzyme inhibition) and had an IC_{50} of 169 nM against GSK-3β in the presence of 10 μM ATP. Molecular modelling showed that inside the GSK-3β ATP binding pocket, the naphthyl group occupied the adenine pocket, whereas the purine core occupied the phosphate location. The carboxamide substituent interacted with Lys183 and is exposed to the solvent system. Significantly, naphthalene **120** at 10 μM in presence of 10 μM ATP displayed good

selectivity for GSK-3β (82% inhibition). All other enzyme activity, with the exception of a weak activity against CK2α (41% inhibition) and TYRO3/SKY (22% inhibition), was unaffected.[259]

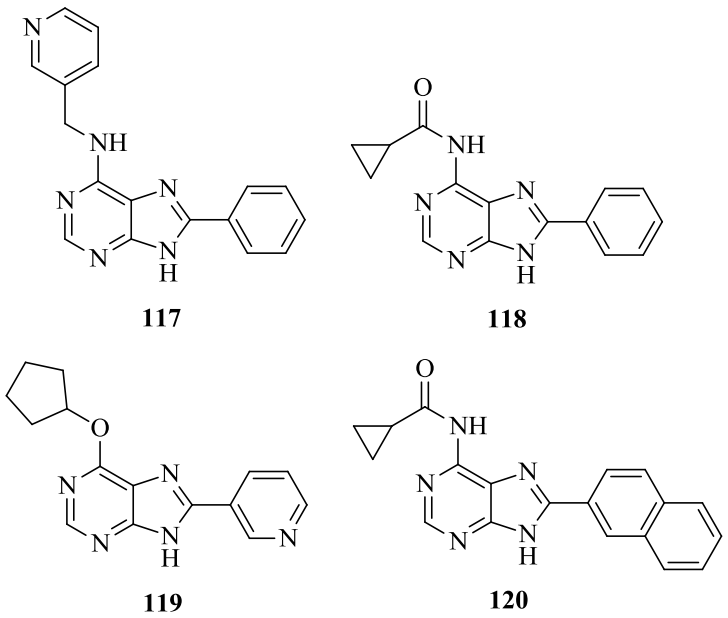

Figure 1.35. Purine derived GSK-3β inhibitors

One of the earliest pyrazolo derivatives that inhibits GSK-3β was reported by Mitsubishi Pharma Corporation with IC_{50} values of below 14 nM on rabbit GSK-3β. The most potent inhibitor from this collection was compound **121** (Fig. 1.36) with an IC_{50} value of 0.61 nM.[260] In another pyrazolo example, the oral inhibitor, compound **122** (Fig. 1.36), inhibited GSK-3β with an IC_{50} value of 2 nM in the presence of 500 nM ATP. In addition, **122** displayed 230-fold selectivity against 27 kinases. JNPL3 mice that were treated with **122** (10 mg/kg twice daily by oral gavage) showed reduced tau phosphorylation in primary neuronal cells and brain tissue.[261]

In 2016, a series of pyrazolopyridine compounds were developed through HTS analysis and cellular assays in an attempt to improve kinome selectivity. Compound **123** (Fig. 1.36) inhibited GSK-3β with an IC_{50} value of 54 nM. A co-crystal structure of **123** bound to human GSK-3β showed that **123** binds in the ATP-binding domain and is anchored to the hinge residues via tridentate hydrogen-bonding interactions within the pyrazolopyridine core. It was suggested that this unique tridentate interaction enhances affinity towards GSK-3 and provides broader kinome selectivity. Further design led to compound **124** (Fig. 1.36) that displayed potent inhibitory activity (GSK-3β IC_{50} = 4 nM), but proved to be synthetically challenging to make. Replacing

the trifluoro group with a cyclopropyl substitute resulted in compound **125** (Fig. 1.36), which retained the desired potency (GSK-3β IC_{50} = 5 nM) while improving the synthetic viability of the route. Furthermore, **124** and **125** displayed concentration-dependent inhibition of tau in SH-SY5Y cells with cellular EC_{50} values of 1.00 and 1.76 μM, respectively. Finally, **124** demonstrated good selectivity against 10 kinases.[262]

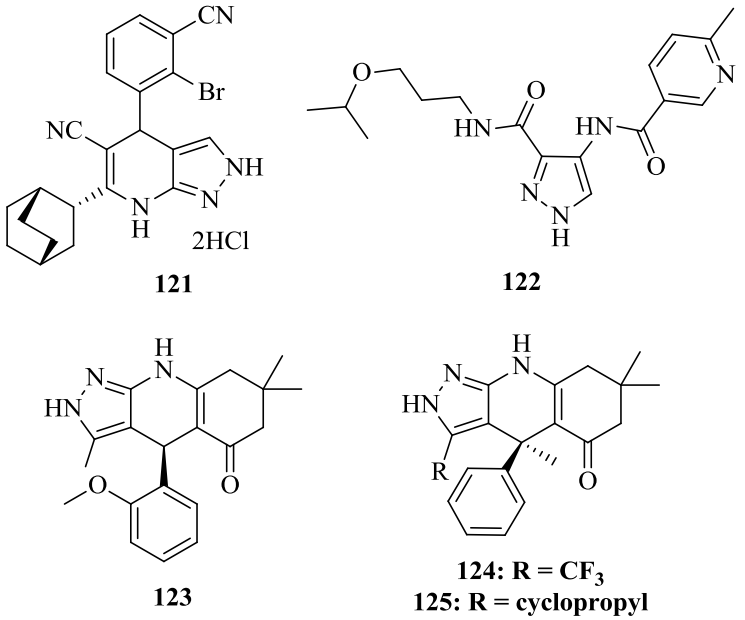

Figure 1.36. Pyrazolo-derived GSK-3β inhibitors

AstraZeneca developed a series of aminopyrazine derivatives that have a strong interaction with Val135 in the hinge region of the ATP-binding pocket. One of the most active compounds of the series, aminopyrazine **126** (Fig. 1.37), inhibited GSK-3β with an IC_{50} value of 4.9 nM and has a 110-fold selectivity over CDK2. Although this compound showed excellent potency and selectivity, it was determined that **126** exhibited lower selectivity against SGK and DYRK1A. A co-crystal structure of **126** bound to GSK-3β showed that the methylpiperazine moiety protruded into the solvent. Of note was that transfected 3T3 fibroblast cells treated with **126** showed reduced ability to phosphorylate tau in a dose-dependent fashion (tau inhibition IC_{50} = 76 nM). Lastly, **126** demonstrated good BBB permeability in bovine endothelial cells (15×10^{-3} cm/min).[263]

It has been determined that many CDK inhibitors are also excellent inhibitors of GSK-3β. An example is the pyrrolopyrazine compound, Aloisine A **127** (Fig. 1.37), that inhibits GSK-3β with an IC_{50} value of 650 nM. Kinetic studies showed that aloisines act as competitive inhibitors for ATP in the ATP binding pocket. Furthermore, the molecule forms two hydrogen bonds with the backbone nitrogen and oxygen atoms of Leu83.[264]

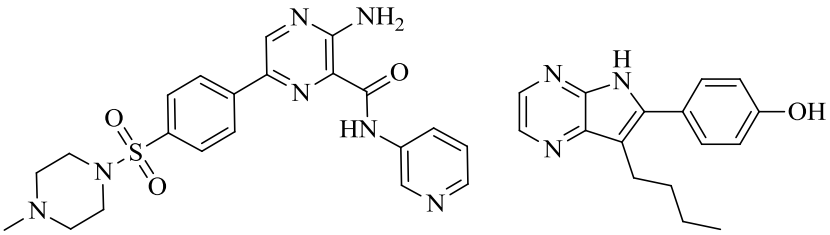

126 **127**

Figure 1.37. Pyrazine-derived GSK-3β inhibitors

1.7.1.4 Azole derivatives

Vertex Pharmaceuticals was one of the first to develop azole-based GSK-3 inhibitors. A large library of pyrrole-pyrazole inhibitors were developed and tested on various kinases such as JNK, JAK, Aurora, AKT, KDR, ERK and GSK-3. Compound **128** (Fig. 1.38), one of the most potent GSK-3 inhibitor in this series, inhibited GSK-3 with an IC_{50} value of <10 μM. Information regarding which GSK-3 isoform it inhibits was not disclosed.[265]

Novo Nordisk developed a library of 2,4-diaminothiazole derivatives for the treatment of metabolic disorders such as diabetes. A large number of these derivatives, including thiazole **129** (Fig. 1.38), inhibited GSK-3β with the activity of **129** being IC_{50} <5 μM.[266]

AR-A014418 **130** (Fig. 1.38) has been described as a potent GSK-3β inhibitor (GSK-3β IC_{50} = 104 nM) and inhibits endogenous Ser396 phosphorylation of tau in 3T3 cells, which stably express human four-repeat tau protein. When treated with 50 μM Aβ over 4 days, hippocampal neurons displayed significant reduction in neuronal loss (>50%) when pre-treated with 10 μM of **130**. In addition, **130** also showed superior selectivity over CDK2 and CDK5 (IC_{50} = >100 μM).[267]

Novo Nordisk identified a novel class of triazole derivatives that inhibit GSK-3β with IC_{50} values in the range of 0.1 to 10 μM. Triazole **131** (Fig. 1.38) inhibited GSK-3β with an IC_{50} value of

0.28 μM in the presence of 100 μM ATP, and against a panel of 31 kinases **131** showed high selectivity for GSK-3β in the presence of 10 μM ATP.[268]

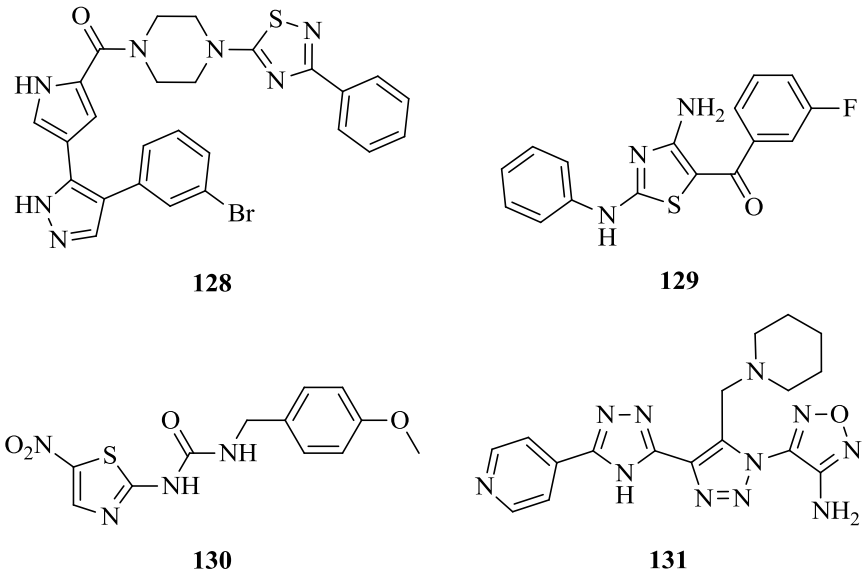

Figure 1.38. Some of the early azole derived GSK-3β inhibitors

Takeda Pharmaceuticals identified dioxolane **132** (Fig. 1.39) as a GSK-3β inhibitor with an IC_{50} value of 65 nM by HTS. The X-ray co-crystal structure of **132** with GSK-3β confirmed the interaction with the ATP-binding site (Fig. 1.39). One oxygen atom of the dioxolane and a neighbouring hydrogen atom formed hydrogen bonds with the amide NH hydrogen and carbonyl oxygen of Val135 in the hinge region. In addition, the nitrogen atoms of the oxadiazole formed a unique hydrogen-bonded network between Lys85-Glu97-Asp200 through two water molecules (Fig. 1.39).[262]

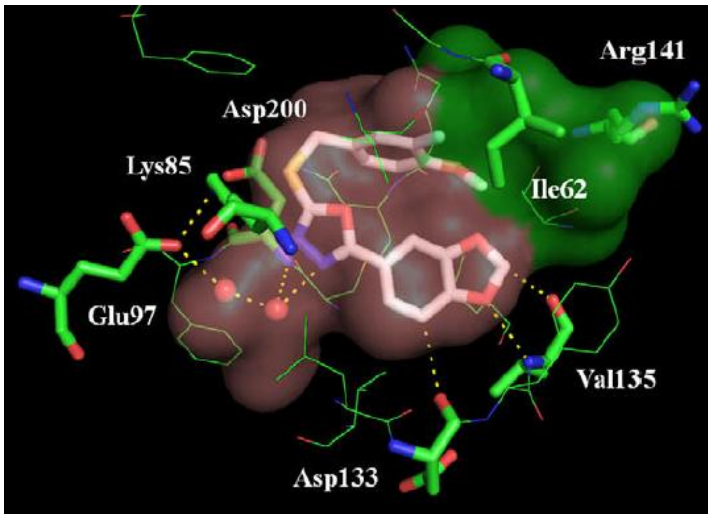

Figure 1.39. X-ray co-crystal structure of dioxolane **132** in complex with GSK-3β[262]

By keeping the 1,3,4-oxadiazole core, further derivatisation of the fused heterocyclic rings offered improved potency. Compounds **133** – **136** (Fig. 1.40) demonstrated low nanomolar potency against GSK-3β (IC_{50} < 7 nM). Compound **136** (GSK-3β IC_{50} = 2.3 nM) was evaluated against a panel of 23 kinases and determined to have more than a 1000-fold selectivity against all the tested kinases including CDK1, CDK2 and CDK5.[269]

Further modification of dioxolane **132** led to the development of a more potent version of the 1,3,4-oxadiazole series. As a result, compound **137** (Fig. 1.40) showed excellent inhibitory activity against both isoforms of GSK-3 (GSK-3α IC_{50} = 4 nM, GSK-3β IC_{50} = 14 nM). Replacement of the dioxolane core with a fused amide heterocycle afforded compound **138** (Fig 1.40) that showed similar potency (GSK-3α IC_{50} = 2 nM, GSK-3β IC_{50} = 17 nM) to **137**.[270]

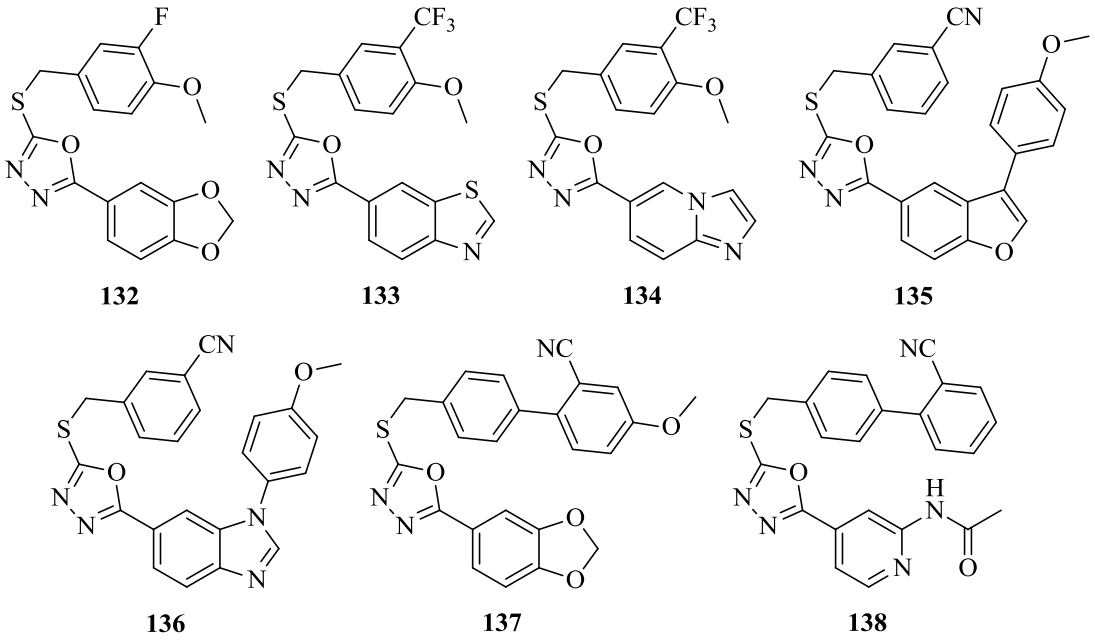

Figure 1.40. Series of 1,3,4-oxadiazoles that demonstrated sub-nanomolar potencies against GSK-3β

1.7.1.5 Maleimide derivatives

Studies have shown that the bisindolyl-maleimide derivatives of staurosporine, GF 109203x **139** and Ro 31-8220 **140** (Fig. 1.41) are potent inhibitors of GSK-3 with IC_{50} values in the nanomolar range. Maleimide **139** inhibited GSK-3β with an IC_{50} value of 190 nM, and maleimide **140** demonstrated stronger activity with an IC_{50} of 2.8 nM. The proposed mechanism of action for the maleimides is thought to be through competition with ATP for the binding site of GSK-3β.[271, 272] Replacing one of the indole groups with a heterocycle revealed good potencies against GSK-3β. Pyrazole-maleimide **141** (Fig. 1.41) inhibited GSK-3β at a K_i value of 48 nM and six-member heteroaryls such as pyrimidine-maleimide **142** (Fig. 1.41) also exhibited excellent potency (GSK-3β K_i = 6 nM). Furthermore, the insertion of a heterocycle instead of a heteroaryl to the maleimide resulted in compound **143** (Fig. 1.41), but it exhibited lower potency (GSK-3β K_i = 84 nM). At concentrations of 10 μM, compounds **141** and **142** inhibited GSK-3β kinase activity by 92% and 96% respectively, in the presence of 100 μM ATP. Meanwhile, compounds **141** and **142** exhibited very weak inhibition against 74 other kinases and moderate inhibition against CDK, RsK and PKB.[273]

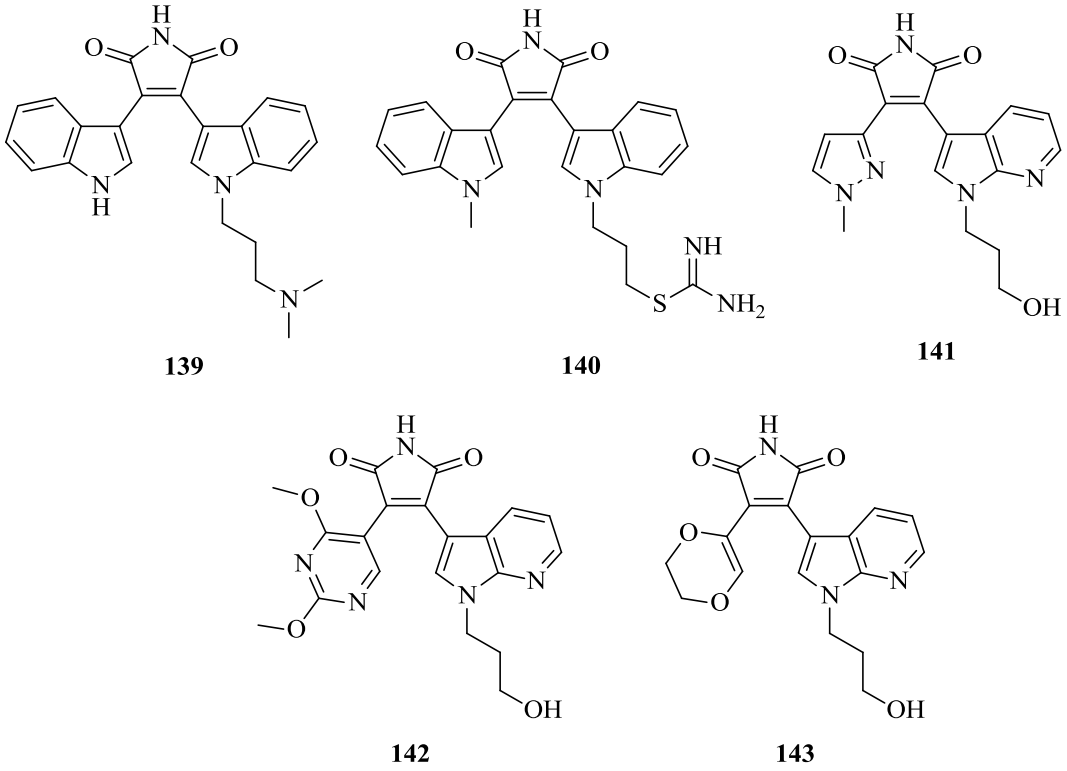

Figure 1.41. Examples of the early indolyl-maleimide derivatives

The introduction of a triazolo-pyridine ring to the indolyl-maleimide produced a series of GSK-3β inhibitors that exhibited IC_{50} values in the low nanomolar range. The insertion of a suitable hydrophilic side chain at the *N*-position of the indole ring, which can form hydrogen bonds with GSK-3β, provided inhibitors with enhanced activity. Compound **144** (Fig. 1.42), with an imidazole group, exhibited potent GSK-3β inhibitory activity with an IC_{50} value of 36 nM. Replacement of the imidazole group with a hydroxyl moiety, as in **145** (Fig. 1.42), resulted in a 3-fold loss in potency (GSK-3β IC_{50} = 121 nM). In addition, introduction of an alkyl side chain such as isopropyl group on the indole nitrogen in **146** (Fig. 1.42) at the *N*-position of the indole led to 37-fold increase in potency (GSK-3β IC_{50} = 13 nM). This suggests that a hydrophobic side chain on the *N*-position of the indole is necessary for enhanced potency. It should be noted that, in a Western blot assay, compound **146** inhibited the phosphorylation of tau in primary neurons.[274]

Replacement of the triazolo-pyridine ring with a furo-pyridine ring resulted in similar observations as for the triazolo-pyridine ring. Isopropyl derivative **147** (Fig. 1.42) displayed the most potent inhibitory activity against GSK-3β of the furo-pyridine series, with an IC_{50} value of

19 nM. No information was disclosed regarding kinase selectivity or whether **147** has the ability to inhibit tau phosphorylation.[275]

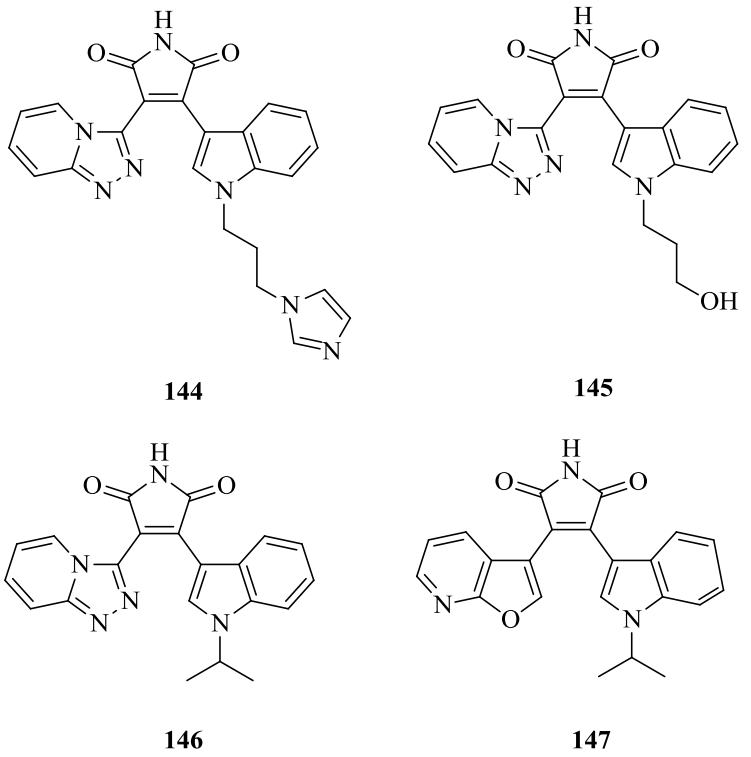

144 **145**

146 **147**

Figure 1.42. Triazolo-pyridine and furo-pyridine maleimide derivatives

1.7.1.6 Indirubin derivatives

Indirubins are indole derivatives and related to the naturally-occurring indigo dyes. Indirubin **148** (Fig. 1.43) inhibits GSK-3β with moderate activity with an IC_{50} value of 600 nM. The insertion of a halogen on the 5-position of **148** dramatically improved the inhibitory activity. 5-Chloroindirubin **149** (Fig. 1.43) was determined to be the most potent GSK-3β inhibitor (IC_{50} = 50 nM) for the series of halogenated indirubins. The incorporation of a monoxime group to the halogenated indirubins further improved the potency. 5-iodoindirubin-3′-monoxime **150** (Fig. 1.43) exhibited the most potent activity against GSK-3β with an IC_{50} value of 9 nM. However, compound **150** demonstrated poor selectivity against CDK1 and CDK5.[276]

Further modifications on the monoxime side chain improved the selectivity against the CDK family. Hydroxyethyloxime **151** (Fig. 1.43) exhibited strong inhibitory activity against GSK-3α/β (IC_{50} = 30 nM) with more than 300 times selectivity against the CDK family.

Replacement of the hydroxyl group with piperazine, as in **152** (Fig. 1.43), improved the potency by ten times (GSK-3α/β IC_{50} = 3.3 nM), but with a 5-fold drop in selectivity over the CDK family.[277] Improved selectivity of the CDK family was achieved by the attachment of an acetate onto the oxime functional group. Acetateoxime **153** (Fig. 1.43) exhibited improved results (GSK-3α/β IC_{50} = 7 nM) and over 4000 times selectivity over the CDK family.[278] In 2007, Meijer *et al.* patented this class of indirubins derivatives and this patent also lists *in vivo* studies on several compounds.[279]

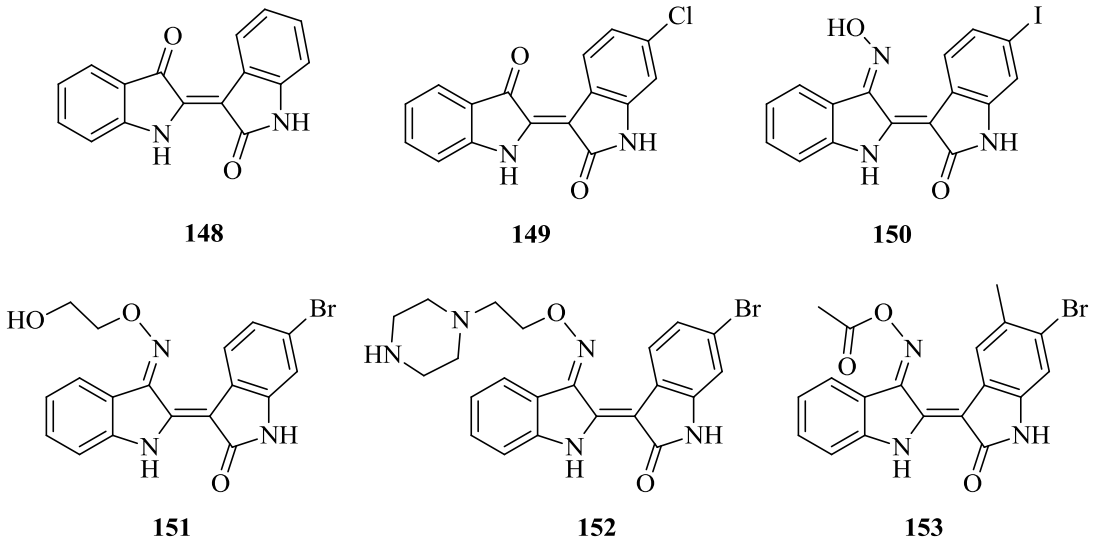

Figure 1.43. Indirubin derivatives that demonstrate potent inhibitory activity against GSK-3β

1.7.1.7 Paullone derivatives

Paullones have been reported as potent ATP competitive inhibitors of GSK-3β and as inhibitors of tau phosphorylation. Alsterpaullone **154** (Fig. 1.44) inhibits GSK-3β with an IC_{50} value of 4 nM in the presence of 15 μM ATP, but showed poor selectivity (about nine times) against the CDK family. **154** also had the ability to inhibit tau phosphorylation of expressed human tau23 in Sf9 cells *in vivo*.[280] Furthermore, alsterpaullone demonstrated the potential to revive death motor neurons.[281]

Inserting a hydrophilic side chain on the paullone scaffold resulted in improved selectivity against the CDK family. Gwenpaullone **155** and C3-paullone **156** (Fig. 1.44) inhibited GSK-3β with IC_{50} values of 40 nM and 30 nM respectively, with slight improvement in selectivity (about 12 times against the CDK family).[282] Further modifications on the side chain resulted in

compound **157** (Fig. 1.44) that demonstrated remarkable potent GSK-3β activity with an IC_{50} value of 0.8 nM. The selectivity against CDK1 was poor (three times) but was good against CDK5 about 38 times). Unfortunately, molecular docking studies could not provide a completely satisfactory explanation for the potency of **157**.[283]

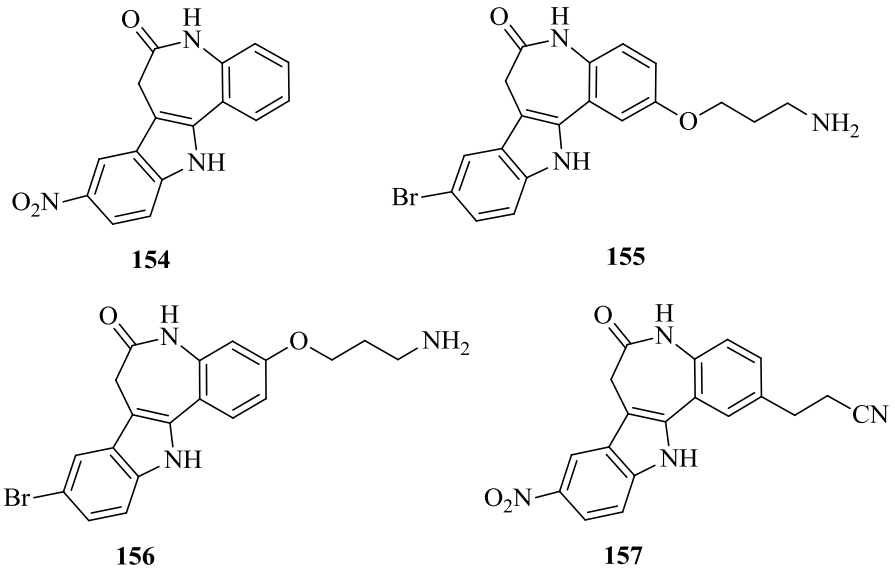

154 **155** **156** **157**

Figure 1.44. Paullone derivatives that inhibit GSK-3β

1.7.1.8 Non-competitive and irreversible GSK-3β inhibitors

The human kinome has over 500 protein kinases that share a high degree of homology in the catalytic site within the ATP-binding pocket. Achieving kinase selectivity is therefore one of the major hurdles in the search and design of protein kinase inhibitors.[284] Designing ATP allosteric GSK-3 inhibitors affords a way to overcome the kinase selectivity problem, since they should bind to unique regions within the kinase providing a more subtle modulation of kinase activity than simply blocking ATP entrance.[238]

The first reported family in this class was the small heterocyclic thiadiazolidinones (TDZD). TDZD-8 **158** (Fig. 1.45) exhibited modest inhibitory activity against GSK-3β with an IC_{50} value of 2 μM, but showed superior selectivity against four other kinases (over 50 times). Kinetic experiments with varying levels of ATP suggested that **158** acts as a non-competitive inhibitor of ATP binding.[285] Although the exact mechanism of action remains unclear, a possible role has

been postulated for interactions with Lys205, Tyr216 and Arg96 residues located in the active site of GSK-3β.[238, 285]

Tideglusib **159** (Fig. 1.45) is an another TDZD that has reached Phase II clinical trials for the treatment of AD and supranuclear palsy.[286] The GSK-3β inhibitory activity of **159** was moderate with an IC_{50} value of 2.4 μM.[287] Enzyme kinetic experiments indicated that tideglusib **159** inhibited GSK-3β irreversibly, as shown by the lack of recovery in enzyme function after removal of the unbound drug.[286] In the preclinical trials, **159** reversed the amyloid load in brain tissue, prevented cell loss and reduced spatial memory deficits. Patients with mild-to-moderate AD exhibited slight improvement in cognitive function after treatment with **159**. However, a Phase IIb trial was aborted due to insignificant statistical differences between the treatment group and the control group.[288]

The library of non-competitive ATP GSK-3β inhibitors has been expanded to include α-halomethylketones (HMK). For instance, thienyl halomethylketone **160** (Fig. 1.45) inhibited GSK-3β with an IC_{50} value of 1 μM. Kinetic experiments with different ATP and **160** levels confirmed that **160** acts as a non-competitive inhibitor of ATP binding. Based on the encouraging results, a second series of HMK derivatives, that contained a phenyl group, was developed. Phenyl HMK **161** (Fig. 1.45) also showed promising GSK-3β inhibition results with an IC_{50} value of 0.5 μM. It was suggested that the electron-withdrawing properties of the halogens play a role in the potency of the inhibitor. No information was disclosed as to whether **161** binds irreversibly to GSK-3β.[289]

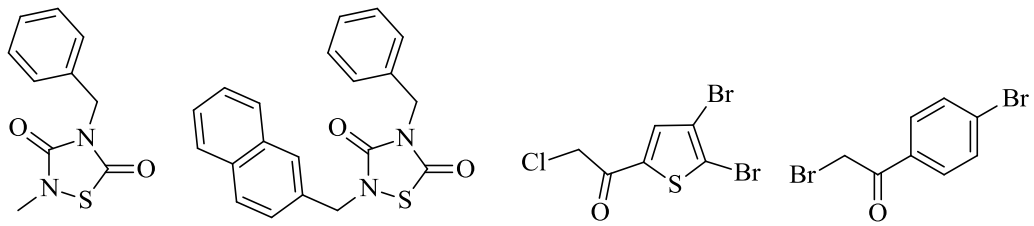

158 **159** **160** **161**

Figure 1.45. Small non-competitive ATP inhibitors of GSK-3β

A theory has been suggested that the inactivation of the GSK-3β is due to the formation of an irreversible covalent sulfur-carbon bond between Cys199 located at the entrance to the ATP site of GSK-3β, and HMK (Fig 1.46).[238, 290]

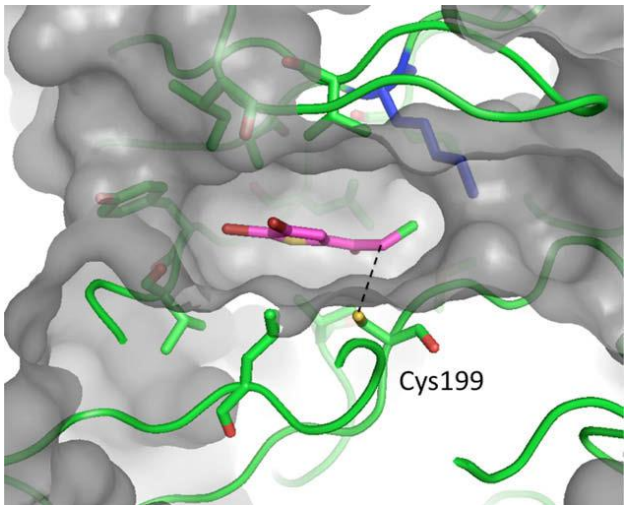

Figure 1.46. Representation of **160** in the ATP-binding site of GSK-3β. The carbon atom bearing the chlorine is above the sulfur atom of Cys199.[290]

To further prove that Cys199 is involved in the inactivation of GSK-3β by incubation with phenyl HMK, known reversible inhibitors were converted into irreversible inhibitors by adding a HMK unit at a strategic position. With the aid of molecular modelling, three structurally distinct known GSK-3β inhibitors, an analogue of ATP **162** (PDB entry 1J1B) and two reversible inhibitors, **163** and **164** (PDB entries 3F88 and 1R0E) (Fig. 1.47), were modified to incorporate a HMK group. The predicted poses derived from docking calculations for **165**, **166** and **167** (Fig. 1.47) revealed that the HMK moiety is suitably positioned for chemical modification by Cys199. All three HMK derivatives, **165**, **166** and **167**, inhibited GSK-3β (IC_{50} = 13.4 μM, 0.58 μM and 0.005 μM respectively) and covalent bonding to GSK-3β was confirmed by MALDI-TOF analyses.[291]

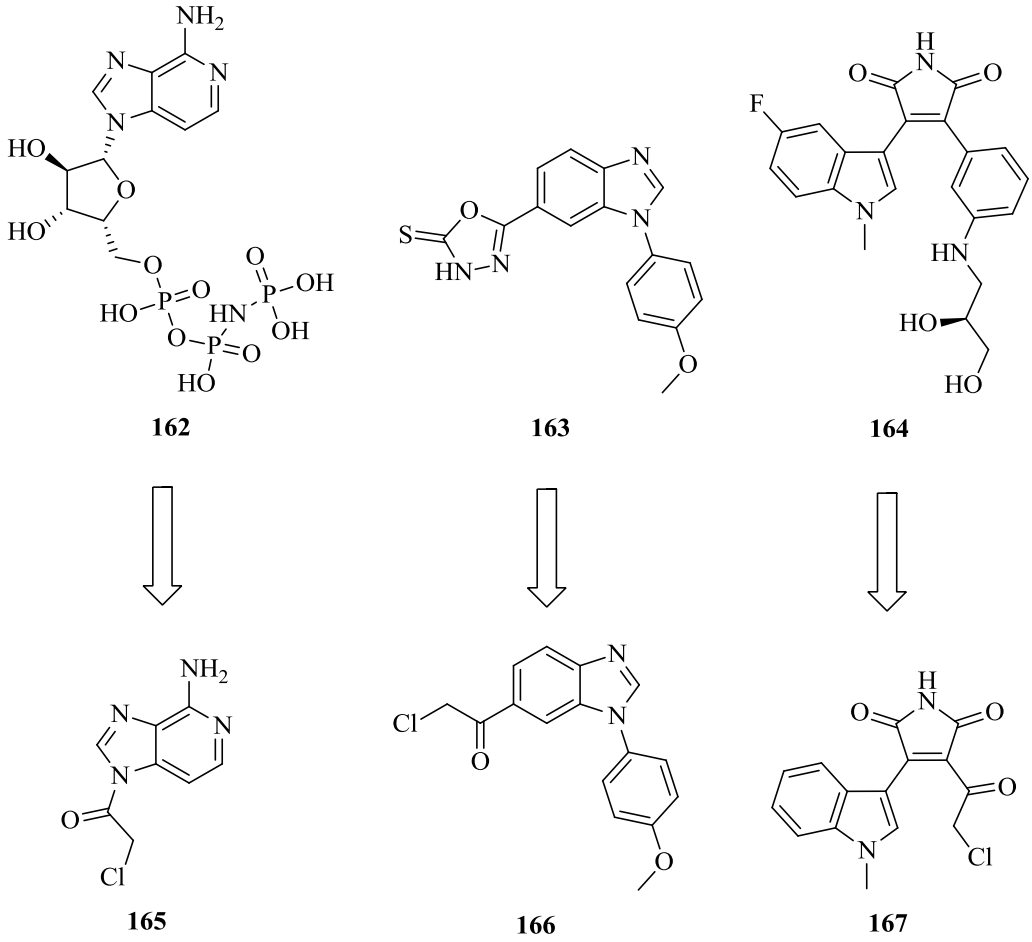

Figure 1.47. Switching from reversible to irreversible GSK-3β inhibitors

1.7.2 Tau aggregation inhibitors

The NFTs comprise dense double helix fibres occupying the cortical pyramidal cell and neurons in the brainstem. These fibres were termed paired helical filaments (PHFs).[292] The difference in the repeat domain fragment from the core of the PHF and from the normal tau is that it is phase shifted with respect to the normal repeats. The length of the repeat domain is exactly three repeats in length, but the positioning of the alternating tubulin-binding segments and the intervening linker segments is reversed. The repeat domain in the PHF core can be used to distinguish between the tau-tau binding interactions and those that pertain to the tau-tubulin binding. Therefore tau aggregation inhibitors could be developed that selectively target the tau-tau binding interaction.[293]

Thionine **168** (Fig. 1.48) was one of the first identified tau aggregation inhibitor that produced a linear inhibition of tau-tau binding over the range from 1:1 to 10:1 molar ratio with respect to tau.[294] With **168**, the K_i of inhibition of tau-tau binding, based on a solid-phase tau-tau binding interaction, was determined to be 98 nM. For tau-tubulin binding, the K_i was found to be 7.9 mM, an 8000-fold difference.[293]

In another example, rhodanines were identified as tau aggregation inhibitors through HTS. Rhodanine-furan **169** (Fig. 1.48) inhibited the assembly of PHF with an IC_{50} value of 0.47 μM. The analysis of the nature of substituents on the flanking regions of the rhodanine showed preference for hydrogen bond donors and acceptors such as carboxylic acids, nitro groups, phenols, sulfonates and sulfonamides.[295]

Furthermore, a ligand-based virtual screening of 200 000 compounds yielded phenylthiazolylhydrazide **170** as one of the hits.[296] Phenylthiazolylhydrazide **170** (Fig. 1.48) demonstrated good activity against 10 μM K19 tau protein (IC_{50} = 1.6 μM and 50% depletion concentration, DC_{50} = 0.7 μM). Analytical data obtained from STD-NMR spectroscopy indicated that **170** bound directly to monomeric tau and that this was mediated through the aromatic ring of the imidazole. Hydrogen-bonding interactions with the nitro group and imidazole amine were also observed.[297, 298] However, the phenylthiazolylhydrazide core was thought to be susceptible to cytochrome P450-mediated oxidative cleavage on the thiazole moiety.[299] Hydrazine is also a potential producer of ROS after oxidative cleavage of the *N*-*N* bond.[300, 301]

In an *in vitro* experiment of aggregated tau, benzothiazole N744 **171** (Fig. 1.48) yielded a dose-dependent decrease in filament numbers and mass. The IC_{50} value for **171** inhibition of htau40 fibrillisation at 24 h was 280 ± 20 nM. It was suggested that **171** potentially interferes with both nucleation and extension phases of tau assembly.[302]

From the screening of 292 000 compounds, aminothienopyridazines (APTZs) were identified as potent inhibitors of P301L K18 tau aggregation. APTZ **172** (Fig. 1.48) was identified as one of the lead candidates (IC_{50} = 5.1 μM at 15 μM P301L K18 tau). Results of size-exclusion chromatography of the supernatant after incubation of tau40 with APTZs showed the presence of monomeric tau, and also the presence of stabilised oligomeric species. Therefore, the data suggests that APTZs prevent tau aggregation and the formation of potentially neurotoxic fibrils. This results in increased availability of tau monomers to stabilise microtubules.[303]

Azaphilones, which occur in fungi, have recently been identified through standard biochemical assays as potential tau aggregation inhibitors. Azaphilone **173** (Fig. 1.48) demonstrated the best activity in the series with an IC_{50} value of 56 μM for dissolving preformed tau filaments *in vitro*, while partially preserving the ability of tau to bind to tubulin and promote microtubule assembly. Quantitative analysis of the filament lengths in the presence of **173** showed no filaments greater than 200 nm in length when compared to the control (>200 nm). These promising results indicate that the azaphilones could be used as a new scaffold with appropriate biological activity for further development.[304]

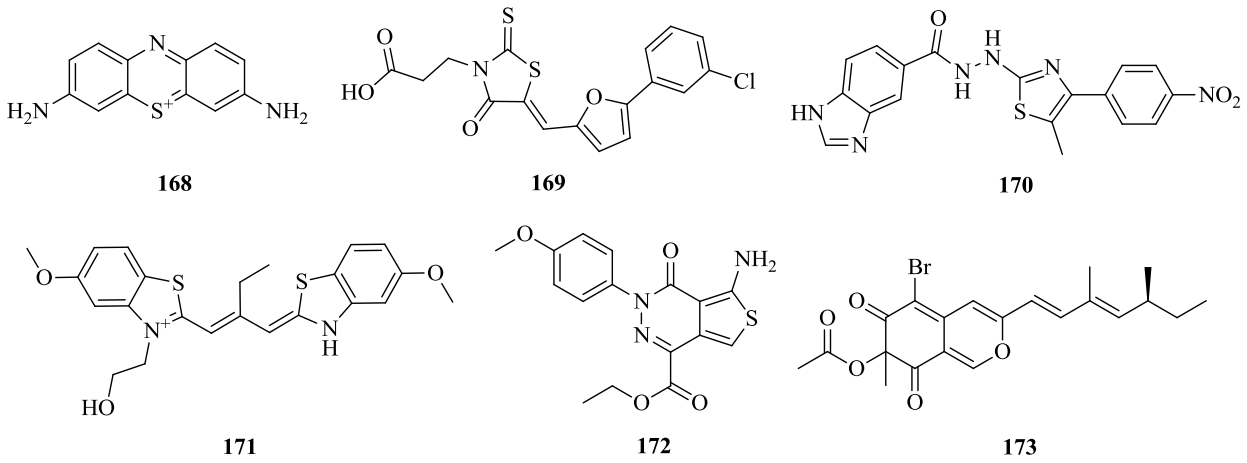

Figure 1.48. Tau aggregation inhibitors

1.8. Acetylcholinesterase

Cholinergic transmission has a vital role in the sleep-wake cycle, circadian rhythms, learning, memory, cognition and cortical activity.[305-308] Acetylcholinesterase (AChE) is a serine-protease that hydrolyses the carboxylic ester of the neurotransmitter acetylcholine to afford choline and acetic acid, thus playing an integral part in cholinergic transmission. AChE is predominantly expressed in plasma, red blood cells, nervous tissue and neuromuscular junctions.[309]

In AD patients, cholinergic neurons undergo extensive degenerative changes, resulting in acetylcholine depletion and cholinergic hypofunction. This contributes to progressive memory deficit and cognitive decline.[310, 311] Furthermore, AChE is also one of the proteins that colocalises with Aβ deposits and promotes Aβ assembly that aggregates in insoluble plaques.[312]

Therefore, the use of AChE inhibitors to treat symptoms caused by cholinergic imbalances represents an attractive option to treat AD.

AChE predominates in the healthy brain, while butyrylcholinesterase (BChE) is considered to play a minor role in the regulation of AChE levels. However, BChE levels increase progressively in patients with AD while AChE activity remains unchanged or declines.[313] While the development of BChE inhibitors is an attractive option, its role in the regulation of cholinergic transmission is not fully understood, thus AChE remains the main target and AChE selectivity over BChE is desired.[314, 315]

1.8.1 Marketed AChE inhibitors

In 1993, tacrine **174** (AChE IC_{50} = 167 nM) (Fig. 1.49) was the first AChE inhibitor to hit the market for the treatment of AD. Tacrine prescriptions were halted after other AChE inhibitors were introduced as it became clear that tacrine caused liver toxicity.[316, 317]

Donepezil **175** (AChE IC_{50} = 5.7 nM) (Fig. 1.49) was the second FDA-approved drug for the treatment of mild to moderate AD. More than 200 clinical trials with **175** have been carried out so far.[317, 318] This drug interacts within the active site of the AChE through aromatic interactions. The benzylpiperidine and indanone groups interact with the indole ring of Trp84 of the anionic subsite and with the indole ring of Trp279 at the peripheral site of the enzyme, respectively.[317]

Rivastigmine **176** (AChE IC_{50} = 4.15 μM) (Fig. 1.49) is a drug widely used for the treatment of AD. This drug belongs to a new generation of cholinesterase inhibitors with a carbamate moiety, which has the ability to react covalently within the active site of AChE. Furthermore, rivastigmine exhibits a ten-fold selectivity for the brain AChE than for the AChE in the peripheral nervous system.[317]

Lastly, Galantamine **177** (AChE IC_{50} = 800 nM) (Fig. 1.49), an alkaloid isolated from different species of the Amaryllidaceae family, acts as a competitive and reversible AChE inhibitor. Galantamine inhibits AChE along with allosteric modulation of nicotinic acetylcholine receptors that leads to increased release of acetylcholine.[317, 319]

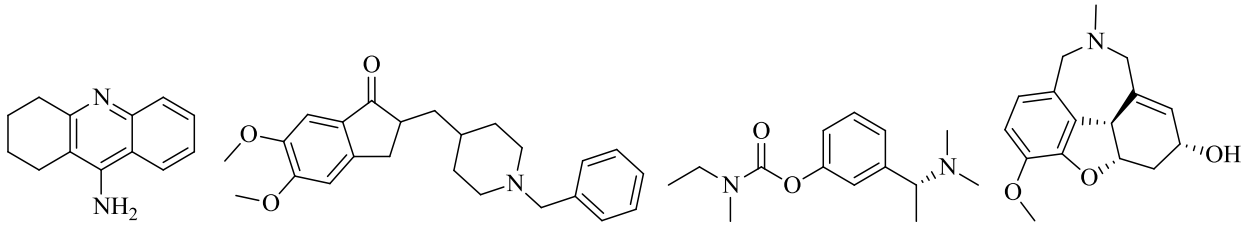

174 **175** **176** **177**

Figure 1.49. AChE inhibitors currently on the market for the treatment of AD

1.8.2 Tacrine derivatives

After the introduction of tacrine **174** (Fig. 1.49) as the first AChE inhibitor,[311, 312] structural changes were made to improve its potency and reduce toxicity. Molecular docking studies revealed two different binding sites for tacrine **174** in AChE, namely, the catalytic site and the peripheral site. The peripheral site is located at the opening of the enzymatic binding pocket and far from the catalytic site at the bottom of the pocket.[320] To exploit this phenomenon, Pang *et al.* introduced an alkyl bridge in tacrine **174** via the NH_2 group to join two tacrine molecules. Heptamethylene tethered tacrine **178** (Fig. 1.50) inhibited rat brain AChE with an IC_{50} of 0.4 nM with a 980-fold selectivity over BChE. This compound was 1 000 times more active than tacrine and 10 000 times more selective towards rat brain AChE. Unfortunately, no information regarding its toxicity was disclosed.[320]

To improve the potency, a protonatable amine group was introduced in the middle of the tether to provide additional interactions with aromatic residues in the active site of AChE. To this end, compound **179** (Fig. 1.50) delivered better potency (K_i = 0.06 nM), but less selectively against BChE (K_i = 6 nM).[321]

Martinéz *et al.* synthesised various heterodimers of tacrine or its 6-chloro derivative (for interaction with the catalytic site) with an indole moiety (for interaction with the peripheral sites), which were linked by a suitable tether with an amide group.[322] Optimisation of the length of the tether and the position of the amide group led to the synthesis of different derivatives with IC_{50} values in the low nanomolar range. For example, compound **180** (Fig. 1.50) was shown to possess the highest activity (bovine AChE IC_{50} = 0.02 nM) and selectivity against bovine BChE (145-fold). Furthermore, at a concentration of 100 μM, **180** inhibited 98% of the AChE-induced $A\beta_{1\text{-}40}$ peptide aggregation.[322]

Rosini *et al.* developed tacrine derivatives with antioxidant properties that demonstrated additional benefits. Lipoic acid, a known antioxidant, has shown to protect neurons against cytotoxicity induced by Aβ and to restore cognitive functions in patients with AD. The combination of tacrine with lipoic acid led to the synthesis of lipocrine derivative **181** (Fig. 1.50) that inhibits human recombinant AChE with an IC_{50} value of 0.253 nM and shows 43-fold selectivity against BChE. Furthermore, **181** was able to protect SH-SY5Y neuronal cells in a dose-dependent fashion against ROS formation by *tert*-butyl hydroperoxide.[323]

Tacrine homodimers with piperazine-ethyl spacers also demonstrated potent activity. Compound **182** (Fig. 1.50) showed an inhibitory activity against human AChE with an IC_{50} value of 4.49 nM and a 339-fold selectivity over BChE. The compounds with an amide group in the tether demonstrated better inhibitory activities in comparison to the compounds without an amide group. This suggested that an amide group in the tether is important for AChE inhibition.[324]

By using click chemistry as a tool for lead optimisation, Manetsch *et al.* developed a series of triazole-linked AChE inhibitors. Triazole compound **183** (Fig. 1.50) inhibits electric eel AChE with a dissociation constant of 99 fM. Co-crystallisation of **183** with AChE revealed hydrogen bonding of the triazole ring with Ser203 and Gly121 via a H_2O molecule.[325]

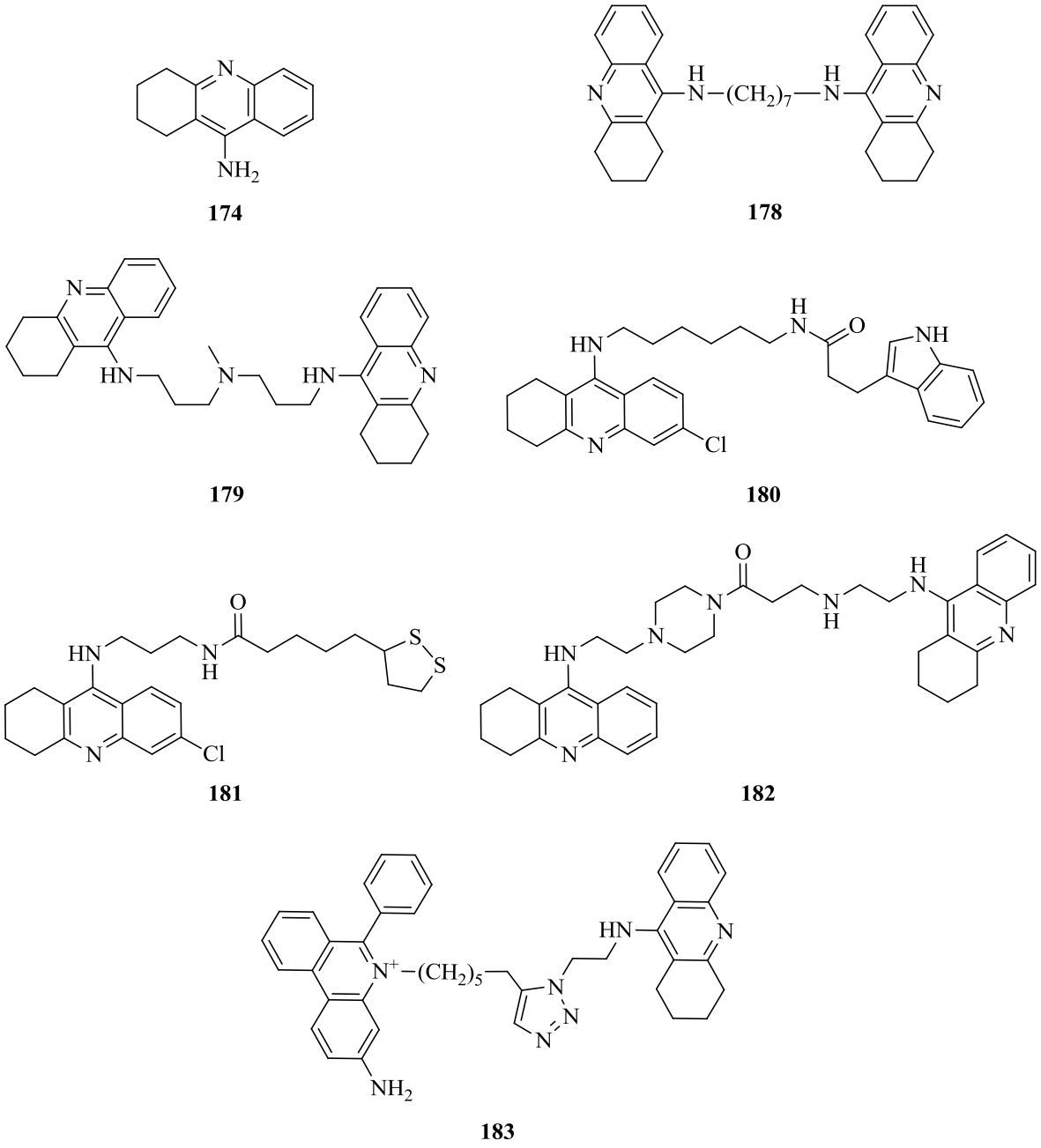

Figure 1.50. Tacrine-derived AChE inhibitors

1.8.3 Donepezil derivatives

The pharmacological profile of donepezil **175** (Fig. 1.49) has spurred researchers to design and synthesise donepezil-like compounds through bioisosteric replacements for the indanone ring system. Villalobos *et al.* identified the benzisoxazole ring structure as a suitable bioisostere for the indanone ring in donepezil **175**. Benzisoxazole **184** (Fig. 51) displayed very high *in vitro*

AChE inhibitory activity (IC_{50} = 2.8 nM) and also a very high selectivity against BChE (over 3200 times). In addition, *in vivo* experiments showed that **184** elevated the acetylcholine levels in mouse forebrain after oral administration. Lastly, **184** was able to reverse hemicholinium-3-induced amnesia with an average of 90% at doses of 3.2 and 5.6 mg/kg.[326]

However, **185** (Fig. 1.51) proved to be metabolically labile, partially undergoing hydrolysis of the acetamide group to produce the corresponding aniline derivative, which was 7-fold less active. To improve the metabolic stability, the acetamide group was converted into a 5-membered heterocycle. This resulted in the development of **185** that displayed improved potency (AChE IC_{50} = 0.33 nM) and increased selectivity against BChE (approximately 22 000 times).[327]

Ismail *et al.* used the indole moiety as the bioisostere for the indanone ring in donepezil. In the Ellman's assay,[328] compound **186** (Fig. 1.51) showed a slight improvement in AChE inhibition (53%) compared with donepezil (40%). When a benzyl moiety was used instead of a phenyl group, as in compound **186**, 55% AChE inhibition was demonstrated. In addition, molecular modelling studies suggested that compounds with the benzyl group were a better fit in the receptor.[329]

Modifications on the benzyl moiety of donepezil to improve potency and selectivity led to the synthesis of **187** (Fig. 1.51). The incorporation of a fluorine group on the benzyl ring improved the potency slightly (hAChE IC_{50} = 32 nM, **175** hAChE IC_{50} = 48 nM), but significantly increased the selectivity against hBChE (400 times, **175** = 66 times). This suggested that small modifications on the benzyl moiety could enhance the selectivity for AChE inhibition.[330]

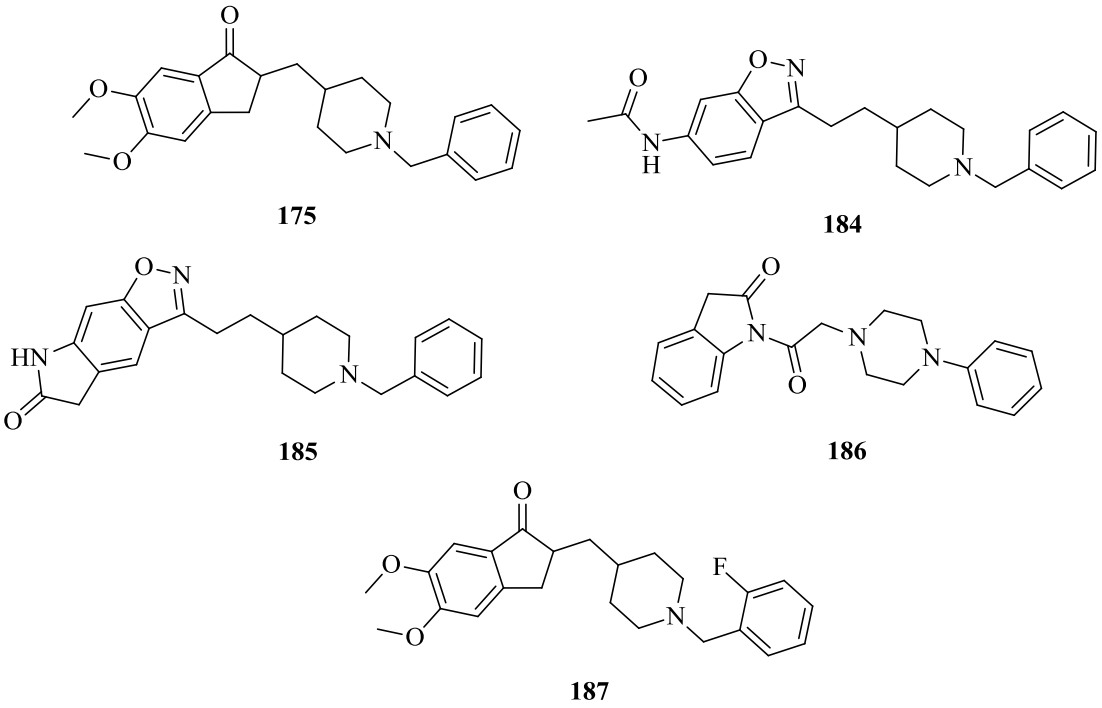

Figure 1.51. Donepezil-derived AChE inhibitors

1.8.4 Rivastigmine derivatives

Bolognesi *et al.* developed a series of conformationally-restricted analogues of rivastigmine **176** by changing the dimethylaminoethylphenyl portion to a tricyclic system, as exemplified by compound **188** (Fig. 1.52). Compound **188** exhibited potent hAChE inhibitory activity (IC_{50} = 8.11 nM), but exhibited poor selectivity against hBChE (1.3-fold). In this series, it was determined that the alkyl substituent at the carbamoyl nitrogen determined the potency of the inhibitor, and that longer alkyl chains showed diminished inhibitory activity against hAChE. A possible explanation was that the longer alkyl chains experienced steric hindrance in the active site.[331]

Through SAR studies, a series of irreversible carbamate inhibitors were developed by Lin *et al.* that targeted the peripheral active site. As an example, carbamate **189** (Fig. 1.52) inhibited AChE the strongest in this series (K_i = 1 μM). The K_i values for electron-withdrawing groups on the benzene ring such as NO_2, CF_3 and Cl were lower than electron-donating groups. The proposed mechanism for the irreversible inhibition was that the inhibitor donates electrons to the aromatic rings of the peripheral site to form non-covalent adducts. This results in a conformational change at Phe330 near the entrance of AChE, causing a partial blockade for the entrance of substrate.[332]

Molecular modelling studies have also shown that the distance between the carbamic carbon and the piperidine nitrogen affects the activity of the compound. Experimenting with the chain length between the carbamate and the piperidine resulted in compound **190** (Fig. 1.52), one of the most active inhibitors in this series (AChE IC_{50} = 14 nM, BChE IC_{50} = 124 nM, nine times selectivity). The dimethylcarbamates were determined to be more active when the phenyl ring was joined to piperidine with a single carbon tether. Increasing the bridge length between the phenyl ring and piperidine resulted in diminished activity.[333]

Other conformationally-constrained derivatives with six- or seven-membered rings were developed by Toda *et al.*, as dual inhibitors for AChE and serotonin transporter (SERT). The racemic seven-membered ring carbamate **191** (Fig. 1.52) inhibited mouse brain AChE with an IC_{50} value of 66 nM and rat SERT with 63 nM. The (*R*)-enantiomer **192** (Fig. 1.52) showed extremely potent inhibitory activities against both AChE (IC_{50} = 14 nM) and SERT (IC_{50} = 6 nM), but the (*S*)-enantiomer **193** (Fig. 1.52) was only somewhat active (AChE IC_{50} = 609 nM, SERT IC_{50} = 930 nM). No information regarding BChE inhibition was disclosed.[334]

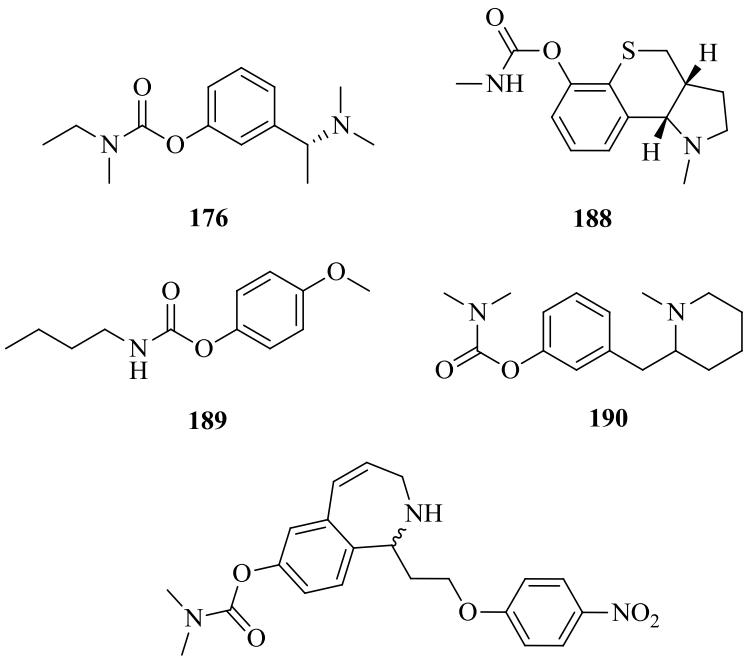

Figure 1.52. Rivastigmine-derived AChE inhibitors

1.8.5 Galantamine derivatives

Mary *et al.* developed one of the earliest galantamine derivatives that consisted of bis-interacting ligands. In this research, different alkyl linkers with a terminal phthalimido group were incorporated on the *N*-demethylgalantamine and 6-*O*-demethylgalantamine. *N*-phthalimidoalkyl **194** (Fig. 1.53) with an 8-carbon bridge exhibited the most AChE inhibitory activity in the *N*-demethylgalantamine series with an IC_{50} value of 10 nM. In the 6-*O*-demethylgalantamine series, *O*-phthalimidoalkyl **195** (Fig. 1.53), with a 10-carbon bridge, was the most active (AChE IC_{50} = 50 nM). Both compounds were also found to be more potent than galantamine (36 times and 7 times respectively). The length of the alkyl linkers was determined to have an effect on the potency and the best inhibitory activities were achieved with eight to ten methylene groups. It was also observed that compounds with a permanent positive charge on the galantamine nitrogen atom showed better activity than the neutral compounds, which suggests that an iminium salt is necessary for enhanced potency.[335]

Herlem *et al.* went on further to synthesise galantamine derivatives with an open D-ring. Unfortunately, the compounds in this series showed only weak activity against AChE, with compound **196** (Fig. 1.53) being the most active (AChE IC_{50} = 580 μM, BChE IC_{50} = 216 μM). This suggests that a closed ring system is necessary for high inhibition activity.[336]

Jia *et al.* developed a library of *N*-substituted galantamine derivatives by incorporating terminal benzylpiperidine, benzylmorpholine, benzylamide and benzyldiethylamine moieties with different alkyl chain linkers. The potency of AChE inhibition was influenced by the chain length as well the type of amine function at the end of the alkyl linker. The benzyl piperidine derivative **197** (Fig. 1.53), with a six methylene bridge, showed the most potent AChE inhibition with an IC_{50} value of 5.62 nM and a 5800 times selectivity against BChE. The morpholine and amide derivatives were the least active of all the compounds, which suggested that for these compounds the terminal group was situated in a hydrophobic domain.[337]

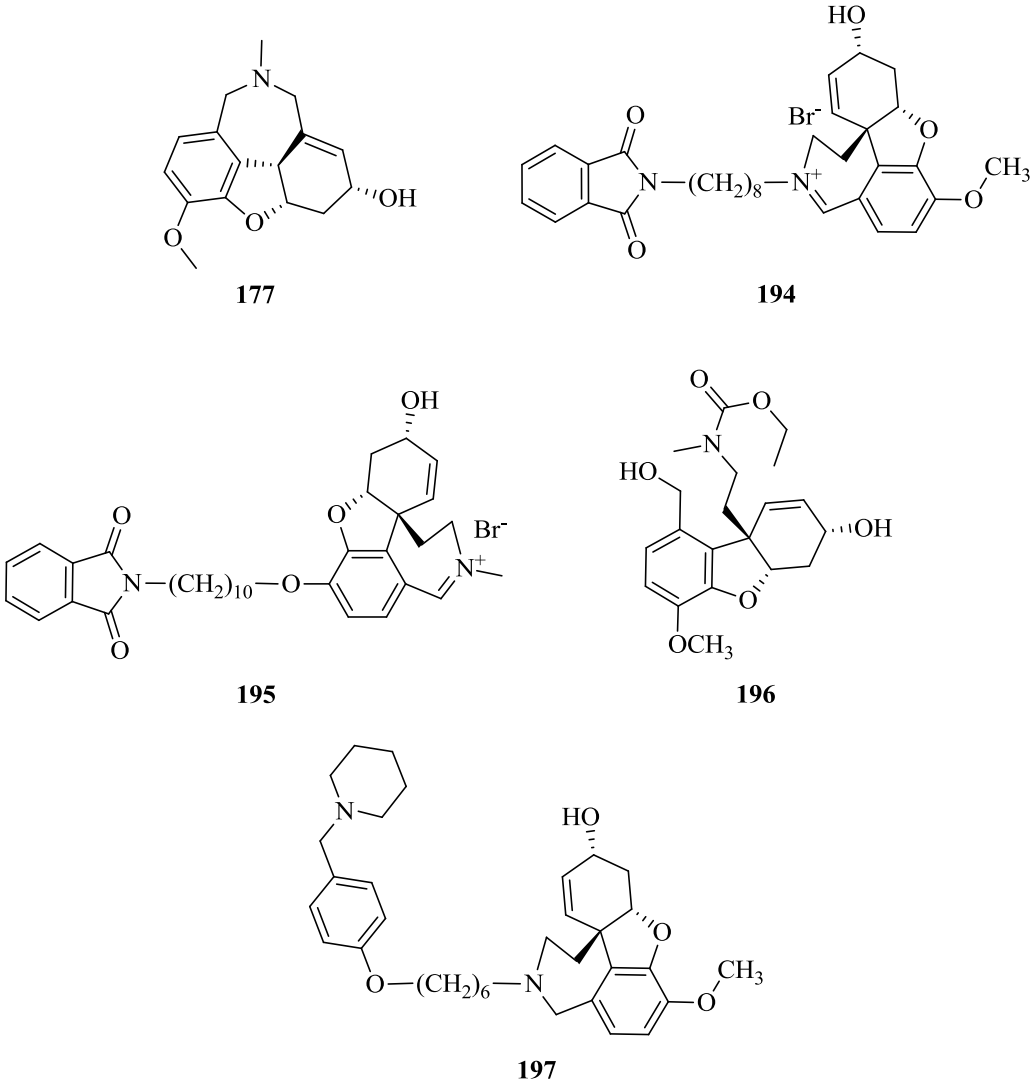

Figure 1.53. Galantamine-derived AChE inhibitors

1.8.6 Miscellaneous AChE inhibitors

Huperzine A **198** (Fig. 1.54), a naturally-occurring sesquiterpene alkaloid found in *Lycopodium* species, produces long-term AChE inhibition in rat brain and an increase in acetylcholine levels up to 40%. Side effects were determined to be mild even at high doses (2 mg/kg i.m.).[338]

An example of inhibitors with a unique scaffold was developed by Tumiatti *et al.*[339] A series of molecules with a benzo[*lmn*][3,8]phenanthroline-1,3,6,8(2*H*,7*H*)-tetraone linker was synthesised to determine whether structural flexibility can influence the potential to inhibit AChE. Results revealed that the insertion of a rigid dipiperidino moiety strongly influenced the ability to inhibit AChE. Dipiperidino **199** (Fig. 1.54) was the best AChE inhibitor (IC_{50} = 0.37 nM) with a 5200

times selectivity against BChE. Furthermore, **199** was able to inhibit the Aβ-self aggregation with an IC_{50} of 9.69 μM.[339]

Berberine **200** (Fig. 1.54), an isoquinoline alkaloid from *Chelidonium majus L.* (AChE IC_{50} = 1.85 μM, 43 times selectivity against BChE),[340] was used as a basic skeleton for the construction of a series of hybrid compounds. In this series, the hybrid compound hydroquine **201** (Fig. 1.54) demonstrated the best AChE inhibitory activity (IC_{50} = 123 nM) with a 17 times selectivity against BChE. Hydroquine **201** also demonstrated excellent antioxidant effects (Trolox equiv. = 3.54), which was stronger than berberine **200** (Trolox equiv. = 0.4), and at a concentration of 20 μM, inhibited 85% of $A\beta_{1-42}$ peptide aggregation.[341]

Studies have shown that β-Carbolines are excellent inhibitors of both AChE and BChE. Rook and co-workers synthesised a series of bivalent β-carboline derivatives as potential dual AChE/BChE inhibitors. A structure-activity study revealed that the inhibitory activity of quaternary N^9-bivalent β-carbolines was higher in comparison to the analogues without a permanent positive charge. β-Carboline **202** (Fig. 1.54), with a nine methylene unit linker, proved to be a potent inhibitor of AChE and BChE (IC_{50} = 0.5 nM and 5.7 nM respectively). In addition, **202** also inhibited the transient glutamate-induced Ca^{2+} excitotoxicity with an IC_{50} value of 1.4 μM.[342]

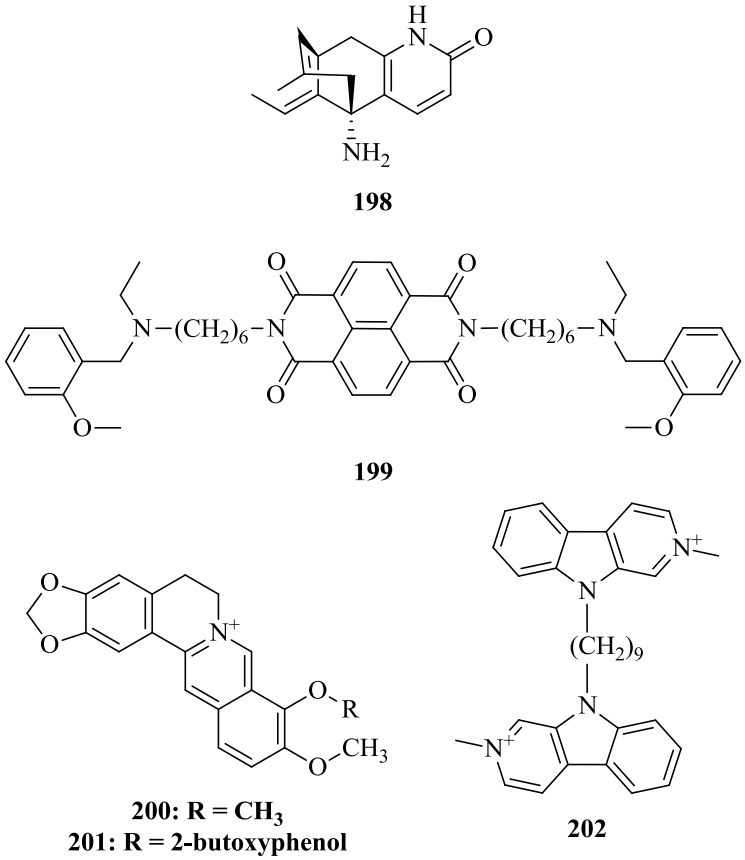

Figure 1.54. AChE inhibitors with different moieties

The AChE inhibitors are one of the main drugs for the management of AD. However, the limited availability of clinical AChE inhibitors prompted the need for further research to develop effective AChE inhibitors that may treat AD patients in more complete manner.

1.9. Conclusions

It has been over 100 years since Alois Alzheimer's observation of the first Aβ plaques and tangles in the brain of Auguste Deter. Since then, our knowledge of AD has grown significantly. Numerous hypotheses have been constructed and investigated to determine the cause of AD. It is clear from these findings that AD is a very complex disease with multiple origins. The fact that AD progresses very slowly makes it difficult to diagnose and effective treatment has proved elusive. Many drugs have reached clinical trials but sadly, most have failed and those that have succeeded only treat the symptoms.

In order to obtain effective disease-modifying approaches, it is critical to know the structures implicated in the origin and the disease progression. Since the development of the amyloid cascade hypothesis, many resources have been invested in the design and development of inhibitors for the associated enzymes. However, the failure of clinical trials that target the clearance of Aβ deposits and the fact that Aβ production overload does not appear to be directly causal of AD, forced researchers to develop other hypotheses that include metal dyshomeostasis, tauopathy and acetylcholinesterase.

These hypotheses provide numerous avenues to explore and to further our understanding of the complex etiology of AD, Hopefully, they will also allow for the development of therapeutics that are able to offer some degree of relief. In the last ten years, new drug prototype candidates have been identified and they are the starting point of a new generation of drugs that has the potential to reach clinical trials and, hopefully, the market.

1.10 Aims and objectives

The aim of this project has been to develop new compounds that have the potential to be irreversible GSK-3β inhibitors. The main scope of the project was to synthesise and characterise new compounds using known techniques and synthetic pathways. For the most part, the adaptation of synthetic organic chemistry techniques and pathways were needed to successfully synthesise the new compounds. The final compounds would then be tested for their biological activity and as well whether it binds irreversibly to GSK-3β.

The second chapter describes the short introduction to GSK-3β and irreversible inhibitors. The molecular modelling studies of the GSK-3β are also discussed. Based on the molecular modelling results, three different series of inhibitors were then identified for synthesis. Each series will be discussed in the next following chapters.

This is followed by the third chapter, which describes the synthesis of the (*E*)-3-(3-aminopyrazin-2-yl)acrylaldehyde derivatives and the quest to find optimal conditions for successful Suzuki-Miyaura reactions.

The fourth chapter describes the synthesis of the (*E*)-1-(3-aminopyrazin-2-yl)prop-2-en-1-one derivatives. This chapter also discusses the synthetic attempts of coupling the electrophilic "warhead" to the aminopyrazine core.

The fifth chapter describes the biological results of the synthesised compounds from chapters four and five. The biological results are then compared with the results of the molecular modelling studies.

The sixth chapter describes the attempted synthesis of the terminal "warheads". This chapter discusses the different methodologies that were explored to find the optimal conditions to synthesise the terminal "warheads".

The seventh chapter gives an overview of conclusions from the work carried out and suggests potential future work that may arise from this project.

The appendix describes additional *Plasmodium falciparum* biological testing that was carried out on the synthesised compounds and the search for the pharmacophore.

1.11 References

1. *Alzheimer's Association*, http://www.alz.org/facts/ Accessed October 2015.
2. H. W. Querfurth and F. M. LaFerla, *New England Journal of Medicine*, 2010, **362**, 329-344.
3. Y. Huang and L. Mucke, *Cell*, 2012, **148**, 1204-1222.
4. E. B. Larson, M.-F. Shadlen, W. Li, W. C. McCormick, J. D. Bowen, L. Teri and W. A. Kukull, *Annals of Internal Medicine*, 2004, **140**, 501-511.
5. D. J. Selkoe and M. B. Podlisny, *Annual Review of Genomics & Human Genetics*, 2002, **3**, 67-99.
6. M. Goedert and M. G. Spillantini, *Science*, 2006, **314**, 777-781.
7. C. F. Lippa, A. M. Saunders, T. W. Smith, J. M. Swearer, D. A. Drachman, B. Ghetti, L. Nee, D. Pulaski-Salo, D. Dickson, Y. Robitaille, C. Bergeron, B. Crain, M. D. Benson,

M. Farlow, B. T. Hyman, P. St. George-Hyslop, A. D. Roses and D. A. Pollen, *Neurology*, 1996, **46**, 406-412.

8. A. J. Hanson, S. Craft and W. A. Banks, *Current Pharmaceutical Design*, 2015, **21**, 114-120.
9. L. Bertram and R. Tanzi, *Journal of Molecular Neuroscience*, 2001, **17**, 127-136.
10. L. Tai, S. Mehra, V. Shete, S. Estus, G. Rebeck, G. Bu and M. LaDu, *Molecular Neurodegeneration*, 2014, **9**, 2.
11. A. Takeda, E. Loveman, A. Clegg, J. Kirby, J. Picot, E. Payne and C. Green, *International Journal of Geriatric Psychiatry*, 2006, **21**, 17-28.
12. T. Gómez-Isla, J. L. Price, D. W. McKeel Jr., J. C. Morris, J. H. Growdon and B. T. Hyman, *The Journal of Neuroscience*, 1996, **16**, 4491-4500.
13. J. Larson, G. Lynch, D. Games and P. Seubert, *Brain Research*, 1999, **840**, 23-35.
14. P. F. Chapman, G. L. White, M. W. Jones, D. Cooper-Blacketer, V. J. Marshall, M. Irizarry, L. Younkin, M. A. Good, T. V. P. Bliss, B. T. Hyman, S. G. Younkin and K. K. Hsiao, *Nature Neuroscience*, 1999, **2**, 271-276.
15. G. M. Shankar, B. L. Bloodgood, M. Townsend, D. M. Walsh, D. J. Selkoe and B. L. Sabatini, *Journal of Neuroscience*, 2007, **27**, 2866-2875.
16. J. J. Palop and L. Mucke, *Archives of Neurology*, 2009, **66**, 435-440.
17. G. G. Glenner and C. W. Wong, *Biochemical and Biophysical Research Communications*, 1984, **122**, 1131-1135.
18. G. G. Glenner and C. W. Wong, *Biochemical and Biophysical Research Communications*, 1984, **120**, 885-890.
19. A. Goate, M.-C. Chartier-Harlin, M. Mullan, J. Brown, F. Crawford, L. Fidani, L. Giuffra, A. Haynes, N. Irving, L. James, R. Mant, P. Newton, K. Rooke, P. Roques, C. Talbot, M. Pericak-Vance, A. Roses, R. Williamson, M. Rossor, M. Owen and J. Hardy, *Nature*, 1991, **349**, 704-706.
20. E. Levy-Lahad, W. Wasco, P. Poorkaj, D. Romano, J. Oshima, W. Pettingell, C. Yu, P. Jondro, S. Schmidt, K. Wang, A. C. Crowley, Y.-H. Fu, S. Y. Guenette, D. Galas, E. Nemens, E. M. Wijsman, T. D. Bird, G. D. Schellenberg and R. E. Tanzi, *Science*, 1995, **269**, 973-977.

21. R. Sherrington, E. I. Rogaev, Y. Liang, E. A. Rogaeva, G. Levesque, M. Ikeda, H. Chi, C. Lin, G. Li, K. Holman, T. Tsuda, L. Mar, J. F. Foncin, A. C. Bruni, M. P. Montesi, S. Sorbi, I. Rainero, L. Pinessi, L. Nee, I. Chumakov, D. Pollen, A. Brookes, P. Sanseau, R. J. Polinsky, W. Wasco, H. A. R. Da Silva, J. L. Haines, M. A. Pericak-Vance, R. E. Tanzi, A. D. Roses, P. E. Fraser, J. M. Rommens and P. H. St George-Hyslop, *Nature*, 1995, **375**, 754-760.
22. D. J. Selkoe, *Neuron*, 1991, **6**, 487-498.
23. J. Hardy and D. J. Selkoe, *Science*, 2002, **297**, 353-356.
24. K. P. Kepp, *Chemical Reviews*, 2012, **112**, 5193-5239.
25. A. Rauk, *Chemical Society Reviews*, 2009, **38**, 2698-2715.
26. A. S. DeToma, S. Salamekh, A. Ramamoorthy and M. H. Lim, *Chemical Society Reviews*, 2012, **41**, 608-621.
27. B. X. Wong, A. Tsatsanis, L. Q. Lim, P. A. Adlard, A. I. Bush and J. A. Duce, *PLoS One*, 2014, **9**, e114174.
28. P. Nathalie and O. Jean-Noël, *Current Alzheimer Research*, 2008, **5**, 92-99.
29. B. Bulic, M. Pickhardt, B. Schmidt, E.-M. Mandelkow, H. Waldmann and E. Mandelkow, *Angewandte Chemie International Edition*, 2009, **48**, 1740-1752.
30. F. Gervais, R. Chalifour, D. Garceau, X. Kong, J. Laurin, J. Mclaughlin, C. Morissette and J. Paquette, *Amyloid*, 2001, **8**, 28-35.
31. P. S. Aisen, D. Saumier, R. Briand, J. Laurin, F. Gervais, P. Tremblay and D. Garceau, *Neurology*, 2006, **67**, 1757-1763.
32. C. Reitz, *International Journal of Alzheimer's Disease*, 2012, **2012**, 11.
33. http://www.alzforum.org/therapeutics/elnd005, Accessed November 2015.
34. F. Yang, G. P. Lim, A. N. Begum, O. J. Ubeda, M. R. Simmons, S. S. Ambegaokar, P. P. Chen, R. Kayed, C. G. Glabe, S. A. Frautschy and G. M. Cole, *Journal of Biological Chemistry*, 2005, **280**, 5892-5901.
35. B. B. Aggarwal, A. Kumar and A. C. Bharti, *Anticancer Research*, 2003, **23**, 363-398.
36. A. A. Reinke and J. E. Gestwicki, *Chemical Biology & Drug Design*, 2007, **70**, 206-215.
37. https://clinicaltrials.gov/ct2/show/NCT01001637, Accessed November 2015.
38. D. Yanagisawa, H. Taguchi, S. Morikawa, T. Kato, K. Hirao, N. Shirai and I. Tooyama, *Biochemistry and Biophysics Reports*, 2015, **4**, 357-368.

39. L. Fang, S. Gou, X. Liu, F. Cao and L. Cheng, *Bioorganic & Medicinal Chemistry Letters*, 2014, **24**, 40-43.
40. K. M. Nelson, J. L. Dahlin, J. Bisson, J. Graham, G. F. Pauli and M. A. Walters, *Journal of Medicinal Chemistry*, 2017, **60**, 1620-1637.
41. K. Watanabe, T. Segawa, K. Nakamura, M. Kodaka, H. Okuno and T. Konakahara, *Journal of Peptide Research*, 2001, **58**, 342-346.
42. L. O. Tjernberg, J. Näslund, F. Lindqvist, J. Johansson, A. R. Karlström, J. Thyberg, L. Terenius and C. Nordstedt, *Journal of Biological Chemistry*, 1996, **271**, 8545-8548.
43. T. Arai, T. Araya, D. Sasaki, A. Taniguchi, T. Sato, Y. Sohma and M. Kanai, *Angewandte Chemie International Edition*, 2014, **53**, 8236-8239.
44. M. Citron, *Nature Reviews Drug Discovery*, 2010, **9**, 387-398.
45. B. De Strooper, R. Vassar and T. Golde, *Nature Reviews Neurology*, 2010, **6**, 99-107.
46. T. E. Golde, L. S. Schneider and E. H. Koo, *Neuron*, 2011, **69**, 201-213.
47. C. Haass, *The EMBO Journal*, 2004, **23**, 483-488.
48. R. Olsauskas-Kuprys, A. Zlobin and C. Osipo, *OncoTargets and therapy*, 2013, **6**, 943-955.
49. A. K. Ghosh, M. Brindisi and J. Tang, *Journal of Neurochemistry*, 2012, **120**, 71-83.
50. O. Descamps, P. Spilman, Q. Zhang, C. P. Libeu, K. Poksay, O. Gorostiza, J. Campagna, B. Jagodzinska, D. E. Bredesen and V. John, *Journal of Alzheimer's Disease*, 2013, **37**, 343-355.
51. S. Sinha, J. P. Anderson, R. Barbour, G. S. Basi, R. Caccavello, D. Davis, M. Doan, H. F. Dovey, N. Frigon, J. Hong, K. Jacobson-Croak, N. Jewett, P. Keim, J. Knops, I. Lieberburg, M. Power, H. Tan, G. Tatsuno, J. Tung, D. Schenk, P. Seubert, S. M. Suomensaari, S. Wang, D. Walker, J. Zhao, L. McConlogue and V. John, *Nature*, 1999, **402**, 537-540.
52. L. Hong, G. Koelsch, X. Lin, S. Wu, S. Terzyan, A. K. Ghosh, X. C. Zhang and J. Tang, *Science*, 2000, **290**, 150-153.
53. R. K. Hom, L. Y. Fang, S. Mamo, J. S. Tung, A. C. Guinn, D. E. Walker, D. L. Davis, A. F. Gailunas, E. D. Thorsett, S. Sinha, J. E. Knops, N. E. Jewett, J. P. Anderson and V. John, *Journal of Medicinal Chemistry*, 2003, **46**, 1799-1802.

54. M. Bäck, J. Nyhlén, I. Kvarnström, S. Appelgren, N. Borkakoti, K. Jansson, J. Lindberg, S. Nyström, A. Hallberg, Å. Rosenquist and B. Samuelsson, *Bioorganic & Medicinal Chemistry*, 2008, **16**, 9471-9486.

55. J. N. Cumming, T. X. Le, S. Babu, C. Carroll, X. Chen, L. Favreau, P. Gaspari, T. Guo, D. W. Hobbs, Y. Huang, U. Iserloh, M. E. Kennedy, R. Kuvelkar, G. Li, J. Lowrie, N. A. McHugh, L. Ozgur, J. Pan, E. M. Parker, K. Saionz, A. W. Stamford, C. Strickland, D. Tadesse, J. Voigt, L. Wang, Y. Wu, L. Zhang and Q. Zhang, *Bioorganic & Medicinal Chemistry Letters*, 2008, **18**, 3236-3241.

56. Y.-S. Wang, C. Strickland, J. H. Voigt, M. E. Kennedy, B. M. Beyer, M. M. Senior, E. M. Smith, T. L. Nechuta, V. S. Madison, M. Czarniecki, B. A. McKittrick, A. W. Stamford, E. M. Parker, J. C. Hunter, W. J. Greenlee and D. F. Wyss, *Journal of Medicinal Chemistry*, 2010, **53**, 942-950.

57. Z. Zhu, Z.-Y. Sun, Y. Ye, J. Voigt, C. Strickland, E. M. Smith, J. Cumming, L. Wang, J. Wong, Y.-S. Wang, D. F. Wyss, X. Chen, R. Kuvelkar, M. E. Kennedy, L. Favreau, E. Parker, B. A. McKittrick, A. Stamford, M. Czarniecki, W. Greenlee and J. C. Hunter, *Journal of Medicinal Chemistry*, 2010, **53**, 951-965.

58. S. Geschwindner, L.-L. Olsson, J. S. Albert, J. Deinum, P. D. Edwards, T. de Beer and R. H. A. Folmer, *Journal of Medicinal Chemistry*, 2007, **50**, 5903-5911.

59. A. Stamford and C. Strickland, *Current Opinion in Chemical Biology*, 2013, **17**, 320-328.

60. C. W. Murray, O. Callaghan, G. Chessari, A. Cleasby, M. Congreve, M. Frederickson, M. J. Hartshorn, R. McMenamin, S. Patel and N. Wallis, *Journal of Medicinal Chemistry*, 2007, **50**, 1116-1123.

61. P. C. May, R. A. Dean, S. L. Lowe, F. Martenyi, S. M. Sheehan, L. N. Boggs, S. A. Monk, B. M. Mathes, D. J. Mergott, B. M. Watson, S. L. Stout, D. E. Timm, E. Smith LaBell, C. R. Gonzales, M. Nakano, S. S. Jhee, M. Yen, L. Ereshefsky, T. D. Lindstrom, D. O. Calligaro, P. J. Cocke, D. Greg Hall, S. Friedrich, M. Citron and J. E. Audia, *Journal of Neuroscience*, 2011, **31**, 16507-16516.

62. I. V. Efremov, F. F. Vajdos, K. A. Borzilleri, S. Capetta, H. Chen, P. H. Dorff, J. K. Dutra, S. W. Goldstein, M. Mansour, A. McColl, S. Noell, C. E. Oborski, T. N. O'Connell, T. J. O'Sullivan, J. Pandit, H. Wang, B. Wei and J. M. Withka, *Journal of Medicinal Chemistry*, 2012, **55**, 9069-9088.

63. J. Madden, J. R. Dod, R. Godemann, J. Kraemer, M. Smith, M. Biniszkiewicz, D. J. Hallett, J. Barker, J. D. Dyekjaer and T. Hesterkamp, *Bioorganic & Medicinal Chemistry Letters*, 2010, **20**, 5329-5333.

64. S. W. Gerritz, W. Zhai, S. Shi, S. Zhu, J. H. Toyn, J. E. Meredith, L. G. Iben, C. R. Burton, C. F. Albright, A. C. Good, A. J. Tebben, J. K. Muckelbauer, D. M. Camac, W. Metzler, L. S. Cook, R. Padmanabha, K. A. Lentz, M. J. Sofia, M. A. Poss, J. E. Macor and L. A. Thompson, *Journal of Medicinal Chemistry*, 2012, **55**, 9208-9223.

65. J. B. Jordan, L. Poppe, X. Xia, A. C. Cheng, Y. Sun, K. Michelsen, H. Eastwood, P. D. Schnier, T. Nixey and W. Zhong, *Journal of Medicinal Chemistry*, 2012, **55**, 678-687.

66. A. A. Thomas, K. W. Hunt, B. Newhouse, R. J. Watts, X. Liu, G. Vigers, D. Smith, S. P. Rhodes, K. D. Brown, J. N. Otten, M. Burkard, A. A. Cox, M. K. Geck Do, D. Dutcher, S. Rana, R. K. DeLisle, K. Regal, A. D. Wright, R. Groneberg, J. Liao, K. Scearce-Levie, M. Siu, H. E. Purkey and J. P. Lyssikatos, *Journal of Medicinal Chemistry*, 2014, **57**, 10112-10129.

67. P. Shah and A. D. Westwell, *Journal of Enzyme Inhibition and Medicinal Chemistry*, 2007, **22**, 527-540.

68. J. E. Audia, D. J. Mergott, S. M. Sheehan and B. M. Watson, Patent: US 2009/275566 A1, 2009.

69. D. Oehlrich, H. Prokopcova and H. J. M. Gijsen, *Bioorganic & Medicinal Chemistry Letters*, 2014, **24**, 2033-2045.

70. B.-M. Swahn, J. Holenz, J. Kihlström, K. Kolmodin, J. Lindström, N. Plobeck, D. Rotticci, F. Sehgelmeble, M. Sundström, S. v. Berg, J. Fälting, B. Georgievska, S. Gustavsson, J. Neelissen, M. Ek, L.-L. Olsson and S. Berg, *Bioorganic & Medicinal Chemistry Letters*, 2012, **22**, 1854-1859.

71. C. R. Butler, M. A. Brodney, E. M. Beck, G. Barreiro, C. E. Nolan, F. Pan, F. Vajdos, K. Parris, A. H. Varghese, C. J. Helal, R. Lira, S. D. Doran, D. R. Riddell, L. M. Buzon, J. K. Dutra, L. A. Martinez-Alsina, K. Ogilvie, J. C. Murray, J. M. Young, K. Atchison, A. Robshaw, C. Gonzales, J. Wang, Y. Zhang and B. T. O'Neill, *Journal of Medicinal Chemistry*, 2015, **58**, 2678-2702.

72. H. F. Dovey, V. John, J. P. Anderson, L. Z. Chen, P. De Saint Andrieu, L. Y. Fang, S. B. Freedman, B. Folmer, E. Goldbach, E. J. Holsztynska, K. L. Hu, K. L. Johnson-Wood, S.

L. Kennedy, D. Kholodenko, J. E. Knops, L. H. Latimer, M. Lee, Z. Liao, I. M. Lieberburg, R. N. Motter, L. C. Mutter, J. Nietz, K. P. Quinn, K. L. Sacchi, P. A. Seubert, G. M. Shopp, E. D. Thorsett, J. S. Tung, J. Wu, S. Yang, C. T. Yin, D. B. Schenk, P. C. May, L. D. Altstiel, M. H. Bender, L. N. Boggs, T. C. Britton, J. C. Clemens, D. L. Czilli, D. K. Dieckman-McGinty, J. J. Droste, K. S. Fuson, B. D. Gitter, P. A. Hyslop, E. M. Johnstone, W. Y. Li, S. P. Little, T. E. Mabry, F. D. Miller, B. Ni, J. S. Nissen, W. J. Porter, B. D. Potts, J. K. Reel, D. Stephenson, Y. Su, L. A. Shipley, C. A. Whitesitt, T. Yin and J. E. Audia, *Journal of Neurochemistry*, 2001, **76**, 173-181.

73. M. Wolfe, *Neurotherapeutics*, 2008, **5**, 391-398.

74. T. A. Lanz, C. S. Himes, G. Pallante, L. Adams, S. Yamazaki, B. Amore and K. M. Merchant, *Journal of Pharmacology and Experimental Therapeutics*, 2003, **305**, 864-871.

75. M. A. Brodney, D. D. Auperin, S. L. Becker, B. S. Bronk, T. M. Brown, K. J. Coffman, J. E. Finley, C. D. Hicks, M. J. Karmilowicz, T. A. Lanz, D. Liston, X. Liu, B.-A. Martin, R. B. Nelson, C. E. Nolan, C. E. Oborski, C. P. Parker, K. E. G. Richter, N. Pozdnyakov, B. G. Sahagan, J. B. Schachter, S. A. Sokolowski, B. Tate, J. W. Van Deusen, D. E. Wood and K. M. Wood, *Bioorganic & Medicinal Chemistry Letters*, 2011, **21**, 2631-2636.

76. B. P. Imbimbo, *Drug Discovery Today: Therapeutic Strategies*, 2008, **5**, 169-175.

77. R. S. Doody, R. Raman, M. Farlow, T. Iwatsubo, B. Vellas, S. Joffe, K. Kieburtz, F. He, X. Sun, R. G. Thomas, P. S. Aisen, E. Siemers, G. Sethuraman and R. Mohs, *New England Journal of Medicine*, 2013, **369**, 341-350.

78. J.-U. Peters, G. Galley, H. Jacobsen, C. Czech, P. David-Pierson, E. A. Kitas and L. Ozmen, *Bioorganic & Medicinal Chemistry Letters*, 2007, **17**, 5918-5923.

79. A. F. Kreft, R. Martone and A. Porte, *Journal of Medicinal Chemistry*, 2009, **52**, 6169-6188.

80. I. Churcher, K. Ashton, J. W. Butcher, E. E. Clarke, T. Harrison, H. D. Lewis, A. P. Owens, M. R. Teall, S. Williams and J. D. J. Wrigley, *Bioorganic & Medicinal Chemistry Letters*, 2003, **13**, 179-183.

81. A. R. Keerti, B. A. Kumar, T. Parthasarathy and V. Uma, *Bioorganic & Medicinal Chemistry*, 2005, **13**, 1873-1878.

82. I. Churcher, S. Williams, S. Kerrad, T. Harrison, J. L. Castro, M. S. Shearman, H. D. Lewis, E. E. Clarke, J. D. J. Wrigley, D. Beher, Y. S. Tang and W. Liu, *Journal of Medicinal Chemistry*, 2003, **46**, 2275-2278.

83. M. F. Parker, D. M. Barten, C. P. Bergstrom, J. J. Bronson, J. A. Corsa, M. S. Deshpande, K. M. Felsenstein, V. L. Guss, S. B. Hansel, G. Johnson, D. J. Keavy, W. Y. Lau, J. Mock, C. V. C. Prasad, C. T. Polson, C. P. Sloan, D. W. Smith, O. B. Wallace, H. H. Wang, A. Williams and M. Zheng, *Bioorganic & Medicinal Chemistry Letters*, 2007, **17**, 4432-4436.

84. C. P. Bergstrom, C. P. Sloan, H. H. Wang, M. F. Parker, D. W. Smith, M. Zheng, S. B. Hansel, C. T. Polson, L. E. Barber, I. Bursuker, V. L. Guss, J. A. Corsa, D. M. Barten, K. M. Felsenstein and S. B. Roberts, *Bioorganic & Medicinal Chemistry Letters*, 2008, **18**, 175-178.

85. S. C. Mayer, A. F. Kreft, B. Harrison, M. Abou-Gharbia, M. Antane, S. Aschmies, K. Atchison, M. Chlenov, D. C. Cole, T. Comery, G. Diamantidis, J. Ellingboe, K. Fan, R. Galante, C. Gonzales, D. M. Ho, M. E. Hoke, Y. Hu, D. Huryn, U. Jain, M. Jin, K. Kremer, D. Kubrak, M. Lin, P. Lu, R. Magolda, R. Martone, W. Moore, A. Oganesian, M. N. Pangalos, A. Porte, P. Reinhart, L. Resnick, D. R. Riddell, J. Sonnenberg-Reines, J. R. Stock, S.-C. Sun, E. Wagner, T. Wang, K. Woller, Z. Xu, M. M. Zaleska, J. Zeldis, M. Zhang, H. Zhou and J. S. Jacobsen, *Journal of Medicinal Chemistry*, 2008, **51**, 7348-7351.

86. C. R. Hopkins, *ACS Chemical Neuroscience*, 2012, **3**, 3-4.

87. K. W. Gillman, J. E. Starrett, M. F. Parker, K. Xie, J. J. Bronson, L. R. Marcin, K. E. McElhone, C. P. Bergstrom, R. A. Mate, R. Williams, J. E. Meredith, C. R. Burton, D. M. Barten, J. H. Toyn, S. B. Roberts, K. A. Lentz, J. G. Houston, R. Zaczek, C. F. Albright, C. P. Decicco, J. E. Macor and R. E. Olson, *ACS Medicinal Chemistry Letters*, 2010, **1**, 120-124.

88. L. Ghezzi, E. Scarpini and D. Galimberti, *Drug Design, Development and Therapy*, 2013, **7**, 1471-1479.

89. V. Coric, C. H. van Dyck, S. Salloway, N. Andreasen, M. Brody, R. W. Richter, H. Soininen, S. Thein, T. Shiovitz, G. Pilcher, S. Colby, L. Rollin, R. Dockens, C. Pachai, E.

Portelius, U. Andreasson, K. Blennow, H. Soares, C. Albright, H. H. Feldman and R. Berman, *Archives of Neurology*, 2012, **69**, 1430-1440.

90. I. Churcher, D. Beher, J. D. Best, J. L. Castro, E. E. Clarke, A. Gentry, T. Harrison, L. Hitzel, E. Kay, S. Kerrad, H. D. Lewis, P. Morentin-Gutierrez, R. Mortishire-Smith, P. J. Oakley, M. Reilly, D. E. Shaw, M. S. Shearman, M. R. Teall, S. Williams and J. D. J. Wrigley, *Bioorganic & Medicinal Chemistry Letters*, 2006, **16**, 280-284.
91. J. Lee, L. Song, G. Terracina, T. Bara, H. Josien, T. Asberom, T. K. Sasikumar, D. A. Burnett, J. Clader, E. M. Parker and L. Zhang, *Biochemistry*, 2011, **50**, 4973-4980.
92. J. D. Best, D. W. Smith, M. A. Reilly, R. O'Donnell, H. D. Lewis, S. Ellis, N. Wilkie, T. W. Rosahl, P. A. Laroque, C. Boussiquet-Leroux, I. Churcher, J. R. Atack, T. Harrison and M. S. Shearman, *Journal of Pharmacology and Experimental Therapeutics*, 2007, **320**, 552-558.
93. R. Xu, D. Cole, T. Asberom, T. Bara, C. Bennett, D. A. Burnett, J. Clader, M. Domalski, W. Greenlee, L. Hyde, H. Josien, H. Li, M. McBriar, B. McKittrick, A. T. McPhail, D. Pissarnitski, L. Qiang, M. Rajagopalan, T. Sasikumar, J. Su, H. Tang, W.-L. Wu, L. Zhang and Z. Zhao, *Bioorganic & Medicinal Chemistry Letters*, 2010, **20**, 2591-2596.
94. T. K. Sasikumar, L. Qiang, D. A. Burnett, D. Cole, R. Xu, H. Li, W. J. Greenlee, J. Clader, L. Zhang and L. Hyde, *Bioorganic & Medicinal Chemistry Letters*, 2010, **20**, 3632-3635.
95. Z. Zhao, D. A. Pissarnitski, H. B. Josien, W.-L. Wu, R. Xu, H. Li, J. W. Clader, D. A. Burnett, G. Terracina, L. Hyde, J. Lee, L. Song, L. Zhang and E. M. Parker, *Journal of Medicinal Chemistry*, 2015, **58**, 8806-8817.
96. S. Weggen, J. L. Eriksen, P. Das, S. A. Sagi, R. Wang, C. U. Pietrzik, K. A. Findlay, T. E. Smith, M. P. Murphy, T. Bulter, D. E. Kang, N. Marquez-Sterling, T. E. Golde and E. H. Koo, *Nature*, 2001, **414**, 212-216.
97. J. L. Eriksen, S. A. Sagi, T. E. Smith, S. Weggen, P. Das, D. C. McLendon, V. V. Ozols, K. W. Jessing, K. H. Zavitz, E. H. Koo and T. E. Golde, *Journal of Clinical Investigation*, **112**, 440-449.
98. G. K. Wilcock, S. E. Black, S. B. Hendrix, K. H. Zavitz, E. A. Swabb and M. A. Laughlin, *The Lancet Neurology*, **7**, 483-493.

99. R. C. Green, L. S. Schneider, D. A. Amato, A. P. Beelen, G. Wilcock, E. A. Swabb and K. H. Zavitz, *JAMA*, 2009, **302**, 2557-2564.

100. Y. Takahashi, I. Hayashi, Y. Tominari, K. Rikimaru, Y. Morohashi, T. Kan, H. Natsugari, T. Fukuyama, T. Tomita and T. Iwatsubo, *Journal of Biological Chemistry*, 2003, **278**, 18664-18670.

101. D. Beher, E. E. Clarke, J. D. J. Wrigley, A. C. L. Martin, A. Nadin, I. Churcher and M. S. Shearman, *Journal of Biological Chemistry*, 2004, **279**, 43419-43426.

102. I. Peretto, S. Radaelli, C. Parini, M. Zandi, L. F. Raveglia, G. Dondio, L. Fontanella, P. Misiano, C. Bigogno, A. Rizzi, B. Riccardi, M. Biscaioli, S. Marchetti, P. Puccini, S. Catinella, I. Rondelli, V. Cenacchi, P. T. Bolzoni, P. Caruso, G. Villetti, F. Facchinetti, E. Del Giudice, N. Moretto and B. P. Imbimbo, *Journal of Medicinal Chemistry*, 2005, **48**, 5705-5720.

103. B. P. Imbimbo, E. Del Giudice, V. Cenacchi, R. Volta, G. Villetti, F. Facchinetti, B. Riccardi, P. Puccini, N. Moretto, F. Grassi, S. Ottonello and A. Leon, *Pharmacological Research*, 2007, **55**, 318-328.

104. A. Hall, R. L. Elliott, G. M. P. Giblin, I. Hussain, J. Musgrave, A. Naylor, R. Sasse and B. Smith, *Bioorganic & Medicinal Chemistry Letters*, 2010, **20**, 1306-1311.

105. M. G. Stanton, J. Hubbs, D. Sloman, C. Hamblett, P. Andrade, M. Angagaw, G. Bi, R. M. Black, J. Crispino, J. C. Cruz, E. Fan, G. Farris, B. L. Hughes, C. M. Kenific, R. E. Middleton, G. Nikov, P. Sajonz, S. Shah, N. Shomer, A. A. Szewczak, F. Tanga, M. T. Tudge, M. Shearman and B. Munoz, *Bioorganic & Medicinal Chemistry Letters*, 2010, **20**, 755-758.

106. Kimura, T., Kawano, K., Doi, E., Kitazawa, N., Shin, K., Miyagawa, T., Kaneko, T., Ito, K., Takaishi, M., Sasaki, T., Patent WO2005115990 A1, 2005.

107. Kimura, T., Kawano, K., Doi, E., Kitazawa, N., Takaishi, M., Ito, K., Kaneko, T., Sasaki, T., Sato, N., Miyagawa, T., Patent US20070117798 A1, 2007.

108. Kimura, T., Kawano, K., Doi, E., Kitazawa, N., Takaishi, M., Ito, K., Kaneko, T., Sasaki, T., Miyagawa, T., Hagiwara, H., Patent US20070117839 A1, 2007.

109. Kimura, T., Kawano, K., Doi, E., Kitazawa, N., Miyagawa, T., Sato, N., Kaneko, T., Shin, K., Ito, K., Takaishi, M., Patent WO2007135970 A1, 2007.

110. Kushida, I., Doi, E., Ito, K., Nakamura, T., Patent WO2007058304 A1, 2007.

111. Shimomura, N., Sato, N., Kaneko, T., Takaishi, M., Wakasugi, K., Yoshikawa, S., Nishikawa, Y., Nakamura, T., Hukuyama, T., Patent WO2007058305 A1, 2007.

112. Shimomura, N., Yoshikawa, S., Hisatake, Y., Imai, A., Patent WO2008140111 A1, 2008.

113. Kushida, I., Sato, N., Sato, Y., Patent WO2009096349 A1, 2009.

114. T. Hashimoto, A. Ishibashi, H. Hagiwara, Y. Murata, O. Takenaka and T. Miyagawa, *Alzheimer's & Dementia*, 2010, **6**, S242.

115. M. Pettersson, D. S. Johnson, C. Subramanyam, K. R. Bales, C. W. am Ende, B. A. Fish, M. E. Green, G. W. Kauffman, R. Lira, P. B. Mullins, T. Navaratnam, S. M. Sakya, C. M. Stiff, T. P. Tran, B. C. Vetelino, L. Xie, L. Zhang, L. R. Pustilnik, K. M. Wood and C. J. O'Donnell, *Bioorganic & Medicinal Chemistry Letters*, 2012, **22**, 2906-2911.

116. M. Pettersson, D. S. Johnson, C. Subramanyam, K. R. Bales, C. W. am Ende, B. A. Fish, M. E. Green, G. W. Kauffman, P. B. Mullins, T. Navaratnam, S. M. Sakya, C. M. Stiff, T. P. Tran, L. Xie, L. Zhang, L. R. Pustilnik, B. C. Vetelino, K. M. Wood, N. Pozdnyakov, P. R. Verhoest and C. J. O'Donnell, *Journal of Medicinal Chemistry*, 2014, **57**, 1046-1062.

117. M. Pettersson, D. S. Johnson, J. M. Humphrey, T. W. Butler, C. W. am Ende, B. A. Fish, M. E. Green, G. W. Kauffman, P. B. Mullins, C. J. O'Donnell, A. F. Stepan, C. M. Stiff, C. Subramanyam, T. P. Tran, B. C. Vetelino, E. Yang, L. Xie, K. R. Bales, L. R. Pustilnik, S. J. Steyn, K. M. Wood and P. R. Verhoest, *ACS Medicinal Chemistry Letters*, 2015, **6**, 596-601.

118. E. Karran, M. Mercken and B. D. Strooper, *Nature Review Drug Discovery*, 2011, **10**, 698-712.

119. J. L. Cummings, T. Morstorf and K. Zhong, *Alzheimer's Research & Therapy*, 2014, **6**, 1-7.

120. C. R. Jack Jr, D. S. Knopman, W. J. Jagust, L. M. Shaw, P. S. Aisen, M. W. Weiner, R. C. Petersen and J. Q. Trojanowski, *The Lancet Neurology*, 2010, **9**, 119-128.

121. A. I. Bush and R. E. Tanzi, *Neurotherapeutics*, 2008, **5**, 421-432.

122. M. A. Smith, K. Wehr, P. L. R. Harris, S. L. Siedlak, J. R. Connor and G. Perry, *Brain Research*, 1998, **788**, 232-236.

123. M. A. Lovell, J. D. Robertson, W. J. Teesdale, J. L. Campbell and W. R. Markesbery, *Journal of the Neurological Sciences*, 1998, **158**, 47-52.

124. M. G. Savelieff, A. S. DeToma, J. S. Derrick and M. H. Lim, *Accounts of Chemical Research*, 2014, **47**, 2475-2482.
125. H. J. Lee, K. J. Korshavn, A. Kochi, J. S. Derrick and M. H. Lim, *Chemical Society Reviews*, 2014, **43**, 6672-6682.
126. K. Leuner, W. E. Müller and A. S. Reichert, *Molecular Neurobiology*, 2012, **46**, 186-193.
127. M. Calkins, M. Manczak and P. Reddy, *Pharmaceuticals*, 2012, **5**, 1103-1119.
128. R. H. Swerdlow, *Biochimica et Biophysica Acta (BBA) - Molecular Basis of Disease*, 2011, **1812**, 1630-1639.
129. L. Pagani and A. Eckert, *International Journal of Alzheimer's Disease*, 2011, Article ID 925050.
130. P. Faller and C. Hureau, *Chemistry – A European Journal*, 2012, **18**, 15910-15920.
131. I. Shcherbatykh and D. O. Carpenter, *Journal of Alzheimer's Disease*, 2007, **11**, 191-205.
132. P. J. Crouch, M. S. Savva, L. W. Hung, P. S. Donnelly, A. I. Mot, S. J. Parker, M. A. Greenough, I. Volitakis, P. A. Adlard, R. A. Cherny, C. L. Masters, A. I. Bush, K. J. Barnham and A. R. White, *Journal of Neurochemistry*, 2011, **119**, 220-230.
133. C. J. Maynard, A. I. Bush, C. L. Masters, R. Cappai and Q.-X. Li, *International Journal of Experimental Pathology*, 2005, **86**, 147-159.
134. P. Zatta, D. Drago, S. Bolognin and S. L. Sensi, *Trends in Pharmacological Sciences*, 2009, **30**, 346-355.
135. J. J. R. Frausto Da Silva and R. J. P. Williams, *The Biological Chemistry of the Elements*, Oxford University Press, Oxford, 2001.
136. P. de Bie, P. Muller, C. Wijmenga and L. W. J. Klomp, *J. Med. Genet.*, 2007, **44**, 673.
137. O. Weinreb, T. Amit and M. B. H. Youdim, *Nutrition and Aging*, 2012, **1**, 27-39.
138. K. A. McCall, C.-c. Huang and C. A. Fierke, *The Journal of Nutrition*, 2000, **130**, 1437S-1446S.
139. D. J. Thiele, *Nucleic Acids Research*, 1992, **20**, 1183-1191.
140. R. Meneghini, *Free Radical Biology and Medicine*, 1997, **23**, 783-792.
141. T. G. Smart, A. M. Hosie and P. S. Miller, *The Neuroscientist*, 2004, **10**, 432-442.
142. M. A. Smith, P. L. R. Harris, L. M. Sayre and G. Perry, *Proceedings of the National Academy of Sciences*, 1997, **94**, 9866-9868.

143. Y. H. Hung, A. I. Bush and R. A. Cherny, *Journal of Biological Inorganic Chemistry*, 2010, **15**, 61-76.
144. M. A. Lovell, *Journal of Alzheimer's Disease*, 2009, **16**, 471-483.
145. A. I. Bush, W. H. Pettingell, G. Multhaup, M. dParadis, J. P. Vonsattel, J. F. Gusella, K. Beyreuther, C. L. Masters and R. E. Tanzi, *Science*, 1994, **265**, 1464.
146. B. R. Roberts, T. M. Ryan, A. I. Bush, C. L. Masters and J. A. Duce, *Journal of Neurochemistry*, 2012, **120**, 149-166.
147. M. P. Cuajungco, L. E. Goldstein, A. Nunomura, M. A. Smith, J. T. Lim, C. S. Atwood, X. Huang, Y. W. Farrag, G. Perry and A. I. Bush, *Journal of Biological Chemistry*, 2000, **275**, 19439-19442.
148. E. Gaggelli, H. Kozlowski, D. Valensin and G. Valensin, *Chemical Reviews*, 2006, **106**, 1995-2044.
149. A. D. Watt, V. L. Villemagne and K. J. Barnham, *Journal of Alzheimer's Disease*, 2013, **33**, S283-S293.
150. R. D. Terry, *Journal of Neuropathology & Experimental Neurology*, 1996, **55**, 1023-1025.
151. K.-H. Cheung, D. Shineman, M. Müller, C. Cárdenas, L. Mei, J. Yang, T. Tomita, T. Iwatsubo, V. M. Y. Lee and J. K. Foskett, *Neuron*, 2008, **58**, 871-883.
152. S. Chakroborty and G. E. Stutzmann, *Science China Life Sciences*, 2011, **54**, 752-762.
153. M. P. Mattson and S. L. Chan, *Cell Calcium*, 2003, **34**, 385-397.
154. S. Chakroborty and G. E. Stutzmann, *European Journal of Pharmacology*, 2014, **739**, 83-95.
155. D. E. Bredesen, R. V. Rao and P. Mehlen, *Nature*, 2006, **443**, 796-802.
156. J. Avila, *Nature Reviews Neurology*, 2010, **6**, 587-588.
157. T. J. A. Craddock, J. A. Tuszynski, D. Chopra, N. Casey, L. E. Goldstein, S. R. Hameroff and R. E. Tanzi, *PLoS One*, 2012, **7**, e33552.
158. A. Budimir, *Acta Pharmaceutica*, 2011, **61**, 1-14.
159. M. A. Santos, K. Chand and S. Chaves, *Coordination Chemistry Reviews*, 2016, **327-328**, 287-303.
160. D. R. C. McLachlan, T. P. A. Kruck, W. Kalow, D. F. Andrews, A. J. Dalton, M. Y. Bell and W. L. Smith, *The Lancet*, 1991, **337**, 1304-1308.

161. R. A. Cherny, J. T. Legg, C. A. McLean, D. P. Fairlie, X. Huang, C. S. Atwood, K. Beyreuther, R. E. Tanzi, C. L. Masters and A. I. Bush, *Journal of Biological Chemistry*, 1999, **274**, 23223-23228.

162. D. Valensin, C. Gabbiani and L. Messori, *Coordination Chemistry Reviews*, 2012, **256**, 2357-2366.

163. K. J. Barnham, V. B. Kenche, G. D. Ciccotosto, D. P. Smith, D. J. Tew, X. Liu, K. Perez, G. A. Cranston, T. J. Johanssen, I. Volitakis, A. I. Bush, C. L. Masters, A. R. White, J. P. Smith, R. A. Cherny and R. Cappai, *Proceedings of the National Academy of Sciences*, 2008, **105**, 6813-6818.

164. D. Valensin, P. Anzini, E. Gaggelli, N. Gaggelli, G. Tamasi, R. Cini, C. Gabbiani, E. Michelucci, L. Messori, H. Kozlowski and G. Valensin, *Inorganic Chemistry*, 2010, **49**, 4720-4722.

165. D. L. Carlson, D. H. Huchital, E. J. Mantilla, R. D. Sheardy and W. R. Murphy, *Journal of the American Chemical Society*, 1993, **115**, 6424-6425.

166. A. Kumar, L. Moody, J. F. Olaivar, N. A. Lewis, R. L. Khade, A. A. Holder, Y. Zhang and V. Rangachari, *ACS Chemical Neuroscience*, 2010, **1**, 691-701.

167. Z. Fang, S. Swavey, A. Holder, B. Winkel and K. J. Brewer, *Inorganic Chemistry Communications*, 2002, **5**, 1078-1081.

168. R. L. Williams, H. N. Toft, B. Winkel and K. J. Brewer, *Inorganic Chemistry*, 2003, **42**, 4394-4400.

169. D.-L. Ma, W.-L. Wong, W.-H. Chung, F.-Y. Chan, P.-K. So, T.-S. Lai, Z.-Y. Zhou, Y.-C. Leung and K.-Y. Wong, *Angewandte Chemie International Edition*, 2008, **47**, 3735-3739.

170. B. Y.-W. Man, H.-M. Chan, C.-H. Leung, D. S.-H. Chan, L.-P. Bai, Z.-H. Jiang, H.-W. Li and D.-L. Ma, *Chemical Science*, 2011, **2**, 917-921.

171. D. J. Hayne, S. Lim and P. S. Donnelly, *Chemical Society Reviews*, 2014, **43**, 6701-6715.

172. V. B. Kenche, L. W. Hung, K. Perez, I. Volitakes, G. Ciccotosto, J. Kwok, N. Critch, N. Sherratt, M. Cortes, V. Lal, C. L. Masters, K. Murakami, R. Cappai, P. A. Adlard and K. J. Barnham, *Angewandte Chemie International Edition*, 2013, **52**, 3374-3378.

173. G. Doshi, G. Sonpavde and C. N. Sternberg, *Expert Opinion on Drug Metabolism & Toxicology*, 2012, **8**, 103-111.

174. X. Mao and A. D. Schimmer, *Toxicology Letters*, 2008, **182**, 1-6.
175. R. A. Cherny, C. S. Atwood, M. E. Xilinas, D. N. Gray, W. D. Jones, C. A. McLean, K. J. Barnham, I. Volitakis, F. W. Fraser, Y.-S. Kim, X. Huang, L. E. Goldstein, R. D. Moir, J. T. Lim, K. Beyreuther, H. Zheng, R. E. Tanzi, C. L. Masters and A. I. Bush, *Neuron*, 2001, **30**, 665-676.
176. G. K. Gouras and M. F. Beal, *Neuron*, 2001, **30**, 641-642.
177. http://www.alzforum.org/news/research-news/pbt2-takes-dive-phase-2-alzheimers-trial, Accessed 12/9/2016.
178. L. M. F. Gomes, R. P. Vieira, M. R. Jones, M. C. P. Wang, C. Dyrager, E. M. Souza-Fagundes, J. G. Da Silva, T. Storr and H. Beraldo, *Journal of Inorganic Biochemistry*, 2014, **139**, 106-116.
179. F. Hirayama and K. Uekama, *Advanced Drug Delivery Reviews*, 1999, **36**, 125-141.
180. D. La Mendola, S. Sortino, G. Vecchio and E. Rizzarelli, *Helvetica Chimica Acta*, 2002, **85**, 1633-1643.
181. V. Oliveri, A. Puglisi, M. Viale, C. Aiello, C. Sgarlata, G. Vecchio, J. Clarke, J. Milton and J. Spencer, *Chemistry – A European Journal*, 2013, **19**, 13946-13955.
182. V. Oliveri, G. I. Grasso, F. Bellia, F. Attanasio, M. Viale and G. Vecchio, *Inorganic Chemistry*, 2015, **54**, 2591-2602.
183. S. Saharan and P. K. Mandal, *Journal of Alzheimer's Disease*, 2014, **40**, 519-529.
184. I. Cacciatore, C. Cornacchia, E. Fornasari, L. Baldassarre, F. Pinnen, P. Sozio, A. Di Stefano, L. Marinelli, A. Dean, S. Fulle, E. S. Di Filippo, R. M. L. La Rovere, A. Patruno, A. Ferrone and V. Di Marco, *ChemMedChem*, 2013, **8**, 1818-1829.
185. B. N. Ramesh, T. S. S. Rao, A. Prakasam, K. Sambamurti and K. S. J. Rao, *Journal of Alzheimer's Disease*, 2010, **19**, 1123-1139.
186. M.-J. R. Howes and E. Perry, *Drugs & Aging*, 2011, **28**, 439-468.
187. E. Perry and M.-J. R. Howes, *CNS Neuroscience & Therapeutics*, 2011, **17**, 683-698.
188. C. Shi, S. Xiao, J. Liu, K. Guo, F. Wu, D. T. Yew and J. Xu, *Platelets*, 2010, **21**, 373-379.
189. J. Birks and J. Grimley Evans, *Cochrane Database of Systematic Reviews*, 2002, **4**, Article No.: CD003120.

190. J. Birks and J. Grimley Evans, *Cochrane Database of Systematic Reviews*, 2009, **1**, Article No.: CD003120.
191. P. Williams, A. Sorribas and M.-J. R. Howes, *Natural Product Reports*, 2011, **28**, 48-77.
192. S. Ghosh, S. Banerjee and P. C. Sil, *Food and Chemical Toxicology*, 2015, **83**, 111-124.
193. R. Hardeland, D. P. Cardinali, G. M. Brown and S. R. Pandi-Perumal, *Progress in Neurobiology*, 2015, **127–128**, 46-63.
194. J. Larson, R. E. Jessen, T. Uz, A. D. Arslan, M. Kurtuncu, M. Imbesi and H. Manev, *Neuroscience Letters*, 2006, **393**, 23-26.
195. J. M. Olcese, C. Cao, T. Mori, M. B. Mamcarz, A. Maxwell, M. J. Runfeldt, L. Wang, C. Zhang, X. Lin, G. Zhang and G. W. Arendash, *Journal of Pineal Research*, 2009, **47**, 82-96.
196. Q. Liu, J.-P. Kou and B.-Y. Yu, *Neurochemistry International*, 2011, **58**, 119-125.
197. W. Yue-Hua and D. Guan-Hua, *Journal of Asian Natural Products Research*, 2009, **11**, 604-612.
198. S. Y. Lee, T. Y. Ha, D. J. Son, S. R. Kim and J. T. Hong, *Neuroscience Research*, 2005, **52**, 330-341.
199. M. Y. Um, J. Y. Ahn, S. Kim, M. K. Kim and T. Y. Ha, *Biological and Pharmaceutical Bulletin*, 2009, **32**, 1516-1520.
200. C. Haass and D. J. Selkoe, *Nature Reviews Molecular Cell Biology*, 2007, **8**, 101-112.
201. I. Grundke-Iqbal, K. Iqbal, Y. C. Tung, M. Quinlan, H. M. Wisniewski and L. I. Binder, *Proceedings of the National Academy of Sciences*, 1986, **83**, 4913-4917.
202. K. S. Kosik, C. L. Joachim and D. J. Selkoe, *Proceedings of the National Academy of Sciences*, 1986, **83**, 4044-4048.
203. K. Iqbal, T. Zaidi, G. Wen, I. Grundke-Iqbal, P. Merz, S. Shaikh, H. Wisniewski, I. Alafuzoff and B. Winblad, *The Lancet*, 1986, **328**, 421-426.
204. Q. Liu, H.-g. Lee, K. Honda, S. L. Siedlak, P. L. R. Harris, A. D. Cash, X. Zhu, J. Avila, A. Nunomura, A. Takeda, M. A. Smith and G. Perry, *Biochimica et Biophysica Acta (BBA) - Molecular Basis of Disease*, 2005, **1739**, 211-215.
205. E. Köpke, Y. C. Tung, S. Shaikh, A. C. Alonso, K. Iqbal and I. Grundke-Iqbal, *Journal of Biological Chemistry*, 1993, **268**, 24374-24384.

206. D.-W. Dong, Y.-S. Zhang, W.-Y. Yang, R.-Q. Wang-Qin, A.-D. Xu and Y.-W. Ruan, *Brain Research*, 2014, **1543**, 280-289.

207. T. Kramer, B. Schmidt and F. Lo Monte, *International Journal of Alzheimer's Disease*, 2012, **2012**, 32.

208. M. von Bergen, P. Friedhoff, J. Biernat, J. Heberle, E.-M. Mandelkow and E. Mandelkow, *Proceedings of the National Academy of Sciences*, 2000, **97**, 5129-5134.

209. A. D. Cash, G. Aliev, S. L. Siedlak, A. Nunomura, H. Fujioka, X. Zhu, A. K. Raina, H. V. Vinters, M. Tabaton, A. B. Johnson, M. Paula-Barbosa, J. Avíla, P. K. Jones, R. J. Castellani, M. A. Smith and G. Perry, *American Journal of Pathology*, **162**, 1623-1627.

210. J. Kuret, C. N. Chirita, E. E. Congdon, T. Kannanayakal, G. Li, M. Necula, H. Yin and Q. Zhong, *Biochimica et Biophysica Acta (BBA) - Molecular Basis of Disease*, 2005, **1739**, 167-178.

211. C.-X. Gong, S. Shaikh, J.-Z. Wang, T. Zaidi, I. Grundke-Iqbal and K. Iqbal, *Journal of Neurochemistry*, 1995, **65**, 732-738.

212. E. M. Jones, M. Dubey, P. J. Camp, B. C. Vernon, J. Biernat, E. Mandelkow, J. Majewski and E. Y. Chi, *Biochemistry*, 2012, **51**, 2539-2550.

213. M. J. Guerrero-Muñoz, J. Gerson and D. L. Castillo-Carranza, *Frontiers in Cellular Neuroscience*, 2015, **9**, Article 464.

214. V. M. Y. Lee, T. K. Kenyon and J. Q. Trojanowski, *Biochimica et Biophysica Acta (BBA) - Molecular Basis of Disease*, 2005, **1739**, 251-259.

215. I. Kelleher, C. Garwood, D. P. Hanger, B. H. Anderton and W. Noble, *Journal of Neurochemistry*, 2007, **103**, 2256-2267.

216. K. S. Kosik and H. Shimura, *Biochimica et Biophysica Acta (BBA) - Molecular Basis of Disease*, 2005, **1739**, 298-310.

217. N. Embi, D. B. Rylatt and P. Cohen, *European Journal of Biochemistry*, 1980, **107**, 519-527.

218. J. R. Woodgett, *The EMBO Journal*, 1990, **9**, 2431-2438.

219. J. A. McCubrey, L. S. Steelman, F. E. Bertrand, N. M. Davis, M. Sokolosky, S. L. Abrams, G. Montalto, A. B. D'Assoro, M. Libra, F. Nicoletti, R. Maestro, J. Basecke, D. Rakus, A. Gizak, Z. Demidenko, L. Cocco, A. M. Martelli and M. Cervello, *Oncotarget 5*, 2014, 2881-2911.

220. S. Patel and J. Woodgett, *Cancer Cell*, **14**, 351-353.
221. M. Maqbool, M. Mobashir and N. Hoda, *European Journal of Medicinal Chemistry*, 2016, **107**, 63-81.
222. S. M. de la Monte, T. Ming, N. Lester-Coll, M. Plater Jr and J. R. Wands, *Journal of Alzheimer's Disease*, 2006, **10**, 89-109.
223. A. Takashima, M. Murayama, O. Murayama, T. Kohno, T. Honda, K. Yasutake, N. Nihonmatsu, M. Mercken, H. Yamaguchi, S. Sugihara and B. Wolozin, *Proceedings of the National Academy of Sciences*, 1998, **95**, 9637-9641.
224. X. Sun, S. Sato, O. Murayama, M. Murayama, J. M. Park, H. Yamaguchi and A. Takashima, *Neuroscience Letters*, 2002, **321**, 61-64.
225. L. K. Chico, L. J. Van Eldik and D. M. Watterson, *Nature Reviews Drug Discovery*, 2009, **8**, 892-909.
226. D. P. Hanger, K. Hughes, J. R. Woodgett, J.-P. Brion and B. H. Anderton, *Neuroscience Letters*, 1992, **147**, 58-62.
227. T. Engel, P. Goñi-Oliver, J. J. Lucas, J. Avila and F. Hernández, *Journal of Neurochemistry*, 2006, **99**, 1445-1455.
228. K. Imahori and T. Uchida, *Journal of Biochemistry*, 1997, **121**, 179-188.
229. A. Takashima, *Journal of Pharmacological Sciences*, 2009, **109**, 174-178.
230. A. P. Babu, S. Chitti, B. Rajesh, V. V. Prasanth, R. J. V. Kishen and K. R. Vali, *Chem-Bio Informatics Journal*, 2010, **10**, 1-12.
231. E. Beurel, S. F. Grieco and R. S. Jope, *Pharmacology & Therapeutics*, 2015, **148**, 114-131.
232. L. Freland and J.-M. Beaulieu, *Frontiers in Molecular Neuroscience*, 2012, **5**, Article 14.
233. G. Manning, D. B. Whyte, R. Martinez, T. Hunter and S. Sudarsanam, *Science*, 2002, **298**, 1912-1934.
234. V. Stambolic, L. Ruel and J. R. Woodgett, *Current Biology*, 1996, **6**, 1664-1669.
235. M. Hong, D. C. R. Chen, P. S. Klein and V. M.-Y. Lee, *Journal of Biological Chemistry*, 1997, **272**, 25326-25332.
236. W. J. Ryves and A. J. Harwood, *Biochemical and Biophysical Research Communications*, 2001, **280**, 720-725.

237. A. Mora, G. Sabio, R. A. González-Polo, A. Cuenda, D. R. Alessi, Juan C. Alonso, J. M. Fuentes, G. Soler and F. Centeno, *Journal of Neurochemistry*, 2001, **78**, 199-206.

238. H. Eldar-Finkelman and A. Martinez, *Frontiers in Molecular Neuroscience*, 2011, **4**, Article 32.

239. W. J. Ryves, R. Dajani, L. Pearl and A. J. Harwood, *Biochemical and Biophysical Research Communications*, 2002, **290**, 967-972.

240. R. Ilouz, O. Kaidanovich, D. Gurwitz and H. Eldar-Finkelman, *Biochemical and Biophysical Research Communications*, 2002, **295**, 102-106.

241. A. Gómez-Ramos, J. Domínguez, D. Zafra, H. Corominola, R. Gomis, J. J. Guinovart and J. Avila, *Journal of Neuroscience Research*, 2006, **83**, 264-273.

242. R. Bertinat, F. Nualart, X. Li, A. J. Yáñez and R. Gomis, *Journal of Clinical & Cellular Immunology*, 2015, **6**, Article 1000285.

243. P. Schultz, D. B. Ring, S. D. Harrison and A. M. Bray, Patent WO1998016528 A1, 1998.

244. S. E. Nikoulina, T. P. Ciaraldi, S. Mudaliar, L. Carter, K. Johnson and R. R. Henry, *Diabetes*, 2002, **51**, 2190-2198.

245. D. B. Ring, K. W. Johnson, E. J. Henriksen, J. M. Nuss, D. Goff, T. R. Kinnick, S. T. Ma, J. W. Reeder, I. Samuels, T. Slabiak, A. S. Wagman, M.-E. W. Hammond and S. D. Harrison, *Diabetes*, 2003, **52**, 588-595.

246. M. L. Selenica, H. S. Jensen, A. K. Larsen, M. L. Pedersen, L. Helboe, M. Leist and J. Lotharius, *British Journal of Pharmacology*, 2007, **152**, 959-979.

247. S. Ding, T. Y. H. Wu, A. Brinker, E. C. Peters, W. Hur, N. S. Gray and P. G. Schultz, *Proceedings of the National Academy of Sciences*, 2003, **100**, 7632-7637.

248. P. Sivaprakasam, X. Han, R. L. Civiello, S. Jacutin-Porte, K. Kish, M. Pokross, H. A. Lewis, N. Ahmed, N. Szapiel, J. A. Newitt, E. T. Baldwin, H. Xiao, C. M. Krause, H. Park, M. Nophsker, J. S. Lippy, C. R. Burton, D. R. Langley, J. E. Macor and G. M. Dubowchik, *Bioorganic & Medicinal Chemistry Letters*, 2015, **25**, 1856-1863.

249. C. Lum, J. Kahl, L. Kessler, J. Kucharski, J. Lundström, S. Miller, H. Nakanishi, Y. Pei, K. Pryor, E. Roberts, L. Sebo, R. Sullivan, J. Urban and Z. Wang, *Bioorganic & Medicinal Chemistry Letters*, 2008, **18**, 3578-3581.

250. M. E. Letelier, P. Izquierdo, L. Godoy, A. M. Lepe and M. Faúndez, *Journal of Applied Toxicology*, 2004, **24**, 519-525.

251. F. P. Guengerich, D. C. Liebler and D. L. Reed, *CRC Critical Reviews in Toxicology*, 1985, **14**, 259-307.

252. L. J. Núñez-Vergara, J. A. Squella, S. Bollo-Dragnic, A. Morello, Y. Repetto, J. Aldunate and M. a. E. Letelier, *Comparative Biochemistry and Physiology Part C: Pharmacology, Toxicology and Endocrinology*, 1997, **118**, 105-111.

253. E. G. Toranzo, T. Gillesse, M. Mendenhall, G. J. Traiger, P. G. Riley, R. P. Hanzlik and R. A. Wiley, *Toxicology and Applied Pharmacology*, 1977, **40**, 415-425.

254. A. J. Peat, J. A. Boucheron, S. H. Dickerson, D. Garrido, W. Mills, J. Peckham, F. Preugschat, T. Smalley, S. L. Schweiker, J. R. Wilson, T. Y. Wang, H. Q. Zhou and S. A. Thomson, *Bioorganic & Medicinal Chemistry Letters*, 2004, **14**, 2121-2125.

255. A. J. Peat, D. Garrido, J. A. Boucheron, S. L. Schweiker, S. H. Dickerson, J. R. Wilson, T. Y. Wang and S. A. Thomson, *Bioorganic & Medicinal Chemistry Letters*, 2004, **14**, 2127-2130.

256. T. L. Smalley Jr, A. J. Peat, J. A. Boucheron, S. Dickerson, D. Garrido, F. Preugschat, S. L. Schweiker, S. A. Thomson and T. Y. Wang, *Bioorganic & Medicinal Chemistry Letters*, 2006, **16**, 2091-2094.

257. Y. Maeda, M. Nakano, H. Sato, Y. Miyazaki, S. L. Schweiker, J. L. Smith and A. T. Truesdale, *Bioorganic & Medicinal Chemistry Letters*, 2004, **14**, 3907-3911.

258. Y. Miyazaki, Y. Maeda, H. Sato, M. Nakano and G. W. Mellor, *Bioorganic & Medicinal Chemistry Letters*, 2008, **18**, 1967-1971.

259. N. Ibrahim, L. Mouawad and M. Legraverend, *European Journal of Medicinal Chemistry*, 2010, **45**, 3389-3393.

260. T. Kohara, K. Fukunaga and T. Hanano, Patent WO2004014910 A1, 2004.

261. Y. Uno, H. Iwashita, T. Tsukamoto, N. Uchiyama, T. Kawamoto, M. Kori and A. Nakanishi, *Brain Research*, 2009, **1296**, 148-163.

262. F. F. Wagner, J. A. Bishop, J. P. Gale, X. Shi, M. Walk, J. Ketterman, D. Patnaik, D. Barker, D. Walpita, A. J. Campbell, S. Nguyen, M. Lewis, L. Ross, M. Weïwer, W. F. An, A. R. Germain, P. P. Nag, S. Metkar, T. Kaya, S. Dandapani, D. E. Olson, A.-L. Barbe, F. Lazzaro, J. R. Sacher, J. H. Cheah, D. Fei, J. Perez, B. Munoz, M. Palmer, K. Stegmaier, S. L. Schreiber, E. Scolnick, Y.-L. Zhang, S. J. Haggarty, E. B. Holson and J. Q. Pan, *ACS Chemical Biology*, 2016, **11**, 1952-1963.

263. S. Berg, M. Bergh, S. Hellberg, K. Högdin, Y. Lo-Alfredsson, P. Söderman, S. von Berg, T. Weigelt, M. Ormö, Y. Xue, J. Tucker, J. Neelissen, E. Jerning, Y. Nilsson and R. Bhat, *Journal of Medicinal Chemistry*, 2012, **55**, 9107-9119.

264. Y. Mettey, M. Gompel, V. Thomas, M. Garnier, M. Leost, I. Ceballos-Picot, M. Noble, J. Endicott, J.-m. Vierfond and L. Meijer, *Journal of Medicinal Chemistry*, 2003, **46**, 222-236.

265. Baker, C., Bemis, G., Cao, J., Green, J., Hale, M., Janetka, J., Maltais, F., Mashall, R., Mullican, M. and Straub, J., Patent WO0157022, 2002.

266. Bowler, A., Olesen, P., Sorensen, A., Hansen, B., Worsaae, H., Kurtzhals, P., Patent US20010039275, 2001.

267. R. Bhat, Y. Xue, S. Berg, S. Hellberg, M. Ormö, Y. Nilsson, A.-C. Radesäter, E. Jerning, P.-O. Markgren, T. Borgegård, M. Nylöf, A. Giménez-Cassina, F. Hernández, J. J. Lucas, J. Díaz-Nido and J. Avila, *Journal of Biological Chemistry*, 2003, **278**, 45937-45945.

268. P. H. Olesen, A. R. Sørensen, B. Ursø, P. Kurtzhals, A. N. Bowler, U. Ehrbar and B. F. Hansen, *Journal of Medicinal Chemistry*, 2003, **46**, 3333-3341.

269. M. Saitoh, J. Kunitomo, E. Kimura, Y. Hayase, H. Kobayashi, N. Uchiyama, T. Kawamoto, T. Tanaka, C. D. Mol, D. R. Dougan, G. S. Textor, G. P. Snell and F. Itoh, *Bioorganic & Medicinal Chemistry*, 2009, **17**, 2017-2029.

270. F. Lo Monte, T. Kramer, J. Gu, M. Brodrecht, J. Pilakowski, A. Fuertes, J. M. Dominguez, B. Plotkin, H. Eldar-Finkelman and B. Schmidt, *European Journal of Medicinal Chemistry*, 2013, **61**, 26-40.

271. A. Martinez, A. Castro, I. Dorronsoro and M. Alonso, *Medicinal Research Reviews*, 2002, **22**, 373-384.

272. I. Hers, J. M. Tavaré and R. M. Denton, *FEBS Letters*, 1999, **460**, 433-436.

273. D. J. O'Neill, L. Shen, C. Prouty, B. R. Conway, L. Westover, J. Z. Xu, H.-C. Zhang, B. E. Maryanoff, W. V. Murray, K. T. Demarest and G.-H. Kuo, *Bioorganic & Medicinal Chemistry*, 2004, **12**, 3167-3185.

274. Q. Ye, W. Mao, Y. Zhou, L. Xu, Q. Li, Y. Gao, J. Wang, C. Li, Y. Xu, Y. Xu, H. Liao, L. Zhang, J. Gao, J. Li and T. Pang, *Bioorganic & Medicinal Chemistry*, 2015, **23**, 1179-1188.

275. Q. Ye, Q. Li, Y. Zhou, L. Xu, W. Mao, Y. Gao, C. Li, Y. Xu, Y. Xu, H. Liao, L. Zhang, J. Gao, J. Li and T. Pang, *Chemical Biology & Drug Design*, 2015, **86**, 746-752.

276. S. Leclerc, M. Garnier, R. Hoessel, D. Marko, J. A. Bibb, G. L. Snyder, P. Greengard, J. Biernat, Y.-Z. Wu, E.-M. Mandelkow, G. Eisenbrand and L. Meijer, *Journal of Biological Chemistry*, 2001, **276**, 251-260.

277. K. Vougogiannopoulou, Y. Ferandin, K. Bettayeb, V. Myrianthopoulos, O. Lozach, Y. Fan, C. H. Johnson, P. Magiatis, A.-L. Skaltsounis, E. Mikros and L. Meijer, *Journal of Medicinal Chemistry*, 2008, **51**, 6421-6431.

278. P. Polychronopoulos, P. Magiatis, A.-L. Skaltsounis, V. Myrianthopoulos, E. Mikros, A. Tarricone, A. Musacchio, S. M. Roe, L. Pearl, M. Leost, P. Greengard and L. Meijer, *Journal of Medicinal Chemistry*, 2004, **47**, 935-946.

279. Meijer, L., Greengard, P., Knockaert, M., Skaltounis, A.L., Patent US20070276025 A1, 2007.

280. M. Leost, C. Schultz, A. Link, Y.-Z. Wu, J. Biernat, E.-M. Mandelkow, J. A. Bibb, G. L. Snyder, P. Greengard, D. W. Zaharevitz, R. Gussio, A. M. Senderowicz, E. A. Sausville, C. Kunick and L. Meijer, *European Journal of Biochemistry*, 2000, **267**, 5983-5994.

281. N. R. Makhortova, M. Hayhurst, A. Cerqueira, A. D. Sinor-Anderson, W.-N. Zhao, P. W. Heiser, A. C. Arvanites, L. S. Davidow, Z. O. Waldon, J. A. Steen, K. Lam, H. D. Ngo and L. L. Rubin, *Nature Chemical Biology*, 2011, **7**, 544-552.

282. M. Knockaert, K. Wieking, S. Schmitt, M. Leost, K. M. Grant, J. C. Mottram, C. Kunick and L. Meijer, *Journal of Biological Chemistry*, 2002, **277**, 25493-25501.

283. C. Kunick, Z. Zeng, R. Gussio, D. Zaharevitz, M. Leost, F. Totzke, C. Schächtele, M. H. G. Kubbutat, L. Meijer and T. Lemcke, *ChemBioChem*, 2005, **6**, 541-549.

284. R. M. Eglen and T. Reisine, *ASSAY and Drug Development Technologies*, 2009, **7**, 22-43.

285. A. Martinez, M. Alonso, A. Castro, C. Pérez and F. J. Moreno, *Journal of Medicinal Chemistry*, 2002, **45**, 1292-1299.

286. J. M. Domínguez, A. Fuertes, L. Orozco, M. del Monte-Millán, E. Delgado and M. Medina, *Journal of Biological Chemistry*, 2012, **287**, 893-904.

287. Padilla, M., Cascon, M., Diaz, I., Gil, A., Pliego, G., Huerta, A., Puerto, M., Patent US20050222220 A1, 2005.

288. J. Godyń, J. Jończyk, D. Panek and B. Malawska, *Pharmacological Reports*, 2016, **68**, 127-138.

289. S. Conde, D. I. Pérez, A. Martínez, C. Perez and F. J. Moreno, *Journal of Medicinal Chemistry*, 2003, **46**, 4631-4633.

290. D. I. Perez, S. Conde, C. Pérez, C. Gil, D. Simon, F. Wandosell, F. J. Moreno, J. L. Gelpí, F. J. Luque and A. Martínez, *Bioorganic & Medicinal Chemistry*, 2009, **17**, 6914-6925.

291. D. I. Perez, V. Palomo, C. Pérez, C. Gil, P. D. Dans, F. J. Luque, S. Conde and A. Martínez, *Journal of Medicinal Chemistry*, 2011, **54**, 4042-4056.

292. M. Kidd, *Nature*, 1963, **197**, 192-193.

293. C. M. Wischik, C. R. Harrington and J. M. D. Storey, *Biochemical Pharmacology*, 2014, **88**, 529-539.

294. C. M. Wischik, P. C. Edwards, R. Y. Lai, M. Roth and C. R. Harrington, *Proceedings of the National Academy of Sciences*, 1996, **93**, 11213-11218.

295. B. Bulic, M. Pickhardt, I. Khlistunova, J. Biernat, E.-M. Mandelkow, E. Mandelkow and H. Waldmann, *Angewandte Chemie International Edition*, 2007, **46**, 9215-9219.

296. L. Gregor, P. Marcus, G. L. David, S. Boris and M. Eckhard, *Current Alzheimer Research*, 2007, **4**, 315-323.

297. M. Pickhardt, G. Larbig, I. Khlistunova, A. Coksezen, B. Meyer, E.-M. Mandelkow, B. Schmidt and E. Mandelkow, *Biochemistry*, 2007, **46**, 10016-10023.

298. B. Bulic, M. Pickhardt and E. Mandelkow, *Journal of Medicinal Chemistry*, 2013, **56**, 4135-4155.

299. R. S. Obach, A. S. Kalgutkar, T. F. Ryder and G. S. Walker, *Chemical Research in Toxicology*, 2008, **21**, 1890-1899.

300. P. Paolo, *Current Drug Metabolism*, 2007, **8**, 839-851.

301. B. K. Park, N. R. Kitteringham, J. L. Maggs, M. Pirmohamed and D. P. Williams, *Annual Review of Pharmacology and Toxicology*, 2005, **45**, 177-202.

302. M. Necula, C. N. Chirita and J. Kuret, *Biochemistry*, 2005, **44**, 10227-10237.

303. A. Crowe, W. Huang, C. Ballatore, R. L. Johnson, A.-M. L. Hogan, R. Huang, J. Wichterman, J. McCoy, D. Huryn, D. S. Auld, A. B. Smith, J. Inglese, J. Q. Trojanowski, C. P. Austin, K. R. Brunden and V. M. Y. Lee, *Biochemistry*, 2009, **48**, 7732-7745.

304. S. R. Paranjape, A. P. Riley, A. D. Somoza, C. E. Oakley, C. C. C. Wang, T. E. Prisinzano, B. R. Oakley and T. C. Gamblin, *ACS Chemical Neuroscience*, 2015, **6**, 751-760.

305. J. P. Wisor, D. M. Edgar, J. Yesavage, H. S. Ryan, C. M. McCormick, N. Lapustea and G. M. Murphy Jr, *Neuroscience*, 2005, **131**, 375-385.

306. M. Sarter, J. P. Bruno and B. Givens, *Neurobiology of Learning and Memory*, 2003, **80**, 245-256.

307. M. Sarter and V. Parikh, *Nature Review Neuroscience*, 2005, **6**, 48-56.

308. D. E. Kuhl, R. A. Koeppe, S. Minoshima, S. E. Snyder, E. P. Ficaro, N. L. Foster, K. A. Frey and M. R. Kilbourn, *Neurology*, 1999, **52**, 691-699.

309. T. Silva, J. Reis, J. Teixeira and F. Borges, *Ageing Research Reviews*, 2014, **15**, 116-145.

310. R. Schliebs and T. Arendt, *Journal of Neural Transmission*, 2006, **113**, 1625-1644.

311. R. Schliebs and T. Arendt, *Behavioural Brain Research*, 2011, **221**, 555-563.

312. N. C. Inestrosa, A. Alvarez, C. A. Pérez, R. D. Moreno, M. Vicente, C. Linker, O. I. Casanueva, C. Soto and J. Garrido, *Neuron*, **16**, 881-891.

313. N. H. Greig, D. K. Lahiri and K. Sambamurti, *International Psychogeriatrics*, 2002, **14**, 77-91.

314. R. M. Lane, M. Kivipelto and N. H. Greig, *Clinical Neuropharmacology*, 2004, **27**, 141-149.

315. R. M. Lane, S. G. Potkin and A. Enz, *International Journal of Neuropsychopharmacology*, 2006, **9**, 101-124.

316. M. Anna, M. Andrea, S. Elena, R. Michela, B. Maria Laura, M. Chiara and T. Vincenzo, *Current Topics in Medicinal Chemistry*, 2013, **13**, 1771-1786.

317. P. Anand and B. Singh, *Archives of Pharmacal Research*, 2013, **36**, 375-399.

318. D. Galimberti and E. Scarpini, *Expert Opinion on Investigational Drugs*, 2016, **25**, 1181-1187.

319. J. Coyle and P. Kershaw, *Biological Psychiatry*, 2001, **49**, 289-299.

320. Y.-P. Pang, P. Quiram, T. Jelacic, F. Hong and S. Brimijoin, *Journal of Biological Chemistry*, 1996, **271**, 23646-23649.

321. L. Savini, A. Gaeta, C. Fattorusso, B. Catalanotti, G. Campiani, L. Chiasserini, C. Pellerano, E. Novellino, D. McKissic and A. Saxena, *Journal of Medicinal Chemistry*, 2003, **46**, 1-4.

322. P. Muñoz-Ruiz, L. Rubio, E. García-Palomero, I. Dorronsoro, M. del Monte-Millán, R. Valenzuela, P. Usán, C. de Austria, M. Bartolini, V. Andrisano, A. Bidon-Chanal, M. Orozco, F. J. Luque, M. Medina and A. Martínez, *Journal of Medicinal Chemistry*, 2005, **48**, 7223-7233.

323. M. Rosini, V. Andrisano, M. Bartolini, M. L. Bolognesi, P. Hrelia, A. Minarini, A. Tarozzi and C. Melchiorre, *Journal of Medicinal Chemistry*, 2005, **48**, 360-363.

324. S. Hamulakova, L. Janovec, M. Hrabinova, P. Kristian, K. Kuca, M. Banasova and J. Imrich, *European Journal of Medicinal Chemistry*, 2012, **55**, 23-31.

325. R. Manetsch, A. Krasiński, Z. Radić, J. Raushel, P. Taylor, K. B. Sharpless and H. C. Kolb, *Journal of the American Chemical Society*, 2004, **126**, 12809-12818.

326. A. Villalobos, J. F. Blake, C. K. Biggers, T. W. Butler, D. S. Chapin, Y. L. Chen, J. L. Ives, S. B. Jones and D. R. Liston, *Journal of Medicinal Chemistry*, 1994, **37**, 2721-2734.

327. A. Villalobos, T. W. Butler, D. S. Chapin, Y. L. Chen, S. B. DeMattos, J. L. Ives, S. B. Jones, D. R. Liston and A. A. Nagel, *Journal of Medicinal Chemistry*, 1995, **38**, 2802-2808.

328. A. Aitken and M. Learmonth, in *The Protein Protocols Handbook*, ed. J. M. Walker, Humana Press, Totowa, NJ, 2009, pp. 1053-1055.

329. M. M. Ismail, M. M. Kamel, L. W. Mohamed and S. I. Faggal, *Molecules*, 2012, **17**, 4811-4823.

330. Z.-M. Wang, P. Cai, Q.-H. Liu, D.-Q. Xu, X.-L. Yang, J.-J. Wu, L.-Y. Kong and X.-B. Wang, *European Journal of Medicinal Chemistry*, 2016, **123**, 282-297.

331. M. L. Bolognesi, M. Bartolini, A. Cavalli, V. Andrisano, M. Rosini, A. Minarini and C. Melchiorre, *Journal of Medicinal Chemistry*, 2004, **47**, 5945-5952.

332. G. Lin, C.-Y. Lai and W.-C. Liao, *Bioorganic & Medicinal Chemistry*, 1999, **7**, 2683-2689.

333. C. Mustazza, A. Borioni, M. R. D. Giudice, F. Gatta, R. Ferretti, A. Meneguz, M. T. Volpe and P. Lorenzini, *European Journal of Medicinal Chemistry*, 2002, **37**, 91-109.

334. N. Toda, K. Tago, S. Marumoto, K. Takami, M. Ori, N. Yamada, K. Koyama, S. Naruto, K. Abe, R. Yamazaki, T. Hara, A. Aoyagi, Y. Abe, T. Kaneko and H. Kogen, *Bioorganic & Medicinal Chemistry*, 2003, **11**, 4389-4415.

335. A. Mary, D. Z. Renko, C. Guillou and C. Thal, *Bioorganic & Medicinal Chemistry*, 1998, **6**, 1835-1850.

336. D. Herlem, M.-T. Martin, C. Thal and C. Guillou, *Bioorganic & Medicinal Chemistry Letters*, 2003, **13**, 2389-2391.

337. P. Jia, R. Sheng, J. Zhang, L. Fang, Q. He, B. Yang and Y. Hu, *European Journal of Medicinal Chemistry*, 2009, **44**, 772-784.

338. X. C. Tang, P. De Sarno, K. Sugaya and E. Giacobini, *Journal of Neuroscience Research*, 1989, **24**, 276-285.

339. V. Tumiatti, A. Milelli, A. Minarini, M. Rosini, M. L. Bolognesi, M. Micco, V. Andrisano, M. Bartolini, F. Mancini, M. Recanatini, A. Cavalli and C. Melchiorre, *Journal of Medicinal Chemistry*, 2008, **51**, 7308-7312.

340. K.-M. Cho, I.-D. Yoo and W.-G. Kim, *Biological and Pharmaceutical Bulletin*, 2006, **29**, 2317-2320.

341. H. Jiang, X. Wang, L. Huang, Z. Luo, T. Su, K. Ding and X. Li, *Bioorganic & Medicinal Chemistry*, 2011, **19**, 7228-7235.

342. Y. Rook, K.-U. Schmidtke, F. Gaube, D. Schepmann, B. Wünsch, J. Heilmann, J. Lehmann and T. Winckler, *Journal of Medicinal Chemistry*, 2010, **53**, 3611-3617.

Chapter 2

Targeting GSK-3β with irreversible inhibitors - short introduction and molecular modelling studies

2.1 Kinases as targets and their relation to Alzheimer's disease

The sequencing of the human genome has enabled the identification of over 500 kinases.[1] Kinases play a dominant role in the regulation of signal transduction and cellular functions in eukaryotic cells. These functions include cell metabolism, cycle progression, transcription, differentiation, apoptosis and cytoskeletal rearrangement.[1] It is no surprise then, that the deregulation of kinases occurs in a variety of diseases including diabetes, inflammatory, cardiovascular and nervous disorders.[2] Furthermore, kinases are known to regulate the axonal transport and modification of the microtubule network through the phosphorylation of motors, adapters and cargoes.[3] Several kinases such as glycogen synthase kinase-3β (GSK-3β), cyclin-dependent kinase 5 (CDK5), protein kinase B (Akt) and p38 mitogen-activated protein kinase (p38 MAPK) are involved in maintaining the integrity of the neuronal and microtubule network.[3] In patients with Alzheimer's disease (AD), these kinases are deregulated, which results in the loss of microtubule stabilisation and an aberrant neuronal network.[4]

In the 1980s, neurofibrillary tangles (NFT) were shown to comprise microtubule-associated protein tau in a hyperphosphorylated, insoluble, and filamentous state. NFT is now known to play an important role in neurodegenerative diseases, including AD.[5] The tau protein is phosphorylated by GSK-3β and in AD patients, it is hyperphosphorylated, which results in the formation of toxic NFT.[6-8] A growing body of evidence suggests that the generation of toxic NFT may drive the onset and progression of AD.[9]

These findings make GSK-3β an attractive target. The reduction in hyperphosphorylation of tau protein could improve the stability of the microtubule network and thereby ultimately prove useful in the development of AD chemotherapy. The focus of this project is thus the synthesis and development of GSK-3β inhibitors.

2.2 Focusing on GSK-3β as the target

2.2.1 The multifaceted roles of GSK-3β in cellular signaling

GSK-3β phosphorylates a large variety of substrates that play a role in signaling systems coupled to receptors for insulin, neurotrophins, a variety of growth factors and transcription factors. Furthermore, the control of GSK-3β activity is an important part in the regulation of the above-mentioned functions, encompassing a wide scope, ranging from survival at the cellular level to mood and cognition at the organism level. Therefore, deregulated GSK-3β activity plays an integral part in certain psychiatric and neurodegenerative diseases.[10]

Glycogen synthase was the first enzyme to be discovered that is inhibited by GSK-3β, through phosphorylation, which halts the glycogen synthesis.[11] Insulin activates glycogen synthase by reducing the phosphate content of this enzyme. Most of the dephosphorylation occurs at a cluster of serine residues on the GSK-3β.[12]

GSK-3β is also involved in the attenuation of insulin signaling by phosphorylation of insulin receptor substrate 1 (IRS-1). The phosphorylation of IRS-1 by GSK-3β results in the inhibition of the tyrosine phosphorylation of IRS-1 by an insulin receptor, which leads to impaired insulin signaling.[13]

GSK-3β phosphorylates several proteins such as tau that contribute to the structural integrity of the cells.[10] Tau is phosphorylated by GSK-3β and binds to microtubules in the phosphorylated state.[14] There is evidence that supports the fact that GSK-3β can regulate the binding of tau to microtubules by controlling the degree of tau phosphorylation and thereby impacting the neuronal structure and neuronal plasticity.[10]

One of the most important roles of GSK-3β is that the kinase is a key regulator of a broad array of transcription factors and has been found to be phosphorylated directly by GSK-3β. Transcription factors and GSK-3β are considered key targets of signaling pathways, because of their involvement in transferring information from the extracellular environment to the nucleus.[10] However, complete inhibition of GSK-3β is not desired and could lead to potential side effects. Only a small percentage inhibition of GSK-3β is required to reset the stoichiometry of tau phosphorylation.[15]

2.2.2 Structural insight on GSK-3β

GSK-3β is a serine/threonine protein kinase and is composed of two domains: an N-terminal domain consisting of a closed β-barrel structure and an α-helical domain at the C-terminal end. The catalytic site that contains the activation loop is sandwiched between the two major domains (Fig. 2.1).[16, 17]

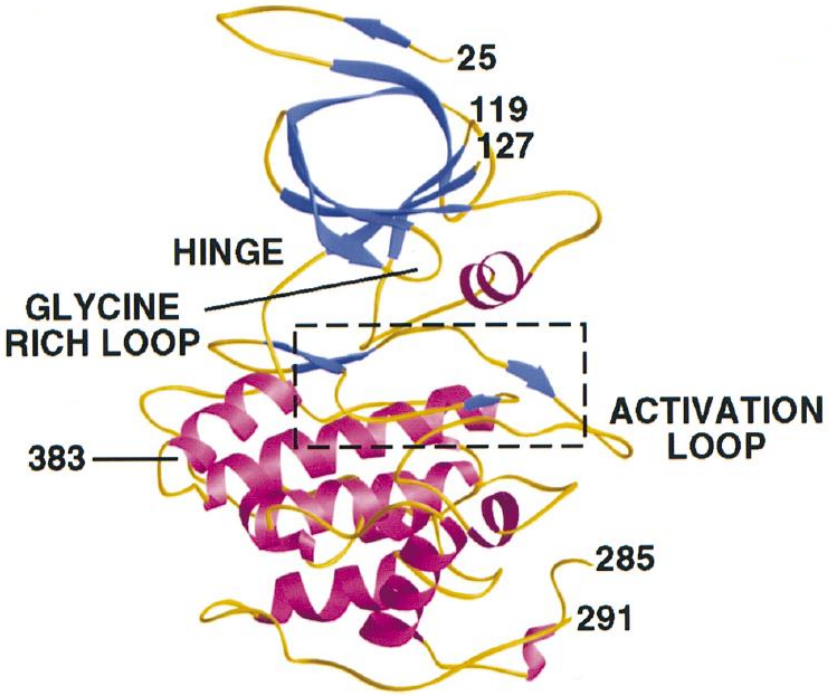

Figure 2.1. The structure of GSK-3β. The N-terminal domain (blue) corresponds to the β-strand domain and the α-helical domain (purple) corresponds to the C-terminal end.[16]

Before GSK-3β can phosphorylate a substrate, its β-strand and α-helical domains aligns into a catalytically active conformation. The polar residues such as arginine and lysine on the β-strand and α-helical domains bind to the phosphate group of the phosphorylated residue (that was phosphorylated by ATP)[17] on the activation loop, which results in the correct alignment of the two domains. This opens up the substrate binding groove and allows the substrate to bind.[16] The blocking of the ATP-binding site would thus prevent substrates from entering the substrate binding groove.

Aoki and co-workers[17] have co-crystallised ADP with GSK-3β to gain structural insight regarding ATP recognition. In Figure 2.2, a crystal structure of the ADP inside the ATP-binding site of GSK-3β is shown. The adenine ring is buried in the hydrophobic pocket

formed by Ile62, Val70, Ala83, Val110, Leu132 and Leu188. The -NH_2 on the purine ring interacts with the O atom on Asp133. A hydrogen bond between the -N atom of the purine ring and Val135's NH is also observed in the hinge loop (Fig. 2.1). The side chain of Lys85 that interacts with the α- and β-phosphoryl groups stabilises the phosphoryl groups during phosphorylation. The magnesium ion (pink sphere in Fig. 2.2), which coordinates to the α- and β-phosphoryl O atoms, creates the correct geometry for phosphoryl transfer.[17]

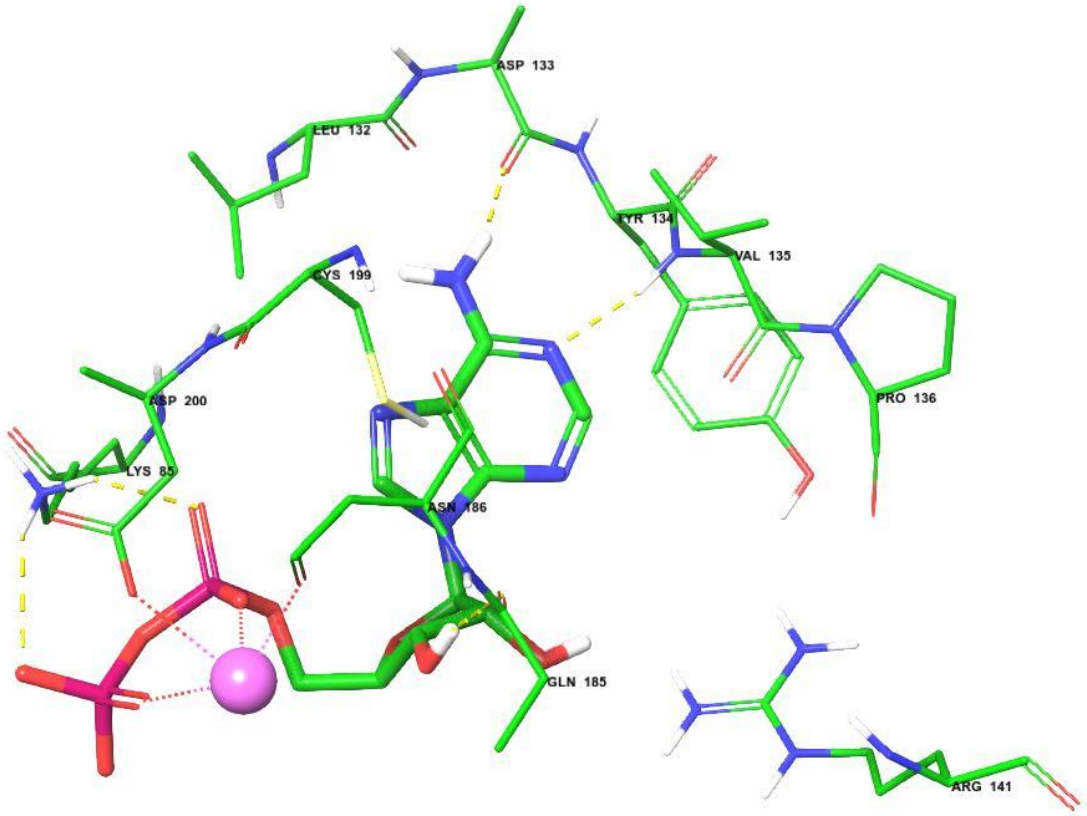

Figure 2.2. Residues participating in binding of ADP in the ATP-binding site of GSK-3β (PDB code: 1J1C, H_2O molecules removed)[17]

Over the years, a plethora of GSK-3β inhibitors have been discovered and most of these demonstrated good-to-excellent inhibitory activity.[18] However, given the structural similarity of many kinases, selectivity remains a challenge. One of the approaches to overcome the challenge is to target the ATP-binding site of the kinase.[19] The structural analysis of ATP inhibitors showed that the establishment of hydrogen bonds with the backbone atoms of Asp133 and Val135 are crucial to achieve enhanced affinity for GSK-3β. Furthermore, additional interactions with Pro136, Lys85, Glu97, Arg141 and Asp200 may increase the activity and selectivity for GSK-3β (Fig. 2.3).[18]

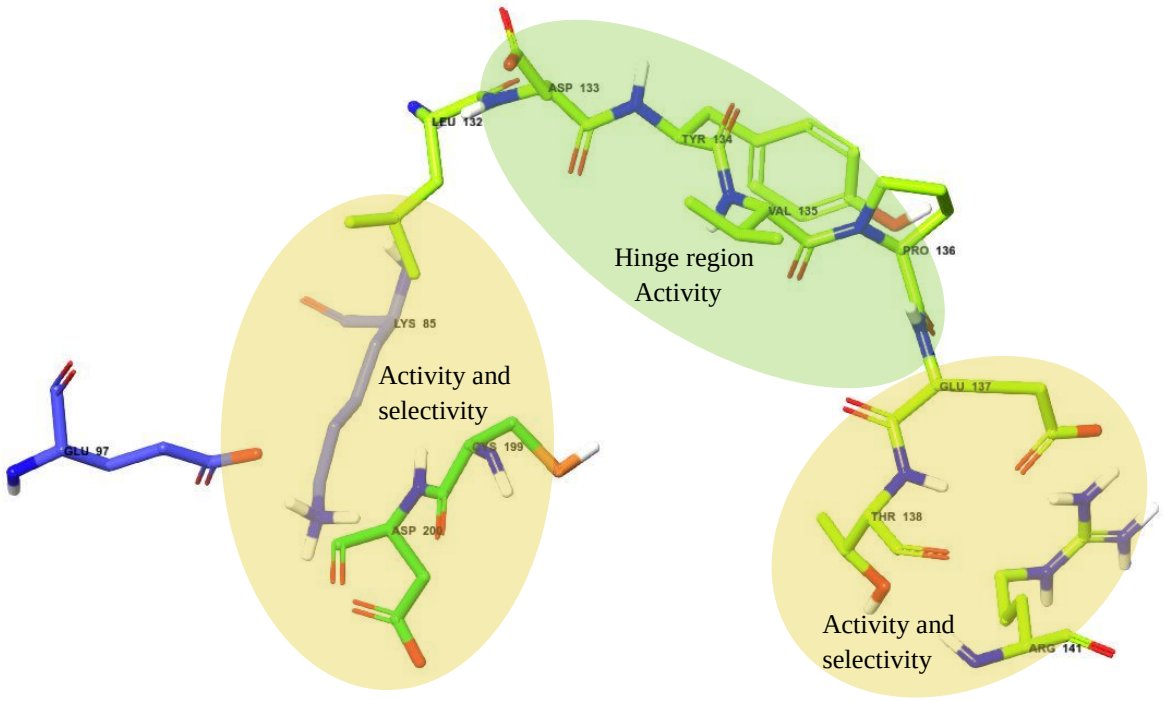

Figure 2.3. Schematic view of the ATP-binding site of GSK-3β that indicates important areas for activity and selectivity.[18]

2.2.3 AstraZeneca's aminopyrazine series

In 2012, through the use of high throughput screening, AstraZeneca identified the aminopyrazine core **203** as a potential starting point for the development of GSK-3β inhibitors. Compound **203** (Fig. 2.4) showed an acceptable potency (GSK-3β IC_{50} = 41 nM), which was below 1 μM, and the aminopyrazine core mimics the adenine ring of ATP.[20]

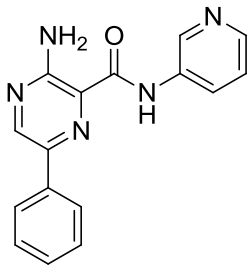

203

Figure 2.4. Aminopyrazine analogue identified through high throughput screening.[20]

A series of pyrazine analogues were synthesised to investigate structure-activity relationships (SAR) and to determine the selectivity with respect to CDK2, a kinase with close homology within the ATP-binding site. From the series, the following pyrazine analogues, **204 – 208**, showed interesting results (Fig. 2.5). Sulfonamide **204** demonstrated one of the lowest

inhibitory activities (GSK-3β K_i = 12 nM) although, with poor selectivity with respect to CDK2 (CDK2 K_i = 100 nM, 8.3 fold). In addition, the Caco2 cell line permeability was below detection level, most likely due to the introduction of two additional hydrogen bond donors from the sulfonamide.[20]

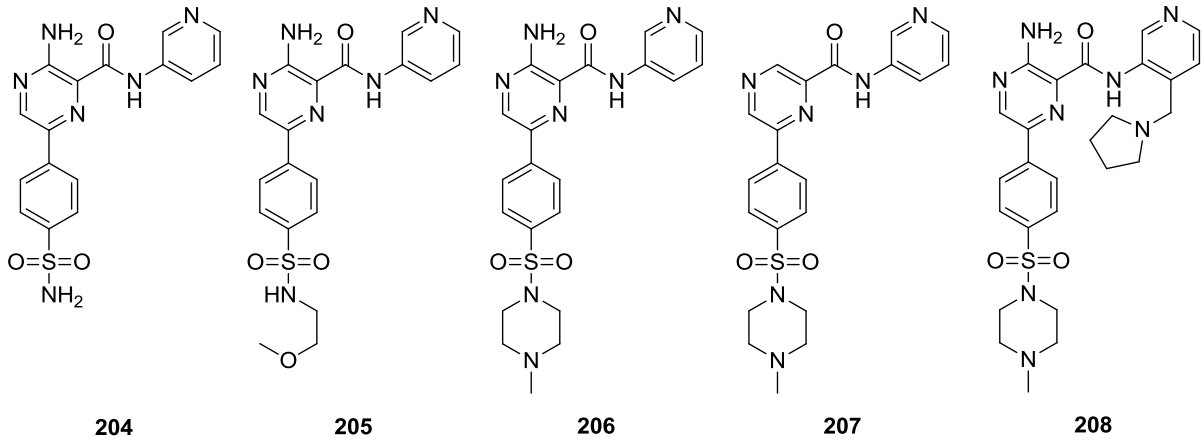

Figure 2.5. Aminopyrazine analogues synthesised by AstraZeneca.[20]

The incorporation of the methoxyethyl side group on the sulfonamide in **205** increased the potency (GSK-3β K_i = 2 nM) and the selectivity with respect to CDK2 (48 fold). In the Caco2 cell assay, good permeability was determined for **205** (20 × 10^{-6} cm/s). The replacement of the methoxyethyl group with methylpiperazine resulted in 2-aminopyridine **206** with lower potency (GSK-3β K_i = 4.8 nM), but improved selectivity with respect to CDK2 (110-fold). The permeability of **206** (Caco2 assay = 14 × 10^{-6} cm/s) was determined to be similar to **205**.

The removal of the -NH_2 group on the pyrazine ring of **207** resulted in a dramatic drop in potency (GSK-3β K_i = 370 nM). This modification in **207** reduced the number of hydrogen-bonding interactions available to the backbone of the hinge region inside the ATP-binding site. This finding suggests that the presence of the -NH_2 group, or a bioisostere thereof, is necessary for potency.

Modification on the pyridine side chain resulted in pyrrolidine **208**, which had one of the best potencies and selectivities (GSK-3β K_i = 0.22 nM; selectivity with respect to CDK2 = 591 fold) in the series, but had a relatively low permeability (Caco2 assay = 2.3 × 10^{-6} cm/s).

The X-ray crystal structure of **206** bound to GSK-3β (Fig. 2.6) indicated that a pyrazine nitrogen and one of the adjacent hydrogens of the -NH_2 formed hydrogen bonds to the

backbone NH of Val135 and the backbone carbonyl of Asp133 in the ATP-binding site, respectively. In addition, the carbonyl in the amide bond of compound **206** likely forms an intramolecular hydrogen bond with -NH_2 on the pyrazine ring, thus directing the nitrogen of the pyridine ring toward Lys85. This would facilitate the formation of a hydrogen bond between the pyridine and the terminal amino group of Lys85. Neither the hydrogen bonds with Val135 and Asp133 nor this conformational 'locking' would occur with **207**. This offers a plausible explanation for the difference in the potency of **206** and **207**.

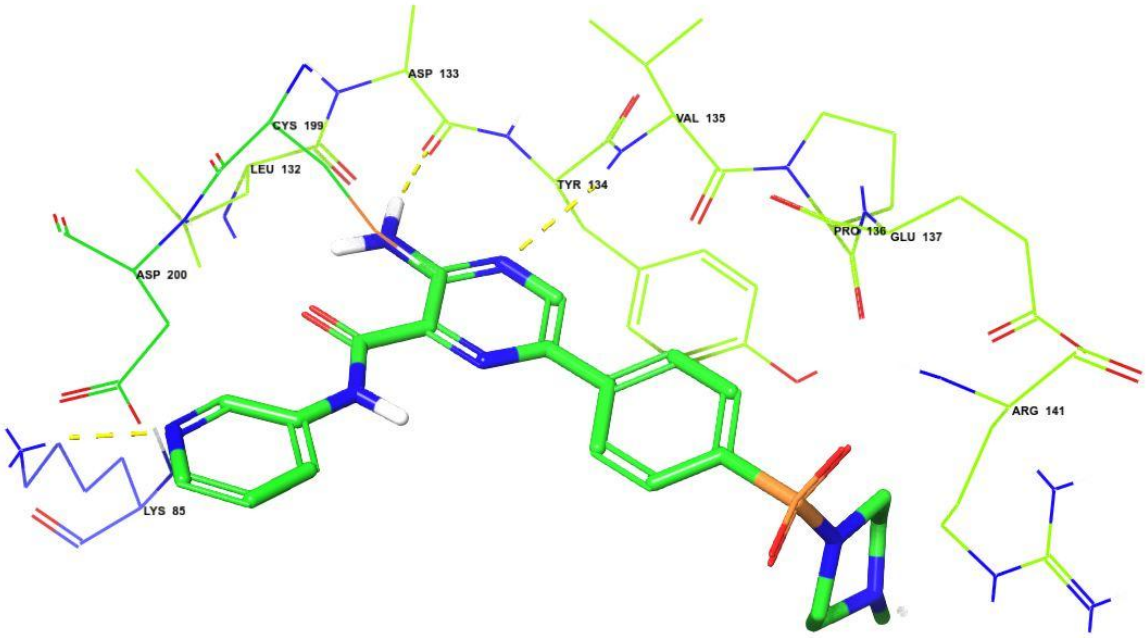

Figure 2.6. X-ray crystal structure of 2-aminopyridine **206** bound to GSK-3β ATP-binding site (PDB: 4ACD).[20]

These results suggest that potential lead compounds based on this aminopyrazine scaffold could be designed to synthesise novel GSK-3β inhibitors. This project thus focuses on using compound **206** as template to design novel irreversible GSK-3β inhibitors.

2.3 The design of irreversible GSK-3β inhibitors

2.3.1 Background on irreversible inhibitors

In general, reversible inhibitors are small molecules that fit snugly in the active site and inhibit the enzyme for as long as they occupy the active site.[21]

Another class of inhibitors are the irreversible ones, which form a covalent bond to a specific nucleophilic amino acid residue located in the ATP-binding site.[22] These irreversible or covalent inhibitors are thus small molecules that contain an electrophilic functional group that reacts with a nucleophilic amino acid residue such as cysteine.[23] Irreversible kinase inhibitors generally consist of a heterocyclic core, which fulfills the same role as reversible inhibitors, by forming hydrogen bonds with the hinge region inside the ATP-binding site, and an electrophilic 'warhead' that forms a covalent bond with a nucleophilic amino acid residue within the ATP-binding site. Irreversible inhibition holds several advantages over ATP competitive inhibition. Irreversible inhibitors are not in competition with high endogenous concentrations of ATP in cells, which means that irreversible inhibitors operate under non-equilibrium binding kinetics, thus the percentage inhibition of the enzyme would increase over time.[24] Furthermore, irreversible inhibition has a longer duration of effect and possesses the ability to deactivate the enzyme even after the free inhibitor has left circulation. Irreversible inhibitors are frequently associated with high selectivity profile and target only kinases with the appropriate cysteine residue in the correct place to form a covalent bond and inhibit irreversibly.[25, 26]

The most frequent warheads present in irreversible inhibitors are Michael acceptors, vinyl sulfones, halomethyl ketones, α-substituted carbonyl derivatives, bromodihydroisoxazoles, imidazole-1-carboxamides, epoxides, β-lactams and strained lactones (Fig. 2.7).[23]

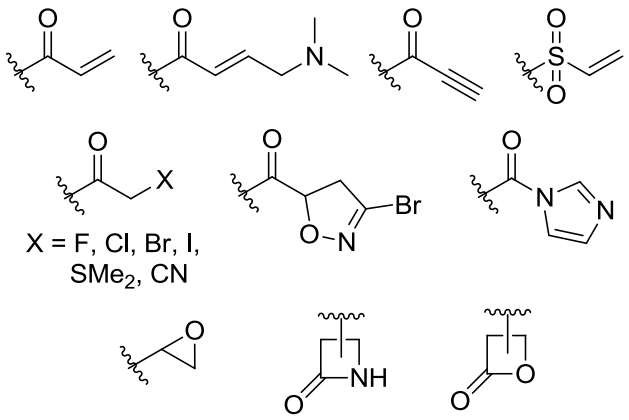

Figure 2.7. Examples of electrophilic functional groups present in irreversible inhibitors.[23]

The mechanism of the covalent bond formation between the warhead and the nucleophilic cysteine can be seen in Figure 2.8. Using the Michael acceptor warhead as an example, the

electron-rich thiol of the cysteine residue reacts at the electrophilic β-carbon of the Michael acceptor. The intermediate enolate then forms the final 1,4-addition product.[26, 27]

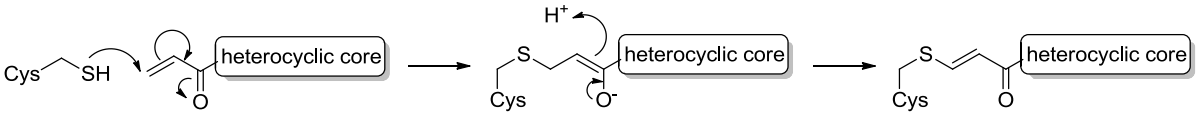

Figure 2.8. Mechanism of the Michael reaction towards the cysteine residue.[26, 27]

The electrophilic functional group, which is also known as the "warhead" needs to be suitably positioned to allow the formation of a covalent bond with the nucleophilic cysteine residue located inside the ATP-binding site.[26] This high biochemical efficiency may translate to lower doses and reduced off-target effects.[28]

2.3.2 Connecting a warhead to the aminopyrazine scaffold

This project focuses on converting the reversible GSK-3β aminopyrazine inhibitor, in particular **206** (see section 2.2.2), into irreversible inhibitors. The goal here is twofold, to develop synthetic methodology associated with creating potential irreversible inhibitors and to ascertain whether this approach is viable with respect to GSK-3β.

The AstraZeneca compound **206** was used as the template for this research (as discussed in section 2.2.2). This molecule can be conceptually divided into two sections: the scaffold and the side chain (Fig. 2.9). The aminopyrazine scaffold is needed for potency[20] and the side chain could be modified to incorporate a warhead. Two general types of warheads were selected for this project, namely Michael acceptors and halomethylketones. Clearly, the position of the warhead relative to the cysteine residue is crucial to afford the possibility of covalent bond formation.

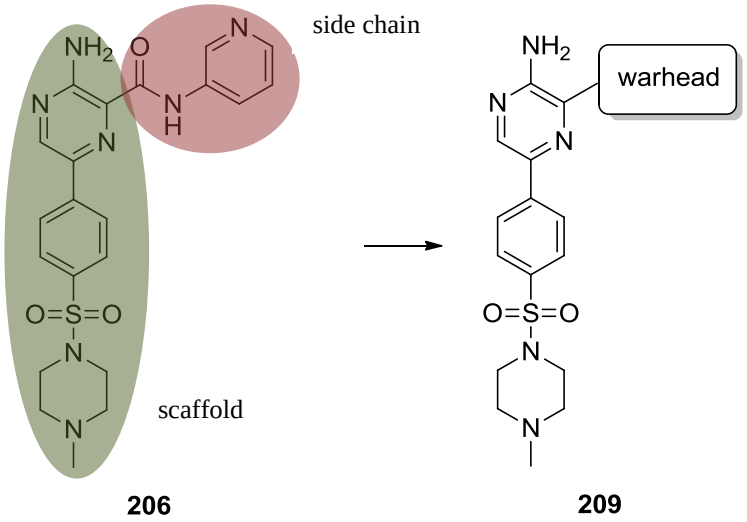

Figure 2.9. Modification of **206** to incorporate a warhead

2.3.3 Molecular modelling of the proposed irreversible inhibitors

The GSK-3β X-ray crystal structure (PDB code: 4ACD) was used to determine the best position for the warhead. Cys199 is a cysteine residue located inside the ATP-binding site and the electron-rich thiol is within 4 Å from the aminopyrazine scaffold (Fig 2.10.).[20] This suggests that the attachment of a warhead to the aminopyrazine scaffold could be within striking distance from the thiol of Cys199.

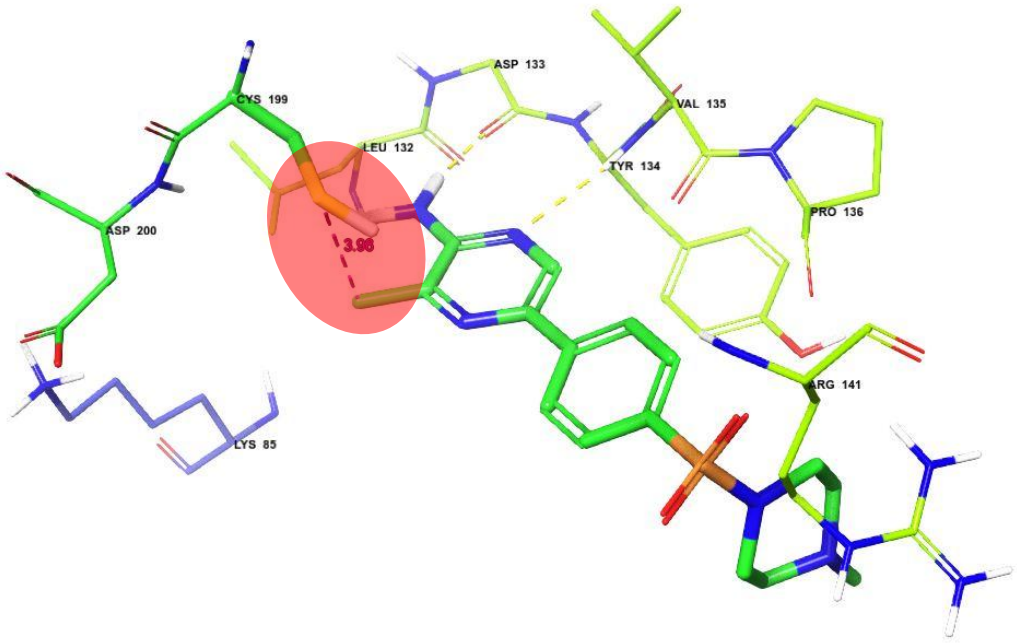

Figure 2.10. The distance between the electron-rich thiol of Cys199 and the potential warhead is within 4 Å.

The position of the warhead needed to be in close proximity to the cysteine to form a covalent bond and the possible arrangements for the two types of warheads was determined (Figure 2.11). The Michael acceptor could be arranged in three ways to assess the different proximities. Two internal arrangements, **210** and **211**, were found to be possible with the carbonyl or the alkene connected to the aminopyrazine scaffold and a side chain coupled to the other side. The third possible arrangement is terminal Michael acceptors, **212** and **213**, with no side chain that could assist in docking and where the carbonyl is directly connected to the aminopyrazine scaffold. For the first library of compounds, the side chain would consist of an amine or a heteroaromatic ring.

For another series, the halomethylketone (HMK) warhead (**214** and **215**) could be positioned directly next to the aminopyrazine scaffold. Bromine and chlorine are generally used in halomethylketone warheads due to the ease of synthesis and will be the focus in the first library of compounds.[29-31]

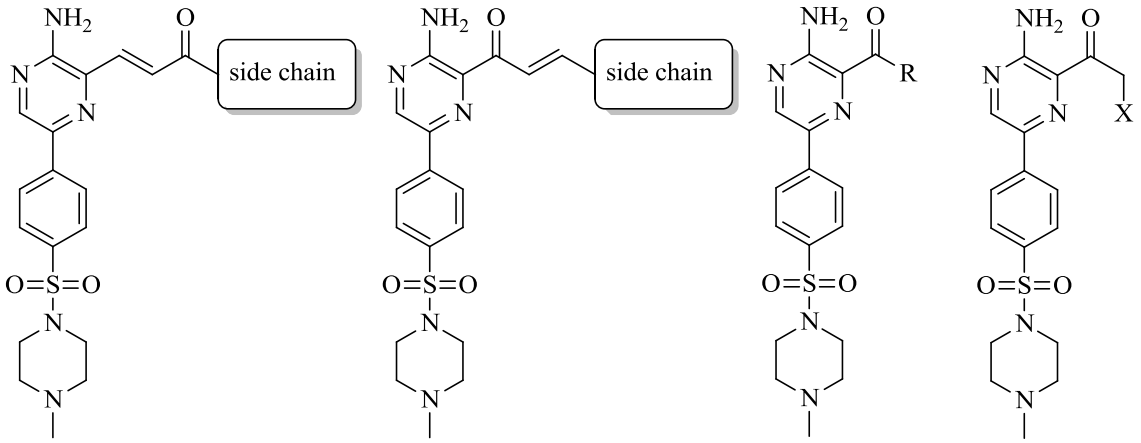

Figure 2.11. Possible arrangements of the warheads

Before the synthesis of these types of irreversible GSK-3β inhibitors could be carried out, molecular modelling techniques were employed to find suitable inhibitors that could fit inside the ATP-binding site and to determine whether the warhead was within striking distance from Cys199 (less than 4 Å).[30] The X-ray crystal structure, 4ACD, obtained from the PDB, was used for these molecular modelling studies.[20]

The GSK-3β X-ray crystal structure, 4ACD, has a resolution of 2.6 Å, which is not sufficiently accurate to identify hydrogen atoms. In general, during the crystallisation process, the molecule is in the solid state and crystal packing may misshape the protein. Therefore, the protein needs to be prepared to minimise the potential problems caused by the aforementioned issues.

The molecular modelling software used in this project was Maestro 11.1, Schrödinger Inc. The protein was prepared using the Protein Preparation Wizard option, which included the addition of hydrogens, missing side chains and loops. The state of the heteroatoms was generated for the pH of 7.0 ± 2.0. The water molecules were then removed manually.
The next step was to generate a receptor grid. Compound **206**, which was co-crystallised with GSK-3β by Berg *et al.*,[20] was used as the ligand to define the receptor grid. All ligands were prepared beforehand with the LigPrep application using OPLS3[32] as the force field, which is most suited for drug-like small molecules. To check whether additional modifications or constraints were needed to obtain accurate docking results, compound **206** was docked into the ATP-binding site. The extra precision (XP) setting, which uses more computational time to eliminate false positives by extensive sampling and advance scoring, was used to obtain the most accurate results. The docking score for compound **206** was determined to be -6.694 kcal/mol and this was used as a standard reference for the docking studies that will be discussed next. The visual representation of the stacked ligands (the co-crystallised **206** and the docked **206**) in Figure 2.12 suggested that no further modifications or constraints were needed.

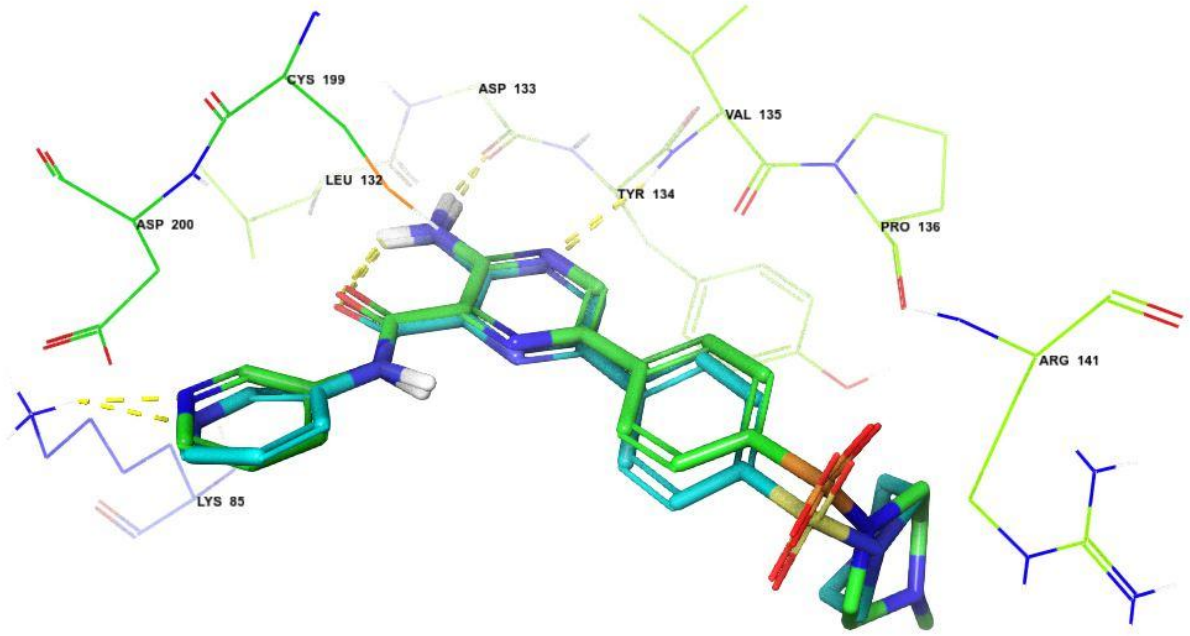

Figure 2.12. Stacked ligands of the co-crystallised- and docked **206**. Green: co-crystallised **206**, blue: docked **206**

The next step was to dock a series of prepared ligands into the ATP-binding site, followed by a post-docking energy minimisation. The docked ligands were then visually inspected for any discrepancies such as strained bond angles. The docking results of the ligands are tabulated in Tables 2.1 and 2.2. The tables are divided in sections based on the type of warhead arrangement. The first two sections are ones based on the internal Michael acceptor warheads and the last section involves the terminal warheads.

The majority of the ligands docked well inside the ATP-binding site of the GSK-3β, when compared to the docked **206**. Compounds **220** and **223** were the only ligands that failed to fit correctly inside the binding site. The possible reasons for the failed docking are steric hindrance and bad interactions between the ligand and the receptor. Specifically, the bulky cyclohexane ring in **220** forced the ligand to dock incorrectly. In addition, the interactions between the N-atom of the pyridine ring in **223** and the receptor resulted in repulsion, which led to incorrect docking of this ligand. Different results were obtained for compounds **232** and **235**, where, presumably, the arrangement of the side chain or the hydrogen bonding allows for a fixed configuration.

Table 2.1. Docking scores of the compounds with an internal Michael acceptor

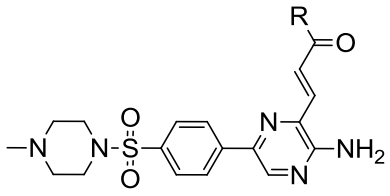

210

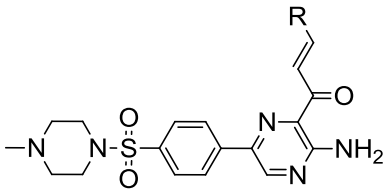

211

R	Docking score	R	Docking score	R	Docking score	R	Docking score
 **216**	-5.751	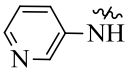 **222**	-8.198	 **228**	-7.746	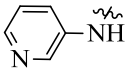 **234**	-6.030
 **217**	-7.205	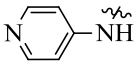 **223**	failed	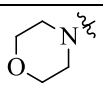 **229**	-5.383	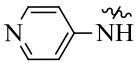 **235**	-5.923
 **218**	-7.439	 **224**	-6.833	 **230**	-4.905	 **236**	-5.862
 **219**	-7.204	 **225**	-9.609	 **231**	-5.338	 **237**	-5.771
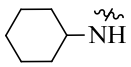 **220**	failed	 **226**	-8.168	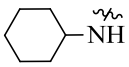 **232**	-5.138	 **238**	-5.931
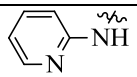 **221**	-7.392	 **227**	-7.808	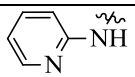 **233**	-5.866	 **239**	-5.794

Table 2.2. Docking scores of the compounds with a terminal Michael acceptor or HMK

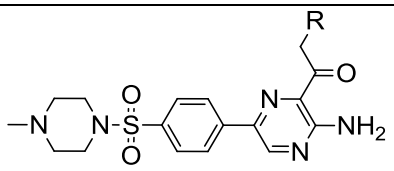

R	Docking score	R	Docking score	R	Docking score	R	Docking score
Br **214**	-5.713	Cl **215**	-5.704	 **212**	-5.193	 **213**	-5.561

The distance between the electrophilic thiol of Cys199 and the β-carbon of Michael acceptors **212-219**, **221**, **222** and **224-239** was measured to be in the region of 3.7 – 4.6 Å.

As an example, Figure 2.13 shows compound **239** docked into the active site. It has hydrogen-bonding interactions with the critical amino acids Asp133 and Val135 in the hinge region (1.8 and 2.5 Å, respectively). Furthermore, a pi-cation interaction between Lys85 and the imidazole ring was observed. Lastly the distance between the thiol of Cys199 and the β-carbon of the Michael acceptor was measured as 3.69 Å.

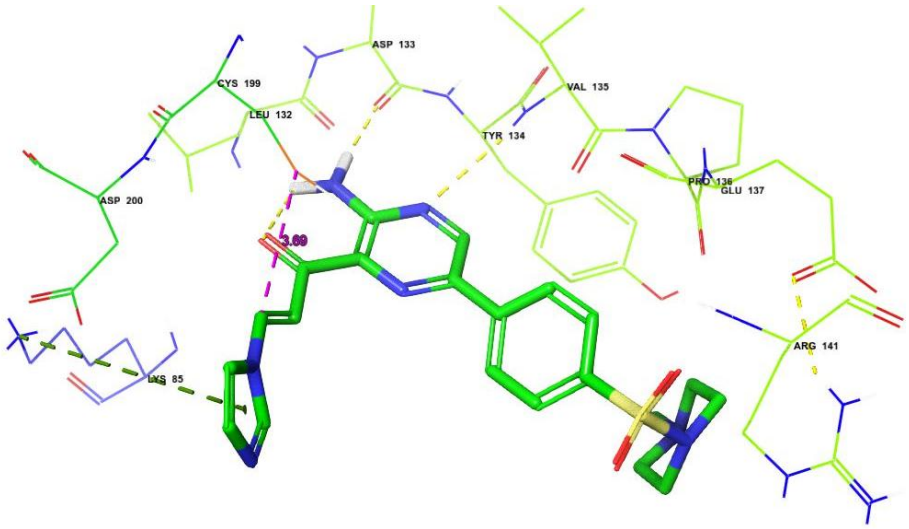

Figure 2.13. Compound **239** interacts with Val135, Asp133 and Lys85. The distance between the thiol of Cys199 and the β-carbon of the Michael acceptor is 3.69 Å

With the aforementioned results in hand, the next step was to run the covalent docking process. Cys199 was selected as the reactive residue and the co-crystallised molecule **206** was used to determine the receptor grid box size (coordinates: x: 23.9 Å, y: -18.8 Å, z: 9.9 Å). The reaction types that were used to simulate the covalent bond formation were Michael addition and nucleophilic substitution. The docking mode was set to thorough pose prediction option, which uses more computational time but provides more accurate docking results. The docking results of the ligands are tabulated in Tables 2.3 and 2.4. The tables are divided in sections based on the type of warhead arrangement in a similar manner to Tables 2.1 and 2.2.

Table 2.3. Covalent docking scores of the compounds with an internal Michael acceptor

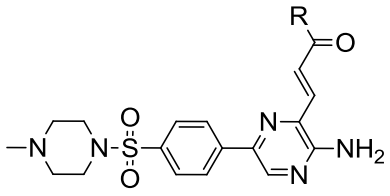

210

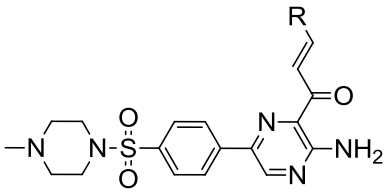

211

R	Docking score	R	Docking score	R	Docking score	R	Docking score
 **216**	-7.903	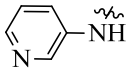 **222**	-5.719	 **228**	-6.242	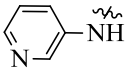 **234**	failed
 **217**	-7.995	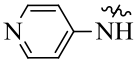 **223**	-	 **229**	-6.460	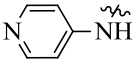 **235**	-5.913
 **218**	-6.378	 **224**	-6.705	 **230**	-6.542	 **236**	-7.325
 **219**	-6.570	 **225**	-7.454	 **231**	-7.394	 **237**	-6.273
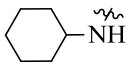 **220**	-	 **226**	-5.772	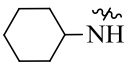 **232**	-5.374	 **238**	-5.658
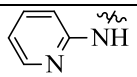 **221**	-5.682	 **227**	-7.479	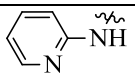 **233**	-5.911	 **239**	-6.345

Table 4. Covalent docking scores of the compounds with a terminal Michael acceptor or HMK

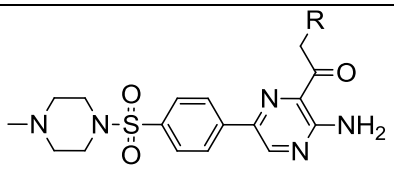

R	Docking score	R	Docking score	R	Docking score	R	Docking score
Br **214**	-6.597	Cl **215**	-5.955	 **212**	-7.065	 **213**	-5.737

The results in general showed that the docked ligands exhibited favourable affinity for covalent docking. Visual inspection of the covalently docked ligands showed that a large group of the ligands retained their interactions with the hinge region after simulated covalent bond formation, while maintaining correct bond geometries. Compared to **222**, compound **234** failed to form a simulated covalent bond with Cys199, which could possibly be explained by the change in shape of the side chain that resulted in a repulsive interaction between the N-atom of the pyridine and the receptor.

Figure 2.14 shows the simulated covalent bond between the thiol of Cys199 and the best docked ligand, compound **236**. This type of result suggests that it is indeed possible to form a covalent bond with Cys199 using the aforementioned warheads without sacrificing the conformation of the ligand and preserving interactions with the hinge region.

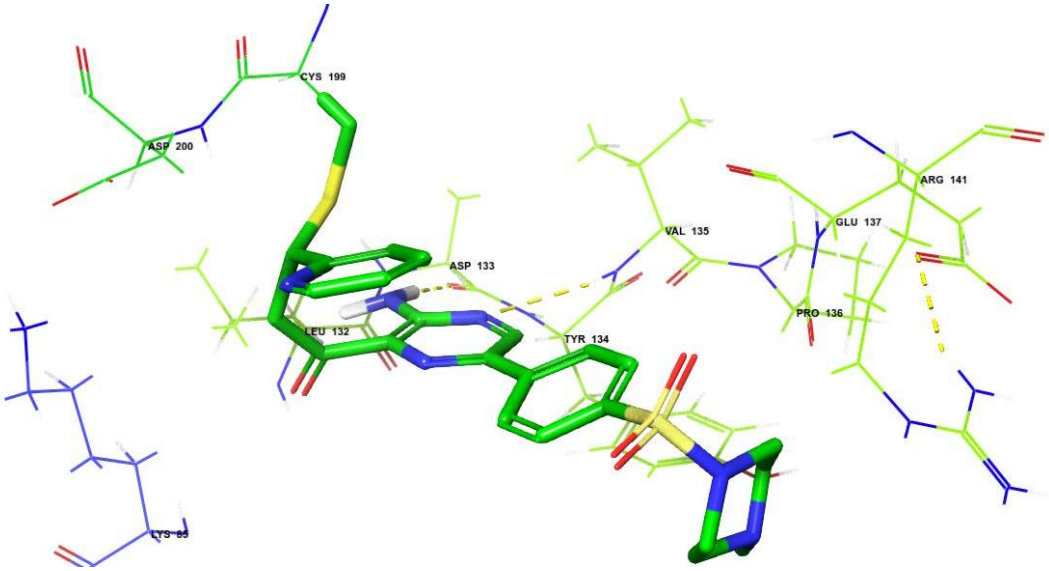

Figure 2.14. Simulated covalent bond formation between the thiol of Cys199 and **236**.

The molecular modelling suggested that this series of molecules was worth pursuing. The next few chapters will discuss the synthesis of some of the molecules that were described here.

2.4 References

1. G. Manning, D. B. Whyte, R. Martinez, T. Hunter and S. Sudarsanam, *Science*, 2002, **298**, 1912-1934.

2. J.-Y. Mérour, F. Buron, K. Plé, P. Bonnet and S. Routier, *Molecules*, 2014, **19**, 19935-19979.
3. K. L. Gibbs, L. Greensmith and G. Schiavo, *Trends in Biochemical Sciences*, 2015, **40**, 597-610.
4. V. M.-Y. Lee, K. R. Brunden, M. Hutton and J. Q. Trojanowski, *Cold Spring Harbor Perspectives in Medicine*, 2011, **1**, a006437.
5. D. M. Holtzman, M. C. Carrillo, J. A. Hendrix, L. J. Bain, A. M. Catafau, L. M. Gault, M. Goedert, E. Mandelkow, E.-M. Mandelkow, D. S. Miller, S. Ostrowitzki, M. Polydoro, S. Smith, M. Wittmann and M. Hutton, *Alzheimer's & Dementia*, 2016, **12**, 1033-1039.
6. T. Arendt, J. T. Stieler and M. Holzer, *Brain Research Bulletin*, 2016, **126**, 238-292.
7. M. Medina, F. Hernández and J. Avila, *Biomolecules*, 2016, **6**, 1-12.
8. M. Medina, J. J. Garrido and F. Wandosell, *Frontiers in Molecular Neuroscience*, 2011, **4**, Article 24.
9. C. Ballatore, V. M. Y. Lee and J. Q. Trojanowski, *Nature Reviews Neuroscience*, 2007, **8**, 663-672.
10. C. A. Grimes and R. S. Jope, *Progress in Neurobiology*, 2001, **65**, 391-426.
11. N. Embi, D. B. Rylatt and P. Cohen, *European Journal of Biochemistry*, 1980, **107**, 519-527.
12. S. E. Plyte, K. Hughes, E. Nikolakaki, B. J. Pulverer and J. R. Woodgett, *Biochimica et Biophysica Acta (BBA) - Reviews on Cancer*, 1992, **1114**, 147-162.
13. H. Eldar-Finkelman and E. G. Krebs, *Proceedings of the National Academy of Sciences*, 1997, **94**, 9660-9664.
14. H. Kadavath, R. V. Hofele, J. Biernat, S. Kumar, K. Tepper, H. Urlaub, E. Mandelkow and M. Zweckstetter, *Proceedings of the National Academy of Sciences*, 2015, **112**, 7501-7506.
15. R. V. Bhat, S. L. Budd Haeberlein and J. Avila, *Journal of Neurochemistry*, 2004, **89**, 1313-1317.
16. E. Haar, J. T. Coll, D. A. Austen, H.-M. Hsiao, L. Swenson and J. Jain, *Nature Structural Biology*, 2001, **8**, 593-596.
17. M. Aoki, T. Yokota, I. Sugiura, C. Sasaki, T. Hasegawa, C. Okumura, K. Ishiguro, T. Kohno, S. Sugio and T. Matsuzaki, *Acta Crystallographica Section D*, 2004, **60**, 439-446.

18. T. Kramer, B. Schmidt and F. Lo Monte, *International Journal of Alzheimer's Disease*, 2012, **2012**, Article ID 381029.
19. M. E. M. Noble, J. A. Endicott and L. N. Johnson, *Science*, 2004, **303**, 1800-1805.
20. S. Berg, M. Bergh, S. Hellberg, K. Högdin, Y. Lo-Alfredsson, P. Söderman, S. von Berg, T. Weigelt, M. Ormö, Y. Xue, J. Tucker, J. Neelissen, E. Jerning, Y. Nilsson and R. Bhat, *Journal of Medicinal Chemistry*, 2012, **55**, 9107-9119.
21. R. Nussinov and C.-J. Tsai, *Annual Review of Pharmacology and Toxicology*, 2015, **55**, 249-267.
22. J. Zhang, P. L. Yang and N. S. Gray, *Nature Reviews Cancer*, 2009, **9**, 28-39.
23. C. González-Bello, *ChemMedChem*, 2016, **11**, 22-30.
24. R. A. Bauer, *Drug Discovery Today*, 2015, **20**, 1061-1073.
25. L. Garuti, M. Roberti and G. Bottegoni, *Current Medicinal Chemistry*, 2011, **18**, 2981-2994.
26. C. Carmi, M. Mor, P. G. Petronini and R. R. Alfieri, *Biochemical Pharmacology*, 2012, **84**, 1388-1399.
27. J. C. Powers, J. L. Asgian, Ö. D. Ekici and K. E. James, *Chemical Reviews*, 2002, **102**, 4639-4750.
28. A. Michalczyk, S. Klüter, H. B. Rode, J. R. Simard, C. Grütter, M. Rabiller and D. Rauh, *Bioorganic & Medicinal Chemistry*, 2008, **16**, 3482-3488.
29. D. I. Perez, S. Conde, C. Pérez, C. Gil, D. Simon, F. Wandosell, F. J. Moreno, J. L. Gelpí, F. J. Luque and A. Martínez, *Bioorganic & Medicinal Chemistry*, 2009, **17**, 6914-6925.
30. D. I. Perez, V. Palomo, C. Pérez, C. Gil, P. D. Dans, F. J. Luque, S. Conde and A. Martínez, *Journal of Medicinal Chemistry*, 2011, **54**, 4042-4056.
31. S. Conde, D. I. Pérez, A. Martínez, C. Perez and F. J. Moreno, *Journal of Medicinal Chemistry*, 2003, **46**, 4631-4633.
32. E. Harder, W. Damm, J. Maple, C. Wu, M. Reboul, J. Y. Xiang, L. Wang, D. Lupyan, M. K. Dahlgren, J. L. Knight, J. W. Kaus, D. S. Cerutti, G. Krilov, W. L. Jorgensen, R. Abel and R. A. Friesner, *Journal of Chemical Theory and Computation*, 2016, **12**, 281-296.

Chapter 3

Synthesis of (*E*)-3-(3-aminopyrazin-2-yl)acrylaldehyde derivatives

3.1 Overview

After the molecular modelling had been completed, the results were used to synthesise the compounds. The boronic acid scaffold **243** was duly synthesised, followed by the attachment of the aminopyrazine core using the Suzuki-Miyaura method. The Suzuki-Miyaura chemistry took significant optimisation to produce acceptable yields. A series of side chains with warheads were then synthesised and finally coupled to the aminopyrazine core to afford the final compounds.

3.2 Retrosynthetic analysis of the library

As shown in Figure 3.1, the final compounds **240** synthesised in this library consist of the scaffold and a side chain. The connection point occurs on the aminopyrazine core of the scaffold. Using a retrosynthetic approach, the molecule can be disconnected to the heteroaryl bromide **241** and the Michael acceptor **242**. In turn, **241** could be disconnected to the boronic acid **242** and 5-bromopyrazin-2-amine **244**. The boronic acid **243** could be readily produced from the sulfonyl chloride **245** and **245** could be obtained from the commercially available bromobenzene **246** by way of sulfonation. Finally, the mono-bromo **244** could be synthesised from commercially available aminopyrazine **247**

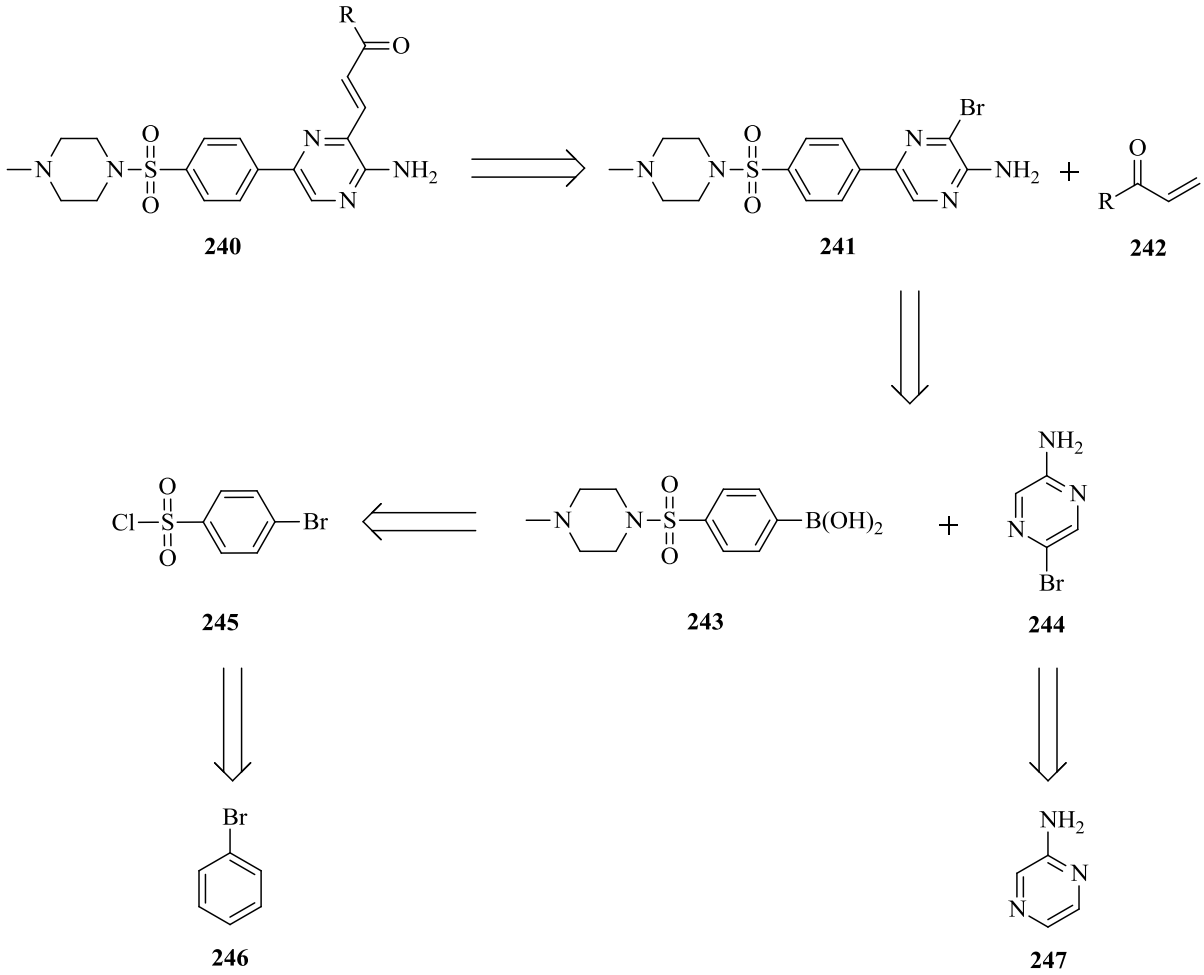

Figure 3.1 Retrosynthetic analysis of the library

3.3 The synthesis of the scaffold

3.3.1 The synthesis of {4-[(4-methylpiperazin-1-yl)sulfonyl]phenyl}boronic acid (243)

According to the disconnection plan in Figure 3.1, the sulfonation of commercially available bromobenzene **246** was carried out using excess chlorosulfonic acid in chloroform. This reaction followed the procedure set out by Samanta *et al.*[1] and is summarised in Scheme 3.1. Chlorosulfonic acid was added dropwise to the solution via a dropping funnel while keeping the temperature below 5 °C. The resulting brown solution was left to stir overnight and then poured onto crushed ice. After purification by column chromatography, the corresponding sulfonated compound was isolated as white-grey solid in a disappointing yield of 38%. An unidentified by-product, which was more polar than **245**, as well as unreacted **245** were seen on the TLC plate.

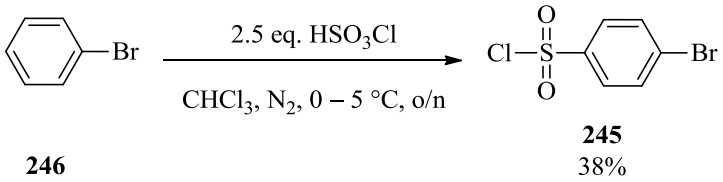

246 **245** 38%

Scheme 3.1. Sulfonation of bromobenzene **246**

To improve the yield, the reaction procedure was modified. The amount of chlorosulfonic acid was increased to 11 eq. to ensure all starting bromobenzene is consumed. To address the problem with the generation of by-products, the reaction was started at -78 °C instead of 0 °C. The reaction was then left to warm gradually to room temperature overnight. This modification afforded the product in a much more acceptable yield of 74%. Two distinctive doublets on the ^{1}H NMR spectrum at 7.91 and 7.77 ppm confirmed the sulfonation of bromobenzene **246** and the values correlated well with data that were reported in the literature.[2]

The next step required the mono-alkylation of piperazine with sulfonyl chloride **245** using an adapted procedure developed by Henderson *et al*. (Scheme 3.2).[3] An excess of piperazine was required to avoid dialkylation, but in an attempt to reduce waste, the number of equivalents was reduced from six to four without significant loss in yield of the desired product. Dissolved 4-bromobenzene-1-sulfonyl chloride **245** was thus added dropwise to a solution of piperazine in dichloromethane. The resulting white slurry was stirred further for two hours before it was worked up with saturated $NaHCO_3$ solution. The product, 1-[(4-bromophenyl)sulfonyl]piperazine **248**, was isolated in an excellent yield of 91% after purification by column chromatography. Mass spectrometry data confirmed that the mono-alkylated product had been obtained (see experimental section). Also, the presence of the piperazine ring was observed on the ^{1}H NMR spectrum as a multiplet at 2.98 – 2.84 ppm.

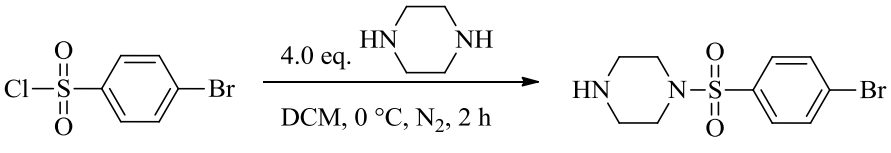

245 **248** 91%

Scheme 3.2. Mono-alkylation of piperazine with **245**

Next, the methylation of **248** was carried out using the adapted procedure shown in Scheme 3.2 in which iodomethane was used as the electrophile (Scheme 3.3). Unfortunately, three different spots (R_f : 0.57, 0.73, 0.93; 9:1 DCM:MeOH) were observed on the TLC plate. It was thus suspected that the piperazine had also quartenised in the presence of iodomethane.

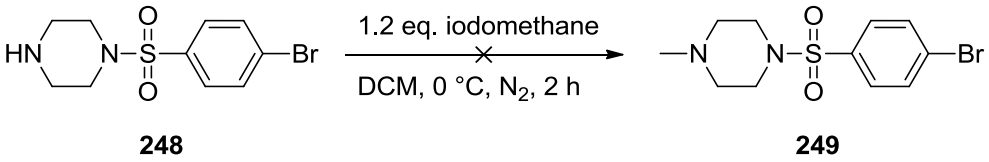

248 **249**

Scheme 3.3. Failed methylation of piperazine **248**

The reductive amination of **248** was then attempted using the modified procedure of a Bristol-Myers Squibb company patent.[4] As shown in Scheme 3.4, $NaCNBH_3$, a general reducing agent for reductive amination, was selected for this reaction.[5-7] The reaction was carried out firstly under basic (Et_3N) conditions as stated in the patent, alternatively under acidic conditions (AcOH) to protonate the formed alcohol. Unfortunately, in both cases, the reaction did not go to completion. Two different products (R_f: 0.64, 0.81; 9:1 DCM:MeOH) were also observed on the TLC plate. In our hands, attempts at separation proved futile. It is possible that one of the products was the double methylated product, although this was not confirmed.

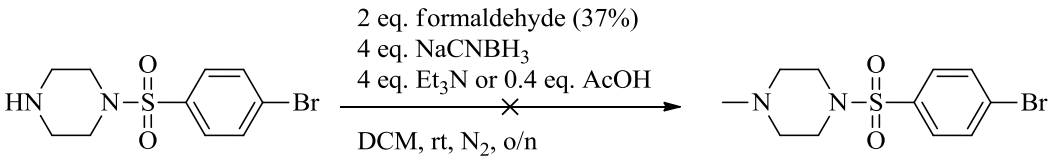

248 **249**

Scheme 3.4. Failed reductive amination of piperazine **248**

A different reductive amination procedure was then attempted, this time using zinc as the electron source in an aqueous acidic medium.[8] It has been shown that the use of zinc in aqueous acetic acid reduces the possibility of over-methylation.[8] As shown in Scheme 3.5, piperazine **248** was added to a solution of dioxane and excess formaldehyde. Zn dust was then added and the resulting grey solution was stirred for one day at room temperature. The solution was then concentrated, diluted with EtOAc and neutralised with a saturated solution of $NaHCO_3$. The product could then be separated from the small amount of dimethylated

by-product using column chromatography and was isolated as white solid in good yield of 85%.

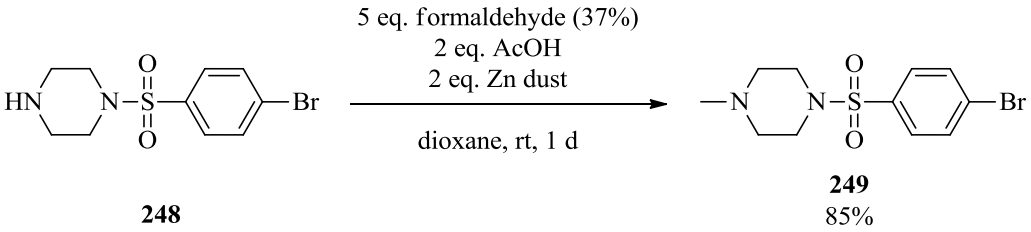

Scheme 3.5. Successful methylation of **248**

In Figure 3.2, the ^{1}H NMR spectrum of methylpiperazine **249** shows a singlet at 2.25 ppm, which integrated for three protons. This indicated the successful mono-methylation of piperazine **248**. The analytical data were in good agreement with the data reported in the literature for this compound.[9]

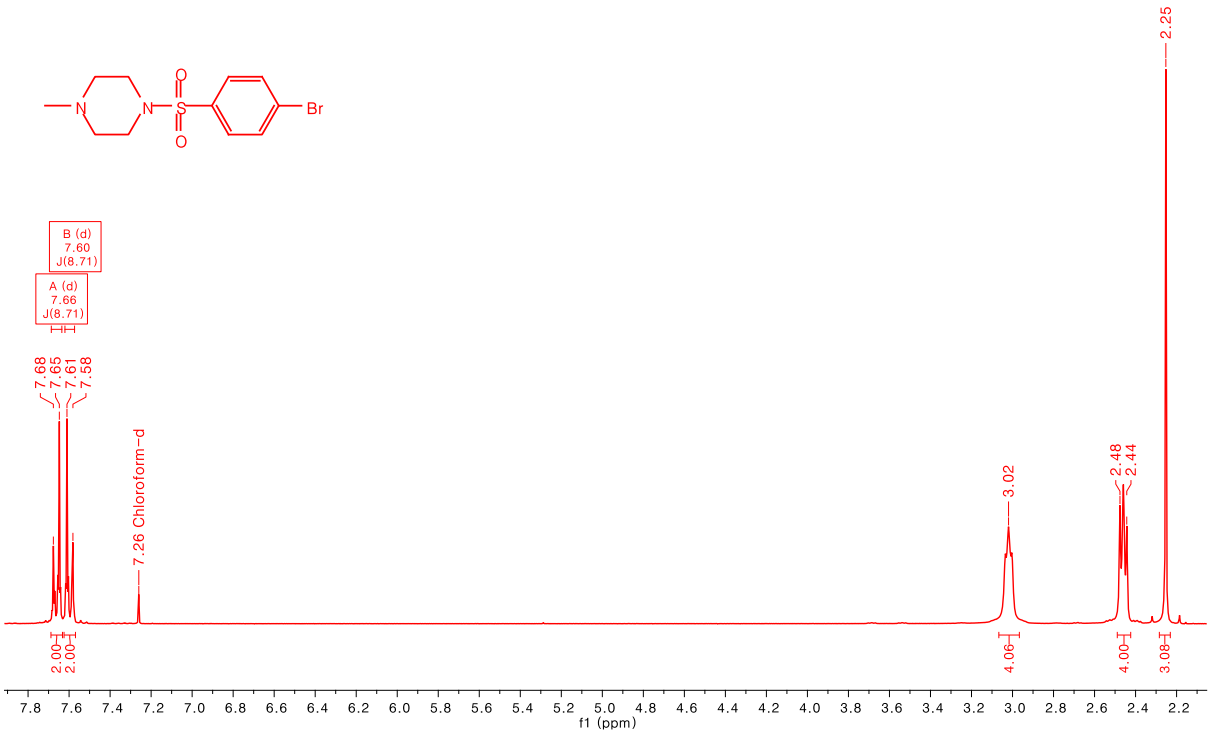

Figure 3.2. ^{1}H NMR spectrum of methylpiperazine **249**

With compound **249** in hand, the next step of the scaffold synthesis required the boronation reaction.[10] To this end, the aryl bromide was first lithiated with *n*-BuLi at –78 °C and stirred for three hours, followed by the addition of trimethyl borate (Scheme 3.6). The resulting dark

orange solution was then stirred for a further three hours before it was warmed to 0 °C and quenched with 2 M HCl. After the quenching, the clear solution was stirred for an additional one hour. The solution was then extracted with Et_2O and concentrated to dryness. After attempts to work up the reaction it became clear that the product was water soluble and that an aqueous work up should be avoided, as no product was isolated.

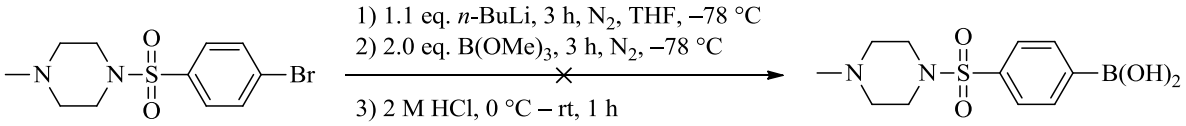

249 **243**

Scheme 3.6. Attempted boronation of compound **249**

To work around the water solubility issue, an alternative procedure was used. This procedure involved the quenching of the reaction with H_2O, followed by concentration under reduced pressure. The mixture was then purified using column chromatography.[11, 12] However, trimethyl borate was used instead of the triisopropyl borate as suggested in the literature.[12] As depicted in Scheme 3.7, **249** and trimethyl borate were dissolved in THF and *n*-BuLi was added dropwise to the solution at –78 °C. The solution was then stirred for two hours at –78 °C and allowed to warm to room temperature whilst stirring for an additional 20 h. Instead of a workup, the reaction was then quenched with a minimum amount of H_2O and the solution was concentrated under reduced pressure. According to the TLC plate, only starting materials were observed. The addition of *n*-BuLi to a solution containing trimethyl borate thus proved to be problematic as the lithium reagent appeared to react with the electrophilic trimethyl borate instead of the aryl bromide.

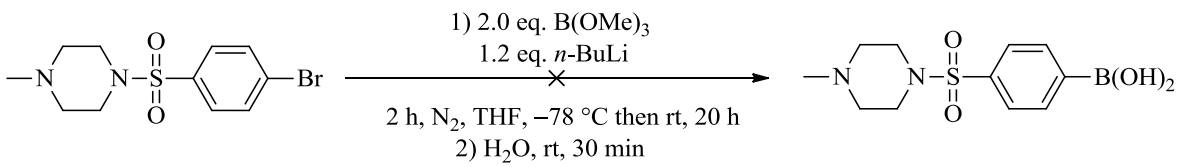

249 **243**

Scheme 3.7. Attempted lithiation of **249**

The procedure was then adapted slightly by changing the order of addition of reagents. *n*-BuLi was thus allowed to react with the aryl bromide, before the addition of trimethyl borate. The reaction was then quenched with 2 M HCl instead of H_2O, to ensure complete

protonation of the formed borate ester species and to promote the consumption of unreacted *n*-BuLi and trimethyl borate. Scheme 3.8 shows the optimised conditions for the boronation of **249**. Since the product **243** is very polar, it was determined that purification by column chromatography was not feasible, although this has been reported in the literature.[11, 12] An alternative method was tried that involved crystallising the crude product. It was also determined experimentally that boronic acid product **243** was poorly soluble in MeOH. The generated LiCl,[13] $B(OH)_3$[14] and the starting material are all soluble in MeOH, and the product could thus be crystallised out of boiling MeOH. In this manner, a white precipitate was isolated that was indeed the boronic acid **243** in 65% yield.

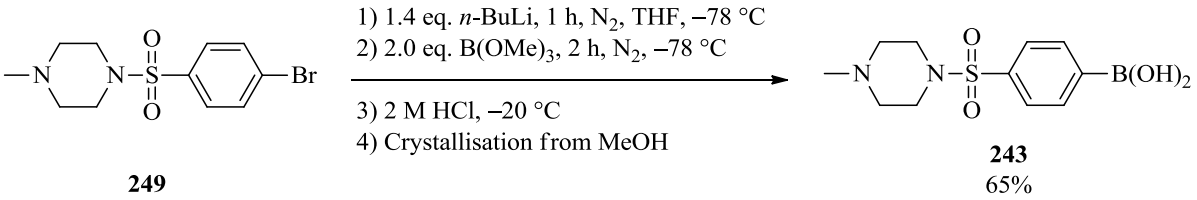

Scheme 3.8. Successful boronation of **249** involving crystallization as the last step

The ^{1}H NMR spectrum of the boronic acid **243** in d_6-DMSO can be seen in Figure 3.3 with the boronic acid OH groups appearing as a broad singlet at 8.44 ppm. In addition, the boronic acid proton peak was not seen in D_2O solvent due to proton exchange. Lastly, mass spectrometry data correlated well with the expected molecular mass of **243**.

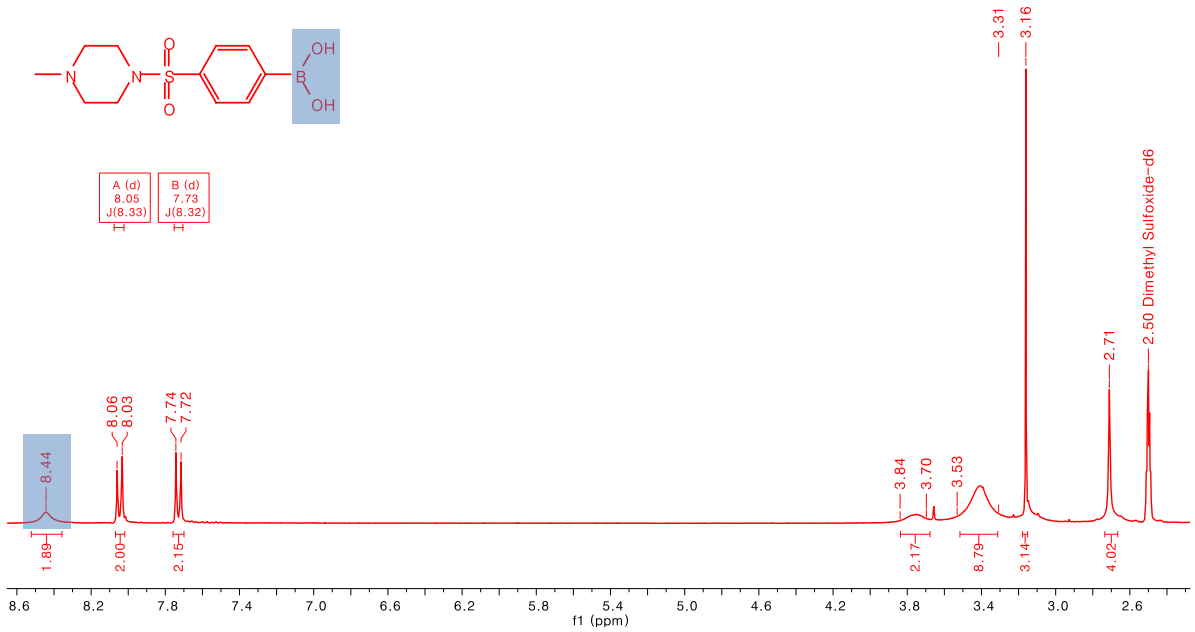

Figure 3.3. ^{1}H NMR spectrum of boronic acid **243**

3.3.2 The synthesis of 5-bromopyrazin-2-amine (244)

The last step of the scaffold synthesis began with the synthesis of the required aminopyrazine core. Pyrazine **247** can undergo an oxidative amination reaction using potassium amide as the nucleophile, liquid NH_3 as the solvent and $KMnO_4$ as the oxidant to form aminopyrazine **250** (Scheme 3.9).[15] This reaction was attempted using sodium amide but after numerous attempts, the product could not be made. For the sake of convenience, the synthesis of aminopyrazine **250** was abandoned and the chemical was purchased from Sigma Aldrich.

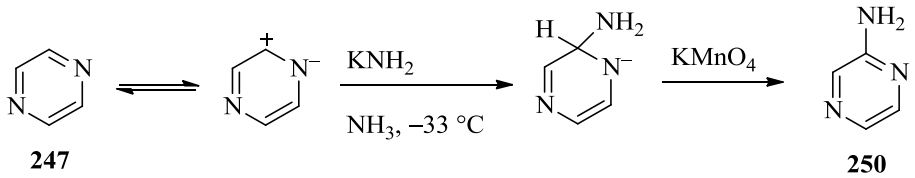

Scheme 3.9. Attempted oxidative amination of pyrazine **250**

The next step was the selective mono-bromination of **250**. Several papers have reported procedures for the bromination of aminopyrazine **250** in various solvents such as DMSO, DCM, DMF and CH_3CN, but the researchers involved obtained low yields or mixtures of mono- and di-brominated compounds.[16-19] The exception to this is the method reported by Mitchell *et al.*[20] They describe mono-bromination of aromatic compounds by adding NBS in DMF dropwise to a solution of an aromatic compound and DMF at room temperature. This method was successfully used to brominate aminopyrazine **250** selectively in the *para* position (Scheme 3.10). After the reaction had been completed, the dark brown solution was poured into ice-water and extracted four times with ethyl acetate. The crude brown residue was then purified using column chromatography to afford the brominated product **244** in a satisfactory 67% yield.

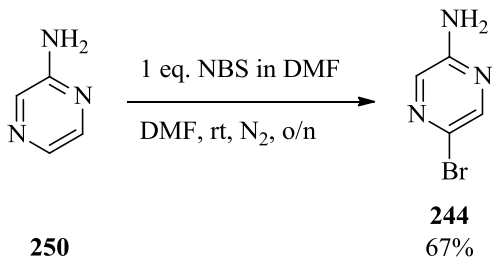

Scheme 3.10. Selective mono-bromination of **250**

Under these conditions, it was determined on the TLC plate that the di-brominated compound had also formed. In addition, the workup was found to be tedious and required copious amounts of ethyl acetate to extract the product out of the DMF-water layer. An improved procedure was thus developed to minimise the formation of the di-brominated compound and to eliminate the workup. As shown in Scheme 3.11, the dissolved NBS was added dropwise to the solution at 0 °C, instead of at room temperature. After completion of the reaction, the solution was concentrated under reduced pressure and the crude reaction mixture was then purified using column chromatography. This resulted in **244** being obtained in a good yield of 86%. The improved conditions resulted in a substantial increase in yield and eliminated the need for a workup. In addition, the lower temperature appeared to reduce the formation of the di-brominated product. Finally, the characterisation data for **244** correlated well with the data reported in the literature.[18]

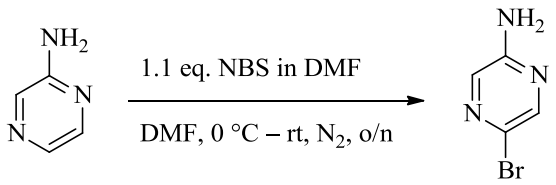

250 **244** 86 %

Scheme 3.11. Improved conditions for the *para*-bromination of **250**

3.3.3 The quest for optimal conditions for the Suzuki-Miyaura reactions

With the boronic acid and the heteroaryl bromide in hand, the scaffold could be assembled via a Suzuki-Miyaura reaction. Hachiya *et al.*[21] have developed a series of aminopyrazine derivatives from **244** through Suzuki-Miyaura couplings. This procedure was adapted for the synthesis of compound **251** and the conditions are depicted in Scheme 3.12. The first Suzuki-Miyaura reaction was carried out in dioxane using $Pd(PPh_3)_4$ as the catalyst and Na_2CO_3 as the base. However, TLC analysis indicated that no product had formed after running the reaction overnight. The addition of water to facilitate the solubility of Na_2CO_3 and heating the reaction to 95 °C unfortunately failed to make a difference.

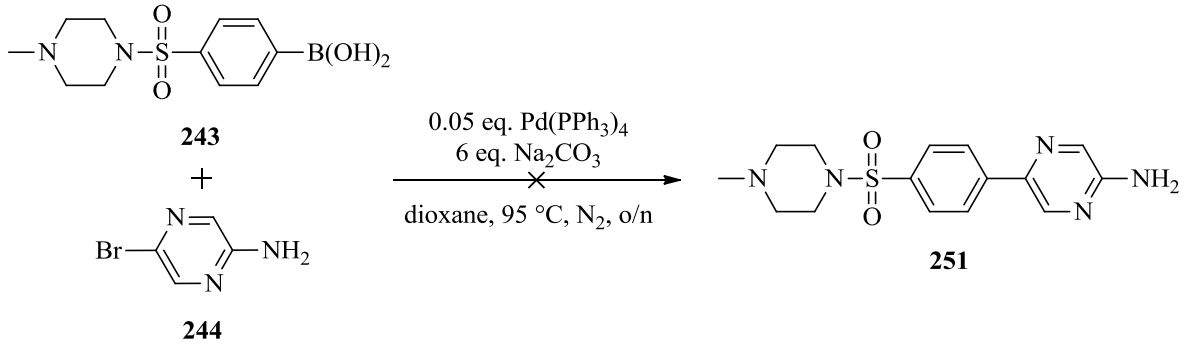

Scheme 3.12. First attempt of the Suzuki-Miyaura reaction

Suzuki-Miyaura reactions are known to frequently require significant optimisation.[22, 23] To this end, different catalysts, bases and solvents were investigated to find the optimum conditions for the Suzuki-Miyaura reaction in this system.

The next catalyst that was investigated was an *N*-heterocyclic carbene (NHC)-palladium complex. Over the years, NHCs have emerged as alternatives to phosphine ligands for the Suzuki-Miyaura coupling. The electron-rich NHC ligands are thought to facilitate the oxidative addition of the aryl halide, while the steric bulkiness increases the rate of the reductive elimination step in the Suzuki-Miyaura cross-coupling cycle.[24, 25]

In our research group, Lonwabo Ngodwana,[26] found success using mesityl-NHC as a ligand for $Pd(OAc)_2$ for his Suzuki-Miyaura reactions. The palladium complex was prepared *in situ* followed by the addition of the starting materials. His procedure was used for the attempted synthesis of **251** and is described in Scheme 3.13. It should be noted that the base was changed to Cs_2CO_3, while the other parameters are the same as in Scheme 3.12. Unfortunately, only starting materials were isolated after stirring the reaction overnight.

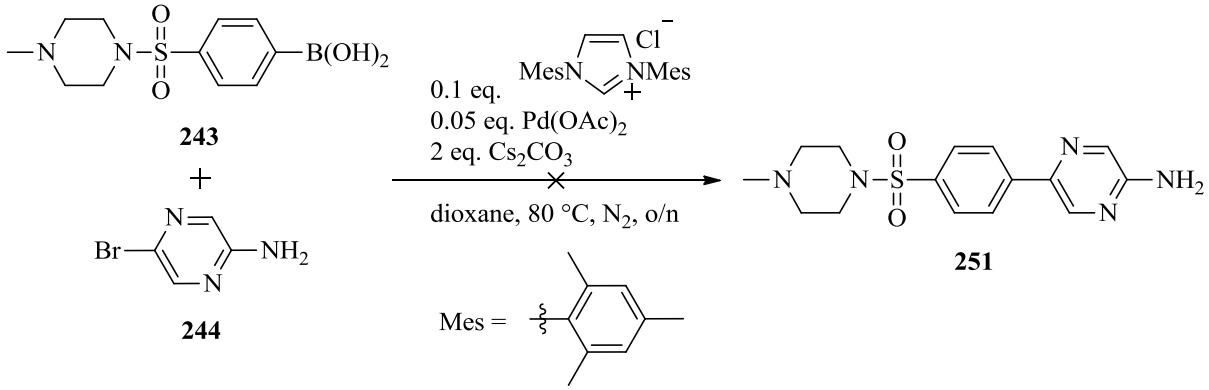

Scheme 3.13. The use of an *N*-heterocyclic carbene-palladium complex for the Suzuki-Miyaura reaction.

Based on the results obtained, it was clear that a specific type of palladium catalyst would be required for the synthesis of **251**. Suzuki-Miyaura reactions with aminopyrazines have been described in a review and one of the catalysts that provided excellent results was Pd(dppf)Cl_2.[27] Compared to other palladium catalysts, the effectiveness of Pd(dppf)Cl_2 can be ascribed to the relatively large P-Pd-P bite angle, which is thought to enhance the rate of the reductive elimination step.[27] In addition, the oxidative addition step of the Suzuki-Miyaura reaction is expected to be facilitated by the electron-rich ferrocene.[28] These properties could improve the Suzuki-Miyaura reaction between the poorly nucleophilic boronic acid **243** and the poorly electrophilic heteroaryl **243**.

However, the price of Pd(dppf)Cl_2 **255** turned out to be prohibitive, and so the catalyst was synthesised using established procedures.[29-31] Scheme 3.14 thus depicts the synthesis of the catalyst Pd(dppf)Cl_2 **255**. The commercially available ferrocene **252** was therefore di-lithiated, followed by the addition of the electrophile, PPh_2Cl, to yield the phosphinated ferrocene ligand **253** in 30% yield.[29] The last step[30] involved the complexation of the ligand **253** with Pd$(CH_3CN)_2Cl_2$ **254**[31] to afford the catalyst **255** in 90% yield. The spectroscopic data of **255** correlated well with the data reported in the literature.[30] Furthermore, a single ^{31}P peak at 34.46 ppm was observed for **255** (referenced to H_3PO_4 in the ^{31}P NMR spectrum).

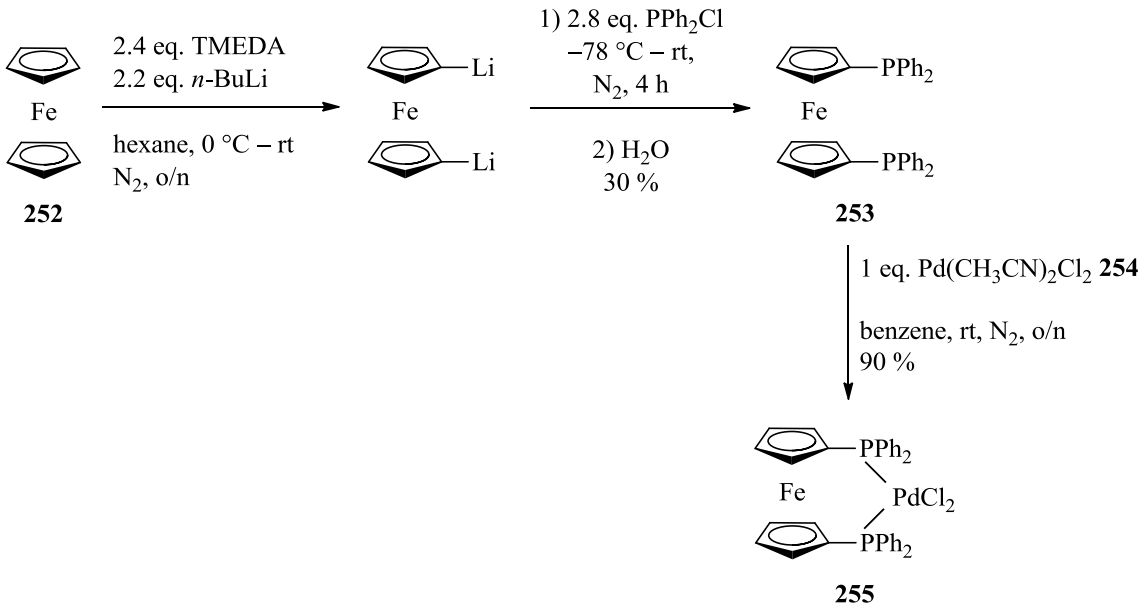

Scheme 3.14. Synthesis of Pd(dppf)Cl_2 **255**

In addition to the catalyst, it is known that the type of base and solvent play important roles in Suzuki-Miyaura reactions.[22, 32] The amount and the strength of the base play a critical role in the transmetallation step[33] and solvents interact directly with the reaction substrates, which can influence the reaction rate and/or selectivity.[34] Therefore, various bases and solvent systems were used to find the optimum conditions for the Suzuki-Miyaura reactions with $Pd(dppf)Cl_2$.

The first attempt of the Suzuki-Miyaura reaction with the $Pd(dppf)Cl_2$ catalyst is shown in Scheme 3.15. The procedure of Berg *et al.*[12] was adapted for this reaction with Na_2CO_3 as the base and a 4:1 ratio of THF:H_2O as the solvent. Electron-poor arylboronic acids are known for their propensity to undergo protodeboronation under basic aqueous conditions.[35] To counteract this, an excess amount of boronic acid is frequently needed.[36] Therefore, in this attempt, 1.5 eq. of the boronic acid **243** was used.

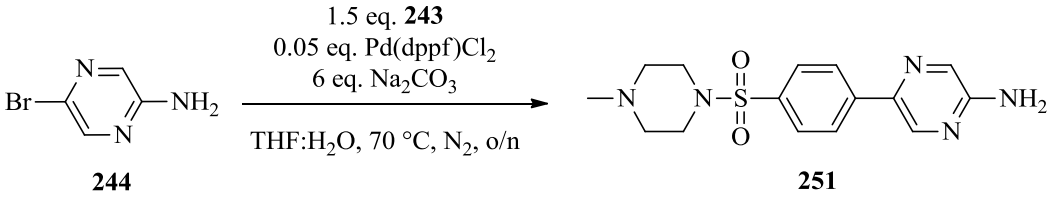

Scheme 3.15. First Suzuki-Miyaura attempt with $Pd(dppf)Cl_2$

The boronic acid **243** was therefore dissolved in THF:H_2O, followed by the addition of Na_2CO_3 and the heteroaryl bromide **244**. The catalyst, $Pd(dppf)Cl_2$, was added last and the yellow-orange solution was heated under reflux overnight. At this point, the TLC plate showed that the starting material, **244**, was fully consumed. The resulting dark brown solution was diluted with ethyl acetate, filtered over celite and then washed with deionized water. Several attempts were performed to purify the crude material using column chromatography (DCM:MeOH 9:1 as eluent) but to no avail. The main reason for this was that byproducts were present, which were difficult to separate from the desired product. Nevertheless, the ^1H NMR spectrum (presence of the methylpiperazine at δ 2.94–2.86, 2.40–2.32 and 2.12 ppm) of the crude **251** suggested that the Suzuki-Miyaura reaction had been a success.

In light of the fact that the reaction with Pd(dppf)Cl_2 did form the desired product, the next step was to change the solvent while keeping the other conditions constant. The reaction was thus repeated in neat DMSO; however the reaction failed to go to completion. After workup, starting materials were recovered and, as before, the product could not be purified using column chromatography. This clearly indicated that the solvent system did indeed play a significant role in the product formation. Berg and *et al.* used another procedure for a Suzuki-Miyaura reaction in which a solvent system of toluene and EtOH in a 4:1 ratio was used, with Na_2CO_3 as the base.[12] After using this procedure, TLC analysis indicated that starting material was still present after stirring overnight, however some formation of the product was evident.

The side products that were formed during the aforementioned attempts were speculated to originate from protodeboronation and/or homocoupling of arylboronic acids. In 2006, Lakmini and co-workers investigated the Pd-catalysed homocoupling of arylboronic acids in the presence of oxygen through electrochemical techniques and proposed a catalytic cycle for this reaction (Fig. 3.4).[37] They proposed that the initial Pd(0) reacts with O_2 to form a Pd(II)peroxo complex **256**. The next step involves the coordination of one oxygen atom of the peroxo complex with one arylboronic acid equivalent, followed by a transfer of the aryl group to the Pd(II) center to produce the peroxo complex **258**. The perboric acid **259** is then released upon hydrolysis. The released perboric acid then reacts with a second equivalent of arylboronic acid to produce the phenol derivative **260**. Lastly, a third arylboronic acid transfers an aryl group to the Ar-Pd(II) and reductively eliminates a homocoupled Ar-Ar product **263**.

The hypothesis that the side products stem from the oxygenated reaction medium was thus put to the test. In the next attempt, the freeze-pump-thaw technique[38] was used to deoxygenate the reaction medium before the Pd catalyst was added. This technique involves the flash freezing of the solution in a Schlenk tube with liquid N_2 and the application of a vacuum thereafter. Upon the subsequent thawing, bubbles of gas escape to the head space of the tube. Repeating the process at least three times removes all the gas from the reaction vessel and delivers a deoxygenated solution.

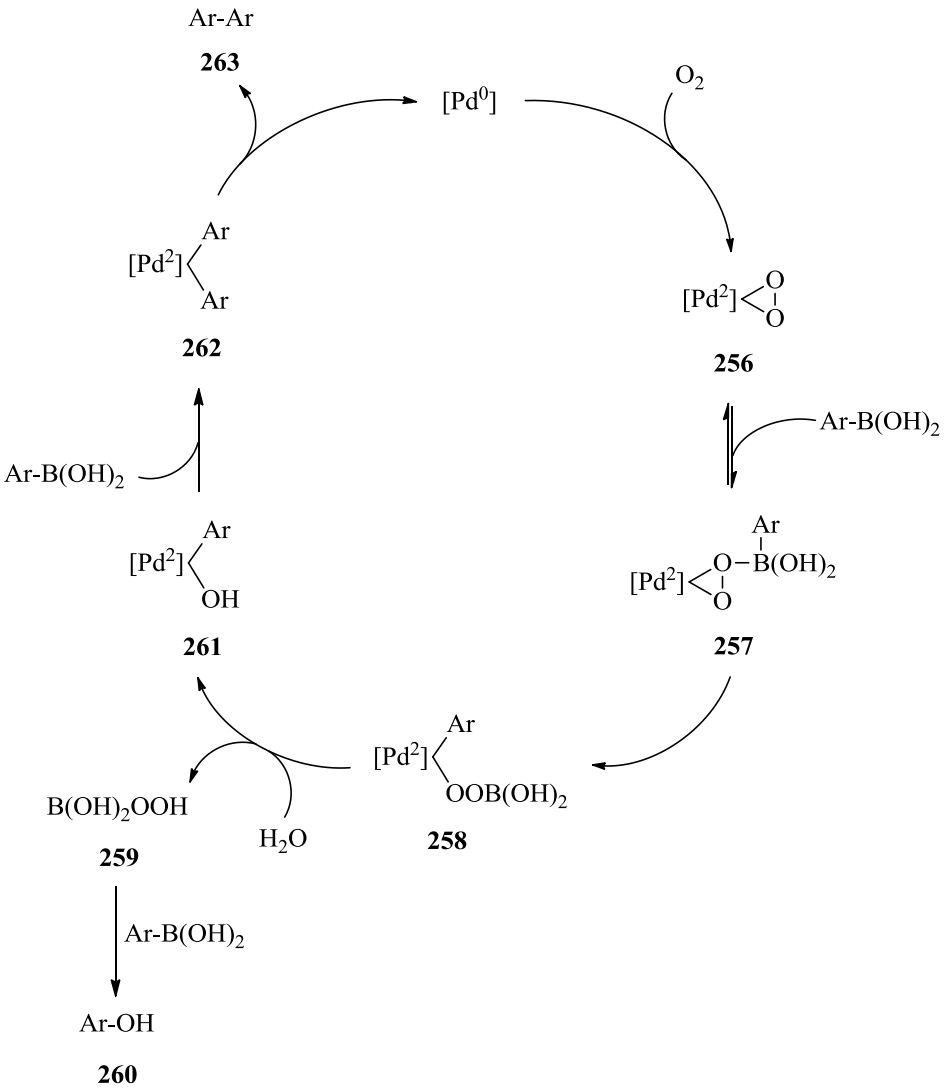

Figure 3.4. Oxidative Pd-catalysed homocoupling of arylboronic acids.[37]

As shown in Scheme 3.16, the heteroaryl bromide **244**, boronic acid **243** and a stronger base, Cs_2CO_3, were dissolved in toluene:EtOH:H_2O (4:1:0.05 ratio) in a Schlenk tube. The reason for the addition of water was to aid the solubility of Cs_2CO_3. The solution was then deoxygenated using the freeze-pump-thaw technique, followed by the addition of Pd(dppf)Cl_2 under argon. The Schlenk tube was then sealed and the dark orange solution was stirred overnight at 80 °C. Under these conditions, a full conversion of **243** was observed on the TLC plate with no detectable side products. The black solution was then diluted with EtOAc and filtered on Celite. The yellow solution was then acidified with 2 M HCl to allow the removal of the spent ferrocene ligand from the solution. The aqueous layer was then basified with saturated $NaHCO_3$ solution and extracted with EtOAc. The organic layer was

concentrated and purified using column chromatography (DCM:MeOH 9:1 as eluent) to produce the product **251** as cream solid (67% yield).

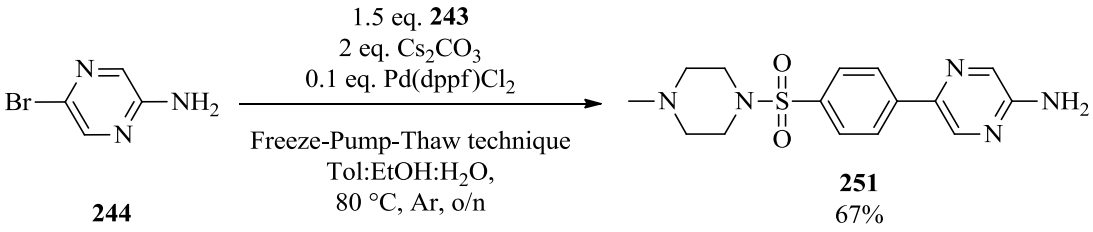

Scheme 3.16. Successful Suzuki-Miyaura reaction using the freeze-pump-thaw technique

The ^{1}H NMR spectrum of **251** (Fig. 3.5) shows the compound in pure form with no side products. The two doublets at 8.02 and 7.80 ppm can be assigned to the aromatic ring and the two doublets at 8.48 and 8.07 ppm to the aminopyrazine ring (see expansion in Fig. 3.5). The -NH_2 peak was observed as the broad singlet at 4.86 ppm and the remaining three peaks (δ 3.07, 2.47 and 2.25 ppm) for the methylpiperazine portion completes the molecule.

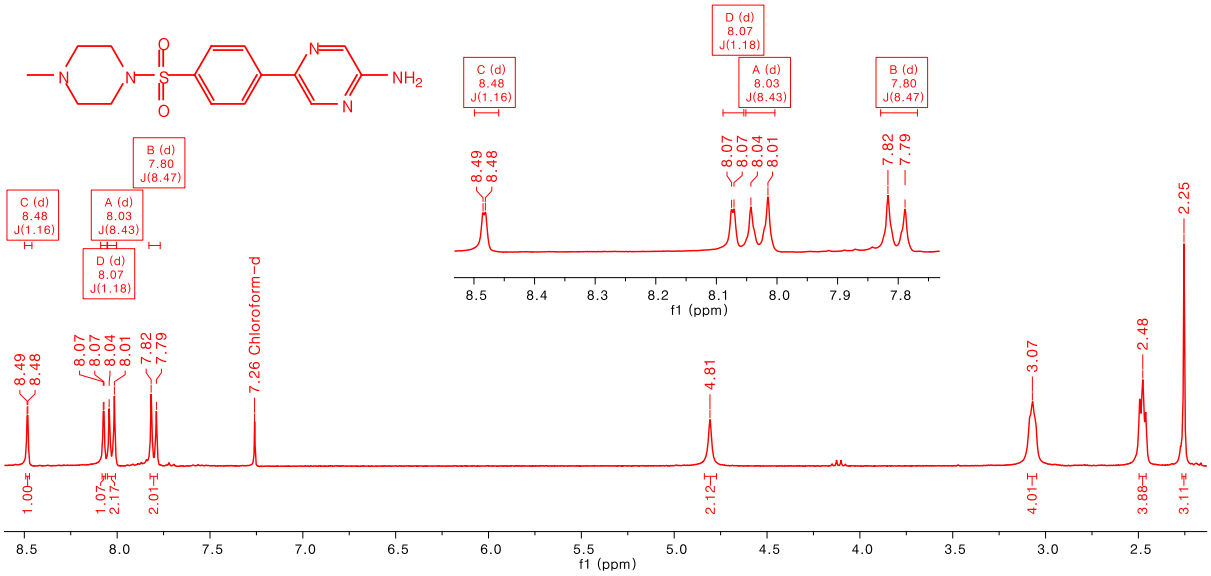

Figure 3.5. ^{1}H NMR spectrum of aminopyrazine **251** provides evidence for successful Suzuki-Miyaura coupling reaction

With the conditions for the Suzuki-Miyaura reaction now optimised, the next step was to improve the yield. In our opinion, the replacement of the halogen on **244** to iodine could potentially increase the reactivity for the oxidative addition step of the Suzuki cycle. Chou *et al.*[39] used *N*-iodosuccinimide (NIS) to iodinate their aminopyrazine precursors and this

procedure was employed for the iodination of the aminopyrazine **250** as laid out in Scheme 3.17.

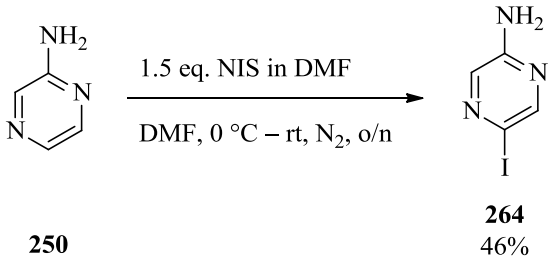

250 **264** 46%

Scheme 3.17. Iodination of aminopyrazine **250**

Since the iodinating agent, NIS, is an expensive reagent, it was synthesised from NBS using a known procedure from Chaikovskii *et al*.[40] The isolated grey solid obtained in this manner was used immediately for the next step. With the freshly prepared NIS in hand, aminopyrazine **250** was iodinated[39] and the procedure is laid out in Scheme 3.17. Aminopyrazine **250** was dissolved in DMF under N_2 and cooled to 0 °C. NIS was next dissolved in DMF and added dropwise to the solution. The yellow solution was then allowed to stir overnight at room temperature. The dark brown-orange solution was then quenched with a saturated solution of $Na_2S_2O_3$, followed by pouring over ice water. The product was extracted with EtOAc three times and the organic layers were pooled and washed once with brine. The crude material was purified using column chromatography (7:3 EtOAc:Hex as eluent) to offer the product **264** as a yellow-cream coloured solid in 46% yield. The spectroscopic data for compound **264** correlated well with the literature data.[39] The procedure of the Suzuki reaction in Scheme 3.16 was carried out with the iodinated aminopyrazine **264** and the product was isolated in 74% yield. This is a moderate 7% improvement over the brominated aminopyrazine **244**. It was then decided that the synthesis of iodo-aminopyrazine was not worth it for future Suzuki-Miyaura reactions.

At this point the effort involved in further optimisation of this reaction was weighed against potential gain in yield. The decision was made to cease further efforts at optimisation and deem the yields sufficiently good to continue with the synthetic plan.

3.3.4 Attempted bromination of 5-{4-[(4-methylpiperazin-1-yl)sulfonyl]phenyl}pyrazine-2-amine (251)

The envisioned route of attachment of the side chains to the aminopyrazine core on the scaffold was by way of a Heck reaction. This required bromination of the aminopyrazine core of **251**. The conditions for the bromination of compound **251** at the *ortho*-position of the aminopyrazine core were adapted from Scheme 3.11. As shown in Scheme 3.18, excess NBS was added portion-wise to promote the bromination at the *ortho*-position related to the -NH_2 group. However, the reaction failed to proceed to completion and only a small amount of the product was isolated. In addition, increasing the amount of NBS to 2 equivalents failed to improve the results.

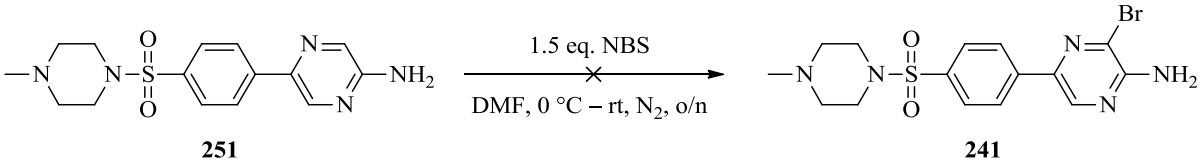

251 **241**

Scheme 3.18. First bromination attempt of **251**

The next attempt was to use the procedure from Jiang *et al.*[16] This team used NBS in DMSO to double brominate aminopyrazine **250** at the *ortho*- and *para*- positions. They isolated the corresponding di-brominated product in 85% yield. This procedure was thus tested on phenylaminopyrazine **251** to see whether it would be possible to brominate the compound at the *ortho* position via this method. In Scheme 3.19, it is shown that compound **251** was dissolved in DMSO:H_2O in a ratio of 3:1 followed by the addition of NBS in portions. The dark orange solution was then stirred overnight at room temperature. However, based on the TLC analysis, it was presumed that no product had formed and the reaction was abandoned.

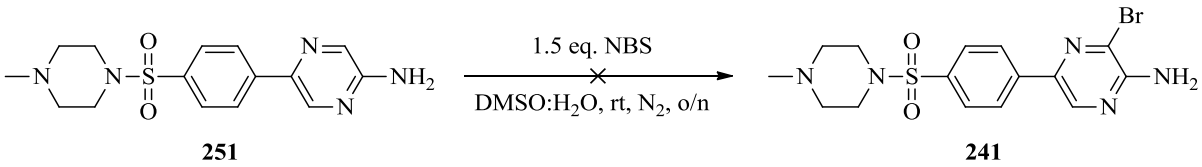

251 **241**

Scheme 3.19. Second bromination attempt of **251**

Recently, Chibale and his team[41] patented their work on anti-malarial agents which are based on aminopyrazine scaffolds. In the patent, there is a procedure that demonstrates the *ortho*

bromination of a *para* substituted aminopyrazine using NBS in DCM, as opposed to the DMSO/H_2O mix used previously. The procedure is laid out in Scheme 3.20. According to this procedure, compound **251** was dissolved in DCM and cooled to 0 °C. NBS was added in portions under N_2 and the resultant black-brown solution was stirred for one hour at room temperature. A full conversion of starting materials was observed on the TLC plate. However, a number of side products were also observed. An acid/base workup with 2 M HCl and a saturated solution of $NaHCO_3$ was carried out to determine whether the product could be separated from the side products. After the workup, the TLC plate showed only one spot, which was presumed to be the desired product, and confirmed by ^{1}H NMR spectral analysis. The brominated compound **241** was sufficiently pure that column purification was not needed. It should be noted that the product was isolated as cream-coloured solid in 46% yield.

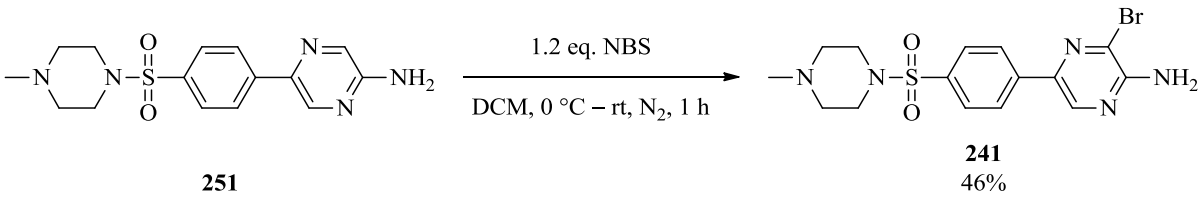

251 **241** 46%

Scheme 3.20 Successful bromination of **251**

The presence of the halogen was confirmed through spectroscopic analysis as the ^{1}H NMR spectrum showed only one heteroaromatic singlet at 8.45 ppm (Fig. 3.6). Compared to the ^{1}H NMR spectrum of compound **251** (Fig. 3.5), the ^5J-coupled doublet peak at 8.07 ppm had disappeared and the ^5J-coupled doublet at 8.48 ppm was now a singlet (8.45 ppm), as shown in Figure 3.6. The presence of the bromine in **251** could also be seen in the IR spectrum at the vibrational frequency of 611 cm^{-1}. Lastly, the molecular mass of compound **241** correlated well with the HRMS data.

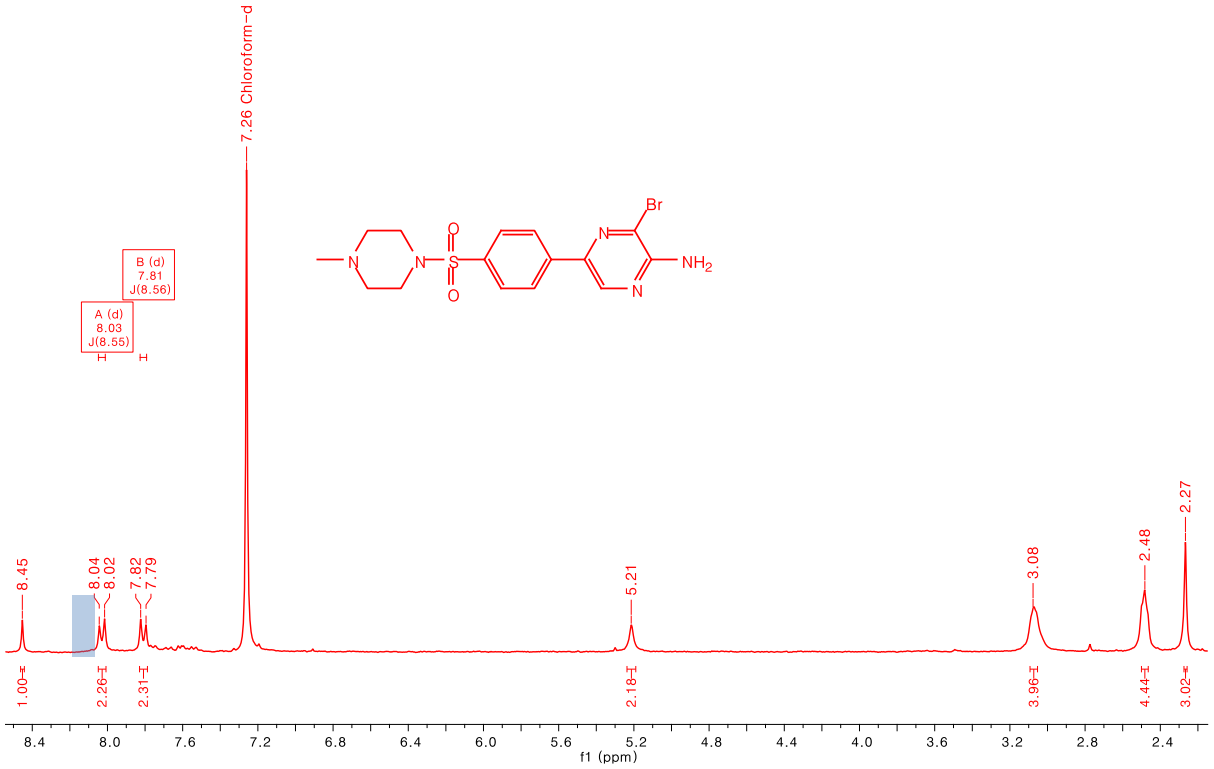

Figure 3.6. ^{1}H NMR spectrum of **241** that indicates the disappearance of the heteroaromatic peak at 8.07 ppm (shaded block)

After the successful bromination of compound **251**, several attempts were carried out to increase the yield using the conditions indicated in Scheme 3.20, but to no avail. It was then decided that this synthesis route was to be discarded because of the poor yield in this final step of the scaffold synthesis. A different route was suggested, which involved the connection of the side chain to the aminopyrazine core before the Suzuki-Miyaura reaction would be carried out with the boronic acid **243**. The different synthetic route will be discussed in the next section.

3.4 A second retrosynthetic analysis of the library

The route that was discussed previously was initially chosen because the Suzuki-Miyaura reaction only has to be carried out once. However, this route proved to be problematic and an alternative route was implemented.

As shown in Figure 3.7, it was envisaged that **240** could be formed by a Suzuki-Miyaura reaction between the boronic acid **243** and the heteroaryl bromide derivatives **266**. Derivatives **266** could, in turn, be disconnected to the di-halogenated aminopyrazine **265** and the Michael acceptors **242** (which could be synthesised from acryloyl chloride and known

amines). Lastly, the di-halogenated aminopyrazine **265** could be obtained by halogenation of 5-bromopyrazin-2-amine **244**.

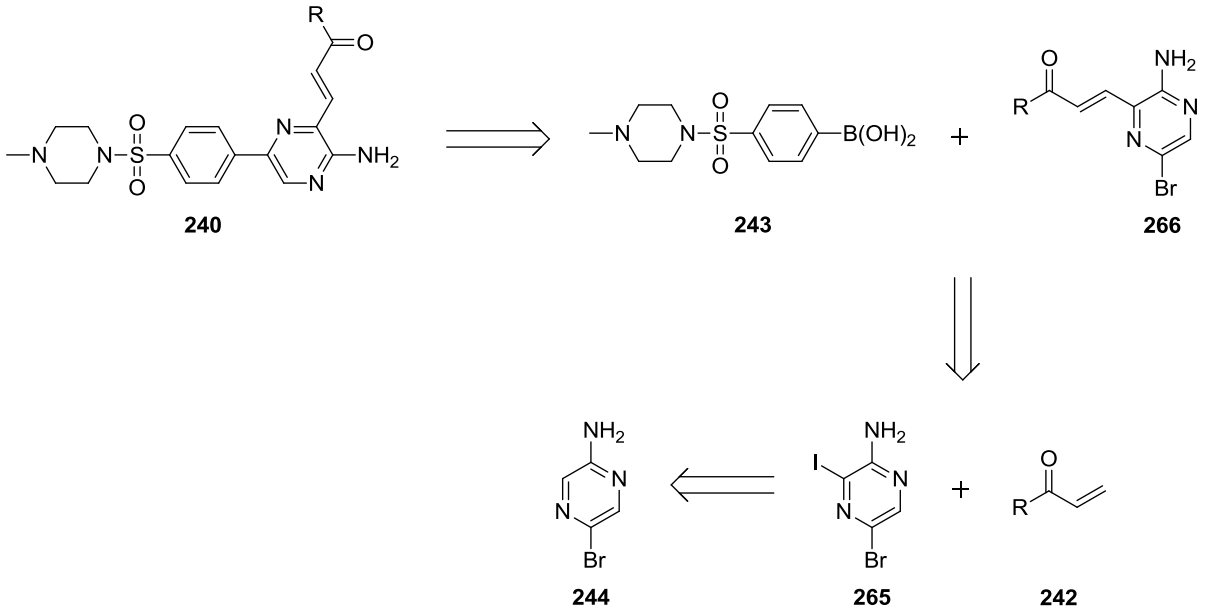

Figure 3.7. Second retrosynthetic analysis of the targeted library

3.5 The synthesis of the Michael acceptor derivatives (266)

3.5.1. The synthesis of 5-bromo-3-iodopyrazin-2-amine (265)

The *ortho*-iodination of the already synthesised 5-bromopyrazin-2-amine **244** involved the use of NIS that was prepared *in situ* from *N*-chlorosuccinimide (NCS) (Scheme 3.21).[42] To this end, NCS was dissolved in DMF at room temperature under N_2 and NaI was added portion-wise. The resulting yellow-brown solution was stirred for one hour before a solution of **247** in DMF was added dropwise. After three hours of stirring at 80 °C, no product was observed on the TLC plate and the temperature was increased to 100 °C for 20 hours. Starting materials were still present and the temperature was increased once again to 130 °C for four hours, but unfortunately no product formed and the starting materials were recovered.

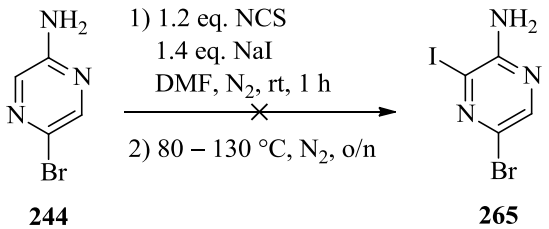

Scheme 3.21. First attempt of iodination of **244**

To eliminate the possibility that the formation of NIS *in situ* from NCS and NaI was causing the failure of the one pot reaction, pure NIS was used instead. Chibale and co-workers[43] used a very similar procedure as in Scheme 3.21 with NIS in dioxane to iodinate **244**. However, compared to their 58% yield, in our hands only trace amounts of the product were isolated. Repeated attempts failed to produce the product in acceptable yield. The obvious solution was thus to use an alternative source of iodine.

Unlike chlorine and bromine, iodine is unreactive towards most aromatic substrates and one thus requires more powerful iodinating species than iodine to synthesise iodinated aromatic substrates.[44] Therefore, in the next attempt, the direct iodination of **244** was conducted with molecular iodine and periodic acid (H_5IO_6), the latter being an oxidising agent and iodinating agent.[45, 46] It should be noted that other research teams have used sodium periodate ($NaIO_4$)[45] or iodic acid (HIO_3),[46] but due to the unavailability of these chemicals in our laboratory at the time, H_5IO_6 was used instead. In H_5IO_6, iodine is in an oxidation state of VII, and this species react with molecular iodine to provide the electrophilic iodonium cation (I^+) (Scheme 3.22).[45]

$$3\ I_2 + I(VII) \rightarrow 7\ I^+$$

Scheme 3.22. Generation of the electrophilic iodinating species

Studies by Kraszkiewicz *et al*.[45] have suggested that the iodination reaction can be carried out in concentrated H_2SO_4, which forms the iodinating intermediate, $IOSO_3H$. The traces of water present in the concentrated H_2SO_4 acts as base to deprotonate the acid. As shown in Scheme 3.23, 5-bromopyrazin-2-amine **244** was dissolved in wet DMSO at room temperature under N_2. Excess I_2 was added to the solution, followed by the addition of H_5IO_6 and H_2SO_4. The resultant black-brown solution was stirred overnight at 60 °C and then quenched with a saturated solution of $Na_2S_2O_3$. At this point, a TLC plate indicated full conversion of the starting materials and only one product spot was observed. The yellow solution was extracted with EtOAc and the organic layer was then washed with brine. The product was purified using column chromatography with EtOAc:Hex 7:3 as eluent to offer 5-bromo-3-iodopyrazin-2-amine **265** as a bright yellow solid in a reasonable yield of 62%.

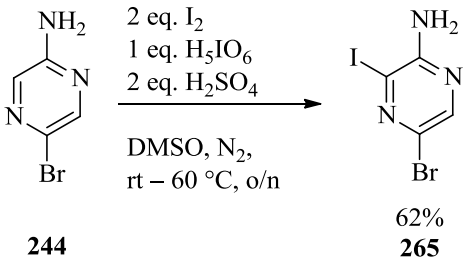

244 **265**

Scheme 3.23. Successful iodination of **244**

In d_6-DMSO, only one heteroaromatic singlet at 8.04 ppm was observed in the ^{1}H NMR spectrum and the singlet at 6.74 ppm could be assigned to the hydrogens of the -NH_2 atoms (Figure 3.7). In addition, these spectroscopic values correlated well with the data reported by Chibale and co-workers.[43]

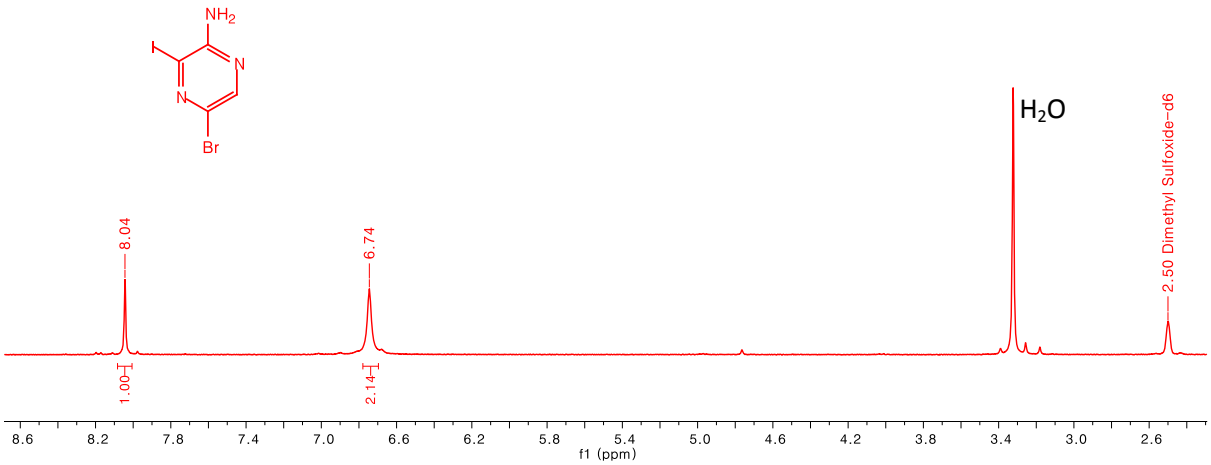

Figure 3.7. ^{1}H NMR spectrum of the iodinated compound **265**

Even though the results that were obtained were positive, a large amount of starting **265** was required for the synthesis of the derivatives **266**, given that a variety of side chains would be added to this core. Therefore, the reaction was scaled up from 100 mg to 500 mg of starting material. Unexpectedly, the yields dropped significantly as the reaction scale increased. Multiple attempts to solve this decrease in yield failed. An alternative procedure that would allow this reaction to be scaled up without sacrificing the yield was thus sought. Several different solvent systems and amounts of iodinating agents were thus investigated.

The iodination procedure of the pyridine version of **244** was reported by de Koning and co-workers[47] and the corresponding product was isolated in 90%. Using their procedure with

a slight adaptation,[48] compound **244** was iodinated and the conditions are laid out in Scheme 3.24. Catalytic amounts of H_5IO_6, H_2SO_4 and AcOH were used to determine whether the necessary iodonium cation species were generated. The starting material **244** was dissolved in CH_3CN, followed by the addition of iodine and the acids. The resulting black-brown solution was then heated overnight at 80 °C, followed by quenching with a saturated solution of $Na_2S_2O_3$. Disappointingly, TLC analysis showed unreacted starting materials and after purification, the product was only isolated in trace amounts.

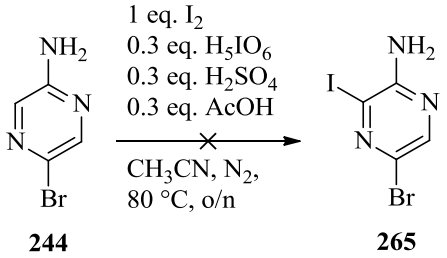

Scheme 3.24. Attempted iodination of **244** in CH_3CN

Nevertheless, the investigation was carried on and in the next attempt, molecular iodine in neat DMSO was used.[49] In a paper by Younis *et al.*,[49] this procedure (Scheme 3.25) was used for the iodination of 3-bromopyridine-2-amine at the 4-position. Given that we had the reagents in hand it was deemed worthwhile to try. Excess molecular iodine was thus added to a solution of **244** and DMSO. The purple-black solution was stirred overnight at 100 °C, followed by quenching with a saturated solution of $Na_2S_2O_3$. An almost full conversion of the starting materials was observed on the TLC plate. However, after purification by column chromatography, only trace amounts of the product were isolated. The fact that only trace amounts of the product were isolated from an almost full conversion of the starting **244** and the presence of an additional product spot on the baseline of the TLC plate suggested a possible formation of an iodinated salt.

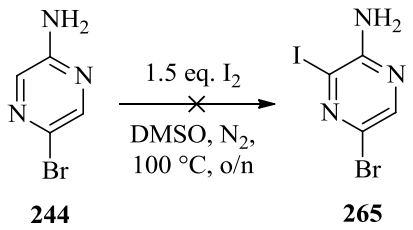

Scheme 3.25. Attempted iodination of **244** with I_2 in DMSO

In the next attempt, the procedure of Scheme 3.23 was modified to determine whether the formation of an iodine salt could be eliminated, this time by carrying out the reaction without H_2SO_4 (Scheme 3.26). The amount of I_2 was also reduced to one equivalent. Full conversion of the starting material **244** was observed on the TLC plate and two additional spots were observed. One of these spots was the iodinated product **265** and the other spot was on the baseline, which was presumably the iodinated salt. No attempts were carried out to isolate the salt. After purification by column chromatography, the desired product **265** was isolated in 52% yield. When the reaction was scaled up from 100 mg to 150 mg, similar results were obtained. However, on further scale up to 250 mg, the yield dropped by 10%. Overall, the reaction went to completion in the absence of H_2SO_4 and with reduced amounts of the I_2 and H_5IO_6.

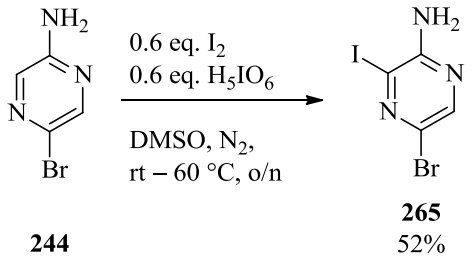

244 **265** 52%

Scheme 3.26. Successful iodination of **244** in the absence of H_2SO_4 (but in moderate yield)

The last attempt for the iodination of **244** was a modification[50] of Scheme 3.24. Instead of using a catalytic amount of AcOH, the reaction was carried out in a solvent system of 1:1 ratio of AcOH:CH_3CN (Scheme 3.27). After stirring the reaction overnight, the TLC indicated a full conversion of the starting materials but again, the product was only isolated in a mediocre yield of 55%.

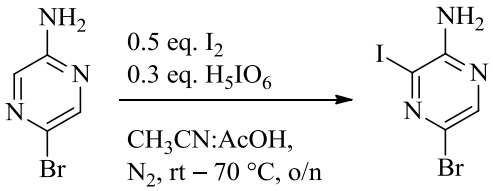

244 **265** 55%

Scheme 3.27. Successful iodination of **244** in a solvent system of CH_3CN:AcOH (but in moderate yield)

Zhao and co-workers faced a similar problem with the bromination of aminopyrazine.[19] Low yields were obtained and when the reaction was scaled up, the yields dropped. They hypothesised that the low yield was due to competitive *N*-bromination, followed by dimerisation with the starting material. Using their hypothesis, the low yields for the iodination of **244** could be explained in Figure 3.8. The *N*-iodination of the starting **244** is largely favoured due to the presence of the starting **244** to form the *N*-iodinated product **267**. The elimination of HI resulted in the formation of the dimer **268** and the next round of *N*-iodination gave the iodinated dimer **269**. Lastly, the elimination of HI gave the azo-dye type compound **270**.

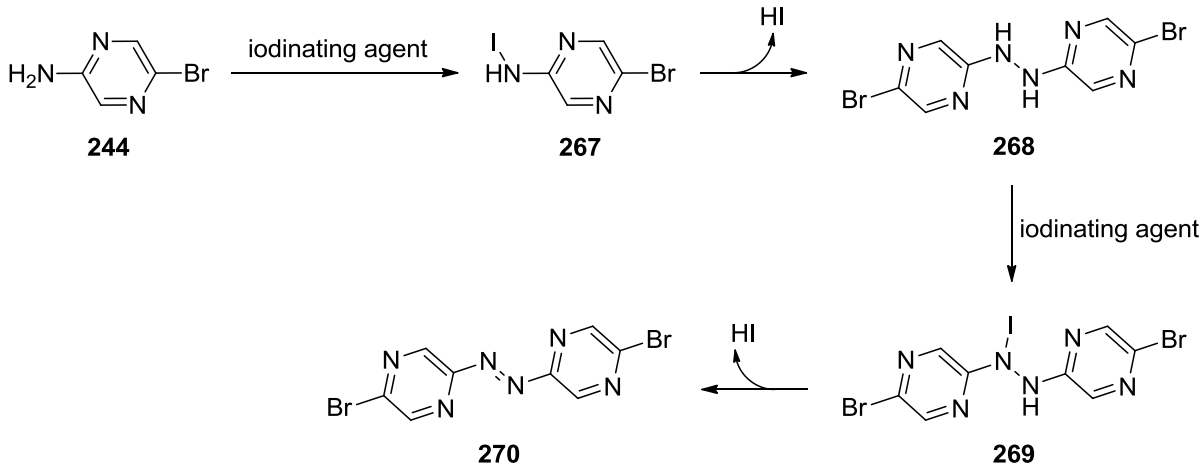

Figure 3.8. Hypothesis for the possible dimerisation of **247**

The optimisation of the yield for the iodination of **244** was subsequently abandon and small scale iodination reactions were carried out using the procedure of Scheme 3.27.

3.5.2 The synthesis of the Michael acceptors (242)

The first four Michael acceptors were synthesised from a commercially available secondary amine and acryloyl chloride. In Scheme 3.28, the four secondary amines **271** – **274** were reacted with acryloyl chloride using the procedure of Tominey *et al.*[51] that had been adapted. The secondary amine and Et_3N were dissolved in DCM at 0 °C under N_2 and acryloyl chloride was then added dropwise. The resulting cloudy solution was then stirred for two hours at room temperature after which the white solution was diluted with EtOAc and washed with a saturated solution of $NaHCO_3$. The crude oil was purified using column chromatography with EtOAc as the eluent to offer the corresponding Michael acceptors

275 – 278 in good yields. The spectroscopic data of these compounds correlated well with the data reported in the literature.[52, 53]

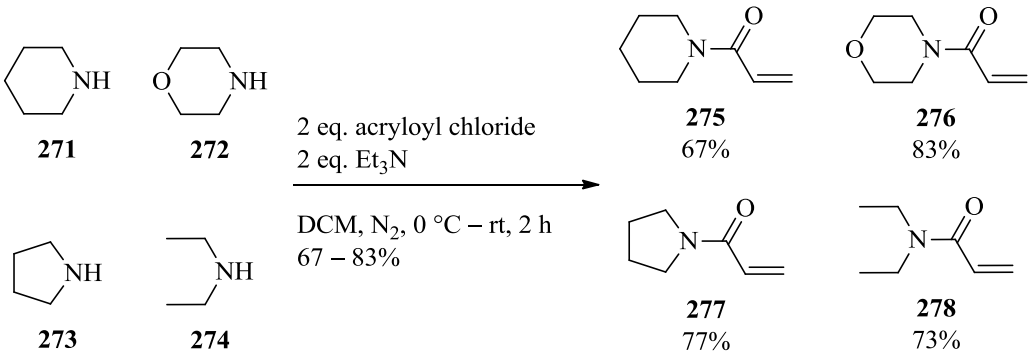

Scheme 3.28. Synthesis of secondary amine-coupled Michael acceptors **275** – **278**

Using Michael acceptor **275** as an example, the ^{1}H NMR spectral data of the acrylic amide can be seen in Figure 3.9. The two doublet of doublets at 6.22 and 5.63 ppm could be assigned to the two non-equivalent protons of C^{10}, each integrating for one proton. The remaining doublet of doublets at 6.56 ppm integrating for one proton originated from the more shielded C^{8}.

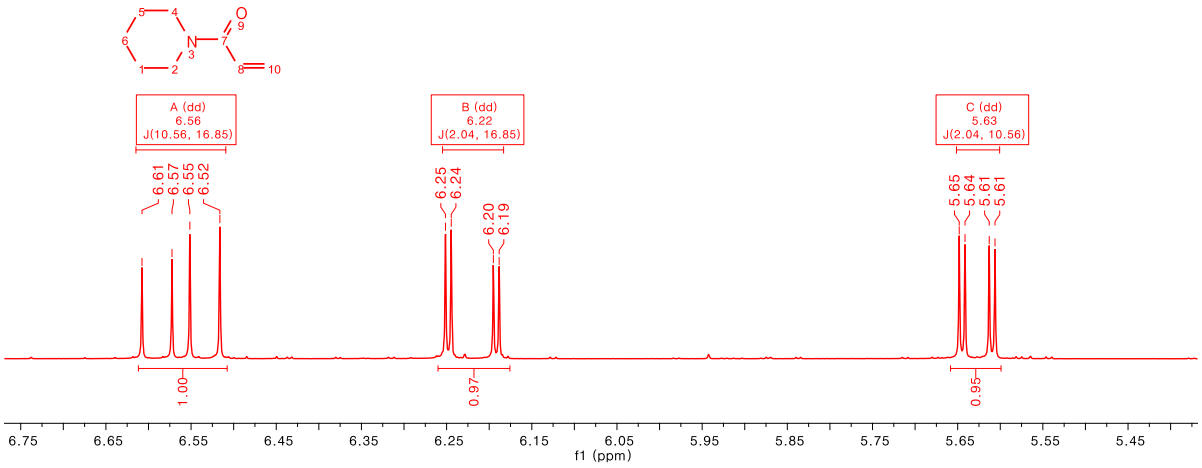

Figure 3.9. ^{1}H NMR spectrum of **275** showing the peaks of the acrylic amide

In addition, three commercially available primary amines **279** – **281** were reacted with acryloyl chloride to form the corresponding Michael acceptors **282** – **284**. In Scheme 3.29, all three reactions followed similar procedures.[51, 54, 55] The primary amines and Et_3N were dissolved in DCM and then cooled to –78 °C, followed by the dropwise addition of acryloyl chloride. The reactions were started at –78 °C to prevent potential over *N*-alkylation. The

solutions were then gradually warmed to room temperature. After stirring the reactions for a specific period of time, dependent on the reactivity of the amine, the solutions were either concentrated immediately or diluted with H_2O and extracted with EtOAc. Purification of the crude material using column chromatography using EtOAc:Hex as eluent then afforded the corresponding Michael acceptors **282** – **284** in moderate to good yields. It should be noted that, the spectroscopic data of these compounds correlated well with the data reported in the literature.[51, 54, 55]

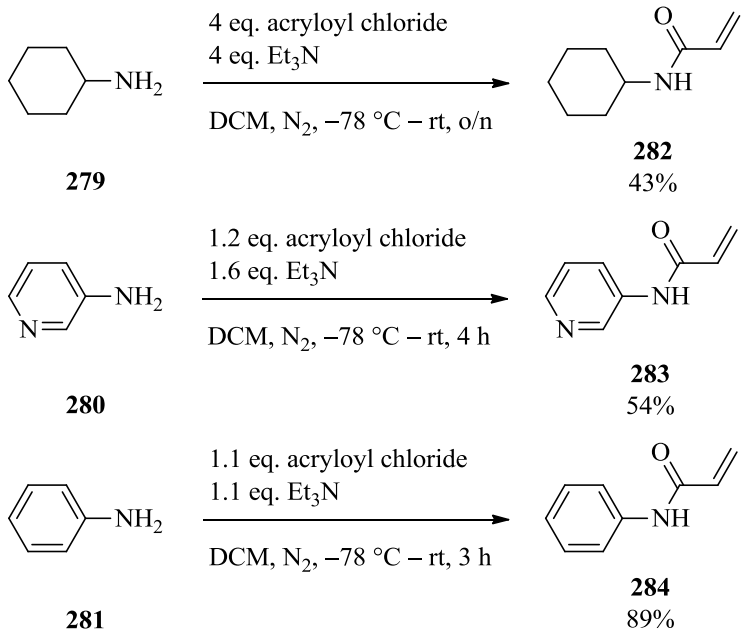

Scheme 3.29. Synthesis of primary amine-coupled Michael acceptors **282** – **284**

Using Michael acceptor **282** as an example, the ^{1}H NMR spectral data of the acrylic amide can be seen in Figure 3.10. One of the doublet of doublets of C^{11} shifted downfield to 6.26 ppm and the other doublet of doublets is observed at 5.62 ppm, both integrating for one proton. The remaining doublet of doublets at 6.05 ppm, integrating for one proton, was assigned to C^9.

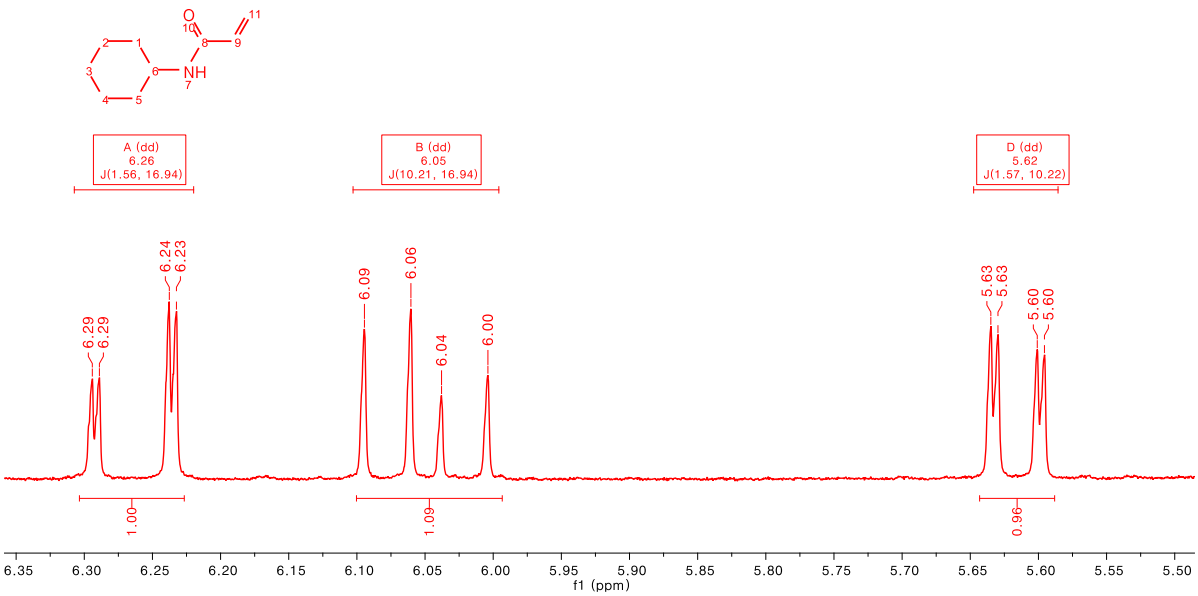

Figure 3.10. ^{1}H NMR spectrum of cyclohexylamine **282** showing the peaks of the acrylic amide

The last Michael acceptor to be synthesised was the 3-pyridine derivative **288** and the procedures are laid out in Scheme 3.30. Commercially available nicotinyl alcohol **285** was first oxidised using excess MnO_2, to afford the aldehyde **286** in 87% yield. The procedure was slightly adapted from that was reported by Quesada *et al.*[56] Due to the low boiling point (78 °C) of the product, the reaction was done with excess MnO_2 in DCM instead of THF, to lower the possibility of evaporation of the product on the rotary evaporator. Nicotinaldehyde **286** then underwent a Grignard reaction[57] with vinyl magnesium bromide in THF to form compound **287** in 98% yield after workup. The last step was the oxidation[57] of **287** with excess MnO_2 to form the Michael acceptor **288**, which was used immediately for the next step due to its air sensitivity and its tendency to polymerise.

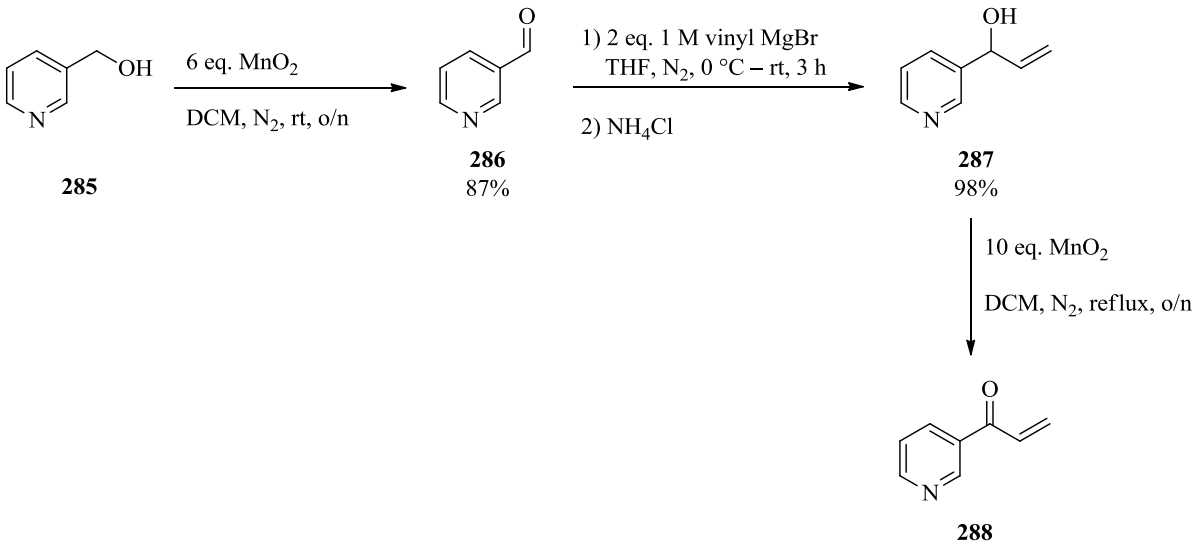

285 **286** 87% **287** 98% **288**

Scheme 3.30. Synthesis of Michael acceptor **288** from 3-pyridinemethanol **285**

3.5.3 The coupling of Michael acceptors to 5-bromo-3-iodopyrazin-2-amine using the Heck reaction

With a library of synthesised Michael acceptor fragments, the next step was the coupling of the warheads to the aminopyrazine core. Following the procedure developed by Slavish *et al.*,[58] a series of the side-chain coupled derivatives of the pyrazine core were chemoselectively prepared using thermal Heck conditions. As described, in Scheme 3.31, Michael acceptor **275** was the first to undergo an iodo-vinyl exchange reaction using phosphine-free Heck conditions. A Schlenk tube was thus charged with compounds **265** and **275** in the presence of $NaHCO_3$ and DMF. The solution was degassed and flushed with N_2 before the addition of $Pd(OAc)_2$. The deep orange-brown solution was subsequently stirred overnight at 70 °C. However, the TLC plate indicated that no product of any kind had formed. The temperature of the reaction was then increased to 100 °C. After an additional 2 days of stirring, unfortunately no formation of the product was observed on the TLC plate.

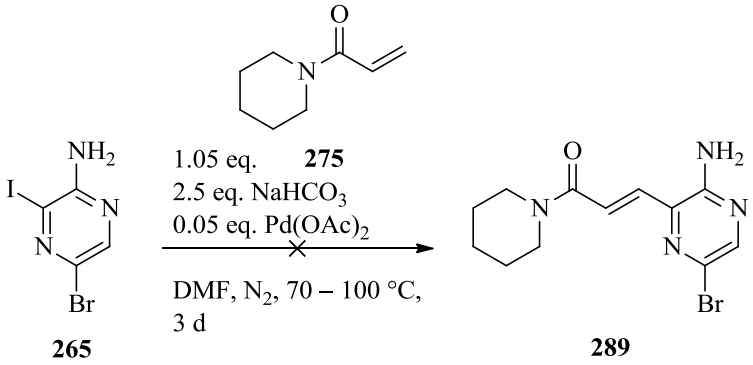

265 289

Scheme 3.31. Attempted regioselective Heck reaction between **265** and **275**

Fang *et al.*[59] have observed that the type of base can influence the outcome of the Heck reaction. They determined that Et_3N delivered optimal results for the Heck reactions with aryl iodide derivatives. Therefore, in the next attempt, the base was changed to Et_3N and the reaction was repeated (Scheme 3.32). After stirring the reaction overnight, full consumption of the starting material **265** was observed on the TLC plate. The black-brown solution was then diluted with EtOAc and filtered on celite. Purification using column chromatography was done with EtOAc:Hex 7:3 as eluent to afford the product **289** as a luminescent yellow solid in 55% yield.

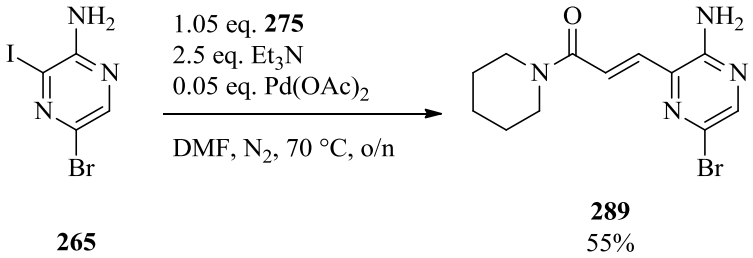

265 **289** 55%

Scheme 3.32. Successful Heck reaction with iodopyrazine **265** and Michael acceptor **275** using Et_3N as the base

This procedure was then used for the Heck reactions with the Michael acceptors **275** – **278**, **282**, **283** and **288** as depicted in Scheme 3.33. It should be noted that improved yields were observed when the base was increased from 2.5 to 4.0 equivalents and the starting Michael acceptors from 1.05 to 1.2 equivalents. The corresponding products **289** – **294** were obtained in low to moderate yields. It should be noted that all the synthesised Michael acceptors exhibited luminescent properties at a wavelength of 365 nm due to the extended conjugation. A variety of aminopyrazine derivatives with extended conjugated network have been reported

to exhibit luminescent properties.[60] It should be noted that the Heck reaction with 1-(pyridin-3-yl)prop-2-en-1-one **288** failed to form the corresponding product and after several attempts, it was abandon. The reason for this failed reaction could be ascribed to the instability of **288**.

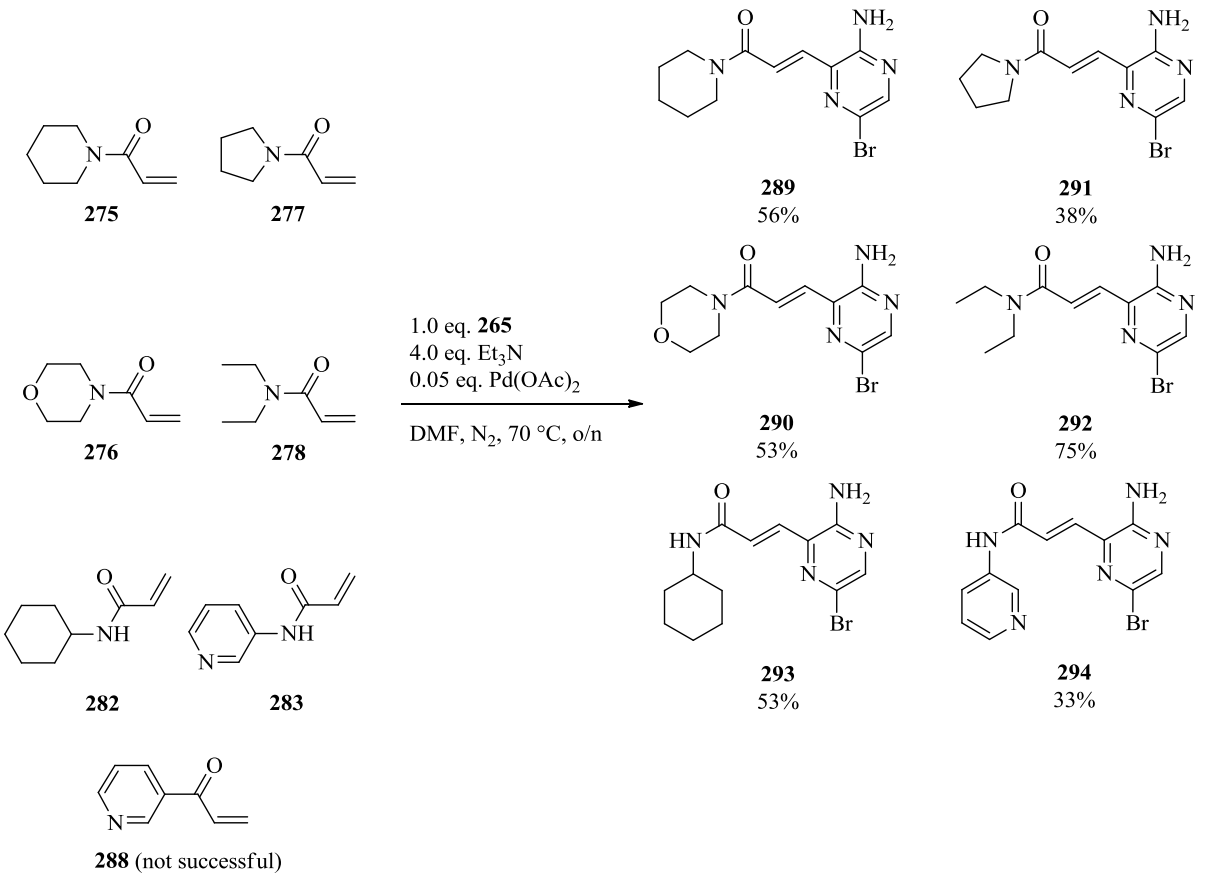

Scheme 3.33. Heck reactions with six different Michael acceptor fragments

The synthesis of the Michael acceptor fragments **284** and **294** were synthesised at a later stage of the project and after receiving the first batch of the biological results (will be discussed in Chapter 5), further work on these two Michael acceptors were abandoned.

The new compounds shown in Scheme 3.33 were all fully characterised. Using **290** as example, the ^{1}H NMR spectrum in Figure 3.11 clearly indicates the (*E*)-configuration of this molecule. The large *J*-coupling values (14.5 Hz) between the doublets at 7.66 and 7.47 ppm clearly indicate that C^{8} and C^{9} are in the *trans*-conformation.[61] The proton of C^{6} is assigned to the singlet at 8.06 ppm and the singlet at 5.15 ppm can be assigned to the -NH_2, integrating

for two protons. Lastly, the multiplet at 3.72 ppm was assigned to the protons of the morpholine ring, integrating for eight protons.

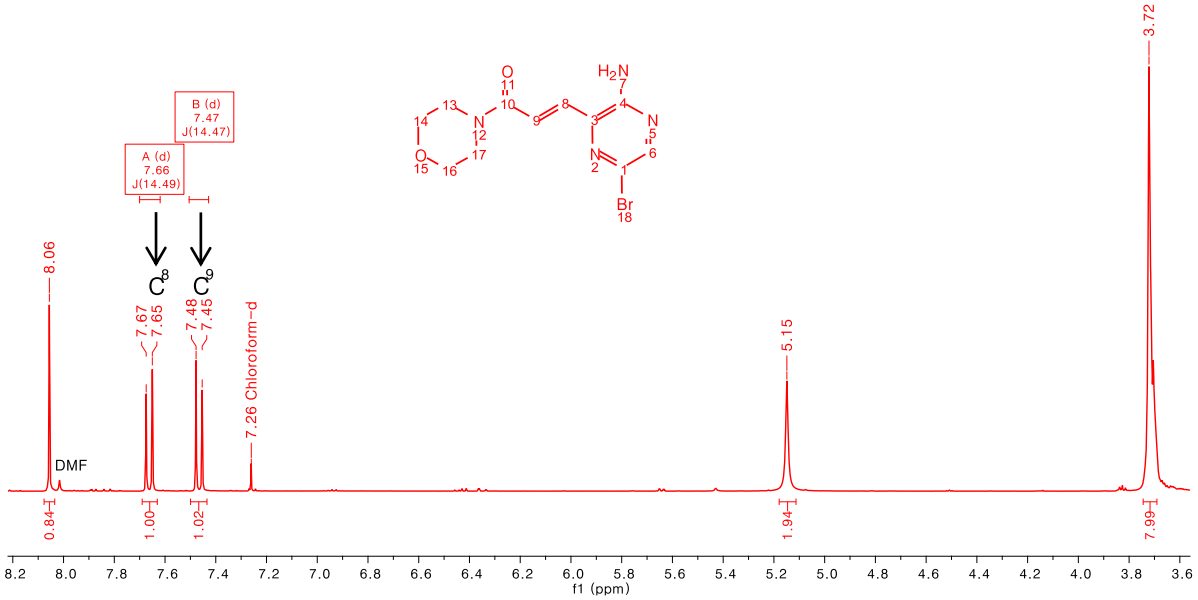

Figure 3.11. ^{1}H NMR spectrum of **290** confirming the (*E*)-configuration of the alkene in the molecule

An interesting phenomenon was observed on the ^{13}C NMR spectrum of **290** (Fig. 3.12). Not two but three carbon peaks were observed for the morpholine ring (66.9, 46.7 and 42.8 ppm). A plausible theory is that the hindered rotation of the amide bond forces C^{13} and C^{17} to be in different chemical environments and this rotameric effect produces two distinctive carbon peaks instead of one peak. The correlation of these three carbon peaks to the multiplet of the morpholine on the HSQC spectrum confirmed the theory (Figure 3.13). The assignment of the carbon peak at 66.9 ppm to C^{14} and C^{16} completes the morpholine ring. The remainders of the carbon peaks were assigned using the aromatic region of the HSQC spectrum as discussed below.

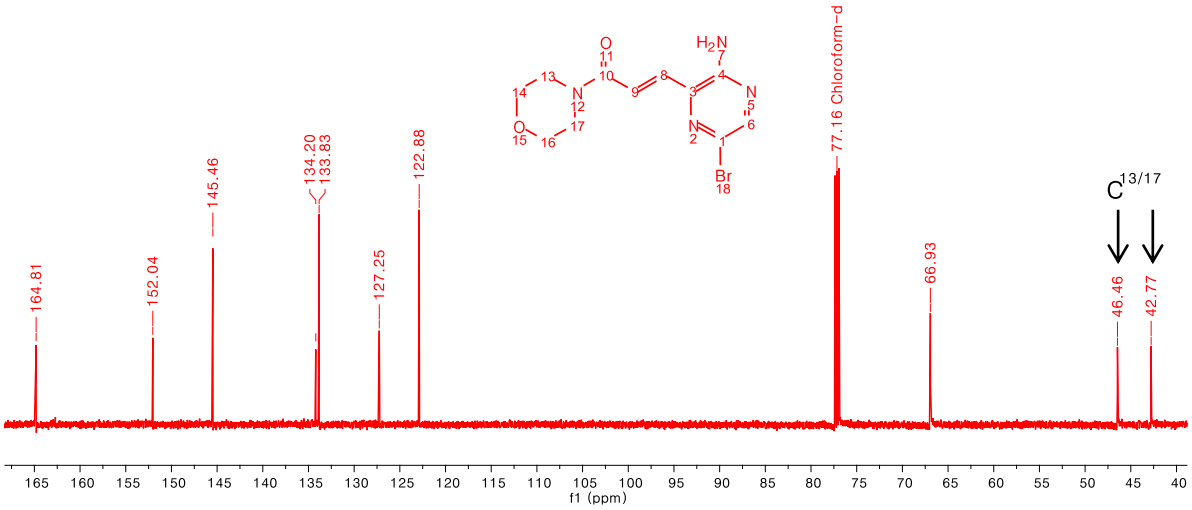

Figure 3.12. ^{13}C NMR spectrum of **290** showing three carbon peaks of the morpholine ring

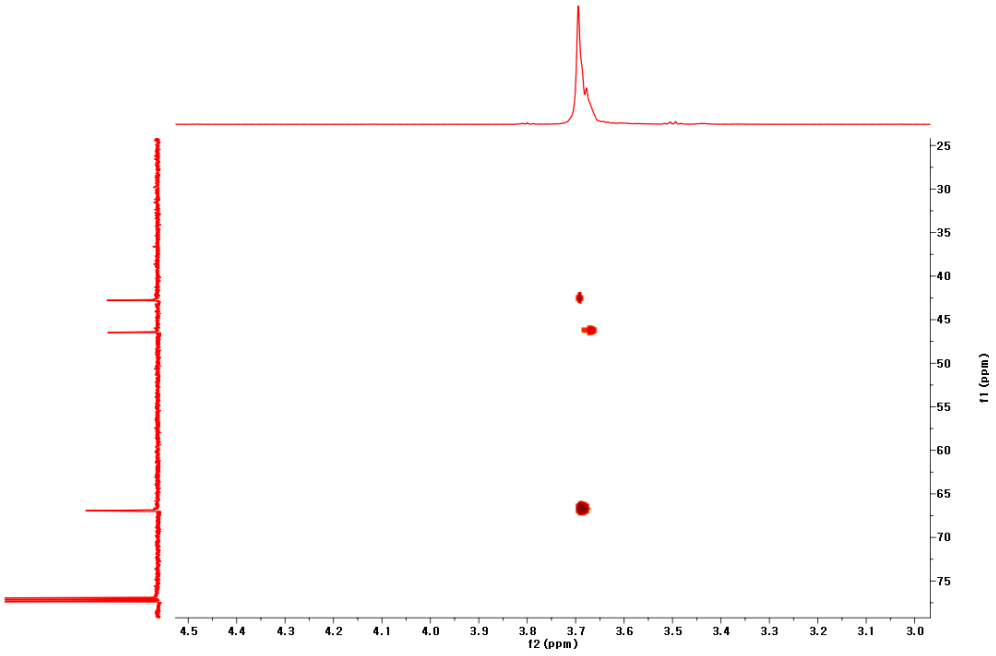

Figure 3.13. Expanded section of the HSQC spectrum of **290** showing the correlation of the three carbon peaks and the multiplet of the morpholine ring

The HSQC spectrum for the aromatic region (Fig. 3.14) showed the correlation between the singlet at 8.02 ppm and the carbon peak at 145.4 ppm, which could be assigned to C^6. In addition, the doublet at 7.63 ppm correlated with the carbon peak at 133.7 ppm, which could be assigned to C^8. The last doublet at 7.44 ppm is C^9, which correlated with the carbon peak at 122.7 ppm. The remaining four carbon peaks could be assigned using the ^{13}C NMR spectrum in Figure 3.14. These included the carbon peak at 164.8 ppm for the carbonyl C^{10}

and the carbon peak at 152.0 ppm for C^4. Due to the deshielding effect of the neighbouring atoms, the carbon peak at 134.2 ppm was assigned to C^3. The last carbon peak at 127.3 ppm was the brominated C^1 which would disappear after the Suzuki-Miyaura reaction (which will be discussed later).

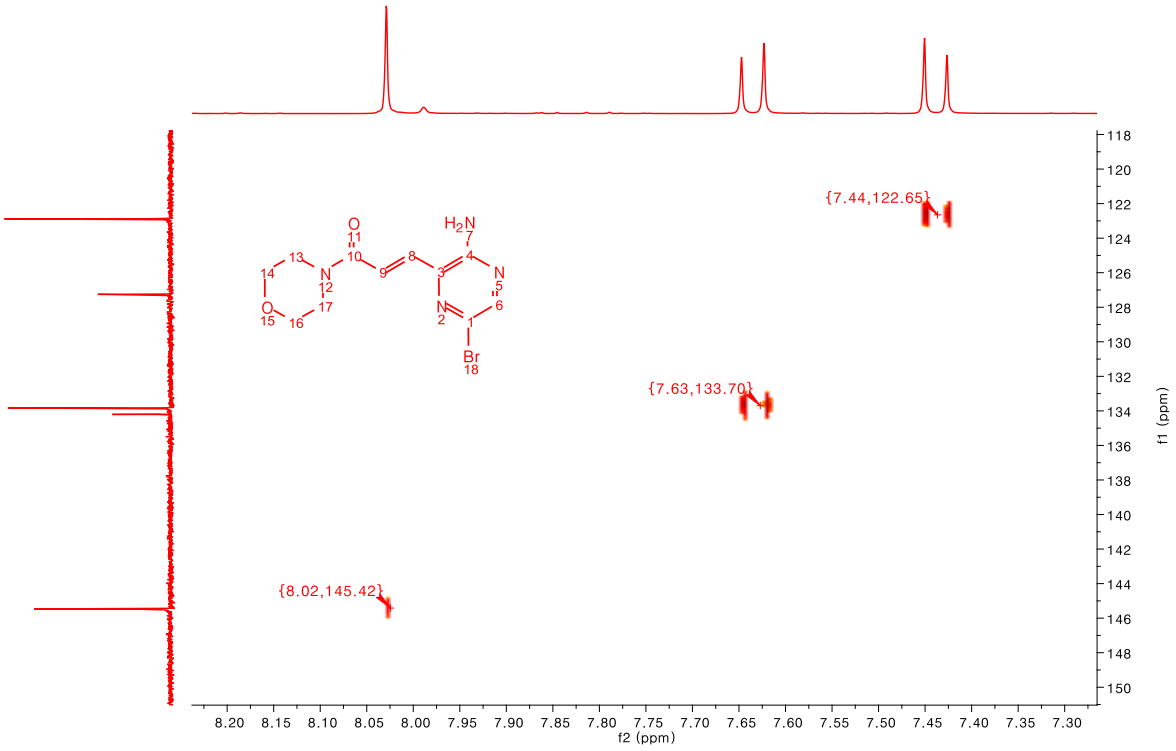

Figure 3.14. HSQC spectrum of **290** showing the aromatic region

3.6 The Suzuki-Miyaura reactions with (*E*)-3-(3-aminopyrazin-2-yl)acrylaldehyde derivatives

With the synthesised warheads coupled to the aminopyrazine core in hand, the Suzuki-Miyaura reaction could now be carried out with the boronic acid **243** to form the final compounds. The procedure was slightly adapted from the one that was reported in Scheme 3.19. The amount of Cs_2CO_3 was increased from 2.0 to 4.0 equivalents to ensure full conversion of the boronic acid **243** to the more reactive borate for subsequent transmetalation.[22] Furthermore, the temperature was decreased from 80 °C to 70 °C to prolong the reactivity of the Pd catalyst. The adapted procedure is set out in Scheme 3.34 and the results are tabulated in Table 4.1. Unfortunately, the Suzuki-Miyaura reaction with **294** formed the corresponding product **221** in trace amounts, which were only soluble in MeOH.

Due to insufficient amounts of starting material, further attempts to improve the yield were not carried out.

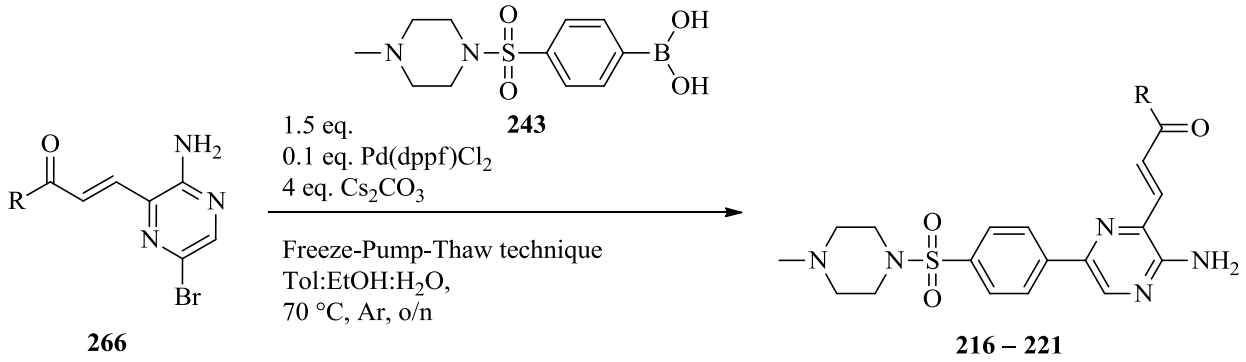

Scheme 3.34. Suzuki-Miyaura reaction between **266** and **243** to form the final compounds **216** – **221**

Table 3.1. Products obtained from the Suzuki reactions with **243** and the six aminopyrazine derivatives **289** - **294**

#	R	Yield
216	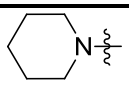	73%
217	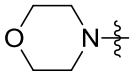	69%
218	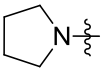	70%
219	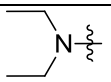	78%
220	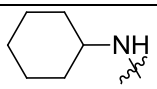	75%
221	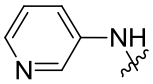	trace amounts

All the new compounds listed in Table 3.1 were fully characterised by ^{1}H, ^{13}C, IR and mass spectrometric analysis. The piperidine derivative **216** was selected as the representative example for the discussion of the NMR spectroscopic characterisation for this series of final compounds. The ^{1}H NMR spectrum of **216** (Fig. 3.15) shows clearly two sets of doublets in the aromatic region, which could be assigned to the phenyl ring ($C^{15/11}$: 8.07 ppm, $C^{12/14}$: 7.82 ppm) and the Michael acceptor (C^{24} : 7.63 ppm, C^{23} : 7.77 ppm) respectively. The singlet at

8.47 ppm, integrating for one proton, was the heteroaryl proton of C^{17}. The singlet at 5.31 ppm, integrating for two protons, was the -NH_2 of C^{19}. Compared to the ^{1}H NMR in Figure 3.6, the peaks at 3.07, 2.49 and 2.26 ppm could be assigned to the methylpiperazine. Therefore, the multiplet integrating for four protons at 3.67 ppm could be assigned to C^{32} and C^{28}. Lastly, the multiplet at 1.67 ppm was assigned to the remaining protons of C^{31}, C^{29} and C^{30}.

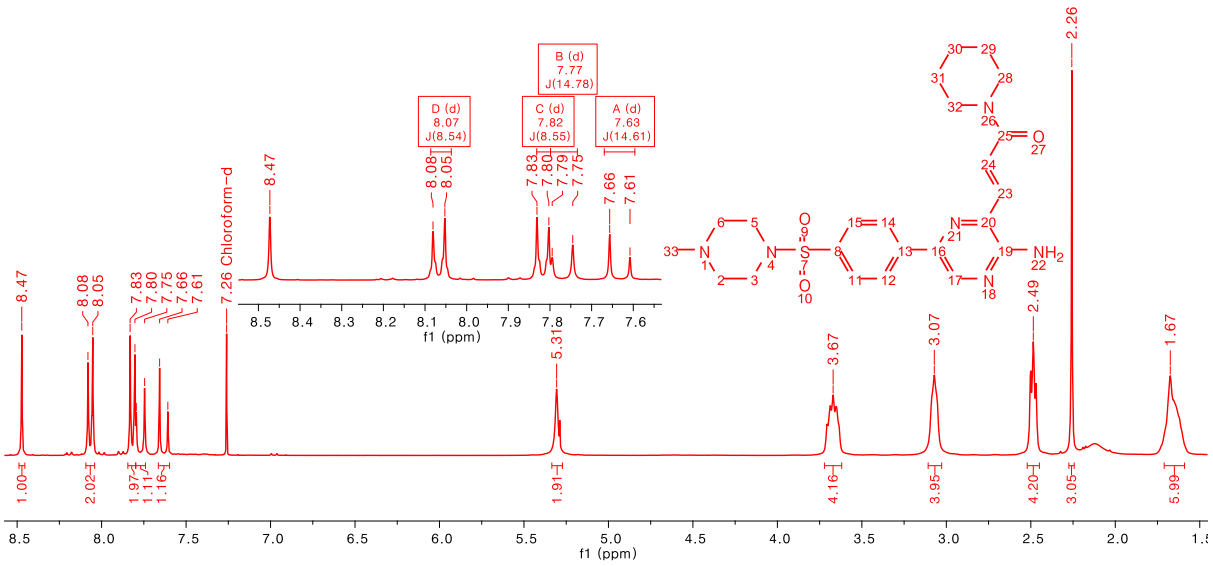

Figure 3.15. ^{1}H NMR spectrum of piperidine **216**

Figure 3.16 shows the ^{13}C NMR spectrum of **216** and in the alkane region, 8 carbon peaks were observed that are easily identifiable. As explained earlier from the ^{13}C NMR spectrum of the morpholine derivative **290** (Fig. 3.12), all these compounds have additional carbon peaks due to the existence of amide rotamers (see experimental section) and this phenomenon was also observed here. The carbon peaks at 47.3 and 43.9 ppm could be assigned to C^{32} and C^{28}. The other two carbons of the piperidine ring, C^{31} and C^{29}, were also observed in different chemical environments and could be assigned to 26.9 and 25.8 ppm. The carbon peak at 24.7 ppm was the last carbon of the piperidine ring, C^{30}. The remaining three carbon peaks in the alkane region could be assigned to the methylpiperazine. The carbon peak at 54.2 ppm could be assigned to C^{33} and the other two carbon peaks at 46.0 and 45.8 ppm are assigned to the piperazine ring, C^2, C^3, C^5 and C^6.

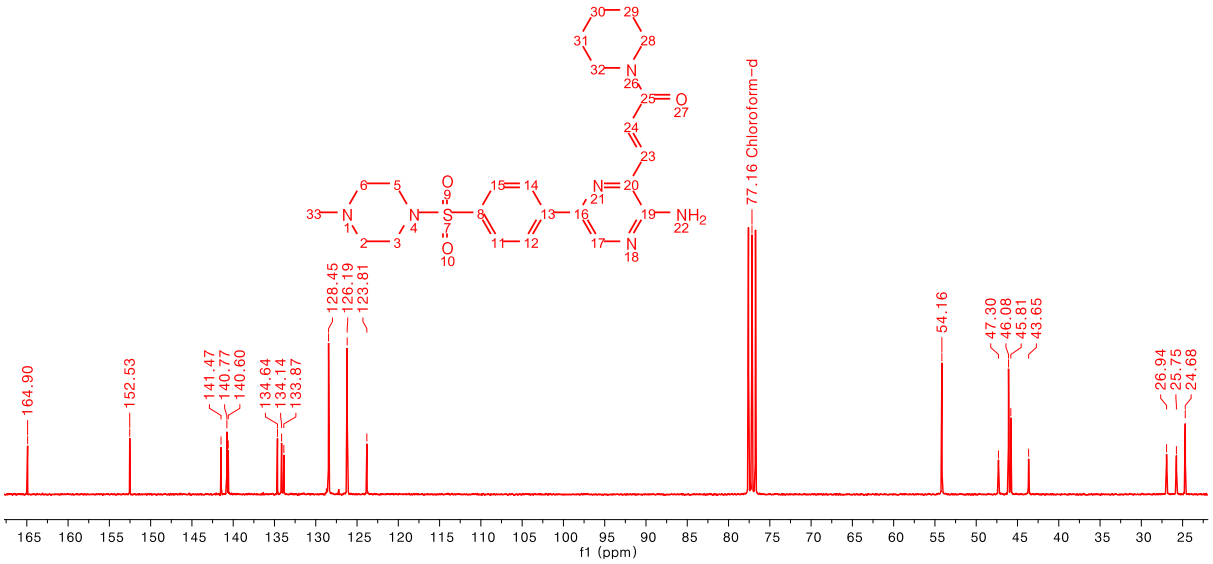

Figure 3.16. ^{13}C NMR spectrum of piperidine **216**

Several carbon peaks in the aromatic region were easily identified since the peaks did not shift much when compared to the starting material **289** (see experimental section). The carbon peaks at 164.9 and 152.6 ppm could be assigned to C^{25} and C^{19} respectively. One carbon peak of the Michael acceptor, C^{24}, could be assigned to the peak at 123.8ppm. The other carbon peak of the Michael acceptor, C^{23}, was sandwiched between the two peaks in the region of 134.6 to 133.9 ppm and could not be identified directly from the ^{13}C spectrum. The remaining carbon peaks were analysed using the HSQC spectrum (Fig. 3.17).

From the HSQC spectrum, the correlation between the doublet at 7.65 ppm and the carbon at 123.8 ppm could be seen and could be assigned to C^{24}. The other doublet of the Michael acceptor at 7.77 ppm correlated with the carbon peak at 134.2 ppm and could now be assigned to C^{23}. The two doublets of the phenyl ring at 8.09 and 7.84 ppm correlated to the carbon peaks at 126.3 and 128.5 ppm and could be assigned to both $C^{15/11}$ and $C^{12/14}$. Lastly, the heteroaromatic proton peak of C^{17} at 8.49 ppm correlated with the carbon peak at 140.8 ppm.

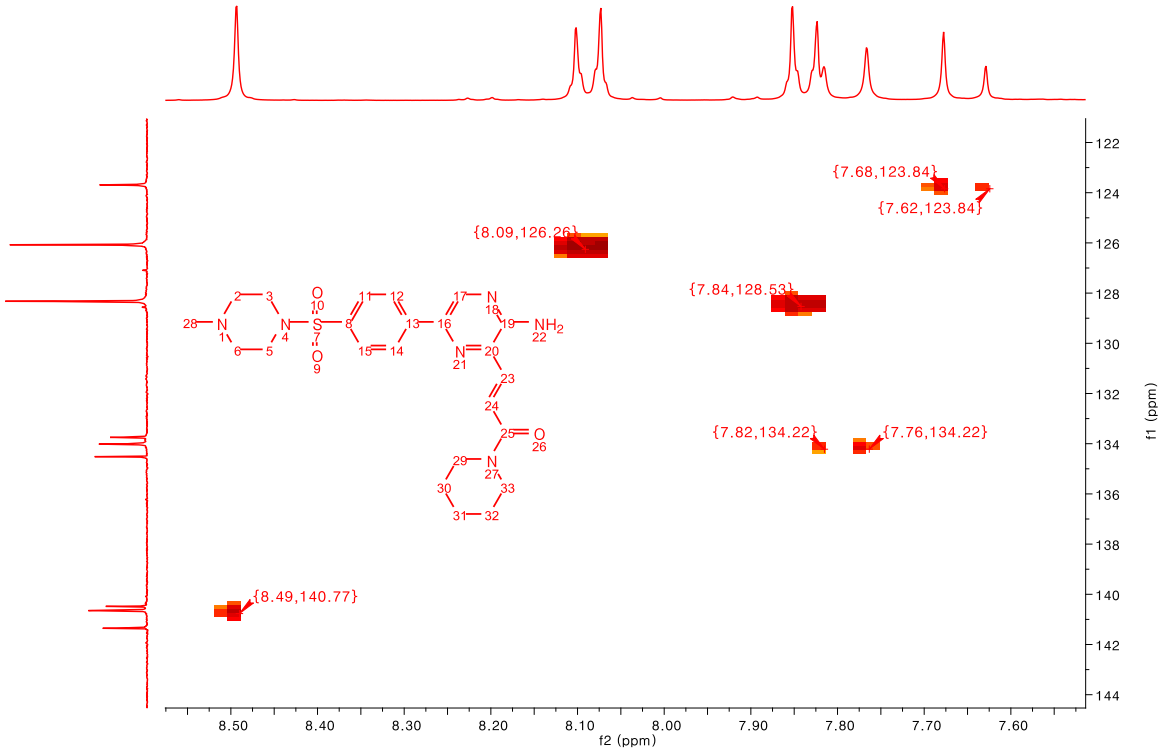

Figure 3.17. HSQC spectrum of piperidine **216**

The HMBC spectrum in Figure 3.18 showed a correlation between the proton of C^{17} at 8.49 ppm to the carbon peaks at 152.4 and 140.5 ppm. The carbon peak at 152.4 ppm had already been assigned to C^{19}, so C^{13} must account for the signal at 140.5 ppm. One of the doublets of the phenyl ring at 8.09 ppm also correlated to the C^{13} and this suggested that the doublet at 8.09 ppm is the proton of C^{11}. The other doublet of the phenyl ring at 7.84 ppm correlated to a carbon peak at 141.4 ppm and therefore was assigned to C^{8}. Both doublets of the Michael acceptor at 7.79 and 7.63 ppm correlated to the same carbon peaks at 164.9 and 133.9 ppm. The carbon peak at 164.9 ppm has already been assigned to C^{25}, thus C^{20} was assigned to be the other carbon peak at 133.9 ppm. The remaining carbon peak at 134.0 ppm could be assigned to C^{16}.

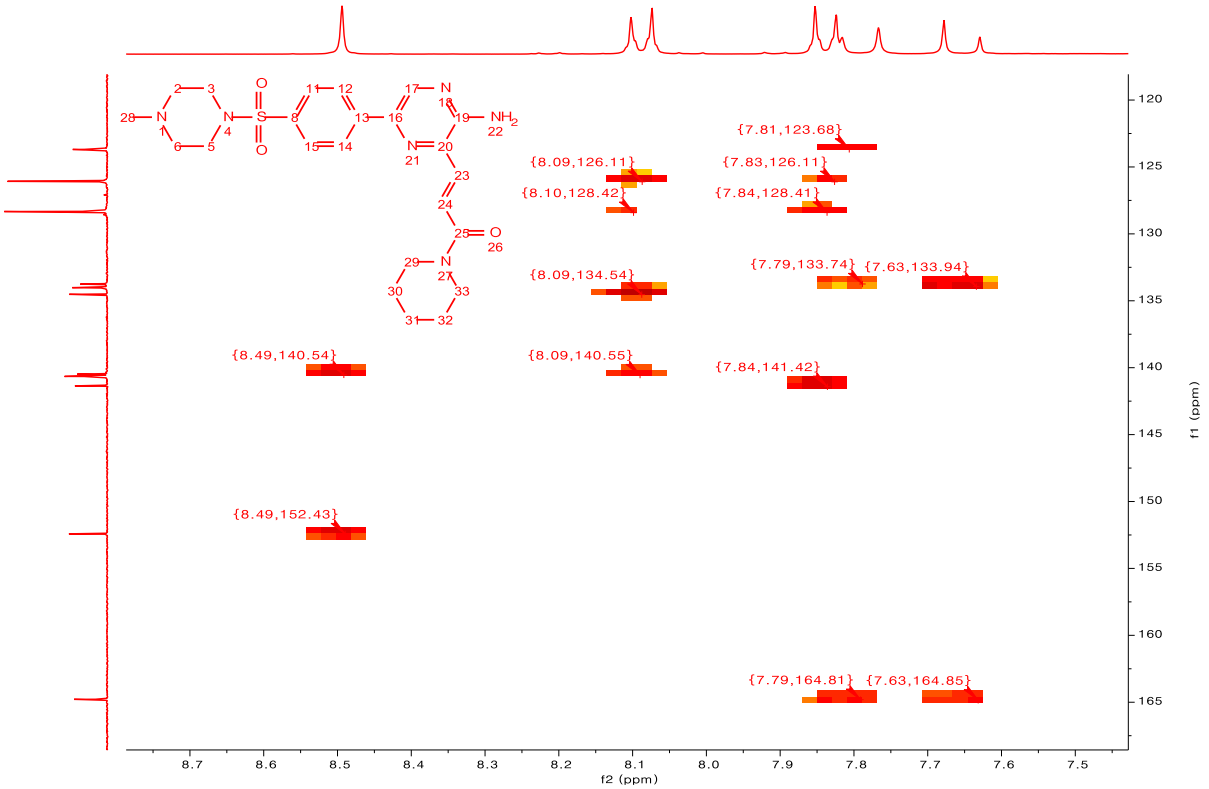

Figure 3.18. HMBC spectrum of piperidine **216**

A series of (*E*)-3-(3-aminopyrazin-2-yl)acrylaldehyde derivatives have been successfully synthesised that involved the Heck and Suzuki-Miyaura methods. The final compounds **216** – **220** have been subjected to biological testing and will be discussed in Chapter 5. After the synthesis of this series, the next chapter will discuss the synthesis of the (*E*)-1-(3-aminopyrazin-2-yl)prop-2-en-1-one derivatives in which the Michael acceptor was rotated 180 °.

3.7 References

1. S. Samanta, K. Srikanth, S. Banerjee, B. Debnath, S. Gayen and T. Jha, *Bioorganic & Medicinal Chemistry*, 2004, **12**, 1413-1423.
2. K. Bahrami, M. M. Khodaei and M. Soheilizad, *Journal of Organic Chemistry*, 2009, **74**, 9287-9291.
3. B. J. Henderson, D. J. Carper, T. F. González-Cestari, B. Yi, K. Mahasenan, R. E. Pavlovicz, M. L. Dalefield, R. S. Coleman, C. Li and D. B. McKay, *Journal of Medicinal Chemistry*, 2011, **54**, 8681-8692.
4. Bristol-Myers Squibb company, Patent US2007/111985 A1, 2007.

5. E. M. Dangerfield, C. H. Plunkett, A. L. Win-Mason, B. L. Stocker and M. S. M. Timmer, *Journal of Organic Chemistry*, 2010, **75**, 5470-5477.
6. C. Kison, N. Meyer and T. Opatz, *Angewandte Chemie International Edition*, 2005, **44**, 5662-5664.
7. M. M. Salter, J. Kobayashi, Y. Shimizu and S. Kobayashi, *Organic Letters*, 2006, **8**, 3533-3536.
8. R. A. da Silva, I. H. S. Estevam and L. W. Bieber, *Tetrahedron Letters*, 2007, **48**, 7680-7682.
9. W. Devine, J. L. Woodring, U. Swaminathan, E. Amata, G. Patel, J. Erath, N. E. Roncal, P. J. Lee, S. E. Leed, A. Rodriguez, K. Mensa-Wilmot, R. J. Sciotti and M. P. Pollastri, *Journal of Medicinal Chemistry*, 2015, **58**, 5522-5537.
10. K.-Y. Wang, C. Chen, J.-F. Liu, Q. Wang, J. Chang, H.-J. Zhu and C. Li, *Organic & Biomolecular Chemistry*, 2012, **10**, 6693-6704.
11. AstraZeneca AB, S. Berg, S. Hellberg, Patent WO2004055009, 2004.
12. S. Berg, M. Bergh, S. Hellberg, K. Högdin, Y. Lo-Alfredsson, P. Söderman, S. von Berg, T. Weigelt, M. Ormö, Y. Xue, J. Tucker, J. Neelissen, E. Jerning, Y. Nilsson and R. Bhat, *Journal of Medicinal Chemistry*, 2012, **55**, 9107-9119.
13. M. Li, D. Constantinescu, L. Wang, A. Mohs and J. Gmehling, *Industrial & Engineering Chemistry Research*, 2010, **49**, 4981-4988.
14. D. Schubert, in *Kirk-Othmer Encyclopedia of Chemical Technology*, John Wiley & Sons, Inc., 2000.
15. H. Hara and H. C. Van Der Plas, *Journal of Heterocyclic Chemistry*, 1982, **19**, 1285-1287.
16. B. Jiang, C.-G. Yang, W.-N. Xiong and J. Wang, *Bioorganic & Medicinal Chemistry*, 2001, **9**, 1149-1154.
17. N. Sato and A. Mizuno, *Journal of Chemical Research*, 2005, **2005**, 747-749.
18. C. B. Aakeroy, P. D. Chopade, C. Ganser and J. Desper, *Chemical Communications*, 2011, **47**, 4688-4690.
19. T. Itoh, S. Kato, N. Nonoyama, T. Wada, K. Maeda, T. Mase, M. M. Zhao, J. Z. Song, D. M. Tschaen and J. M. McNamara, *Organic Process Research & Development*, 2006, **10**, 822-828.
20. R. H. Mitchell, Y.-H. Lai and R. V. Williams, *The Journal of Organic Chemistry*, 1979, **44**, 4733-4735.

21. S. Hachiya, D. Hashizume, S. Maki, H. Niwa and T. Hirano, *Tetrahedron Letters*, 2010, **51**, 1401-1403.
22. C. F. R. A. C. Lima, A. S. M. C. Rodrigues, V. L. M. Silva, A. M. S. Silva and L. M. N. B. F. Santos, *ChemCatChem*, 2014, **6**, 1291-1302.
23. I. Maluenda and O. Navarro, *Molecules*, 2015, **20**, 7528-7557.
24. N. Hadei, E. A. B. Kantchev, C. J. O'Brie and M. G. Organ, *Organic Letters*, 2005, **7**, 1991-1994.
25. M. S. Szulmanowicz, A. Gniewek, W. Gil and A. M. Trzeciak, *ChemCatChem*, 2013, **5**, 1152-1160.
26. L. Ngodwana, S. Bose, V. J. Smith, W. A. L. van Otterlo and G. E. Arnott, *European Journal of Inorganic Chemistry*, 2017, **2017**, 1923-1929.
27. N. I. Nikishkin, J. Huskens and W. Verboom, *Organic & Biomolecular Chemistry*, 2013, **11**, 3583-3602.
28. P. G. Gildner and T. J. Colacot, *Organometallics*, 2015, **34**, 5497-5508.
29. D. A. Khobragade, S. G. Mahamulkar, L. Pospíšil, I. Císařová, L. Rulíšek and U. Jahn, *Chemistry – A European Journal*, 2012, **18**, 12267-12277.
30. T. Hayashi, M. Konishi, Y. Kobori, M. Kumada, T. Higuchi and K. Hirotsu, *Journal of the American Chemical Society*, 1984, **106**, 158-163.
31. M. Rimoldi, F. Ragaini, E. Gallo, F. Ferretti, P. Macchi and N. Casati, *Dalton Transactions*, 2012, **41**, 3648-3658.
32. F. Proutiere and F. Schoenebeck, *Angewandte Chemie International Edition*, 2011, **50**, 8192-8195.
33. N. Miyaura and A. Suzuki, *Chemical Reviews*, 1995, **95**, 2457-2483.
34. P. J. Dyson and P. G. Jessop, *Catalysis Science & Technology*, 2016, **6**, 3302-3316.
35. F. C. Fischer and E. Havinga, *Recueil des Travaux Chimiques des Pays-Bas*, 1974, **93**, 21-24.
36. G. A. Molander, B. Canturk and L. Kennedy, *Journal of Organic Chemistry*, 2009, **74**, 973-980.
37. C. Adamo, C. Amatore, I. Ciofini, A. Jutand and H. Lakmini, *Journal of the American Chemical Society*, 2006, **128**, 6829-6836.
38. http://depts.washington.edu/eooptic/linkfiles/Freeze_Pump_Thaw.pdf, Accessed 27 August 2017.
39. C.-M. Chou, Y.-W. Tung, M.-I. Ling, D. Chan, W. Phakhodee and M. Isobe, *Heterocycles*, 2012, **86**, 1323-1339.

40. V. K. Chaikovskii, V. I. Skorokhodov and V. D. Filimonov, *Russian Journal of Organic Chemistry*, 2001, **37**, 1503-1504.
41. Y. Younis, K. Chibale, M. J. Witty, D. Waterson, Patent WO2013121387 A1, 2013.
42. C. Poriel, M. Lachia, C. Wilson, J. R. Davies and C. J. Moody, *Journal of Organic Chemistry*, 2007, **72**, 2978-2987.
43. Y. Younis, F. Douelle, D. González Cabrera, C. Le Manach, A. T. Nchinda, T. Paquet, L. J. Street, K. L. White, K. M. Zabiulla, J. T. Joseph, S. Bashyam, D. Waterson, M. J. Witty, S. Wittlin, S. A. Charman and K. Chibale, *Journal of Medicinal Chemistry*, 2013, **56**, 8860-8871.
44. E. B. Merkushev, *Synthesis*, 1988, **1988**, 923-937.
45. L. Kraszkiewicz, M. Sosnowski and L. Skulski, *Synthesis*, 2006, **2006**, 1195-1199.
46. B. R. Patil, S. R. Bhusare, R. P. Pawar and Y. B. Vibhute, *Tetrahedron Letters*, 2005, **46**, 7179-7181.
47. T. C. Leboho, S. F. van Vuuren, J. P. Michael and C. B. de Koning, *Organic & Biomolecular Chemistry*, 2014, **12**, 307-315.
48. S. Hildbrand, H. J. Mair, R. N. Radinov, Y. Ren, J. A.Wright, Patent US20110028511 A1, 2011.
49. Y. Younis, F. Douelle, T.-S. Feng, D. G. Cabrera, C. L. Manach, A. T. Nchinda, S. Duffy, K. L. White, D. M. Shackleford, J. Morizzi, J. Mannila, K. Katneni, R. Bhamidipati, K. M. Zabiulla, J. T. Joseph, S. Bashyam, D. Waterson, M. J. Witty, D. Hardick, S. Wittlin, V. Avery, S. A. Charman and K. Chibale, *Journal of Medicinal Chemistry*, 2012, **55**, 3479-3487.
50. N. M. Barl, E. Sansiaume-Dagousset, K. Karaghiosoff and P. Knochel, *Angewandte Chemie International Edition*, 2013, **52**, 10093-10096.
51. A. F. Tominey, J. Liese, S. Wei, K. Kowski, T. Schrader and A. Kraft, *Beilstein Journal of Organic Chemistry*, 2010, **6**, Article No. 66.
52. R. N. Shakhmaev, A. U. Ishbaeva and V. V. Zorin, *Russian Journal of Organic Chemistry*, 2012, **48**, 908-913.
53. M. Fu, L. Chen, Y. Jiang, Z.-X. Jiang and Z. Yang, *Organic Letters*, 2016, **18**, 348-351.
54. J. Eriksson, O. Åberg and B. Långström, *European Journal of Organic Chemistry*, 2007, **2007**, 455-461.
55. F. Wang, H. Yang, H. Fu and Z. Pei, *Chemical Communications*, 2013, **49**, 517-519.
56. E. Quesada and R. J. K. Taylor, *Tetrahedron Letters*, 2005, **46**, 6473-6476.

57. G. Zhang, T. Kumamoto, T. Heima and T. Ishikawa, *Tetrahedron Letters*, 2010, **51**, 3927-3930.

58. P. J. Slavish, Q. Jiang, X. Cui, S. W. Morris and T. R. Webb, *Bioorganic & Medicinal Chemistry*, 2009, **17**, 3308-3316.

59. X. Fang, X. Yang, X. Yang, M. Zhao, G. Chen and F. Wu, *Tetrahedron Letters*, 2006, **47**, 8231-8234.

60. S. Achelle, C. Baudequin and N. Plé, *Dyes and Pigments*, 2013, **98**, 575-600.

61. G. M. Lampman, D. L. Pavia, G. S. Kriz and J. R. Vyvyan, *Spectroscopy*, 4th edn., Brooks/Cole, 2010, page A-14.

Chapter 4

Synthesis of (*E*)-1-(3-aminopyrazin-2-yl)prop-2-en-1-one derivatives

4.1 Overview

The second portion of the internal Michael acceptors was synthesised and coupled to the boronic acid scaffold using the established Suzuki-Miyaura method. The "warhead" was first installed on the aminopyrazine core before the synthesis of the side chains commenced. The side chains were synthesised via substitution and aldol condensation. Various synthetic routes that included Friedel-Crafts acylation, amine protection and Weinreb coupling were explored to find a viable route for the coupling of the "warhead" to the aminopyrazine core.

4.2 Retrosynthetic analysis of the library

The final compounds **295** in this library comprise the same aminopyrazine-sulfonamide scaffold as discussed in Chapter 3, but with side chains consisting of an electrophilic α, β enone warhead in a different position. In this library, the Michael acceptor was rotated 180 ° and the carbonyl moiety was attached to the aminopyrazine core. The retrosynthetic evaluation depicted in Figure 4.1, shows these molecules can be synthesised via Suzuki-Miyaura chemistry from the boronic acid **243** and Michael acceptor derivatives **296**. The synthesis of **296** could be envisaged from a Michael addition reaction between **297** or an Aldol condensation with **298**. Compound **297** and **298** could be further disconnected to the commercially available 2-amino nicotinic acid **299**.

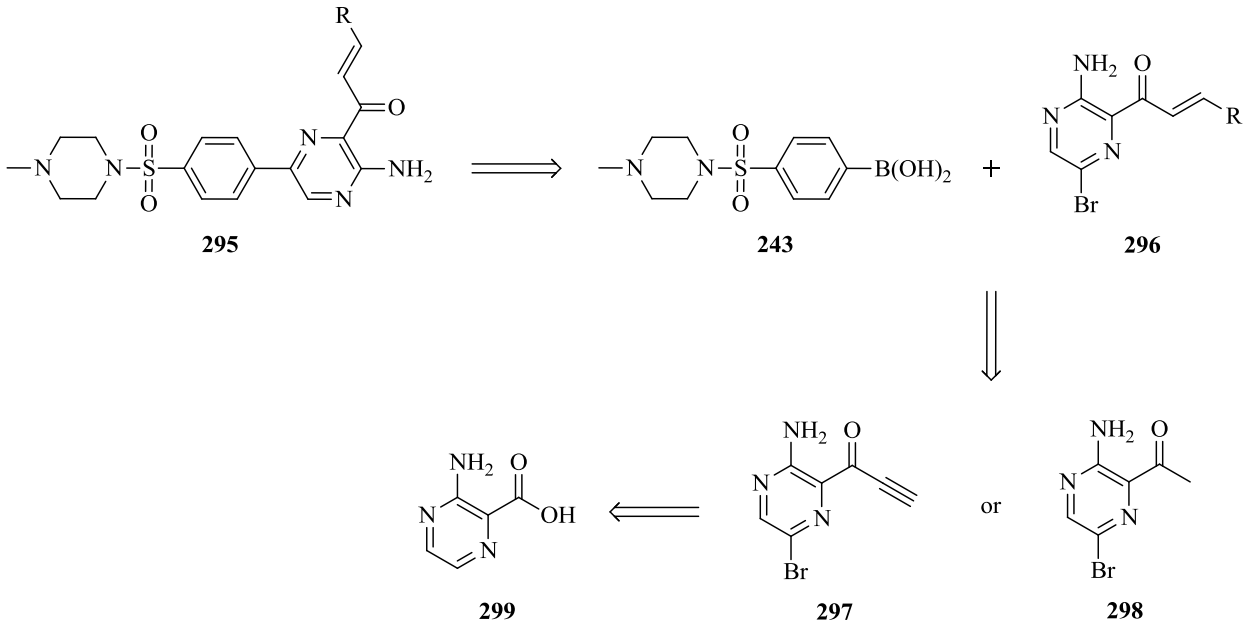

Figure 4.1. Retrosynthesis of the targeted library

4.3 Synthesis of 1-(3-amino-6-bromopyrazin-2-yl)prop-2-yn-1-one (297)

Various methods were employed to synthesise compound **297** and will be discussed in the different sections that follow. These methods included the use of a Friedel Crafts acylation, amine protection and lastly, the Weinreb coupling reaction.

4.3.1 The Friedel-Crafts acylation route

As shown in Scheme 4.1, commercially available 2-amino nicotinic acid **299** was brominated using NBS and sodium hydroxide, followed by quenching the reaction with acetic acid.[1] The solubility of **299** was found to be very low in dimethylformamide and the intramolecular H-bond proton exchange between the amine and the carboxylic acid made the molecule less reactive. This problem was overcome by the addition of sodium hydroxide to disrupt the proton exchange and a clear solution was obtained. After quenching the reaction with acetic acid, the solution was diluted with dichloromethane and washed with iced water. The organic layer was concentrated and the product was isolated as a cream-coloured solid. However, it should be noted that the product was contaminated with dimethylformamide even after several extractions with

dichloromethane. The high polarity of the product **300** (R_f = 0.07 in DCM:MeOH 9:1) made purification via regular column chromatography unviable. In addition, the use of ^{1}H NMR spectroscopy to determine the structure of **300** was inconclusive because the obtained solid was too impure and thus no percentage yield is listed.

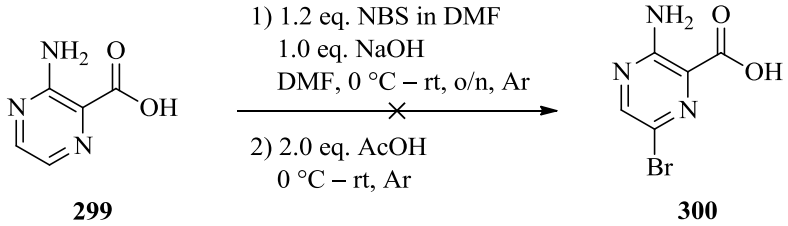

299 **300**

Scheme 4.1 Attempted bromination of **299** using NBS under basic conditions

The aforementioned problems could be avoided by converting the carboxylic acid into an ester before the bromination step.[2, 3] As shown in Scheme 4.2, 2-amino nicotinic acid **299** was added to methanol and the suspension was cooled to 0 °C. Concentrated sulphuric acid was then added dropwise and the suspension was stirred for three days at room temperature. Over time, the suspension gradually became a dark brown solution. The solution was then slowly neutralised with a saturated solution of $NaHCO_3$ and extracted with dichloromethane. After workup, the crude material was recrystallised using water to afford the ester product **301** as an orange coloured solid in 72% yield. In terms of structure elucidation, the ^{1}H NMR spectrum of **301** indicated the presence of the methyl ester (3.85 ppm) and the rest of the spectroscopic data correlated well with that reported in the literature.[3]

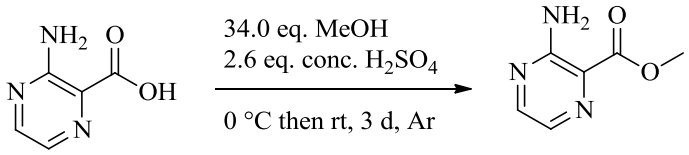

299 **301**
72%

Scheme 4.2. Esterification of 2-amino nicotinic acid **299**

Methyl-3-aminopyrazine-2-carboxylate **301** could now be conveniently brominated with NBS using the procedure of Charrier *et al.*[4] As shown in Scheme 4.3, ester **301** was dissolved in

acetonitrile and cooled to 0 °C. The dissolved NBS was then added dropwise and the brown solution was stirred overnight at room temperature. The dark brown solution was concentrated and diluted with ethyl acetate. After a work up with iced water and brine, the crude material was purified via column chromatography using dichloromethane as eluent to afford the brominated product **302** as peach-white coloured solid in 73% yield. The presence of one heteroaryl proton peak at 8.42 ppm in the ^{1}H NMR spectrum confirmed the successful bromination of ester **301**.

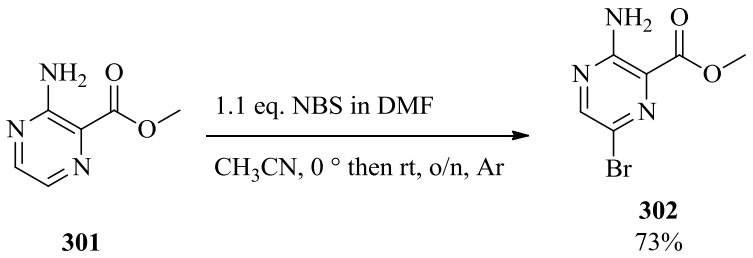

301 **302** 73%

Scheme 4.3. Bromination of methyl-3-aminopyrazine-2-carboxylate **301** using NBS

Compound **302** was then hydrolysed under basic conditions to regenerate the carboxylic acid (Scheme 4.4).[4] To this end, compound **302** and lithium hydroxide was dissolved in methanol and water (1:1 ratio) and the resulting dark orange solution was stirred at 90 °C for 2.5 hours. The dark brown solution was then cooled in ice and neutralised with concentrated hydrochloric acid. The white precipitate was basified with a saturated solution of $NaHCO_3$ and extracted with ethyl acetate. Finally, the aqueous layer was concentrated to a minimum amount to allow the product **300** to crystallize out as yellow needles (66% yield).

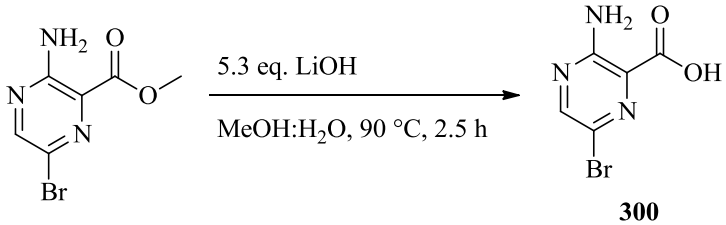

302 **300** 66%

Scheme 4.4. Hydrolysis of methyl-3-amino-6-bromopyrazine-2-carboxylate **302** under basic conditions

With compound **300** in hand, the next step was the Friedel Crafts acylation. The route for the synthesis of the Michael acceptor **297** is summarised in Scheme 4.5. The first step required the reaction of **300** with thionyl chloride to form the acid chloride product, followed by a Friedel Crafts reaction with 1,2-*bis*(trimethylsilyl)ethyne in the presence of the Lewis acid, aluminium chloride, to afford compound **304**. The last step involved a deprotection reaction with K_2CO_3 to give the desired compound **297**.

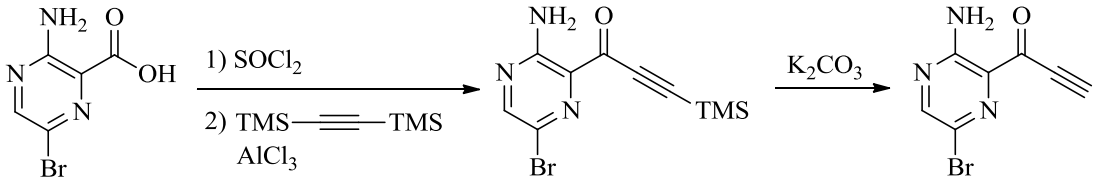

300 **304** **297**

Scheme 4.5. Proposed synthesis of 1-(3-amino-6-bromopyrazin-2-yl)prop-2-yn-1-one **297** using the Friedel Crafts acylation method

A known procedure[5] for the reaction of 2-amino benzoic acid with thionyl chloride was used for the first step and is shown in Scheme 4.6. Due to the fact that 3-amino-6-bromopyrazine-2-carboxylic acid **300** is highly polar and possibly in the zwitterionic form, the reaction was carried out in dimethyl sulfoxide. Unfortunately, the solution thickened over time which suggested a polymerisation reaction. In retrospect, it was determined that thionyl chloride had possibly reacted with the dimethyl sulfoxide.[6]

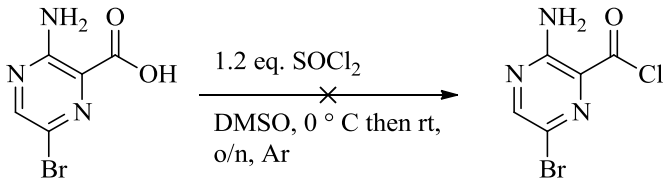

300 **305**

Scheme 4.6. Attempted synthesis of acid chloride **305** in DMSO

The reaction was then repeated in neat thionyl chloride (Scheme 4.7). However, the starting material did not dissolve completely and no changes were observed after stirring the reaction overnight. The cream suspension was then stirred at 90 °C for four hours and the solution has

gradually decreased in turbidity and became clear in terms of transparency. The solution was dark brown-red after four hours and the excess thionyl chloride was removed by evaporation. Unfortunately, the NMR spectroscopy data was inconclusive, which suggested that the isolated material has possibly decomposed.

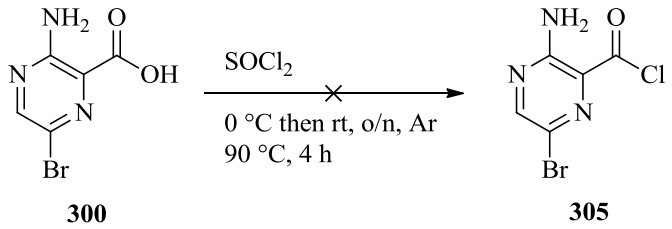

300 **305**

Scheme 4.7. Attempted synthesis of **305** in neat thionyl chloride

In a patent from Pfizer,[7] a procedure for the reaction of 6-chloropyrazine-2-carboxylic acid with thionyl chloride in acetonitrile was described. This starting material is similar to carboxylic acid **300**, except that it lacks the amine functionality. Nevertheless, this procedure was used for the synthesis of acid chloride **305** and this is shown in Scheme 4.8. After the addition of thionyl chloride, the resulting cream suspension was stirred at 90 °C for two hours. The suspension was not completely homogenous and turned dark brown after two hours of stirring. The excess thionyl chloride was then removed by evaporation to provide the crude acid chloride **305** that was used immediately for the next step. Bichler *et al.*[8] carried out the required Friedel Crafts acylation in dichloromethane, but for the second step in our synthesis, (Scheme 4.8) the acylation was carried out in dimethylformamide to facilitate the solubility of the starting reagents. The crude acid chloride **305** was thus dissolved in dimethylformamide and 1,2-*bis*(trimethylsilyl)ethyne was added to the solution at 0 °C. $AlCl_3$ was then added portion-wise and the dark brown solution was stirred overnight at room temperature, followed by quenching the reaction with 2 M HCl. Unfortunately, HPLC analysis of the solution indicated that no product had formed and only the starting carboxylic acid **300** was present.

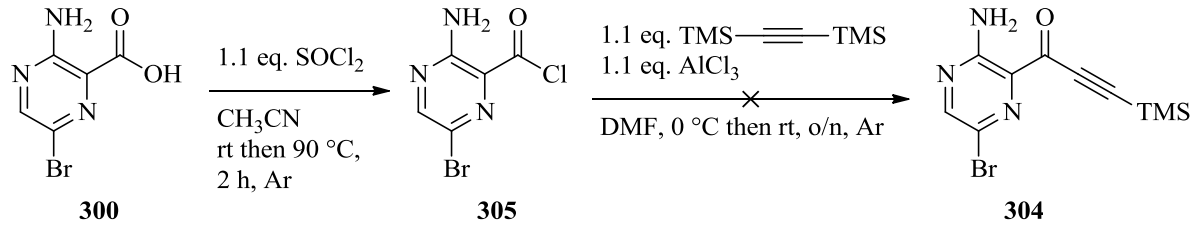

Scheme 4.8. Attempted synthesis of **305** in CH_3CN, followed by acylation in DMF

Usually, Friedel Crafts acylations are carried out in dichloromethane.[9-12] Therefore, this reaction was repeated in dichloromethane, despite the fact that **300** is poorly soluble in dichloromethane (Scheme 4.9). Catalytic amount of dimethylformamide was added to improve the solubility of **300** in dichloromethane. In addition, dimethylformamide reacts with thionyl chloride to generate the Vilsmeier reagent, which is a more reactive chlorinating species than thionyl chloride.[13] Unfortunately, after the workup, HPLC analysis again indicated only the presence of the starting material **300**.

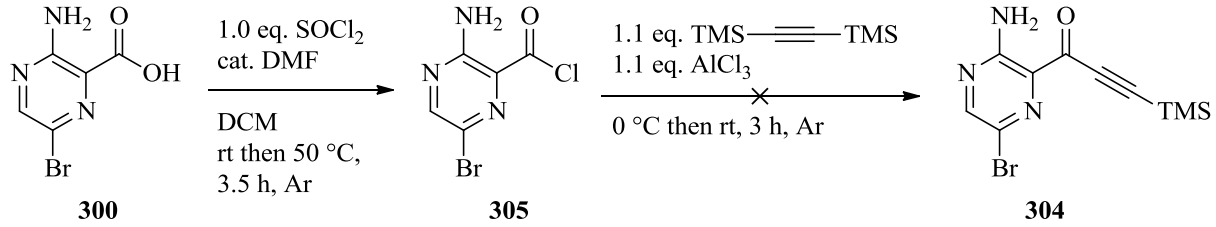

Scheme 4.9. Attempted synthesis of **304** using catalytic amount of dimethylformamide in dichloromethane

The aforementioned findings suggested two possible reasons as to why the Friedel Crafts acylation of **303** failed to form the desired product. Firstly, the zwitterionic form of **300** could prevent the carboxylic acid from reacting with thionyl chloride. Secondly, even if the acid chloride **305** did form, the amine of **305** could potentially react with $AlCl_3$ to form a salt. To test this hypothesis, the reaction was repeated with several modifications.[14] As shown in Scheme 4.10, $AlCl_3$ and 1,2-*bis*(trimethylsilyl)ethyne were replaced with *n*-butyl amine and Et_3N. *n*-Butyl amine was selected as the nucleophile based on the fact that it would lower the polarity of the molecule, thus making it possible to purify the compound using column chromatography. If the acid chloride did form then *n*-butyl amine would react with

3-amino-6-bromopyrazine-2-carbonyl chloride **305** to form the amide product **306**. The reaction was thus conducted as specified, and after the workup and purification using column chromatography, the amide product was isolated as cream solid in 45% yield.

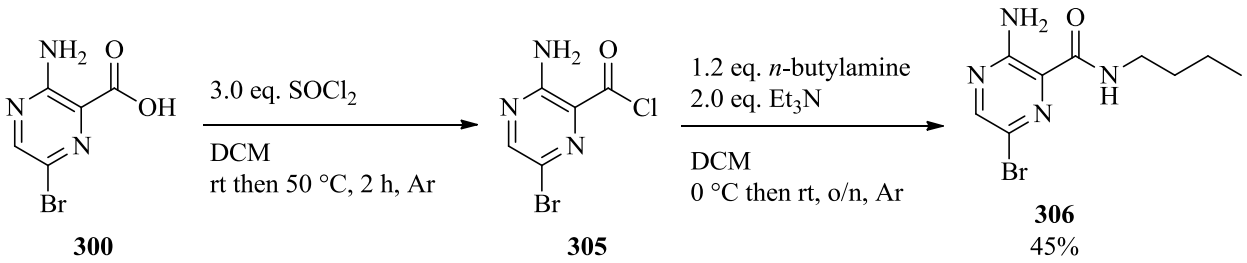

Scheme 4.10. Successful synthesis of butyl amide **306**, which indicated that the acid chloride **305** did form

The ^{1}H NMR spectrum of butyl amide **306** (Fig. 4.2) clearly showed the presence of the amide N-H functional group at 7.66 ppm. In addition, the proton peak at 8.20 ppm could be assigned to C^{2}. The remaining peaks in the alkane region, integrated for nine protons, were assigned to the butyl chain. Since this was a test reaction to confirm whether the acid chloride **305** had formed, no further spectroscopic analysis was carried out.

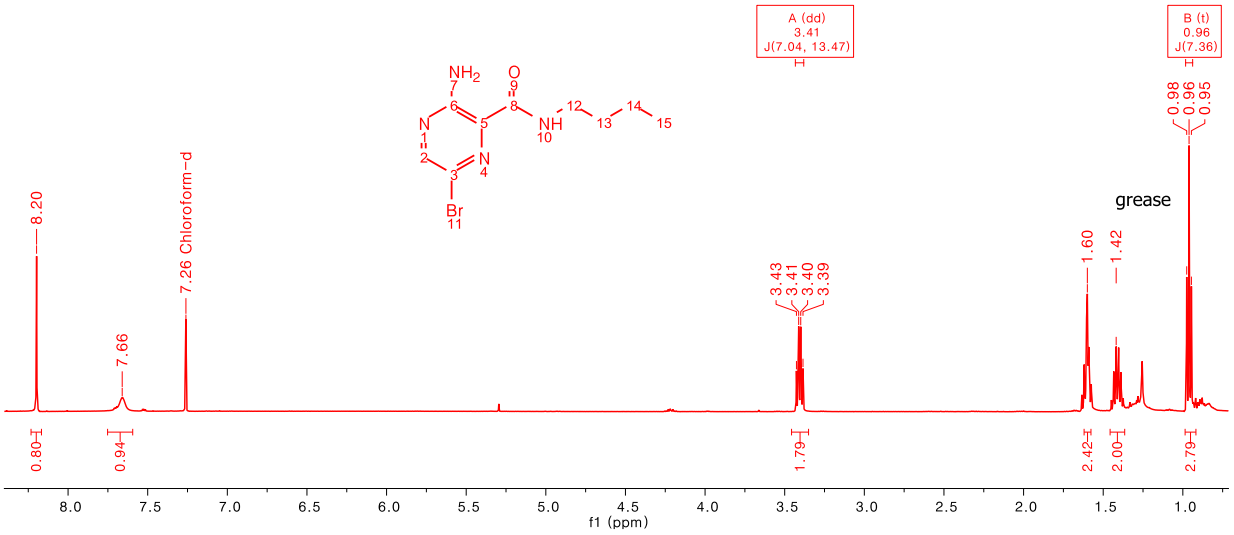

Figure 4.2. ^{1}H NMR spectrum of butyl amide **306**

These findings suggested that the acid chloride **305** did indeed form and was thus not the source of the problem. This meant that the amine of **305** reacted with $AlCl_3$ to form a salt, which deactivated the acylation reaction. To overcome this problem, a synthetic route was developed which involved protection of the amine before the compound underwent a Friedel Crafts acylation. This synthetic route will be discussed in the next section.

4.3.2 The aminopyrazine protection route

The general scheme for the amine protection followed by Friedel Crafts acylation is depicted in Scheme 4.11. The first step involved the protection of the amine with a suitable reagent and the next step the formation of the acid chloride, followed by the Friedel Crafts acylation to afford compound **308**. Lastly, both protecting groups needed to be removed to provide compound **297**.

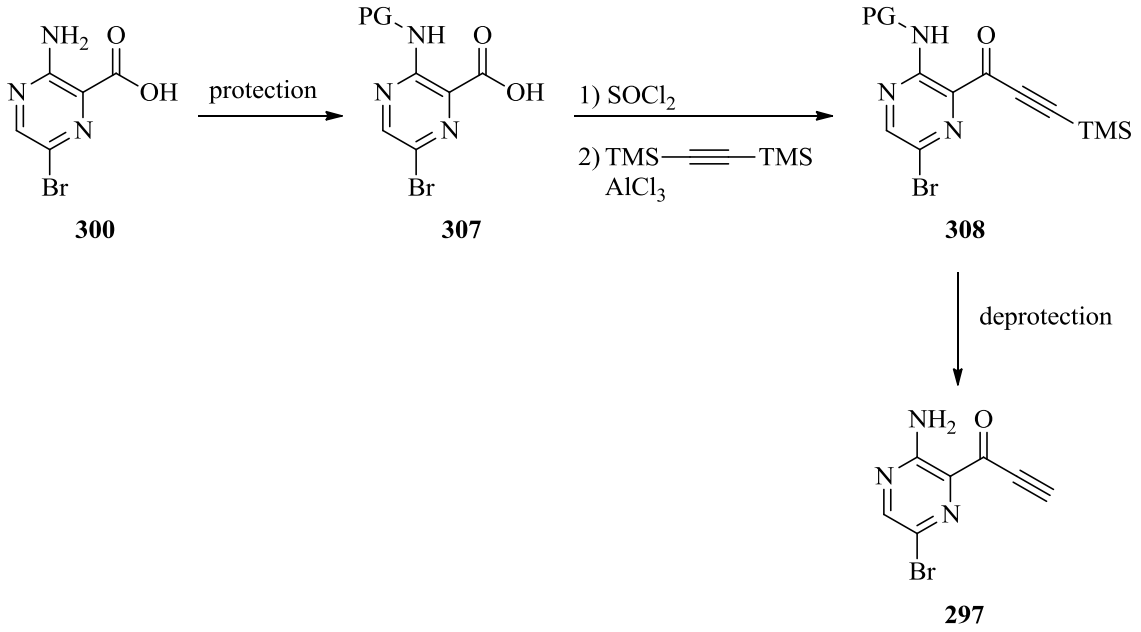

300 **307** **308** **297**

Scheme 4.11. General procedure for the protection of the amine group, followed by Friedel Crafts acylation

Since the trimethylsilyl group can be removed under basic conditions, the protecting group on the amine should also be labile under basic conditions to allow for the simultaneous deprotection of both groups. An example of this type of protecting group is the trifluoroacetamide group that can be removed using K_2CO_3.[15-17]

As shown in Scheme 4.12, 3-amino-6-bromopyrazine-2-carboxylic acid **303** underwent an amine protection reaction with trifluoroacetic anhydride to yield compound **309**.[18] Compound **303** and pyridine were added to dichloromethane at room temperature and the resulting cream suspension was cooled to 0 °C. Trifluoroacetic anhydride was then added dropwise. After workup, the isolated product was identified through TLC and ^{1}H NMR analysis as the starting material **303**. Repeating the reaction firstly with excess Et_3N (5 eq.) instead of pyridine, and then with neat trifluoroacetic anhydride and excess Et_3N (10 eq.) unfortunately proved futile.

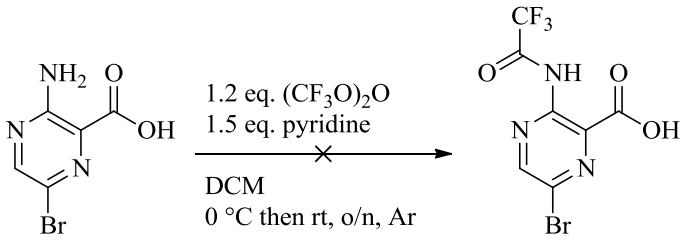

300 **309**

Scheme 4.12. Attempted protection of the amine group of **303** with trifluoroacetic anhydride

The amine group of **300** was found to be very unreactive towards electrophilic attack. 5-Bromo anthranilic acid, can be protected with trifluoroacetic anhydride[19] which suggests that the pyrazine ring of **300** may deactivate the amine towards nucleophilic substitution. Therefore, further work on this route was abandoned and a new route was implemented, which will be discussed in the next section.

4.3.3 The Weinreb coupling route

As explained in the previous section, the amine group of **300** proved to be a stumbling block in terms of reactivity towards electrophiles. Therefore, an alternative approach was considered focusing on the carboxylic acid. As shown in Scheme 4.13, the carboxylic acid **299** can be converted into a Weinreb amide **310**, followed by bromination using NBS to form compound **311**. The last step involved a Grignard reaction with ethynylmagnesium bromide to afford the desired compound **297**.

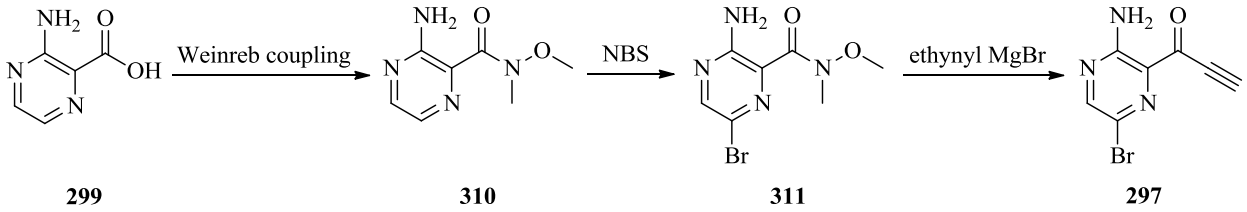

Scheme 4.13. The Weinreb coupling route towards the synthesis of 1-(3-amino-6-bromopyrazin-2-yl)prop-2-yn-1-one **297**

Bruce *et al.*[20] used *N*-(3-dimethylaminopropyl)-*N*′-ethylcarbodiimide hydrochloride (EDC) to activate the carboxylic acid of **299** for the reaction with the Weinreb reagent, *N*-methoxy-*N*-methylamine hydrochloride, to synthesise the Weinreb amide **310**. Due to the unavailability of EDC, the reagent was replaced with 1,1′-carbonyldiimidazole (CDI) and the procedure for the synthesis of **310** was performed as laid out in Scheme 4.14. The starting material **299** was dissolved in DMF at 60 °C and CDI was then added portion-wise to the dark orange solution. After three hours of stirring, the Weinreb reagent was added in one portion and the solution was stirred further at 60 °C overnight. The workup of this reaction with ethyl acetate proved to be difficult due to the miscibility of DMF and water. In addition, after column purification with dichloromethane and MeOH, trace amounts of DMF were present in the product. This problem was solved by allowing the solution to stir at 60 °C overnight in the open as the DMF evaporated under these conditions. The dark brown slurry was then directly purified using column chromatography to afford the product **310** as a pale yellow solid in 94% yield. The ^{1}H NMR spectroscopic analysis revealed two methyl singlets at 3.76 and 3.38 ppm, which indicated the successful synthesis of the Weinreb amide **310**.

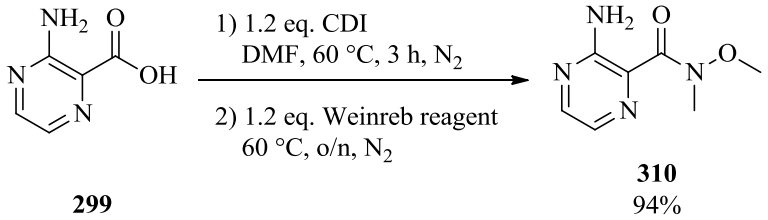

Scheme 4.14. Synthesis of 3-amino-*N*-methoxy-*N*-methylpyrzine-2-carboxamide **310**

The next step required the regioselective *para*-bromination of the Weinreb amide **310** using NBS (Scheme 4.15). This procedure was adapted from the literature.[21] The Weinreb amide **310** was dissolved in chloroform and the solution was cooled to 0 °C. NBS was added portion-wise and the resulting yellow suspension was stirred at 40 °C overnight. Due to the electron donating properties of the -NH_2 group, only one product was observed on the TLC which was later identified as the *para*-brominated product. The solution was then concentrated under reduced pressure and purified using column chromatography with 7:3 Hex:EtOAc as eluent to afford the brominated product **311** as white yellow solid in a good 90% yield.

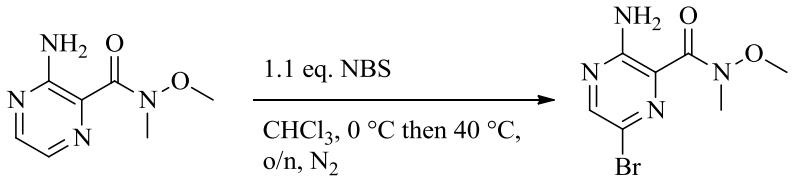

310 **311** 90%

Scheme 4.15. Bromination of **310** using NBS

The last step towards the synthesis of **297** made use of a procedure that was reported in a patent (Scheme 4.16).[20] As in this research, compound **311** was dissolved in THF and cooled to 0 °C. Ethynylmagnesium bromide was then added dropwise and the resulting deep orange-yellow solution was stirred at 0 °C for two hours. The ice bath was then removed and the solution was stirred at room temperature for one hour. Before quenching the reaction with 2 M HCl, the solution was cooled to –10 °C using an ice bath of NaCl and ice. After workup, the column purification was carried out using 8:2 Hex:EtOAc as eluent to afford the product as a luminescent peach-orange solid in a satisfactory 86% yield.

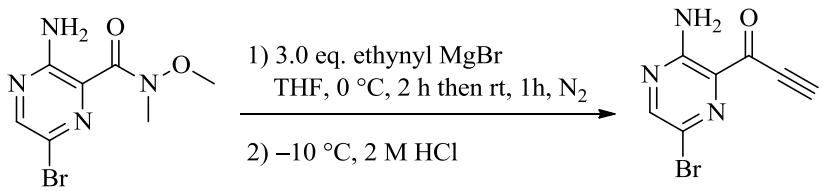

311 **297** 86%

Scheme 4.16. Grignard reaction of **311** with ethynylmagnesium bromide

In terms of characterisation of this new compound, the ^{1}H NMR spectrum of the compound **297** in Figure 4.3 clearly indicated the presence of a terminal alkyne by the presence of a singlet at 3.61 ppm. Due to the proton exchange between the amine and the ketone, the singlet peak of N^{7} at 5.75 ppm was very broad. Lastly, the mass spectrometric data confirmed the molecular mass of this compound as the experimental value of 225.9615 amu corresponded well with that expected for $C_7H_5N_3OBr$ (225.9616 amu).

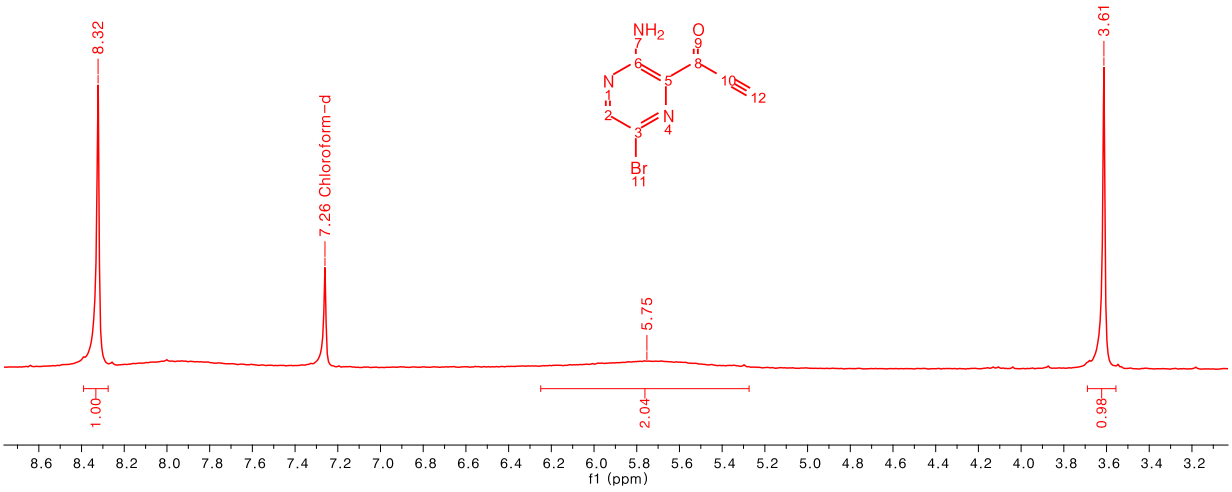

Figure 4.3. ^{1}H NMR spectrum of **297** showing the terminal alkyne proton signal at 3.61 ppm

Based on the successful synthesis of **297**, the procedure shown in Scheme 4.16 was also used for the synthesis of compound **298**. As shown in Scheme 4.17, methylmagnesium bromide was used as the Grignard reagent and the methyl ketone **298** was subsequently isolated as bright yellow solid in 83% yield.

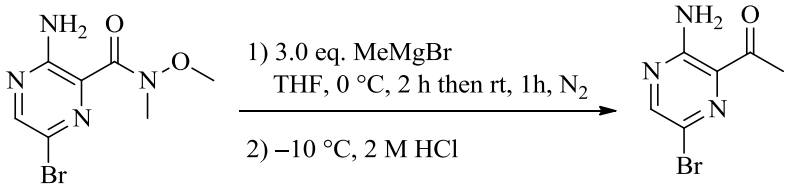

311 **298** 83%

Scheme 4.17. Grignard reaction of **311** with methylmagnesium bromide

With compound **297** and **298** in hand, the synthesis of the side chains could now be completed. The next section will discuss the synthesis of the side chain derivatives **296**.

4.4 Synthesis of 1-(3-amino-6-bromopyrazin-2-yl)prop-2-en-1-one derivatives (296)

Following a procedure developed by Aciro *et al.*,[22] a series of the side chain-coupled derivatives of the pyrazine core were stereoselectively prepared using a Michael addition approach. As shown in Scheme 4.18, compound **297** was dissolved in dichloromethane at 0 °C and morpholine was added dropwise to the orange suspension. The suspension cleared up immediately and the deep orange solution was stirred at room temperature for two hours. The solution was then concentrated under reduced pressure and the mixture was purified using column chromatography using dichloromethane to 95:5 DCM:MeOH as eluent, to afford the product as a yellow solid in 93% yield.

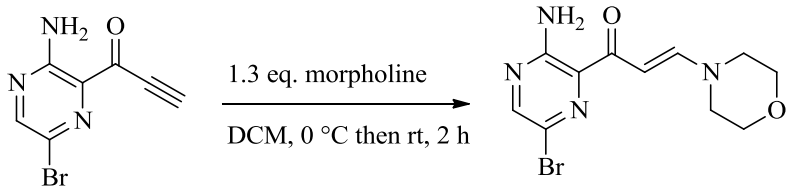

297 **312** 93%

Scheme 4.18. Michael addition reaction of **297** with morpholine

As shown in Figure 4.4, the two doublets at 7.71 and 6.55 ppm have large *J*-coupling values (12.9 Hz), which indicated that the morpholine derivative **312** possesses the (*E*)-configuration. In addition, the heteroaromatic singlet at 8.15 ppm could be assigned to C^6 and the two multiplets at 3.76 and 3.47 ppm, integrating for eight protons, could be assigned to the morpholine ring methylene groups.

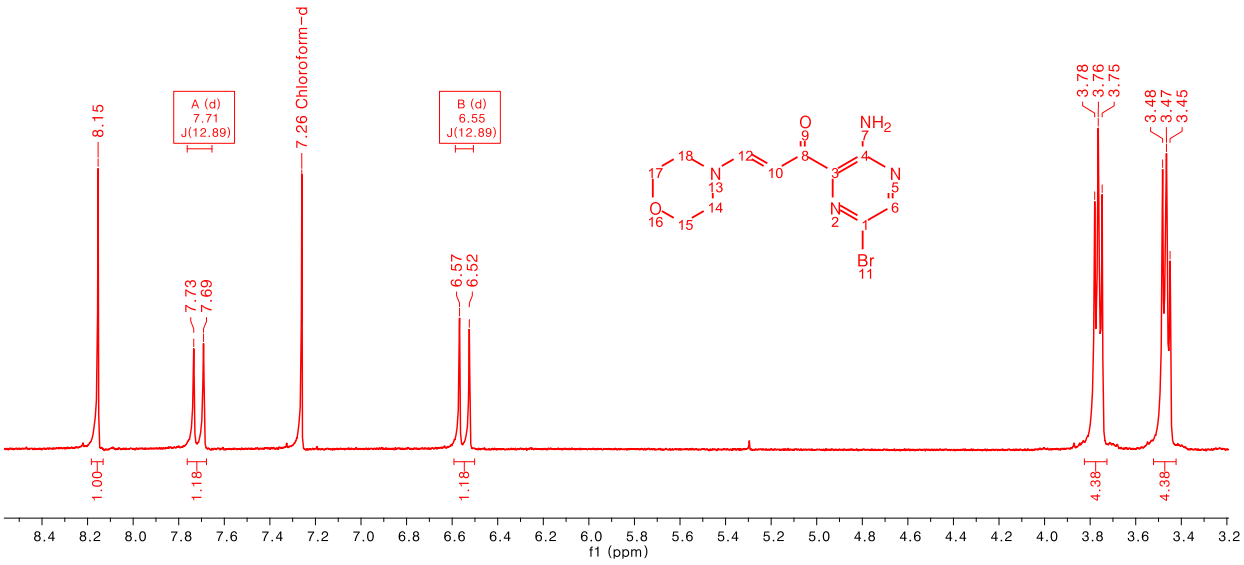

Figure 4.4. ^{1}H NMR spectrum of morpholine **312** confirming the (*E*)-configuration of the molecule

Furthermore, a similar feature of additional carbon peaks due to the extended conjugation system was observed for **312**. The phenomenon, which can be seen in Figure 4.5, is more intense due to the delocalisation of the N-lone pair of the morpholine which restricts the rotation around the N-C bond of the enone. To be able to see the peaks in the alkane region, the NMR spectroscopy experiment had to be carried out for a longer period of time (over 2000 scans) with a concentrated sample. In the alkane region, the carbon peak at 66.5 ppm could be assigned to C^{15} and C^{17}. The remaining two peaks could be assigned to either C^{14} or C^{18}. Since the carbon peaks of the aminopyrazine core have already been analysed in the previous chapter (section 3.5.3), the peaks could be readily identified. In the aromatic region, the carbon peak at 188.2 ppm was the carbonyl C^{8} and the carbon peak at 154.1 ppm could be assigned to C^{6}. The carbon peaks at 148.2 and 123.6 ppm could be assigned to C^{2} and C^{3} respectively, while the carbon peak at 131.8 ppm could be assigned to C^{5}. The two unknown carbon peaks at 152.7 and 91.8 ppm could now be assigned to C^{12} and C^{10} respectively. Finally, the mass spectrometric analysis confirmed the molecular mass of **312** (see experimental section).

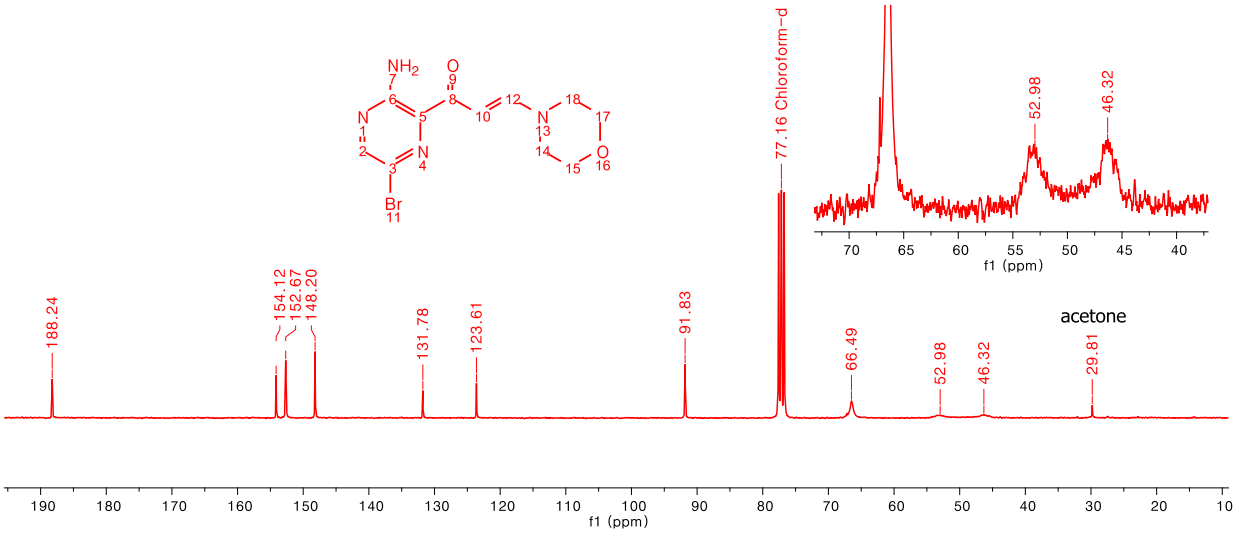

Figure 4.5. ^{13}C NMR spectrum of **312** showing the three broad carbon peaks in the enlarged alkane region

A crystal structure of **312** was also obtained to gain further insight in terms of the structural elucidation. To support the fact that the peaks at 53.0 and 46.3 ppm in the ^{13}C NMR spectrum are not contaminants but carbon atoms of the morpholine ring, a crystal structure of **312** was obtained. Towards this end, compound **312** was dissolved in boiling MeOH and slow evaporation of the cooled solvent resulted small, yellow, block-shaped crystals of diffraction quality. Compound **312** crystallised in the triclinic space group, P1, with one molecule in the asymmetric unit (Figure 4.6 (a)). Hydrogen bonding between the amino group of one molecule and the pyrazine nitrogen of a second molecule link the molecules to form dimers that then pack in three dimensions. From the crystal structure it is evident that the confirmation of the double bond is (*E*), as initially determined by NMR (above) and that the morpholine ring is indeed present.

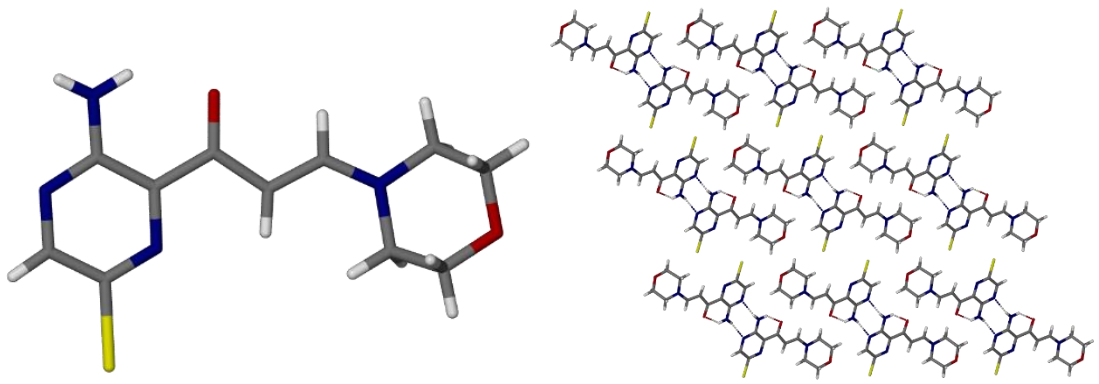

(a) (b)

Figure 4.6. (a) Asymmetric unit of **312** confirming the (*E*)-conformation as well as the presence of the morpholine ring and (b) the packing diagram of **312** viewed down the *a* axis showing the hydrogen-bonding interactions between the molecules.

A series of secondary amines then underwent similar Michael addition reactions with compound **297** and the procedure is shown in Scheme 4.19. For the imidazole **319**, chloroform was needed to improve the solubility and the reaction was carried out at 40 °C overnight. All four products **317** – **320** were isolated in high yields and the (*E*)-configuration was confirmed for all four compounds by means of NMR analysis.

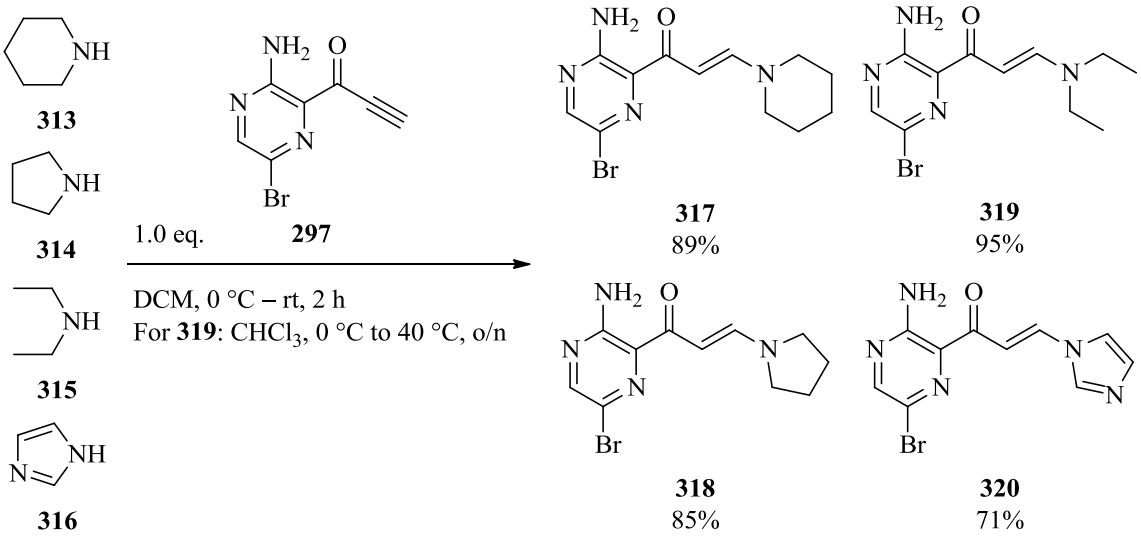

Scheme 4.19. Michael addition reactions of the secondary amines with alkyne **297**

The procedure for the Michael addition reactions of primary amines with alkyne **297** was similar to that mentioned in Scheme 4.19. Cyclohexylamine **321** was the first primary amine to react with alkyne **297** and the procedure is laid out in Scheme 4.20.[23] Alkyne **297** was dissolved in dichloromethane and cooled to 0 °C. A solution of cyclohexylamine in dichloromethane was then added dropwise and the solution was gradually warmed to room temperature over 3 hours. The deep orange solution was concentrated and purified using column chromatography using 1:1 Hex:EtOAc as eluent to afford the product as a dark cream-coloured solid in 93% yield. However, according to the ^{1}H NMR spectrum that will be discussed next, and in contrast to compounds **312**, **317** –**320** the isolated product was the undesired (*Z*)-isomer.

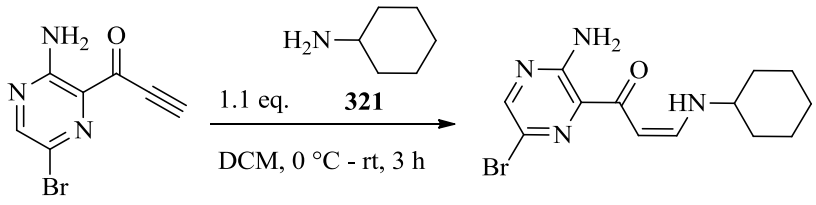

297 **322** 93%

Scheme 4.20. Michael addition reaction of cyclohexylamine with alkyne **297**

The confirmation that compound **322** possessed the (*Z*)-configuration is supplied in Figure 4.7. In the aromatic region of the ^{1}H NMR spectrum, two proton peaks at 7.06 and 6.30 ppm have *J*-coupling constants of 7.5 Hz, which is characteristic of the alkene being in the *cis*-conformation.[24] Furthermore, the doublet of doublets at 7.06 ppm can be assigned to C^{12} and the doublet at 6.30 ppm to C^{10}. The broad singlet, integrating for one proton, at 10.17 ppm can be assigned to N^{13}. The last proton peak at 8.10 ppm is the heteroaromatic proton of C^{2}. The proton peaks of the cyclohexane ring have been assigned with no difficulty and will not be discussed here. Lastly, mass spectrometric data confirmed the molecular mass of this compound as the experimental value of 325.0657 amu corresponded well with that expected for $C_{13}H_{18}N_4OBr$ of 325.0664 amu.

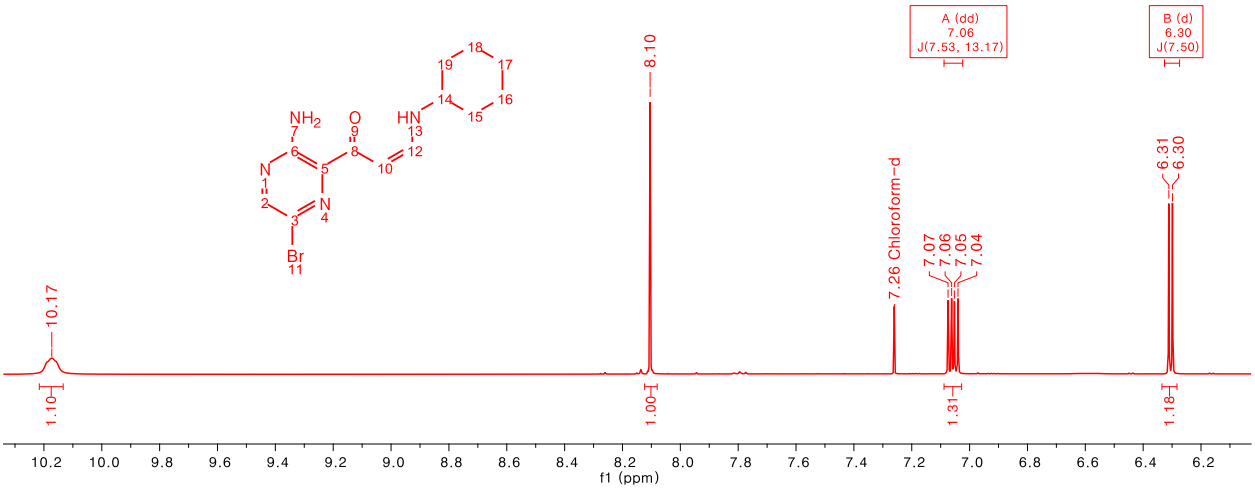

Figure 4.7. ^{1}H NMR spectrum of **322** showing the *cis*-conformation

The reason as to why only the (*Z*)-isomer was observed is possibly due to the tendency of **322** to form an intramolecular hydrogen bond.[25] To determine whether the hydrogen bonding could be disrupted by using protic solvents, the reaction in Scheme 4.20 was repeated in methanol. Unfortunately, similar results were obtained. Repeating the reaction at –78 °C and gradually warming the solution to room temperature delivered similar results which suggested that the (*E*)-isomer cannot be obtained by running the reaction under kinetic control.

Several research teams have reported using Lewis acids for various types of Michael reactions.[26-30] Therefore, an attempt was made to determine whether the use of a Lewis acid or a Brønsted acid could promote the formation of the (*E)*-isomer by interacting with the carbonyl moiety and subsequently disrupting the intramolecular hydrogen bonding. Using the conditions from Scheme 4.21, the acids used and the results obtained are tabulated in Table 4.1.

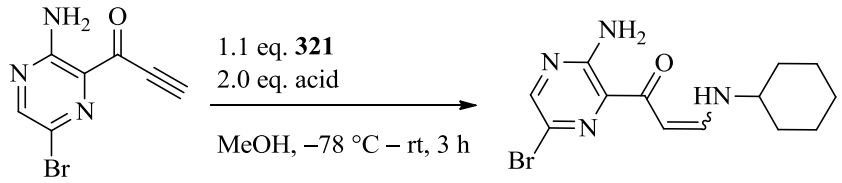

297

322 = *Z*
323 = *E*

Scheme 4.21. Michael addition reactions of cyclohexylamine **321** with alkyne **297** in the presence of various acids

According to the ^{1}H NMR spectroscopic data, none of the acids afforded the (*E*)-isomer. Both $CeCl_3.7H_2O$ and citric acid, provided the (*Z*)-isomer which contained traces of unidentified impurities. The reaction with $TiCl_4$ was carried out in THF, which yielded a mixture that could not be identified by ^{1}H NMR spectrum as the proton peaks of the cyclohexylamine were not present.

Table 4.1. Results obtained with various acids used for the Michael addition reaction of cyclohexylamine **321** with alkyne **301**

#	Acid	*E/Z*
1	$B(OH)_3$	*Z*
2	$CeCl_3.7H_2O$	*Z* (crude)
3	$TiCl_4$ (in THF)	inconclusive
4	AcOH	*Z*
5	citric acid	*Z* (crude)
6	4-nitrophenol	*Z*
7	TsOH	*Z*
8	1M HCl	*Z*

Despite numerous attempts, unfortunately no conditions provided the (*E*)-isomer. As this strategy did not seem to be yielding any of the desired isomer, the decision was made to go back to the drawing board and pursue a different route.

Aldol condensation reactions were thus also implemented to incorporate pyridine systems onto the side chains. Using the procedure of Bhambra *et al.*,[31] 3-pyridinecarboxaldehyde **324** readily underwent an aldol condensation with methyl ketone **298** (Scheme 4.22). These reagents were dissolved in dioxane at room temperature and $LiOH{\cdot}H_2O$ was then added portion-wise to the solution. The yellow solution, with the undissolved $LiOH{\cdot}H_2O$, was then heated at 50 °C for four hours. However, no changes were observed on the TLC plate and MeOH was then added to facilitate the solubilisation of the $LiOH{\cdot}H_2O$. The solution had turned dark orange upon the addition of methanol and after an additional stirring of 19 hours at 50 °C, the solution had turned black-red. The solution was then quenched with water, which resulted in the formation of a

brown slurry. Full conversion of the starting materials was observed on the TLC plate; however, three different spots, one possibly representing the desired product, were visible. In addition, during the workup of the solution, the brown slurry did not dissolved in ethyl acetate or in water and so this approach was abandoned.

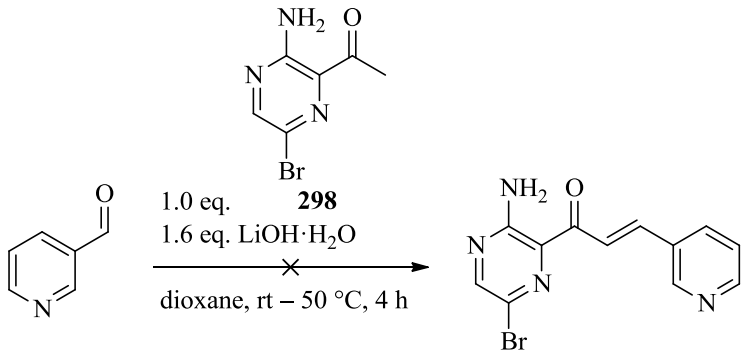

324 **325**

Scheme 4.22. Attempted aldol condensation of 3-pyridine carboxaldehyde **324** with **298**

The reaction was repeated with several modifications.[32] As shown in Scheme 4.23, the solvent system was changed to EtOH:DCM in a 4:1 ratio. In addition, the base was changed to sodium hydroxide and was used in excess. After stirring the solution overnight at room temperature, the black-brown solution was quenched with water. The TLC plate indicated that there was full conversion of the starting materials, but also that a large number of side products had formed (EtOAc as eluent). Only trace amounts of a solid could be isolated after work up, which was not purified further.

Bhambra *et al.*[31] have suggested that the use of protic solvents such as methanol could have an effect on the aldol condensation of **324**. They determined that in methanol, the aldol condensation with **324** could lead to the formation of the diketone product. The reaction in Scheme 4.22 was thus then repeated albeit with a different solvent system. As shown in Scheme 4.23, the aldol condensation reaction of 3-pyridinecarboxaldehyde **324** and methyl ketone **298** was carried out in a solvent system of dioxane and H_2O in a ratio of 15:1 respectively. After stirring overnight at room temperature, the solution had formed a yellowish suspension instead of the black-red solution that was previously observed (Scheme 4.22). A full conversion of the

starting materials was again observed on the TLC plate with only one product spot. Furthermore, the product spot was yellow and could be seen with the naked eye. After the workup, this product was purified using column chromatography using Hex:EtOAc 7:3 as eluent, to afford the product as bright yellow solid in quantitative yield. Spectroscopic analysis of this product confirmed the structure of the desired molecule **325** (see characterisation later in this section).

The reaction was repeated for the other two pyridine starting materials, 2-pyridinecarboxaldehyde **326** and 4-pyridinecarboxaldehyde **328**, and the corresponding products were again isolated in quantitative yields. For the preparation of the NMR spectroscopy samples, a trend was observed for the solubility of the products **325**, **327** and **329**. It was observed that *ortho*-pyridine **327** dissolves moderately in chloroform and that the *meta*-pyridine **325** required an additional ten drops of MeOH. Lastly, *para*-pyridine **329** was insoluble in chloroform and required DMSO to fully dissolve the compound.

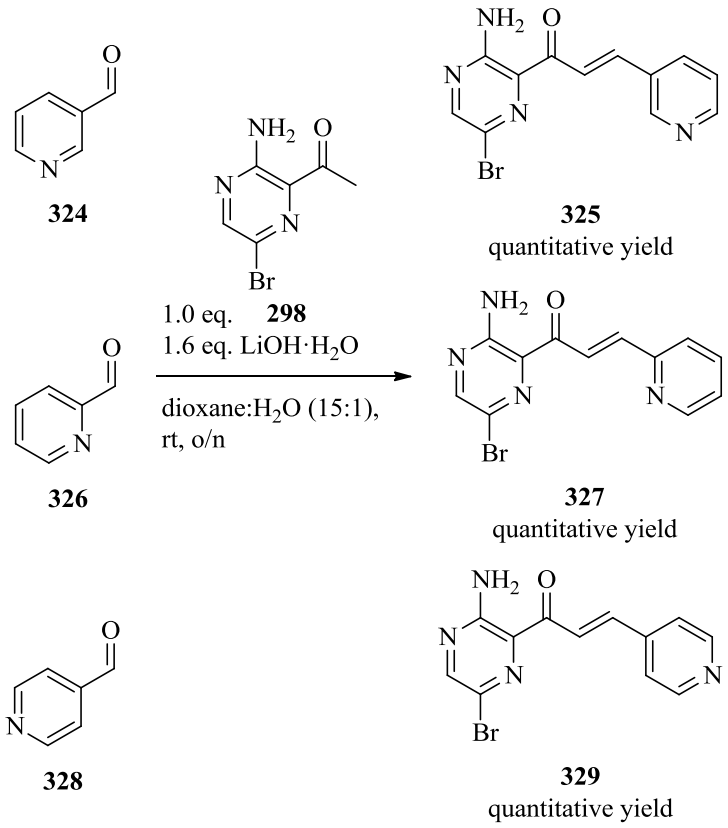

324 **326** **328**

325 quantitative yield

327 quantitative yield

329 quantitative yield

Scheme 4.23. Successful aldol condensation of various pyridinecarboxaldehydes with **298**

The novel compounds **325**, **327** and **329** were analytically characterised and compound **327** was selected to discuss the ^{1}H NMR spectrum (Fig. 4.8). The large *J*-coupling values of the two doublets at 8.59 and 7.84 ppm indicated that **327** had the (*E*)-configuration.[24] These two doublets could be assigned to C^{12} and C^{10} respectively. Due to the deshielding effect of the neighbouring N-atom, C^{15} could be assigned to the doublet at 8.72 ppm. However, it was expected that this peak would be a doublet of doublets, but due to the low resolution of the NMR spectroscopy instrument, the peak was detected as a doublet. The doublet of doublet of doublets at 7.30 ppm could distinctively be assigned to C^{16}. The doublet at 7.61 ppm could be assigned to C^{18} and again this peak was expected to be a doublet of doublets. Lastly, the triplet of doublets at 7.75 ppm could be assigned to C^{17}.

As sometimes occurs with extensively conjugated systems, not all carbon peaks were observed in the ^{13}C spectrum. A possible explanation for this phenomenon is that the asymmetric pyridine ring (**325** and **327**) has five distinctive aromatic chemical environments and will produce only five carbon peaks. For *para*-pyridine **329**, which has a symmetric pyridine ring, only three aromatic peaks were detected.

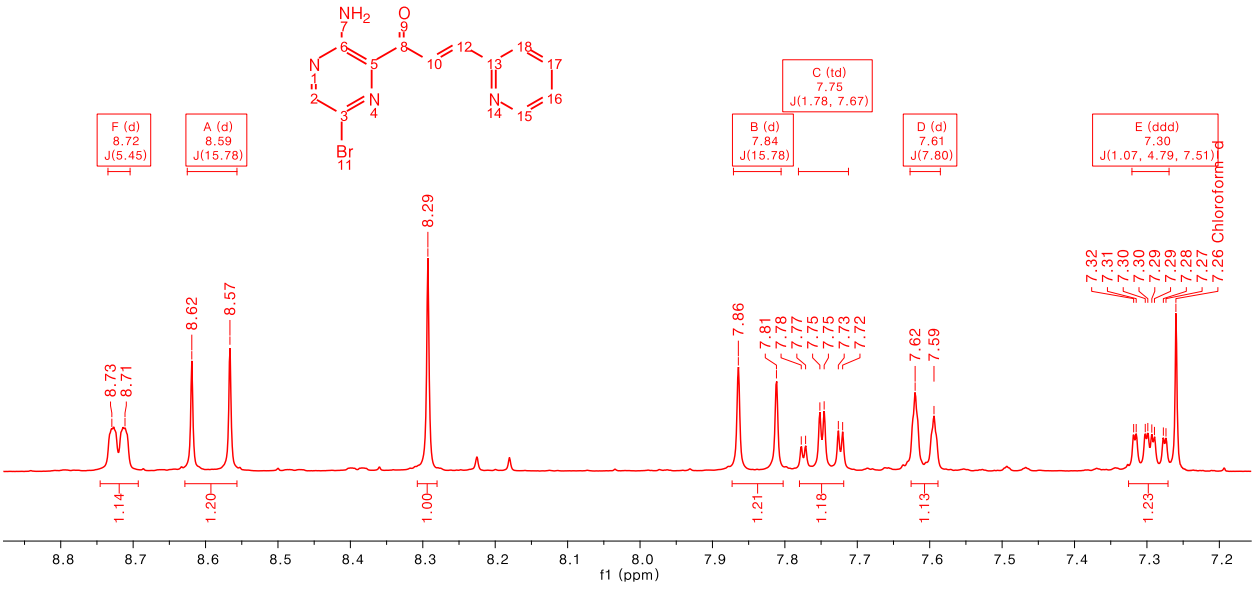

Figure 4.8. ^{1}H NMR spectrum of *ortho* pyridine **327** showing the (*E*)-configuration of the molecule

With the synthesised warheads in hand, the next step was to carry out a Suzuki-Miyaura reaction with boronic acid **243** to produce the desired final compounds. The synthesis of the final compounds will be discussed in the next section.

4.5 The Suzuki-Miyaura reactions with 1-(3-amino-6-bromopyrazin-2-yl)prop-2-en-1-one derivatives

The procedure used for the Suzuki-Miyaura reactions was similar to that mentioned in Scheme 3.36. All synthesised warheads **317** – **320**, **325** and **327** readily underwent a Suzuki-Miyaura reaction with boronic acid **243**, except for *para*-pyridine **329** due to solubility issues. The procedure and the results are shown in Scheme 4.24 and Table 4.1. For the imidazole derivative **239**, two spots were observed on the TLC plate (R_f: 0.50 and 0.56, 9:1 EtOAc:MeOH) that could not be separated using column chromatography. Several attempts to obtain product **239** in pure form proved futile.

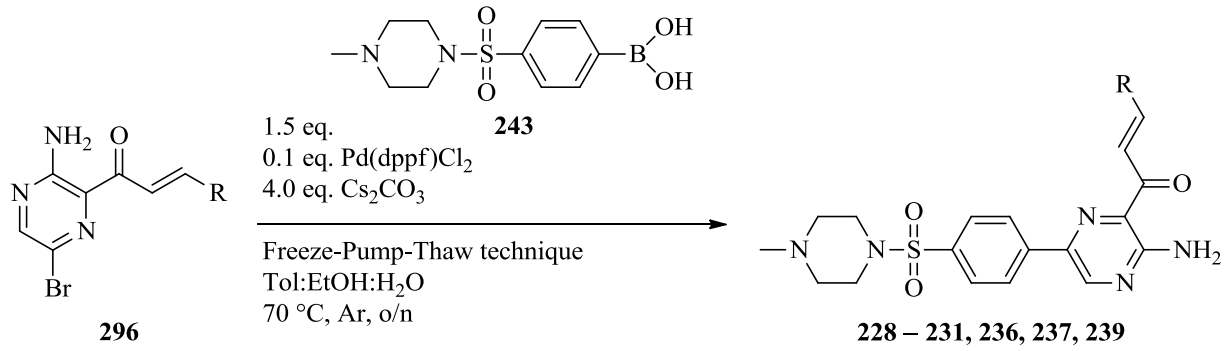

Scheme 4.24. Suzuki reaction with Michael acceptor derivatives **300** to form the final compounds **299**

Table 4.1. Products obtained from the Suzuki reactions with boronic acid **243** and the six aminopyrazine derivatives **317 - 320**, **325** and **327**

#	R	Yield
228	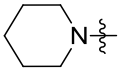	73%
229	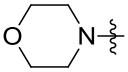	69%
230	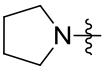	76%
231	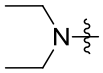	86%
236	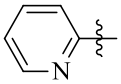	40%
237	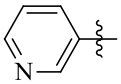	43%
239	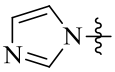	failed

The piperidine derivative **228** was selected for the discussion of NMR spectroscopic characterisation for this series of final compounds. Since the proton peaks of the scaffold have already been identified in Section 3.6, it could be readily applied to this compound and using the spectroscopic data from Figure 4.4, the proton peaks of the side chain could also be identified. As shown in Figure 4.9, one of the doublets of the Michael acceptor was buried under the proton peak of $C^{13/15}$ at 7.84 – 7.80 ppm and could be assigned to C^{27}. The other doublet could be located at 6.71 ppm with a *J*-coupling value of 12.8 Hz. The singlet at 8.58 ppm was the heteroaromatic C^{18} and the doublet at 8.08 ppm was $C^{16/12}$. The multiplet at 3.45 ppm, integrating for four protons, could be assigned to $C^{29/33}$ and the other multiplet at 1.70 ppm, integrating for six protons, could be assigned to $C^{30,31,32}$. Finally, the proton peaks 3.08, 2.49 and 2.27 ppm could be assigned to the methylpiperazine group.

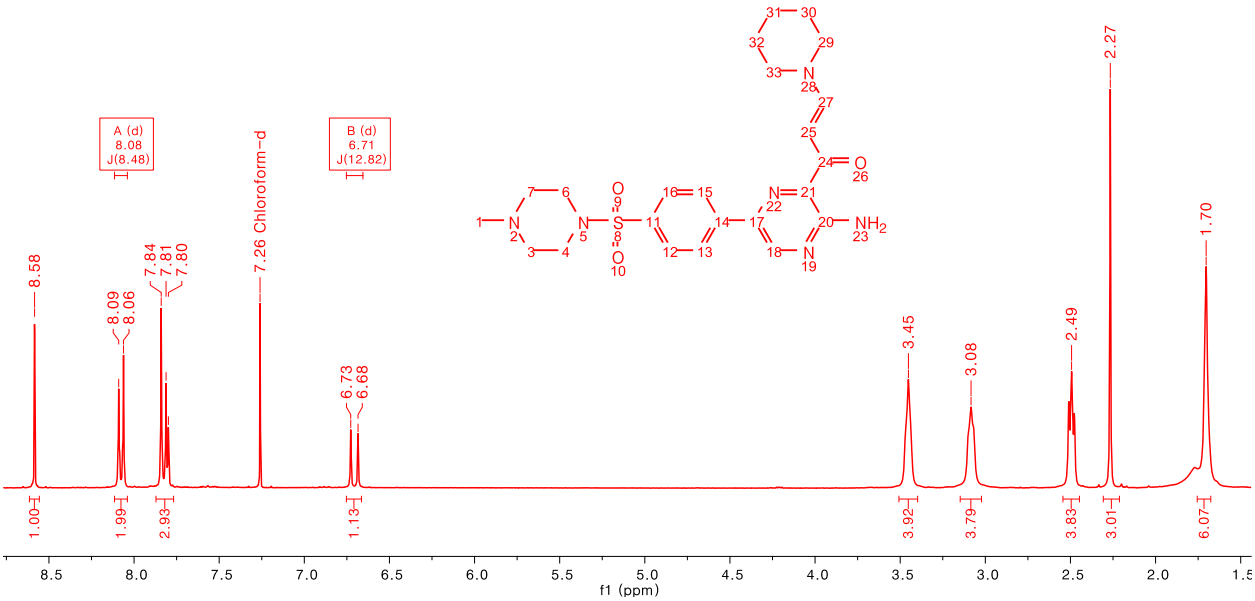

Figure 4.9. ^{1}H NMR spectrum of piperidine **228** showing the successful Suzuki-Miyaura coupling

The ^{13}C NMR spectrum of **228** is shown in Figure 4.10 and several peaks from the aromatic region could be readily assigned using the data from Figure 4.5. The carbon peak at 189.0 ppm was the carbonyl C^{24} and the carbon peak at 154.6 ppm was C^{20}. The carbon peaks at 153.1 and 90.7 ppm could be assigned to C^{27} and C^{25} respectively. The carbon peak at 132.0 ppm was C^{21}. In the alkane region, the carbon peaks at 55.5 and 46.8 ppm could be either C^{33} or C^{29}. The carbon peaks at 26.7 and 25.2 ppm were C^{32} or C^{30}. The carbon peak of the piperidine ring, C^{31}, was 24.2 ppm. The last three peaks that could be readily assigned were 54.2, 46.1 and 45.8 ppm, which belong to the methylpiperazine group. From the spectroscopic data that was covered in section 3.6, the carbon peaks at 128.5 and 126.0 ppm could be assigned to $C^{15/13}$ and $C^{16/12}$ respectively. The carbon peaks at 141.7, 138.1 and 134.3 ppm could be assigned to C^{11}, C^{14} and C^{17} respectively. From the HSQC spectrum (not shown), the carbon peak at 143.2 ppm was identified as C^{18}.

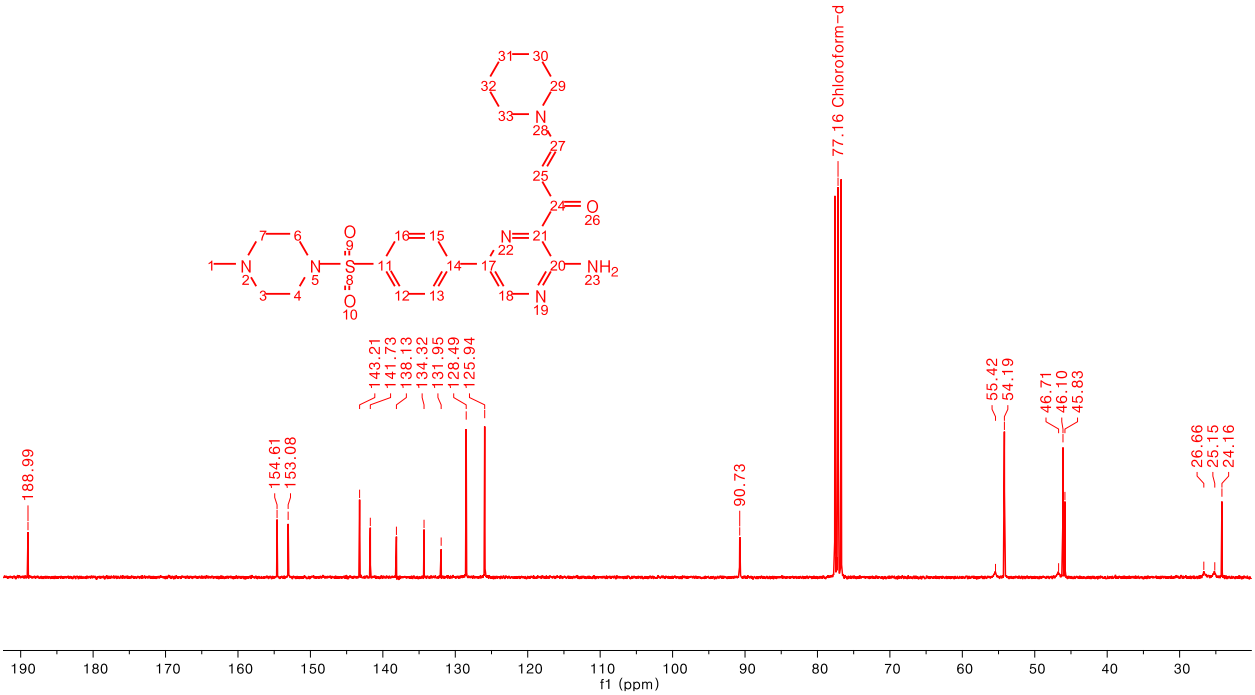

Figure 4.10. ^{13}C NMR spectrum of **228**

A series of (*E*)-1-(3-aminopyrazin-2-yl)prop-2-en-1-one derivatives have been successfully synthesised that involved the Weinreb coupling, Grignard, aldol condensation and Suzuki-Miyaura methods. The final compounds **228** - **231**, **236** and **237** have been subjected to biological testing and will be discussed in the next chapter.

4.6 References

1. J. Pelleter and F. Renaud, *Organic Process Research & Development*, 2009, **13**, 698-705.
2. R. C. Ellingson, R. L. Henry and F. G. McDonald, *Journal of the American Chemical Society*, 1945, **67**, 1711-1713.
3. H. Duan, M. Ning, X. Chen, Q. Zou, L. Zhang, Y. Feng, L. Zhang, Y. Leng and J. Shen, *Journal of Medicinal Chemistry*, 2012, **55**, 10475-10489.
4. J.-D. Charrier, S. J. Durrant, J. M. C. Golec, D. P. Kay, R. M. A. Knegtel, S. MacCormick, M. Mortimore, M. E. O'Donnell, J. L. Pinder, P. M. Reaper, A. P. Rutherford, P. S. H. Wang, S. C. Young and J. R. Pollard, *Journal of Medicinal Chemistry*, 2011, **54**, 2320-2330.

5. K. Mahiwal, P. Kumar and B. Narasimhan, *Medicinal Chemistry Research*, 2012, **21**, 293-307.
6. D. D. Wirth, S. Vikas and P. Jagadish, in *Encyclopedia of Reagents for Organic Synthesis*, John Wiley & Sons, Ltd, 2001.
7. S. Ninkovic, J. F. Braganza, M. R. Collins, J. C. Kath, H. Lui, D. T. Richter, Patent WO2010/16005, 2010.
8. P. Bichler, W. A. Chalifoux, S. Eisler, A. L. K. Shi Shun, E. T. Chernick and R. R. Tykwinski, *Organic Letters*, 2009, **11**, 519-522.
9. C. W. Bradshaw, H. Fu, G. J. Shen and C. H. Wong, *Journal of Organic Chemistry*, 1992, **57**, 1526-1532.
10. C. D. Smith, K. Tchabanenko, R. M. Adlington and J. E. Baldwin, *Tetrahedron Letters*, 2006, **47**, 3209-3212.
11. R. Suzuki, H. Tsukuda, N. Watanabe, Y. Kuwatani and I. Ueda, *Tetrahedron*, 1998, **54**, 2477-2496.
12. D. J. Yee, V. Balsanek and D. Sames, *Journal of the American Chemical Society*, 2004, **126**, 2282-2283.
13. S. V. Vinogradova, V. A. Pankratov, V. V. Korshak and L. I. Komarova, *Bulletin of the Academy of Sciences of the USSR, Division of Chemical Science*, 1971, **20**, 450-455.
14. S. Shang, D. Zhang-Negrerie, Y. Du and K. Zhao, *Angewandte Chemie International Edition*, 2014, **53**, 6216-6219.
15. X. Li, Y. Zhang, Y. Jiang, J. Wu, E. S. Inks, C. J. Chou, S. Gao, J. Hou, Q. Ding, J. Li, X. Wang, Y. Huang and W. Xu, *European Journal of Medicinal Chemistry*, 2017, **134**, 185-206.
16. L. Perrin, M. Legros and R. Mercier, *Macromolecules*, 2015, **48**, 323-336.
17. P. Yang and M. G. Moloney, *RSC Advances*, 2016, **6**, 111276-111290.
18. B. R. Ambler, S. Peddi and R. A. Altman, *Organic Letters*, 2015, **17**, 2506-2509.
19. P. Zhang, E. A. Terefenko and J. Slavin, *Tetrahedron Letters*, 2001, **42**, 2097-2099.
20. I. Bruce, E. Budd, L. Edwards, C. Howsham, Patent US20090239847 A1, 2009.
21. M. Schlosser, A. Ginanneschi and F. Leroux, *European Journal of Organic Chemistry*, **2006**, 2956-2969.

22. C. Aciro, V. A. Steadman, S. N. Pettit, K. G. Poullennec, L. Lazarides, D. K. Dean, N. A. Dunbar, A. J. Highton, A. J. Keats, D. S. Siegel, K. K. Karki, A. J. Schrier, P. Jansa, R. Mackman, Patent WO2010/16005, 2013.
23. J. D. Winkler and J. R. Ragains, *Organic Letters*, 2006, **8**, 4031-4033.
24. G. M. Lampman, D. L. Pavia, G. S. Kriz and J. R. Vyvyan, *Spectroscopy*, 4th edn., Brooks/Cole, 2010, page A-14.
25. J. Yang, C. Wang, X. Xie, H. Li and Y. Li, *European Journal of Organic Chemistry*, 2010, **2010**, 4189-4193.
26. T. C. Wabnitz and J. B. Spencer, *Organic Letters*, 2003, **5**, 2141-2144.
27. T. C. Wabnitz, J.-Q. Yu and J. B. Spencer, *Chemistry – A European Journal*, 2004, **10**, 484-493.
28. S. Kobayashi, K. Kakumoto, Y. Mori and K. Manabe, *Israel Journal of Chemistry*, 2001, **41**, 247-250.
29. M. K. Chaudhuri, S. Hussain, M. L. Kantam and B. Neelima, *Tetrahedron Letters*, 2005, **46**, 8329-8331.
30. J. Bah and J. Franzén, *Chemistry – A European Journal*, 2014, **20**, 1066-1072.
31. A. S. Bhambra, K. C. Ruparelia, H. L. Tan, D. Tasdemir, H. Burrell-Saward, V. Yardley, K. J. M. Beresford and R. R. J. Arroo, *European Journal of Medicinal Chemistry*, 2017, **128**, 213-218.
32. M. Y. Fosso, H. LeVine 3rd, K. D. Green, O. V. Tsodikov and S. Garneau-Tsodikova, *Organic & Biomolecular Chemistry*, 2015, **13**, 9418-9426.

Chapter 5

Biological results

5.1 Overview

In this chapter, the biological results of the synthesised GSK-3β inhibitors that were discussed in chapter three and four will be reviewed. The first biological testing of the compounds involved the determination of the IC_{50} values. The compounds that exhibited an IC_{50} value lower than 10 μM were subjected to the GSK-3β time-dependent studies to determine whether or not these compounds bind irreversibly to the GSK-3β.

5.2 Biological results of the (*E*)-3-(3-aminopyrazin-2-yl)acrylaldehyde derivatives

The five compounds (**216** – **220**) that were synthesised as described in section 3.6 were sent for *in vitro* testing using the radiometric and luminescent assays[1] on the human recombinant GSK-3β enzyme. Each compound was incubated with the enzyme for 20 minutes (see experimental section, Chapter 8.5) and a full dose-response analysis was performed on all compounds to determine the concentration inhibiting 50% of enzyme activity (IC_{50}). The values are shown in Table 5.1. Alsterpaullone **298**, a known reversible GSK-3β inhibitor,[2] was used as a reference standard.

Table 5.1. GSK-3β IC_{50} values of compounds **216** – **220** with the obtained docking scores (Chapter 2.3.3)

#	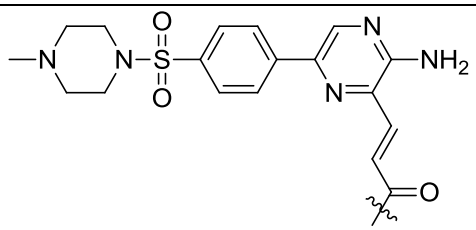	**IC_{50} (GSK-3β) (μM)**	**Docking score (kcal/mol)**
216	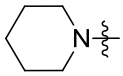	5.29 ± 0.22	-5.751
217	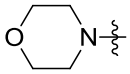	7.47 ± 0.19	-7.205
218	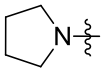	3.63 ± 0.28	-7.439
219	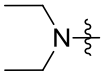	>10 (39%)	-7.204
220	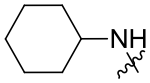	9.90 ± 0.49	failed
298	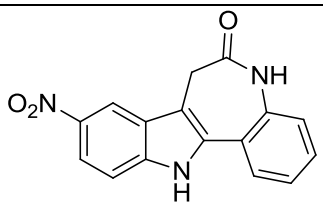	0.004	-

The results for the *in vitro* assay against the human recombinant GSK-3β were very poor when compared to the reference standard and the IC_{50} values were in the lower micromolar range. From these results it can be seen that the position of the carbonyl moiety is critical to obtain nanomolar activity, as seen in compounds **204** – **208** (Chapter 2, Fig. 4), regardless the type of side chains present. From the aforementioned results, the type of amine group on the side chain does not give clear insight as to what is required for potency.

A scatter plot of IC_{50} versus the docking scores (Fig. 5.1) was constructed to compare the biological results with the docking scores (Chapter 2.3.3). The biological activities of the compounds correlated poorly with the results of the molecular modelling as described in chapter 2. It appears that the binding mode used in the molecular modeling does not appear to be

a reliable predictor of efficacy. This could mean that the molecules interact at a different site on the enzyme or inhabit this binding site in a manner unpredicted by the molecular modeling. Lastly, this series does not provide potent inhibitors for GSK-3β and that any future work on this series should be carefully thought through.

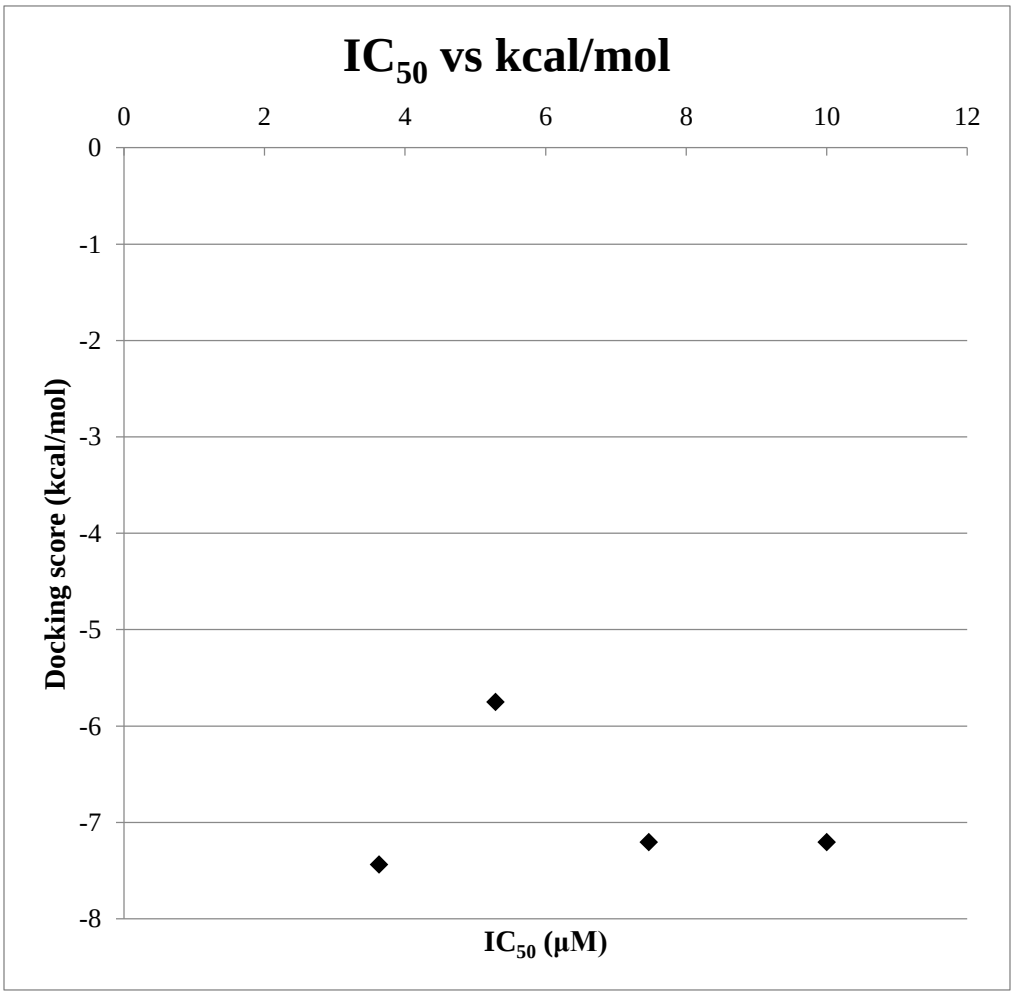

Figure 5.1. A scatter plot of the IC_{50} versus the docking scores for compounds **216** – **219**

Further biological testing included time-dependent studies[1] to determine whether or not each compound binds irreversibly to the GSK-3β. Using the reversible inhibitor, alsterpaullone **298**, as the standard reference, the enzyme was incubated several times with the synthesised compounds. The results shown in Figure 5.2 demonstrated that all of the synthesised compounds exhibited a gradual and sustained increase in inhibitory activity over time in comparison to

alsterpaullone **298**. This suggests that the compounds may indeed exhibit irreversible inhibitory activity on the GSK-3β, albeit at a high concentration.

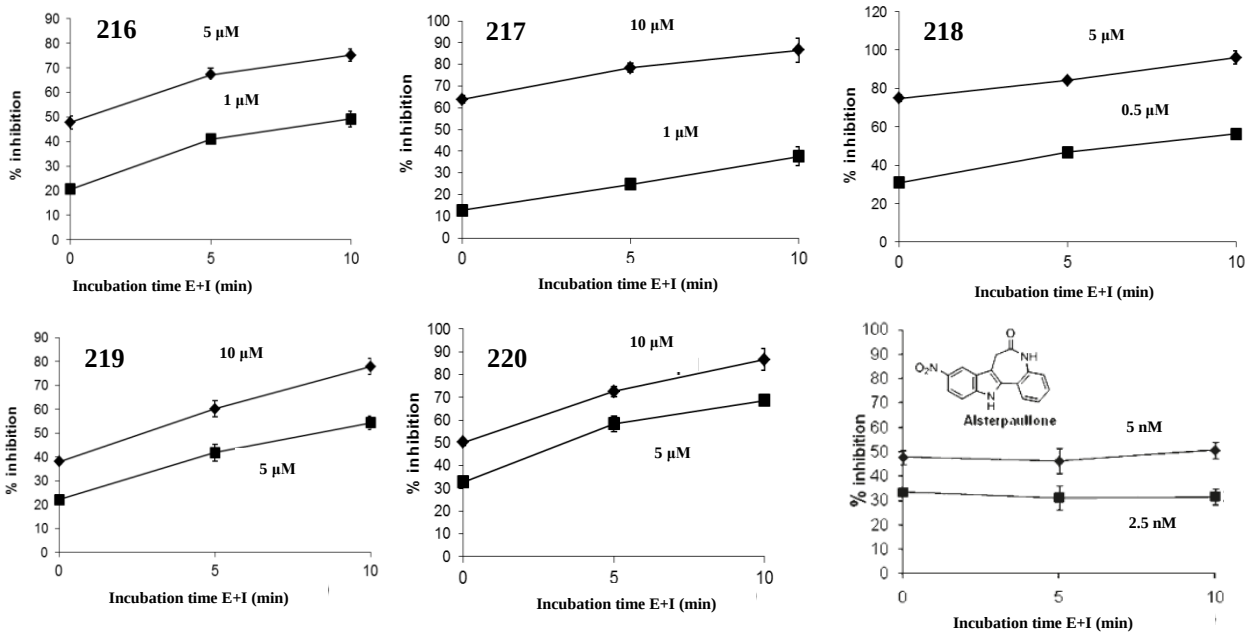

Figure 5.2. GSK-3β time-dependent studies on **216** – **220** and alsterpaullone **298**

These biological results provided bittersweet information regarding the activity of the compounds. All the compounds exhibited poor inhibitory activity but showed the ability to inhibit GSK-3β irreversibly at high concentration. Further studies on irreversible GSK-3β inhibition to obtain better insight were not carried out due to poor biological results and, as a result, further work on this moiety was aborted.

5.3 Biological results of the (*E*)-1-(3-aminopyrazin-2-yl)prop-2-en-1-one derivatives

Six compounds (**228** – **231**, **236** – **237**) that were synthesised as described in chapter 4 were sent for *in vitro* testing using the radiometric and luminescent assays[1] on the human recombinant GSK-3β enzyme. A full dose-response analysis was performed on all compounds to determine the concentration inhibiting 50% of enzyme activity (IC_{50}) and the values are shown in Table 5.2. Alsterpaullone **298**, a known reversible GSK-3β inhibitor,[2] was used as a reference standard.

Table 5.2. GSK-3β IC_{50} values of compounds **228** – **231**, **236** – **237** with the obtained docking scores (Chapter 2.3.3)

#	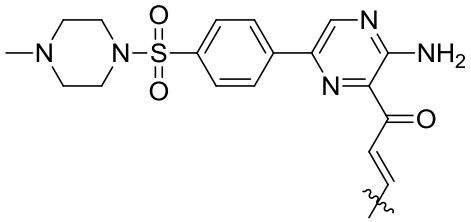	**IC_{50} (GSK-3β) (μM)**	**Docking score (kcal/mol)**
228	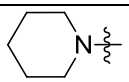	0.91 ± 0.05	-7.746
229	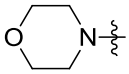	0.54 ± 0.04	-5.383
230	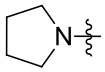	0.40 ± 0.04	-4.905
231	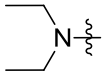	0.35 ± 0.03	-5.338
236	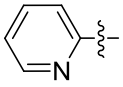	0.12 ± 0.02	-5.862
237	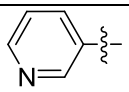	0.20 ± 0.03	-5.771
298	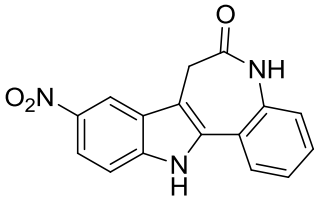	0.004	-

The results for the *in vitro* assay against the human recombinant GSK-3β were substantially better than the aforementioned series (section 5.2) and the IC_{50} values were in the submicromolar range. From the results it can be seen that the position of the carbonyl moiety plays an integral part in the potency of the compound. The size and type of amine group on the side chain does influence the potency of the inhibitor. Compounds **230** and **231,** with smaller amine groups in comparison to compounds **228** and **229,** exhibited stronger inhibitory activity on the GSK-3β.

The pyridine series, compounds **236** and **237**, delivered the most potent activities in this series. As discussed in Chapter 2, the potency could be ascribed to the interaction of the pyridine ring to Lys85 inside the ATP-binding site.

A scatter plot of IC_{50} versus the docking scores (Fig. 5.3) was constructed to compare the biological results with the docking scores (Chapter 2.3.3). However, no correlations could be made between the docking scores and the biological results.

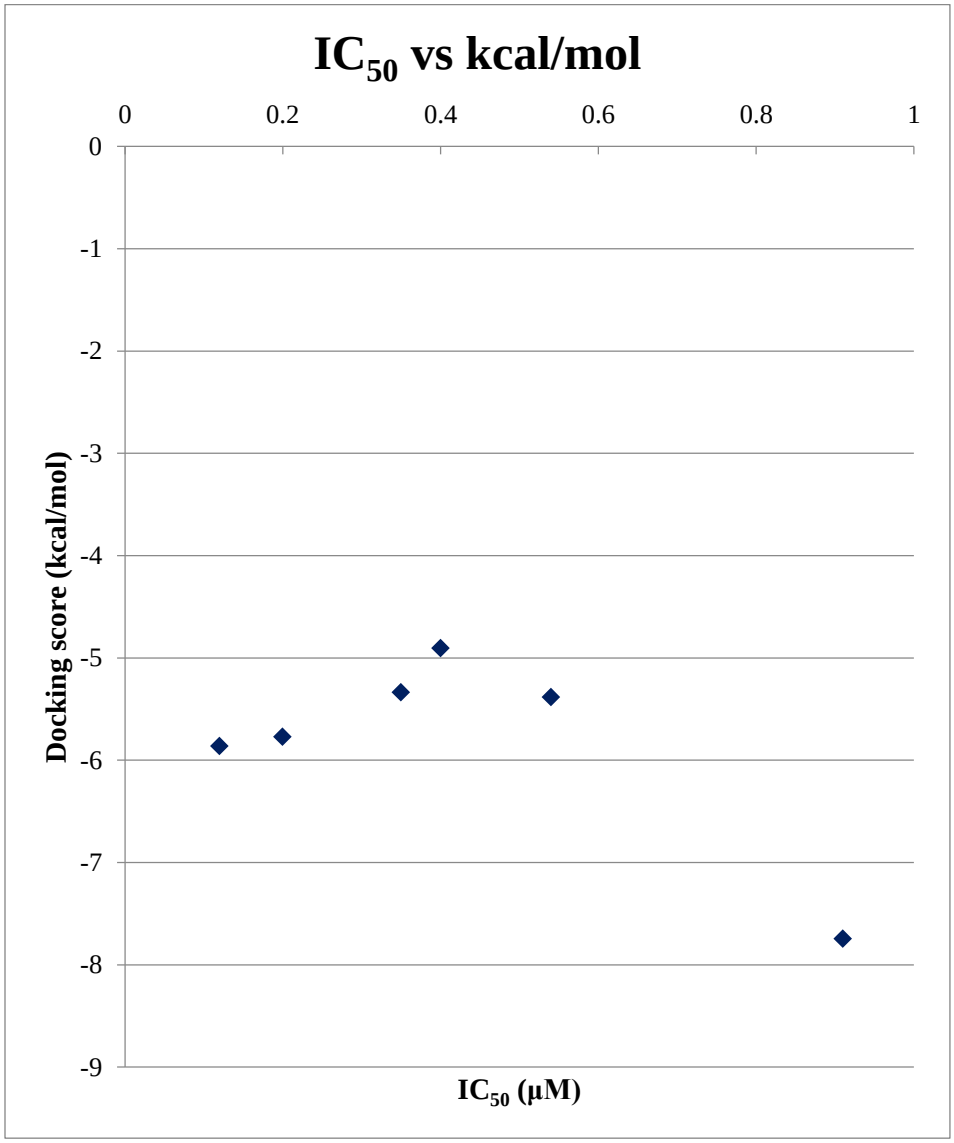

Figure 5.3. A scatter plot of the IC_{50} versus the docking scores for compounds **228** – **231** and **236** – **237**

The results of the time-dependent studies[1] on the GSK-3β for **227** – **230** are shown in Figure 5.2. Using the reversible inhibitor, alsterpaullone **298**, as the standard reference, the enzyme was incubated several times with the synthesised compounds. It should be noted that **236** and **237** were synthesised at the last stage of this project and the time-dependent studies will thus be carried out in the near future. The results demonstrated that at low concentrations, the synthesised compounds exhibited a gradual and sustained increase in inhibitory activity over time when compared to alsterpaullone **298**. This suggests that the compounds may exhibit irreversible inhibitory activity on the GSK-3β.

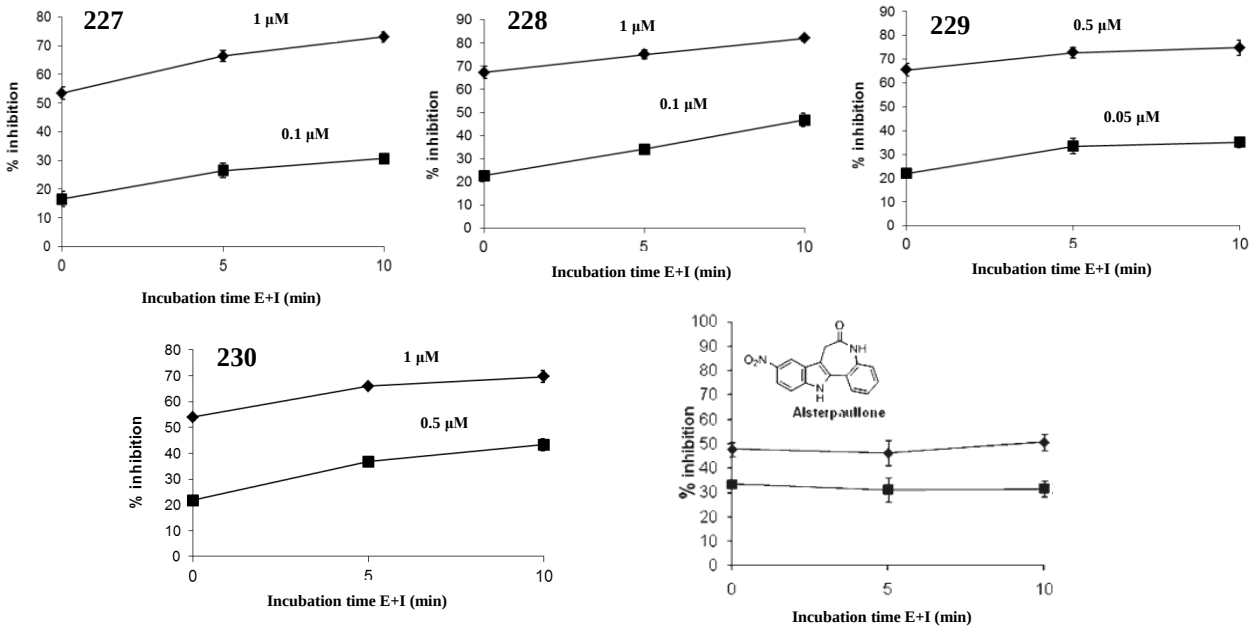

Figure 5.2 GSK-3β time-dependent studies on **227** – **230** and alsterpaullone **298**

These biological results are in good agreement with the docking studies carried out (Chapter 2, section 2.3.3). Compounds **236** and **237**, with the most potent IC_{50} values of 0.12 and 0.20 µM respectively, obtained good docking scores (-5.862 and -5.771 kcal/mol respectively). However, compounds **229** and **231**, with IC_{50} values of 0.54 and 0.35 µM, obtained similar docking scores (-5.383 and -5.338 kcal/mol respectively), which suggests that the pyridine ring in **236** and **237** is involved in an additional role such as pi-sigma interactions with the amino acid residue, Lys85, which could increase the potency of the compound. Overall, these biological results suggest that this moiety has the potential to inhibit GSK-3β irreversibly at nanomolar

concentration. Further work on confirming the covalent nature of the interaction of the inhibitors will be discussed as future work in chapter 7. In addition, these results warrant the development of a 2nd generation of irreversible GSK-3β inhibitors and will be discussed in chapter 7.

5.4 References

1. D. I. Perez, V. Palomo, C. Pérez, C. Gil, P. D. Dans, F. J. Luque, S. Conde and A. Martínez, *Journal of Medicinal Chemistry*, 2011, 54, 4042-4056.
2. M. Leost, C. Schultz, A. Link, Y.-Z. Wu, J. Biernat, E.-M. Mandelkow, J. A. Bibb, G. L. Snyder, P. Greengard, D. W. Zaharevitz, R. Gussio, A. M. Senderowicz, E. A. Sausville, C. Kunick and L. Meijer, *European Journal of Biochemistry*, 2000, 267, 5983-5994.

Chapter 6

Attempted synthesis of terminal electrophilic “warheads”

6.1 Overview

This section describes the last few months of this PhD project that were used to carry out a variety of synthetic procedures, in an attempt to incorporate a terminal electrophilic “warhead”. The concept of this terminal “warhead” was to determine whether improved biological results could be obtained, in comparison to the two previous series that consisted of an internal “warhead”.

6.2 Retrosynthetic analysis of the library

The retrosynthetic approach for the synthesis of terminal electrophilic “warheads” followed similar routes of the internal “warheads” as discussed in chapter three and four. For the synthesis of a terminal electrophilic “warhead” (Fig. 6.1), it was envisaged that **334** could be formed by using the already established Suzuki-Miyaura procedure between boronic acid **243** and **335**. In addition, terminal “warhead” derivatives **335** could be obtained from the already synthesised Weinreb amide **311** (see section 4.3.3).

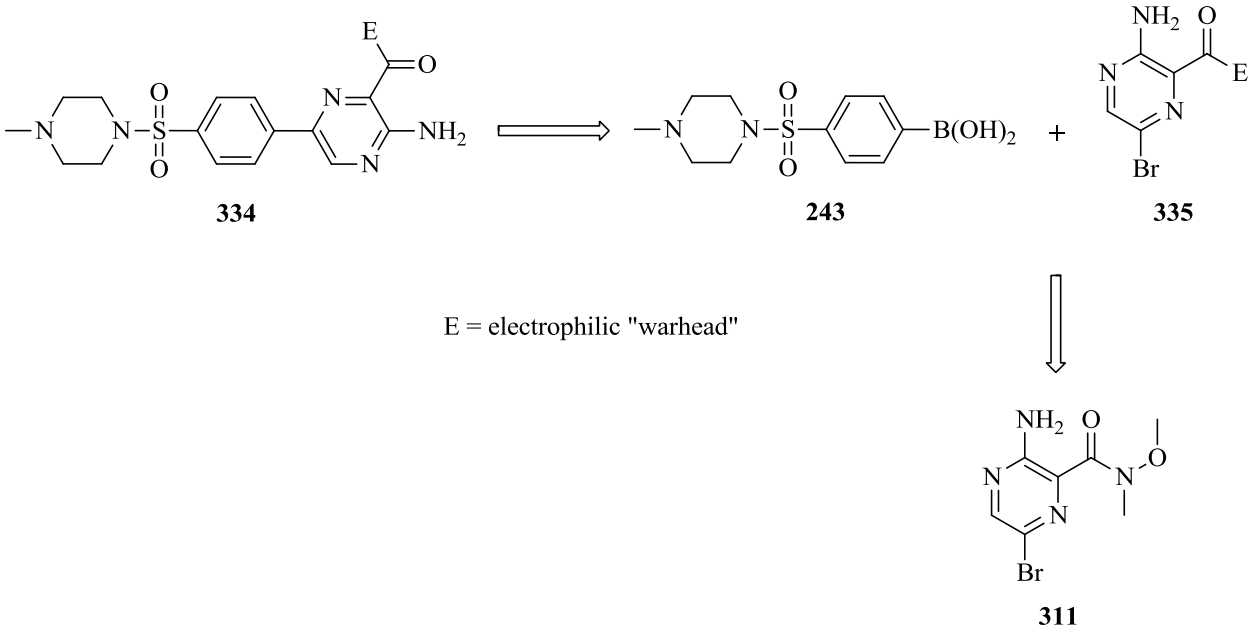

Figure 6.1. Retrosynthetic analysis of the targeted library.

6.3 Synthesis of the terminal Michael acceptor precursors

As shown in Scheme 6.1, the synthesis of the Michael acceptor **336** followed the same procedure mentioned in Chapter 4.2.3 for the alkyne **301**. As such, Weinreb amide **311** was reacted with three equivalents of vinylmagnesium bromide and after purification by column chromatography the Michael acceptor **332** was isolated as yellow solid in an acceptable 62% yield.

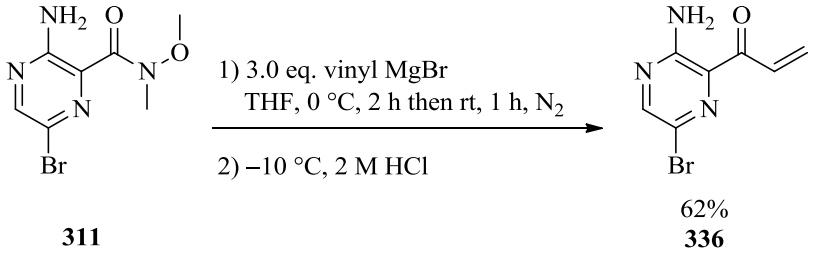

Scheme 6.1. Synthesis of Michael acceptor **336**

As shown, in Figure 6.2, the presence of the vinyl functional group could readily be identified in the ^{1}H NMR spectrum. The two doublet of doublets at 6.54 and 5.90 ppm could be assigned to the terminal protons of C^{12} and the doublet of doublets at 7.85 ppm could be assigned to the

remaining vinyl proton of C^{11}. Finally, the singlet at 8.28 ppm was for the heteroaromatic proton at C^2.

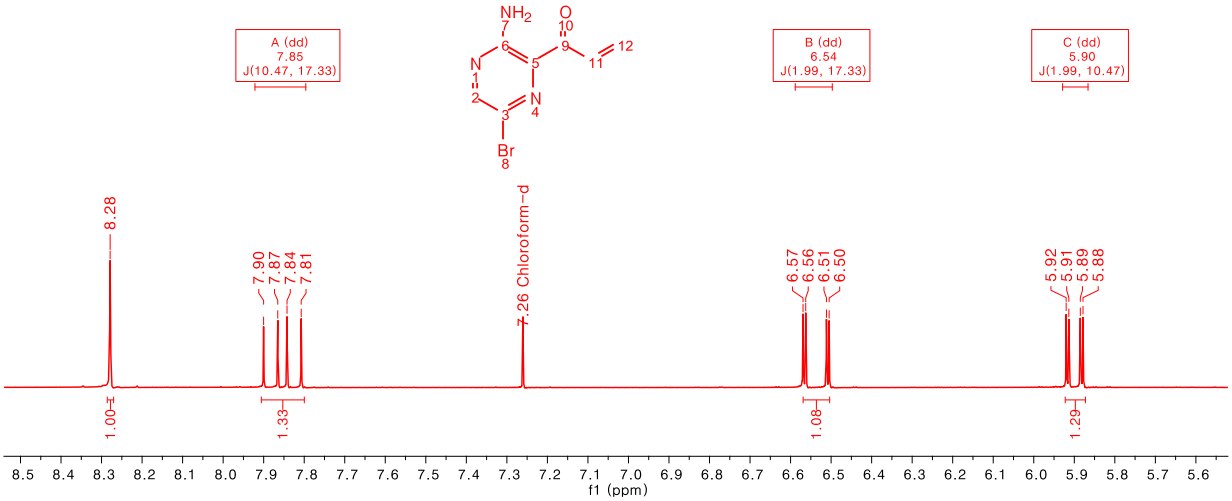

Figure 6.2. ^{1}H NMR spectrum of **336**

With the two different Michael acceptors, **297** (Chapter 4.2.3) and **336**, in hand (Fig. 6.3), the next step was the Suzuki-Miyaura reaction with boronic acid **243** (Fig. 6.3). The next section will discuss the attempted synthesis of these final compounds.

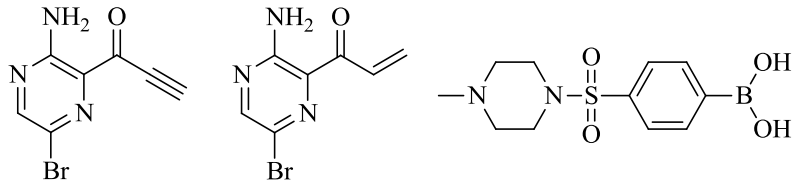

297 **336** **243**

Figure 6.3. Synthesized Michael acceptors **301**, **336** and the boronic acid **243**

6.4 Attempted synthesis of terminal Michael acceptor compounds

Michael acceptor **297** was the first terminal "warhead" derivative to undergo a Suzuki-Miyaura reaction with boronic acid **243** and the procedure is shown in Scheme 6.2. After stirring overnight, full consumption of the starting **297** was observed and one product spot was seen on the TLC plate. A yellow solid was isolated after column chromatography purification. Unfortunately, ^{1}H NMR spectroscopic analysis indicated that a mixture of products had formed. The additional peaks in the aromatic and alkane regions of this spectrum suggested that the

Suzuki-Miyaura coupling appeared to be successful, but that, in addition, the ethanol in the solution had reacted with the Michael acceptor.

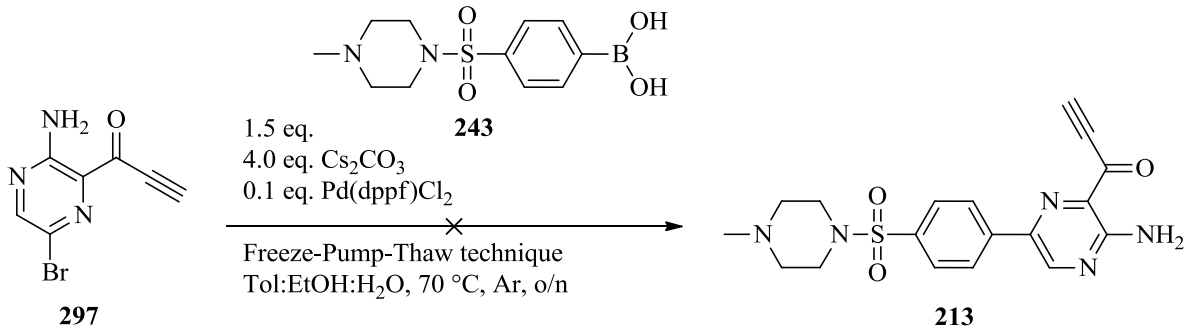

Scheme 6.2. Attempted Suzuki reaction with **297**

The mass spectrometric data gave further support to the idea that ethanol had reacted with **213**. As shown in Table 6.1, three mass to charge (*m/z*) peaks were observed in the high resolution mass spectrometry spectrum. Two of the three peaks suggested the possible formation of the mono- and di-alkylated products **337** and **338**. The structure of the molecule accounting for the third *m/z* peak, 464.1961 amu, could not be identified. In addition, the *m/z* peak for **213** was not detected.

Table 6.1. The structures of the molecules related to the *m/z* values.

Molecule	Calculated mass (M+H) (g/mol)	*m/z* (M+H) (amu)
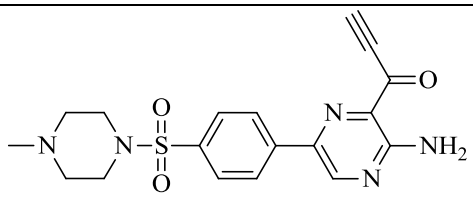 **213**	385.4402	not detected
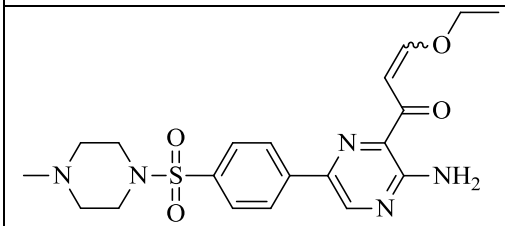 **337**	432.1705	432.1704

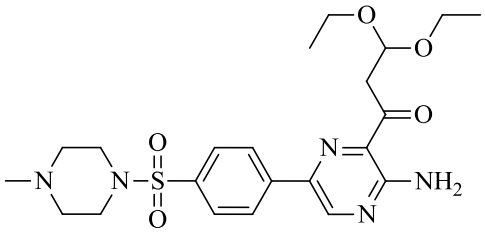 **338**	478.2124	478.2130
unknown	–	464.1961

The reaction was repeated with a solvent system that comprised toluene, *t*-BuOH and water. In comparison to ethanol, *t*-BuOH is a more sterically hindered nucleophilic solvent and should therefore be less reactive. As with the first attempt, the starting material, **297**, was fully consumed after stirring overnight. However, analysis of the ^{1}H NMR spectroscopic data again showed that a mixture of products had formed, which could be the deboronated and/or homocoupled compounds. Replacing *t*-BuOH with dimethoxyethane, a non-nucleophilic solvent, did not improve the results either.

An alternative route, which reversed the synthetic sequence, was explored. This was to do the Suzuki-Miyaura coupling before the addition of the Michael acceptor. This way, the reaction of the Michael acceptor with the ethanol in the Suzuki-Miyaura reaction could be avoided. As shown in Scheme 5.3, Weinreb amide **311** readily underwent a Suzuki-Miyaura reaction with boronic acid **243** to form the corresponding phenylaminopyrazine **337** in 75% yield. Two singlets at 3.87 and 3.52 ppm, both integrating for three protons in the ^{1}H NMR spectrum, confirmed the presence of the Weinreb amide on the new structure **337**. In addition, the presence of five aromatic protons in total confirmed the construction of the biaryl bond.

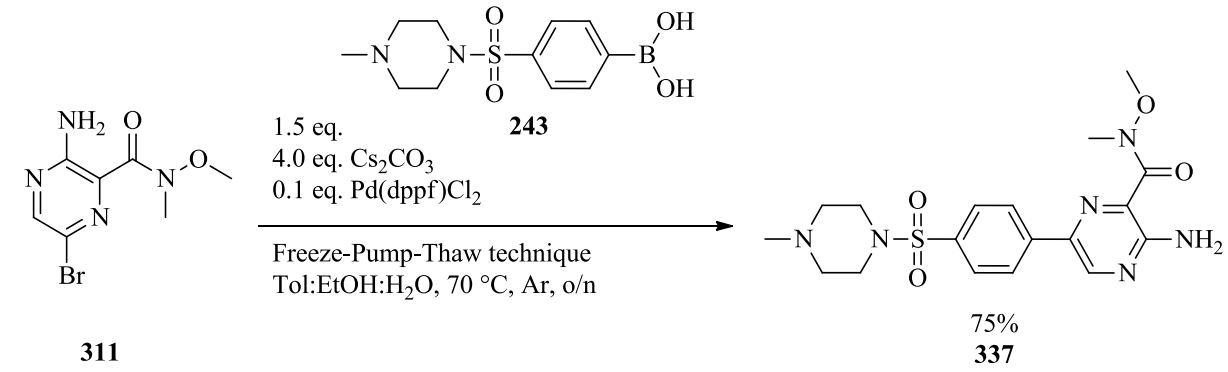

Scheme 6.3. Suzuki reaction of Weinreb amide **311**

As shown in Scheme 6.4, the next step involved the Grignard reaction with ethynyl magnesium bromide utilising a procedure similar to the one that was reported earlier (Section 4.2.3). Unfortunately, after this reaction, only trace amounts of products were isolated with full conversion of the starting material. It was considered that during the quenching of the reaction, the acid labile methylpiperazine could have been protonated to form an amine salt. Therefore, the reaction was repeated and quenched with saturated NH_4Cl solution, but similar disappointing results were obtained.

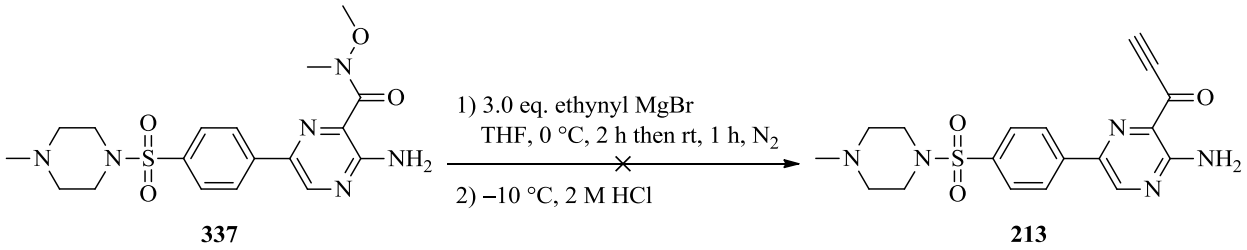

Scheme 6.4. Attempted Grignard reaction with **335**

In the next attempt, a different Grignard intermediate was used to react with **337** (Scheme 6.5).[1] Trimethylsilyl acetylene **338** was first lithiated with *n*-BuLi in THF before a solution of **337** in THF was added. The resulting deep orange solution was then allowed to warm to room temperature over two hours before the reaction was quenched with saturated NH_4Cl solution. The solution was diluted with EtOAc and washed with water. On the TLC plate, the determination of whether the reaction has gone to completion was complicated by the fact that

the product had a similar R_f value to the starting material **337**. As the mixture could not be separated, the crude mixture was carried to the next step.

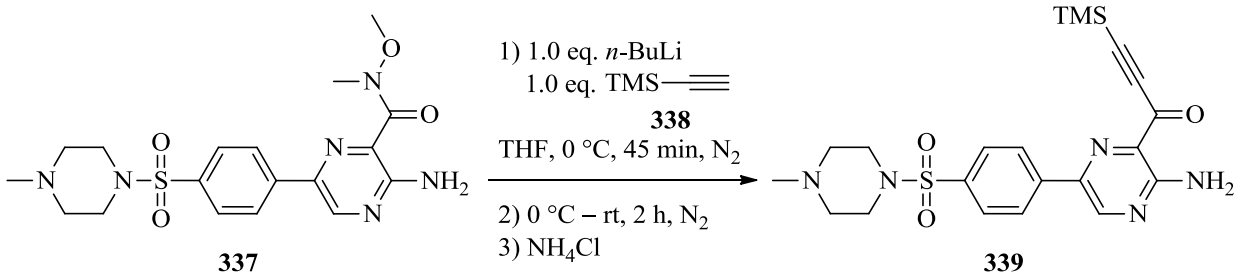

Scheme 6.5. Grignard reaction with trimethylsilyl acetylene **338**

The next step required the deprotection of the alkyne-TMS group and this procedure is shown in Scheme 6.5.[2] The crude mixture from the previous step was dissolved in THF and subsequently cooled to 0 °C. Tetra-*n*-butylammonium fluoride (TBAF·$3H_2O$) was then added portion-wise and the resultant brown solution was stirred for one hour at room temperature. It should be noted that no significant changes were observed on the TLC plate and the reaction was deemed a failure.

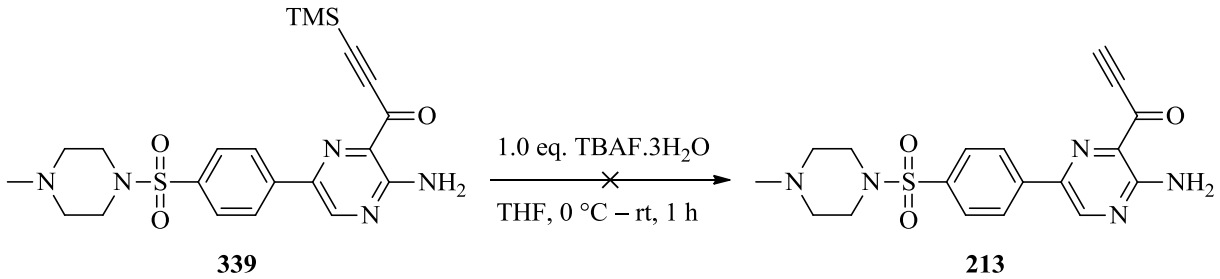

Scheme 6.6. Attempted deprotection of **337** with TBAF·$3H_2O$

After this failed attempt, it was decided to abandon this synthetic route of coupling the terminal Michael acceptors onto the aminopyrazine core.

6.5 Attempted synthesis of halomethyl ketone compounds

The synthesis of a different terminal electrophilic "warhead", the halomethylketone, was pursued after the aforementioned attempts failed to produce compounds with a terminal Michael acceptor. The synthesis of the halomethylketone compounds will be discussed next.

Compound **298** (see chapter 4, Scheme 4.17) readily underwent a Suzuki-Miyaura reaction with boronic acid **243** (Scheme 6.7) and the product **340** was isolated as yellow solid in 71% yield. In terms of NMR spectroscopic analysis, the presence of the methyl ketone was observed as a proton singlet at 2.80 ppm and a carbonyl peak at 202.7 ppm.

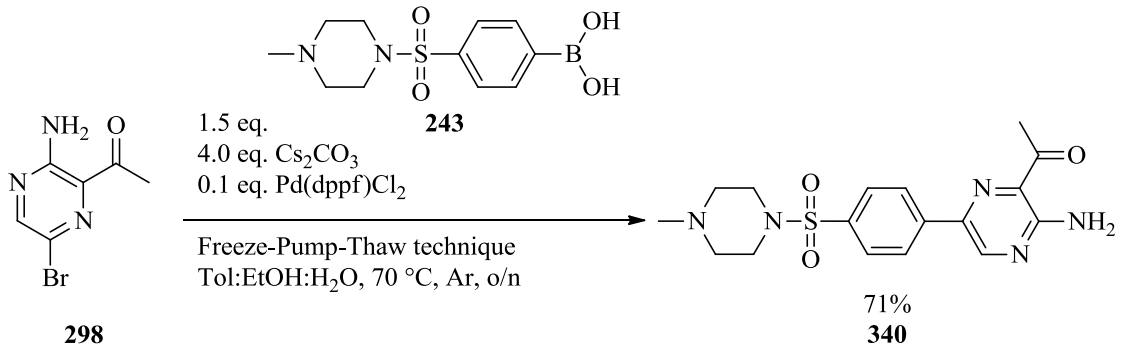

Scheme 6.7. Suzuki reaction of methyl ketone **298** with **243**

The next step involved the bromination of the methyl ketone **340**. Using the procedure of Kharaman *et al*.,[3] methyl ketone **340** was thus brominated with molecular bromine in chloroform (Scheme 6.8). According to the TLC plate, three product spots had formed, which suggested the formation of mono-, di- and tribrominated products in an unknown ratio and could not be separated. Unreacted starting material was also observed on the TLC plate. It has been documented that the bromination of a methyl ketone with bromine can lead to the formation of polybrominated products, as was experienced in our synthetic attempts.[4, 5]

To eliminate the formation of polybrominated products, it was proposed that the reaction could be carried out under acidic conditions.[6-9] The reaction in Scheme 6.8 was thus repeated in neat acetic acid and the solution was stirred overnight. This time, only one product spot and unreacted starting methyl ketone **340** were observed on the TLC plate. However, after purification by

column chromatography, the desired product **214** was only isolated in trace amounts. The reaction proved to be sluggish and further attempts with molecular bromine as the brominating agent were abandoned. An alternative synthetic route was pursued and will be discussed next.

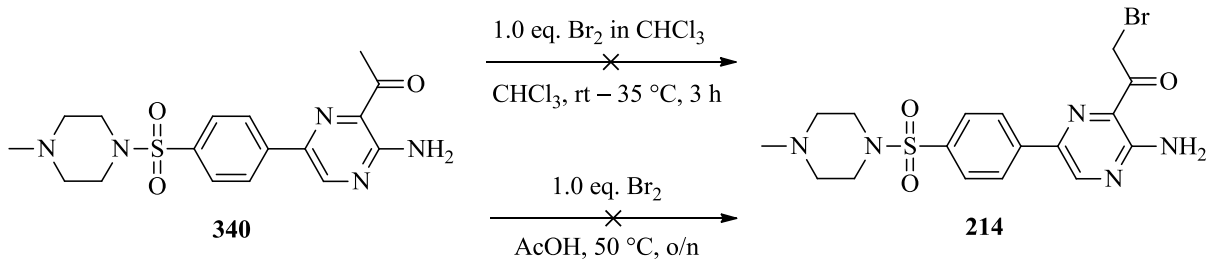

Scheme 6.8. Attempted bromination of methyl ketone **340**

Copper bromide, a known brominating agent,[10, 11] in chloroform-ethyl acetate is known to react with methyl ketones to give selectively the corresponding α-bromo ketones.[12] Following the procedure of Boominathan *et al.*,[13] a solution of methyl ketone **340**, copper bromide, chloroform and ethyl acetate (1:1 ratio) was heated under reflux overnight (Scheme 6.9). Unfortunately, only the starting **340** was observed on the TLC plate after stirring overnight.

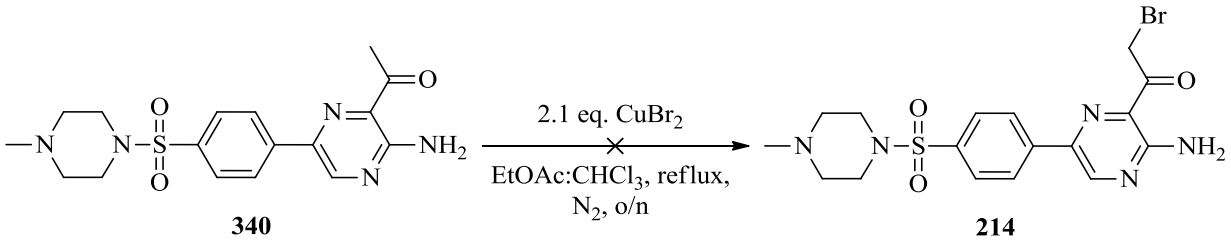

Scheme 6.9. Attempted bromination of **340** with copper bromide

Trimethylphenylammonium tribromide (PTAB) is another brominating agent that selectively forms α-bromo ketones.[14-16] The procedure of Perner *et al.*[17] was slightly adapted and is shown in Scheme 6.10. The reaction was carried out at 30 °C instead of at room temperature. Methyl ketone **340** was dissolved in THF and PTAB was added in several portions. The dark orange solution was stirred for three days, but according to the TLC plate, only starting materials were present.

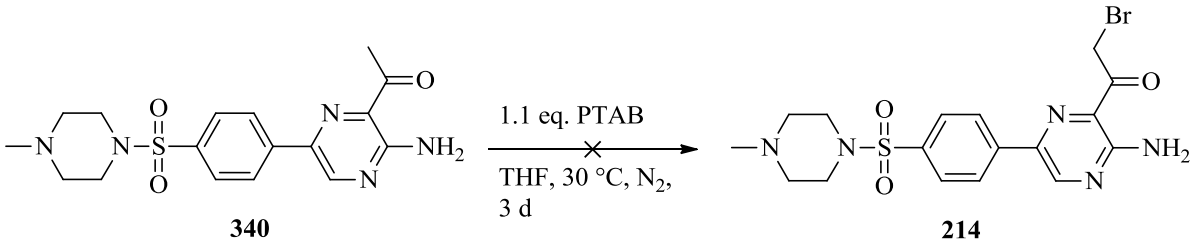

Scheme 6.10. Attempted bromination of **340** with PTAB

A different brominating source was used for the last attempt. Several papers have reported the successful mono-bromination of acetophenone using NBS and catalytic amount of *para*-toluenesulfonic acid (PTSA).[18-22] The procedures are all similar, varying only in the solvent and the temperature at which the reactions were carried out. The procedure for the mono-bromination of methyl ketone **340** with NBS and catalytic amount of PTSA is shown in Scheme 6.11. Methyl ketone **340** and PTSA was thus dissolved in chloroform and NBS was added in several portions. The reaction was first carried out at room temperature to minimise the risk of over-bromination and the solution was stirred overnight. Unfortunately, three product spots and unreacted starting material were observed on the TLC plate, which suggested that over-bromination has once again occurred. In addition, the three products could not be separated by using column chromatography

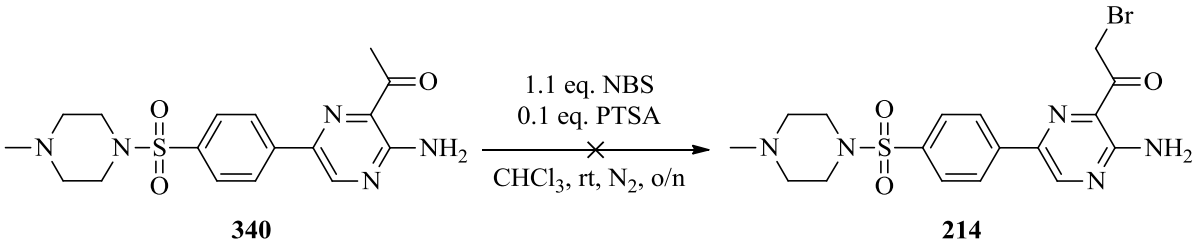

Scheme 6.11. Attempted bromination of **340** with NBS and PTSA

Due to the failed attempts to mono-brominate the methyl ketone **340**, it was decided to abandon the synthesis of halomethyl ketone derivatives. To obtain potential irreversible inhibitors with these structural features, a new synthetic route would have to be implemented that would overcome the aforementioned issues. This will be discussed in the future work section of chapter 7.

6.6 References

1. R. V. Somu, H. Boshoff, C. Qiao, E. M. Bennett, C. E. Barry and C. C. Aldrich, *Journal of Medicinal Chemistry*, 2006, **49**, 31-34.
2. P. A. Donets, K. Van Hecke, L. Van Meervelt and E. V. Van der Eycken, *Organic Letters*, 2009, **11**, 3618-3621.
3. D. C. Kahraman, G. Hanquet, L. Jeanmart, S. Lanners, P. Sramel, A. Bohac and R. Cetin-Atalay, *MedChemComm*, 2017, **8**, 81-87.
4. H.-J. Ha, S.-K. Lee, Y.-J. Ha and J.-W. Park, *Synthetic Communications*, 1994, **24**, 2557-2562.
5. C. Rappe, *Acta Chemica Scandinavica*, 1966, **20**, 376-384.
6. A.-M. Liberatore, J. Schulz, C. Favre-Guilmard, J. Pommier, J. Lannoy, E. Pawlowski, M.-A. Barthelemy, M. Huchet, M. Auguet, P.-E. Chabrier and D. Bigg, *Bioorganic & Medicinal Chemistry Letters*, 2007, **17**, 1746-1749.
7. V. P. Boyarskii, T. E. Zhesko, E. V. Larionov and V. A. Polukeev, *Russian Journal of Applied Chemistry*, 2007, **80**, 571-575.
8. S. Ling, Z. Xin, Z. Qing, L. Jian-Bing, J. Zhong and F. Jian-Xin, *Synthetic Communications*, 2007, **37**, 199-207.
9. M. Devocelle, A. Mortreux, F. Agbossou and J.-R. Dormoy, *Tetrahedron Letters*, 1999, **40**, 4551-4554.
10. E. M. Kosower, W. J. Cole, G. S. Wu, D. E. Cardy and G. Meisters, *The Journal of Organic Chemistry*, 1963, **28**, 630-633.
11. C. E. Castro, E. J. Gaughan and D. C. Owsley, *The Journal of Organic Chemistry*, 1965, **30**, 587-592.
12. L. C. King and G. K. Ostrum, *The Journal of Organic Chemistry*, 1964, **29**, 3459-3461.
13. S. S. K. Boominathan, W.-P. Hu, G. C. Senadi and J.-J. Wang, *Advanced Synthesis & Catalysis*, 2013, **355**, 3570-3574.
14. Y. Usui, F. Uehara, S. Hiki, K. Watanabe, H. Tanaka, A. Shouda, S. Yokoshima, K. Aritomo, T. Adachi, K. Fukunaga, S. Sunada, M. Nabeno, K.-I. Saito, J.-i. Eguchi, K. Yamagami, S. Asano, S. Tanaka, S. Yuki, N. Yoshii, M. Fujimura and T. Horikawa, *Bioorganic & Medicinal Chemistry Letters*, 2017, **27**, 3726-3732.

15. A. Nitta, H. Fujii, S. Sakami, M. Satoh, J. Nakaki, S. Satoh, H. Kumagai and H. Kawai, *Bioorganic & Medicinal Chemistry Letters*, 2012, **22**, 7036-7040.
16. A. Boulangé, J. Parraga, A. Galán, N. Cabedo, S. Leleu, M. J. Sanz, D. Cortes and X. Franck, *Bioorganic & Medicinal Chemistry*, 2015, **23**, 3618-3628.
17. R. J. Perner, J. R. Koenig, S. DiDomenico, A. Gomtsyan, R. G. Schmidt, C.-H. Lee, M. C. Hsu, H. A. McDonald, D. M. Gauvin, S. Joshi, T. M. Turner, R. M. Reilly, P. R. Kym and M. E. Kort, *Bioorganic & Medicinal Chemistry*, 2010, **18**, 4821-4829.
18. S. Sharma, A. K. Pandey, P. K. Shukla and A. K. Saxena, *Bioorganic & Medicinal Chemistry Letters*, 2011, **21**, 6476-6481.
19. I. Pravst, M. Zupan and S. Stavber, *Tetrahedron Letters*, 2006, **47**, 4707-4710.
20. C. Correa, M. d. C. Cruz, F. Jiménez, L. G. Zepeda and J. Tamariz, *Australian Journal of Chemistry*, 2008, **61**, 991-999.
21. U. Rashid, W. Ahmad, S. F. Hassan, N. A. Qureshi, B. Niaz, B. Muhammad, S. Imdad and M. Sajid, *Bioorganic & Medicinal Chemistry Letters*, 2016, **26**, 5749-5753.
22. V. V. Angeles-Dunham, D. M. Nickerson, D. M. Ray and A. E. Mattson, *Angewandte Chemie International Edition*, 2014, **53**, 14538-14541.

Chapter 7

Conclusions and future work

7.1 Conclusions

The initial aim of this project was to synthesise three libraries of compounds with electrophilic "warheads" such as Michael acceptors and halomethyl ketones that could be tested on GSK-3β to determine their biological activity and also whether they bind irreversibly to the enzyme. This is also the first attempt to synthesise irreversible inhibitors attached to the aminopyrazine class of compounds. Two libraries that consisted of a total of 11 compounds with an internal "warhead" were successfully synthesised. The third library, which consist of a terminal "warhead" could not be synthesised due to various synthetic complications. In addition, our research group also develop antimalarial inhibitors, thus the synthesised compounds were also tested on a chloroquine sensitive strain of *P. falciparum*, NK54, to determine their antiplasmodial activity. As one of the molecules showed surprising good efficacy, a small number of fragments of this molecule were made to see if the pharmacophore could be identified.

The key Suzuki-Miyaura chemistry was thoroughly explored to find the optimal conditions for the synthesis of the scaffold, 5-{4-[(4-methylpiperazin-1-yl)sulfonyl]phenyl}pyrazin-2-amine **251**. The conditions were determined to be 1.5 equivalents of boronic acid **243**, 0.1 equivalents of Pd(dppf)Cl_2 and 4.0 equivalents of Cs_2CO_3 in a solvent system of toluene:ethanol:water (4:1:0.05 ratio). In addition, the reaction mixture need to be deoxygenated thoroughly using the freeze-pump-thaw technique before the catalyst was added.

Five (*E*)-3-(3-aminopyrazin-2-yl)acrylaldehyde derivatives were successfully synthesised and analytically characterised. The compounds were obtained in good yields, ranging from 69 – 78%. *m*-Aminopyridine **221** was only isolated in trace amounts and further attempts to improve the yield were not carried out due to insufficient amounts of starting material. All five of the compounds were sent for biological testing on the GSK-3β and were found to be poor (3.63 – >10 μM). The most potent compound was pyrrolidine **218** with an IC_{50} value of 3.63 μM. The

time-dependent studies on the GSK-3β suggested that all five compounds possibly might exhibit irreversible inhibitory activity at high concentrations (≥ 1 μM).

Six (*E*)-1-(3-aminopyrazin-2-yl)prop-2-en-1-one derivatives were also successfully synthesised and analytically characterised. Imidazole derivative **239** could not be isolated as attempts to obtain the product in pure form proved futile. Overall, the compounds were isolated in moderate to good yields, ranging from 40 – 86%. All six of the compounds were sent for biological testing on the GSK-3β and were found to be better inhibitors than the first five compounds tested. All compounds exhibited IC_{50} values of under 1 μM, with *o*-pyridine **236** being the most active (IC_{50} value of 0.12 μM). The time-dependent studies on the GSK-3β suggested that four of the six compounds may exhibit irreversible inhibitory activity at low concentrations (≤ 1 μM). The GSK-3β time-dependent studies of pyridines **236** and **237** will be carried out in the near future by one of our collaborators.

7.2 Future work

7.2.1 Future modification on the synthesised compounds

This project represents the first approach of electrophilic "warheads" attached to the aminopyrazine core and therefore has the potential to be further expanded to include a second generation with more focused properties.

The results of the (*E*)-1-(3-aminopyrazin-2-yl)prop-2-en-1-one derivatives (chapter 4) suggested that pyridine rings may play a critical role in achieving minimum IC_{50} concentration. By looking at the work of Berg *et al.*[1] (Fig. 7.1, **208** GSK-3β K_i = 0.22 nM), modifications on the pyridine ring may offer an option to improve the potency of the compounds. As shown in Figure 7.1, a moiety that consists of a pyrrolidine (**341**), diethylamine (**342**), dimethylamine (**343**) or a methoxy group (**344**) could be inserted onto the pyridine ring. These modifications may allow the compounds to fit better inside the GSK-3β ATP-binding site and they have improved interactions with the amino acid residues. However, these suggestions have to be modelled first inside the GSK-3β ATP-binding site.

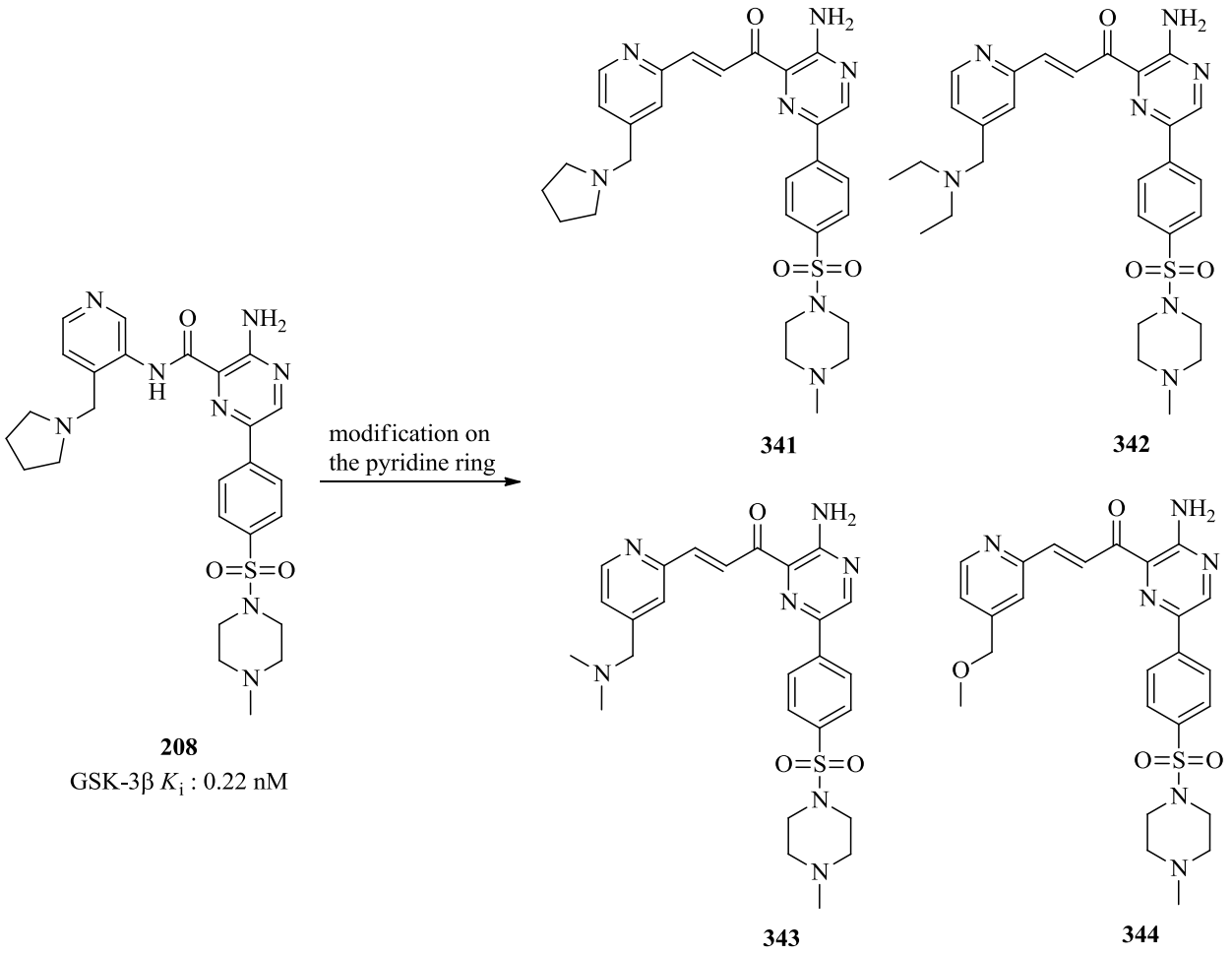

Figure 7.1. Possible future modifications on the pyridine ring to improve the potency of the GSK-3β inhibitors

Another option to improve the potency would be to reposition the pyridine ring (Fig. 7.2, **345**) or install a different heteroaromatic moiety (Fig. 7.2), such as a triazole (**346**), furan (**347**) or pyrrole (**348**) ring system. This would offer insight into whether the rearrangement or the type of heteroaromatic ring plays a role in the inhibitory activity of the GSK-3β. Again, these suggestions have to be modelled first inside the GSK-3β ATP-binding site before the synthesis of the modified molecules could be carried out.

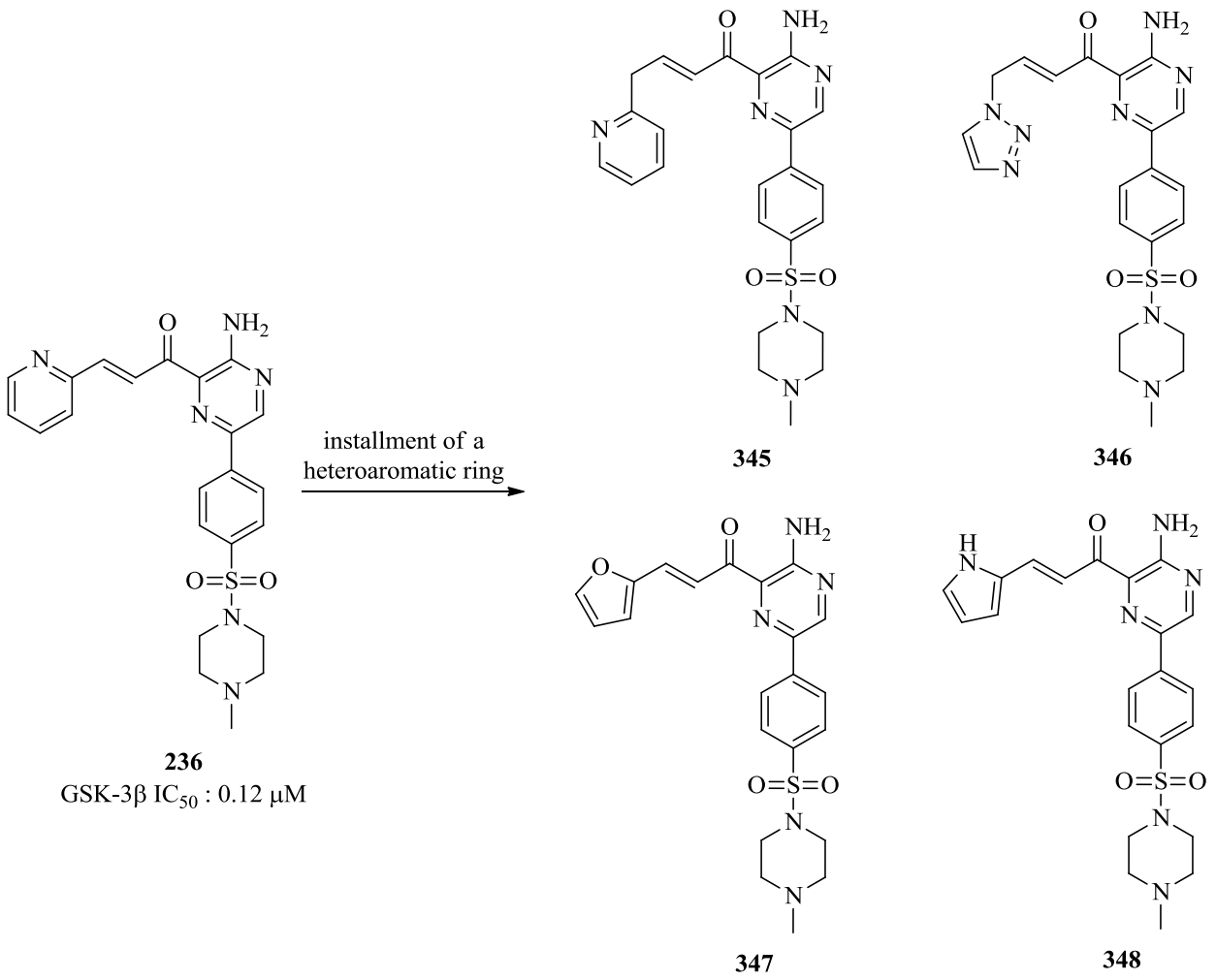

Figure 7.2. Installment of a heteroaromatic ring to improve the potency of the GSK-3β inhibitors

Lastly, the covalent binding of the compounds to GSK-3β could be confirmed biophysically by MALDI-TOF analyses.[2] Each compound could be combined with GSK-3β, and allowed to interact with the enzyme for a specific amount of time. The excess unreacted enzyme could be washed off and mass analysis of the bound inhibitor-enzyme complex could reveal whether one peak is observed, which would suggest the combined mass of the compound and GSK-3β. This could possibly indicate that the compound had bound irreversibly to the enzyme. The presence of two peaks would indicate that the compound had not bound covalently to GSK-3β, which then suggests that the compound is a reversible inhibitor.

Another experiment that could be carried out is the synthesis of a saturated derivative of compound **231** (Fig. 7.3). The double bond of the Michael acceptor could be reduced to

deactivate the "warhead" and this new compound, **340**, could be subjected to time-dependent studies on the GSK-3β. The results could then prove whether compound **340** exhibit a gradual and sustained increase in inhibitory activity over time, which would suggest a different mode of inhibitory action.

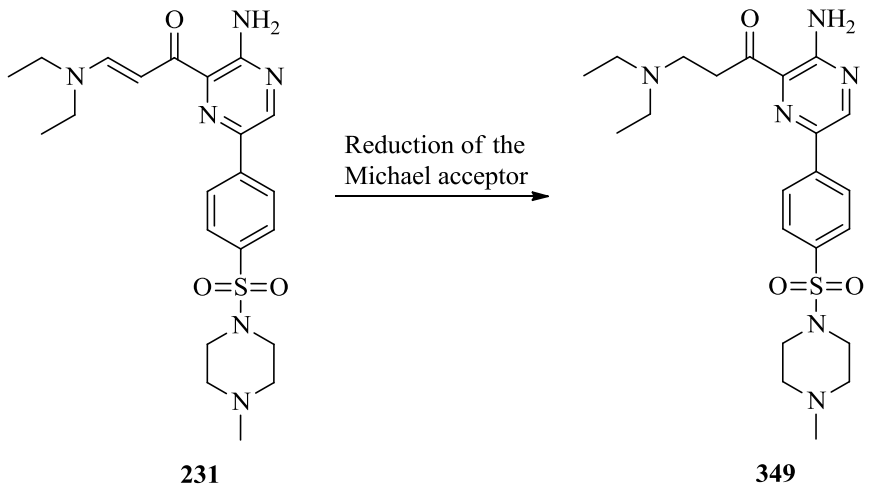

231 **349**

Figure 7.3. Reduction of the Michael acceptor to deactivate the "warhead"

7.2.2 Future synthetic attempts to synthesise GSK-3β halomethyl ketone inhibitors

The synthesis of the terminal "warheads" proved to be a stumbling block as described in chapter 6. As shown in Scheme 7.1, alternative brominating sources could be used to mono-brominate methyl ketone **340**. One example is the use of bromotrimethylsilane (TMSBr) and potassium nitrate (KNO_3) in a non-nucleophilic solvent such as DCM to afford the corresponding product **214**.[3] In this reaction, nitryl bromide (NO_2Br) is generated *in situ* from TMSBr and KNO_3, which then reacts with the α-methylketone to give the corresponding α-brominated product.

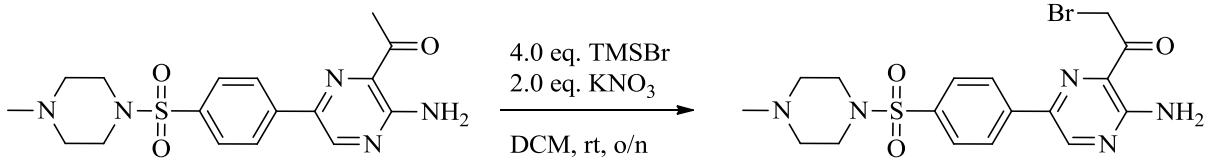

340 **214**

Scheme 7.1. Monobromination of methyl ketone **340** with TMSBr and KNO_3

Another option to selectively synthesise the monobrominated compound would be to form enamine **350**, which could be then be selectively mono-brominated, followed by hydrolysis of the intermediate brominated immonium salt to give the corresponding product **214** (Scheme 7.2).[4] The formation of the salt would prevent the molecule from entering another round of bromination to form the undesired dibrominated product.

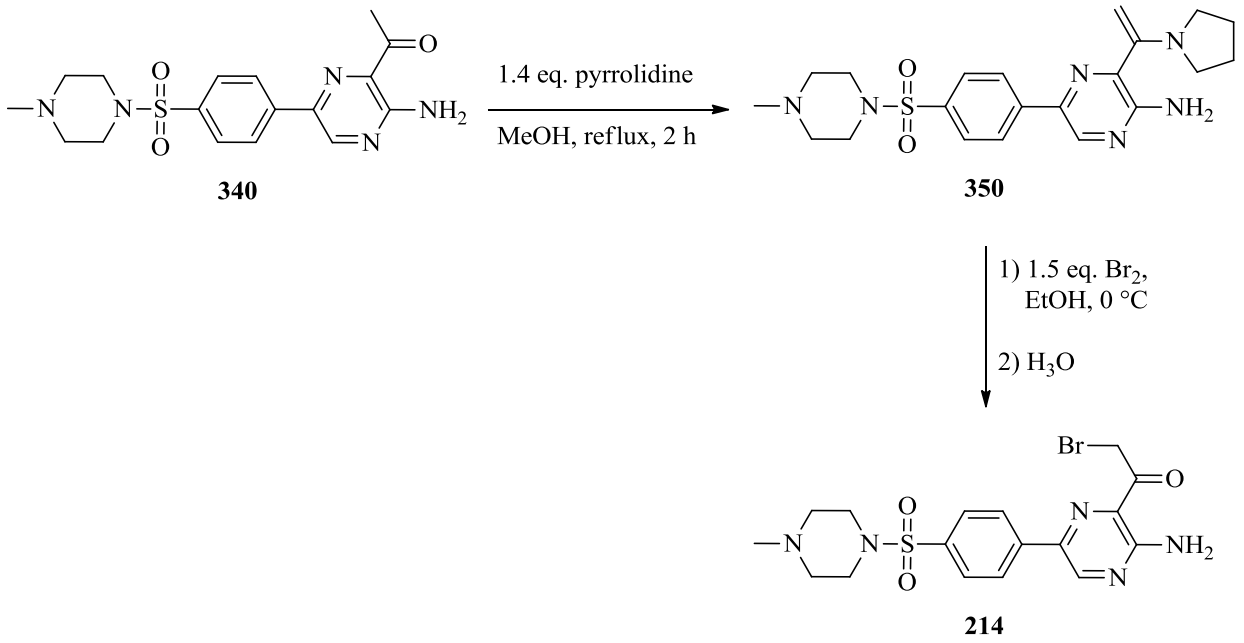

340 **350** **214**

Scheme 7.2. Suggested method to synthesise α-brominated **214** via the enamine

7.3 References

1. S. Berg, M. Bergh, S. Hellberg, K. Högdin, Y. Lo-Alfredsson, P. Söderman, S. von Berg, T. Weigelt, M. Ormö, Y. Xue, J. Tucker, J. Neelissen, E. Jerning, Y. Nilsson and R. Bhat, *Journal of Medicinal Chemistry*, 2012, **55**, 9107-9119.
2. D. I. Perez, V. Palomo, C. Pérez, C. Gil, P. D. Dans, F. J. Luque, S. Conde and A. Martínez, *Journal of Medicinal Chemistry*, 2011, **54**, 4042-4056.
3. G. K. S. Prakash, R. Ismail, J. Garcia, C. Panja, G. Rasul, T. Mathew and G. A. Olah, *Tetrahedron Letters*, 2011, **52**, 1217-1221.
4. E. Claudel, C. Arbez-Gindre, V. Berl and J. Lepoittevin, *Synthesis*, 2009, **20**, 3391-3398.

Chapter 8

Experimental section

8.1 General procedures

All chemicals used in this project were purchased from Aldrich or Merck. Tetrahydrofuran was distilled under nitrogen from sodium sand with benzophenone as an indicator. Dichloromethane was distilled under nitrogen from calcium hydride. Where necessary, purification of other reagents was performed according to standard literature procedures.[1] The molarity of alkyl lithiums was determined using a method as described in the literature.[2]

All reactions were performed under anhydrous conditions and a positive pressure of nitrogen. Low temperature reactions were performed in a Dewar or plastic bowl using dry ice in acetone (–78 °C) or ice in water (0 °C).

Column chromatography was performed on Merck silica gel 60 (particle size 0.040–0.063 mm) using combinations of hexane (Hex), ethyl acetate (EtOAc), methanol (MeOH) and dichloromethane (DCM) as solvent. Thin layer chromatography (TLC) was carried out on aluminium-backed Merck silica gel 60 F254 plates. Visualisation was achieved with a UV lamp, using iodine on silica or by dipping the TLC plate into a Cerium Ammonium Molybdate solution (CAM) or ninhydrin solution (NIN) followed by heating.

All ^{1}H, ^{13}C nuclear magnetic resonance spectra were obtained using a 300 MHz Varian VNMRS (75.5 MHz for ^{13}C), 400 MHz (100 MHz for ^{13}C) or 600 MHz (150 MHz for ^{13}C) using deuterated solvents. Chemical shifts (δ) were recorded using the residual peaks of deuterated solvents ($CDCl_3$ = δ 7.26 and DMSO–D_6 = δ 2.50 in ^{1}H NMR, $CDCl_3$ = δ 77.2 and DMSO–D_6 = δ 39.5 in ^{13}C NMR). All chemical shifts are reported in ppm. Spectra were obtained at 25 °C. Melting points were obtained using a Gallenkamp Melting Point Apparatus and are uncorrected. Infrared spectra were obtained using a Nexus Thermo-Nicolet FT-IR instrument using the ATR attachment. High resolution mass spectrometry was performed by the CAF (Central Analytical Facility) Institute at Stellenbosch University using a Waters API Q-TOF Ultima spectrometer.

Additional spectroscopic data can be found at this Google Drive link: https://drive.google.com/open?id=14nAI0J6EXssDMP2QhoiRrrHjiGU7iU-i

8.2 Chapter 3

4-Bromobenzenesulfonyl chloride (245)

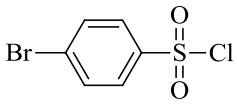

Bromobenzene (5.0 mL, 47 mmol) was dissolved in $CHCl_3$ (180 mL) and precooled to –78 °C. Excess HSO_3Cl (35.0 mL, 517 mmol) was added dropwise to the solution via a pressure-equalising dropping funnel. The reaction was allowed to stir overnight while gradually warming to room temperature. The brown solution was then poured over crushed ice and extracted with DCM (3 × 35 mL). The organic layer was dried over anhydrous $MgSO_4$, filtered and concentrated under reduced pressure. Chromatography was done using 7:3 Hex:DCM as eluent to afford the product as an off-white solid (8.9 g, 74% yield). R_f = 0.57 (Hex:DCM, 7:3); ^{1}H NMR ($CDCl_3$, 300 MHz): δ = 7.91 (d, *J* = 8.5 Hz, 2H, CH), 7.78 (d, *J* = 8.5 Hz, 2H, CH). The spectroscopic data were in agreement with the reported data.[3]

1-[(4-Bromophenyl)sulfonyl]piperazine (248)

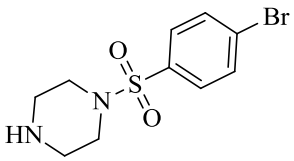

Piperazine (6.7 g, 78 mmol) was dissolved in DCM (120 mL) and cooled to 0 °C. Sulfonyl chloride **245** (5.0 g, 20 mmol) was dissolved in DCM (10 mL) and added dropwise to the solution at 0 °C while stirring vigorously. The resulting white solution was left to stir for two hours and then washed with a saturated solution of $NaHCO_3$ (3 × 30 mL). The organic layer was dried over anhydrous $MgSO_4$, filtered, and concentrated under reduced pressure. Purification was done using column chromatography with DCM and then 9:1 DCM:MeOH as eluent to afford the product as a white solid (5.4 g, 91% yield). Mp 163–165 °C (neat); R_f = 0.43 (DCM:MeOH, 9:1); IR (ATR): 2969 (w), 2916 (w), 2859 (w), 1573 (m), 1342 (m), 1161 (vs), 751 (vs) cm^{-1}; ^{1}H NMR ($CDCl_3$, 300 MHz): δ = 7.65 (d, *J* = 8.5 Hz, 2H, CH), 7.58 (d, *J* = 8.5 Hz, 2H, CH), 2.98–2.84 (m, 8H, CH_2), 1.64 (s, 1H, NH); ^{13}C NMR ($CDCl_3$, 75.5 MHz): δ = 134.8 (1C, CH), 132.5 (2C, CH), 129.4 (2C, CH), 128.1 (1C, CH), 47.0 (2C, CH_2), 45.4 (2C, CH_2); HRMS–ES+: *m/z* $[M+H]^+$ calcd for $C_{10}H_{14}N_2O_2SBr$: 304.9959; found: 304.9962.

1-[(4-Bromophenyl)sulfonyl]-4-methylpiperazine (249)

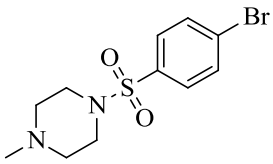

Compound **248** (4.7 g, 15 mmol) was dissolved in dioxane (40 mL). Formaldehyde (37%, 4.6 mL, 77 mmol) and acetic acid (1.8 mL, 31 mmol) was added to the solution followed by the addition of zinc (2.0 g, 31 mmol) in one portion. The resulting grey solution was stirred for one day at room temperature and the solid was then removed by filtration. The filtrate was concentrated under reduced pressure and diluted with EtOAc (35 mL). The organic layer was washed with a saturated solution of $NaHCO_3$ (25 mL) and dried over anhydrous $MgSO_4$. The product was purified using column chromatography with 95:5 DCM:MeOH as eluent and was isolated as a white solid (4.2 g, 85% yield). R_f = 0.40 (DCM:MeOH, 95:5); ^{1}H NMR ($CDCl_3$, 300 MHz): δ = 7.66 (d, *J* = 8.7 Hz, 2H, CH), 7.60 (d, *J* = 8.7 Hz, 2H, CH), 3.03–3.00 (m, 4H, CH_2), 2.48–2.44 (m, 4H, CH_2), 2.25 (s, 3H, CH_3); ^{13}C NMR ($CDCl_3$, 75.5 MHz): δ = 134.6 (1C, C), 132.4 (2C, CH), 129.4 (2C, CH), 128.0 (1C, C), 54.1 (2C, CH_2), 46.0 (2C, CH_2), 45.8 (1C, CH_3). The spectroscopic data were in agreement with the reported data.[4]

{4-[(4-Methylpiperazin-1-yl)sulfonyl]phenyl}boronic acid (243)

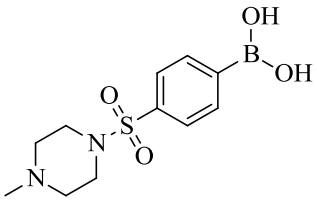

Compound **249** (1.0 g, 3.1 mmol) was dissolved in THF (14 mL) and precooled to –78 °C. *n*-BuLi (0.88 M, 5.0 mL, 4.4 mmol) was added dropwise to the solution. The resulting dark yellow solution was stirred further for one hour followed by the addition of $B(OMe)_3$ (0.70 mL, 6.3 mmol). The light yellow solution was stirred further at –78 °C for two hours or until the yellow colour had disappeared. The solution was quenched with 2 M HCl (20 mL) and then concentrated to dryness. The white solid was dissolved in boiling MeOH (5 mL) and upon cooling the product precipitated out. The pale yellow mother liquor was removed with a pipette and the white solid was washed twice with MeOH (5 mL), followed by concentration to dryness. The product was obtained as a white solid (0.58 g, 65% yield) and was sufficiently pure to carry through to the next reaction. Mp 189–191 °C (neat); R_f = 0.10 (DCM:MeOH, 95:5); IR (ATR): 3551 (s), 3350 (br), 2693 (m), 2614 (m), 1324 (m), 1156 (m), 943 (m) cm^{-1}; ^{1}H NMR (DMSO–D_6, 300 MHz): δ = 8.45 (br s, 2H, OH), 8.05 (d, *J* = 8.3 Hz, 2H, CH), 7.73 (d, *J* = 8.3 Hz, 2H, CH), 3.82–3.67 (m, 2H, CH_2), 3.43–3.37 (m, 2H, CH_2), 3.16 (s, 3H, CH_3), 2.71 (m, 4H, CH_2); ^{13}C NMR (DMSO–D_6, 75.5 MHz): δ = 135.6

(1C, CH), 135.0 (1C, CH), 126.4 (1C, CH), 51.5 (1C, CH_3), 43.0 (2C, CH_2), 41.9 (2C, CH_2); HRMS–ES+: *m/z* $[M+H]^+$ calcd for $C_{11}H_{18}N_2O_4SB$: 285.1080; found: 285.1078.

5-Bromopyrazin-2-amine (244)

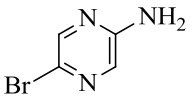

Aminopyrazine (1.0 g, 11 mmol) was dissolved in DMF (10 mL) and cooled to 0 °C. *N*-Bromosuccinamide (NBS) (1.9 g, 11 mmol), dissolved in DMF (10 mL), was added dropwise slowly. The resulting dark brown solution was then stirred at room temperature overnight and poured over crushed ice (100 mL). The solution was washed with EtOAc (4 × 40 mL) and the organic layers were combined followed by washing with brine (25 mL). The organic layer was dried over anhydrous $MgSO_4$, filtered and concentrated under reduced pressure. Purification using column chromatography was done with 1:1 Hex:EtOAc as eluent to afford the product as a cream solid (1.1 g, 63% yield). R_f = 0.56 (Hex:EtOAc, 1:1); ^{1}H NMR ($CDCl_3$, 300 MHz): δ = 8.09 (d, *J* = 1.3 Hz, 1H, CH), 7.77 (d, *J* = 1.3 Hz, 1H, CH), 4.65–4.50 (br s, 2H, NH_2). The spectroscopic data were in agreement with the reported data.[5]

5-(4-((4-Methylpiperazin-1-yl)sulfonyl)phenyl)pyrazin-2-amine (251)

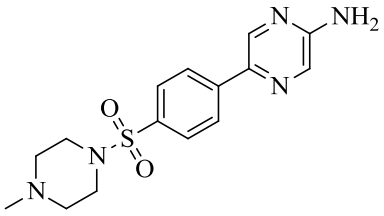

5-Bromopyrazine **244** (0.10 g, 0.45 mmol), boronic acid **243** (0.14 g, 0.68 mmol) and Cs_2CO_3 (0.29 g, 0.90 mmol) were charged to a Schlenk tube and dissolved in Tol:EtOH:H_2O (6 mL, 3:1:0.05). The reaction mixture was degassed three times using the freeze-pump-thaw method and then heated at 80 °C overnight. The black-brown solution was then diluted with EtOAc and filtered through celite. The orange-brown solution was washed with brine (20 mL) and the organic layer was acidified with 2M HCl (2 × 10 mL). The layers were separated and the aqueous layer was then basified with a saturated solution of $NaHCO_3$ (25 mL) and extracted with EtOAc (2 × 20 mL). The organic layers were collected, dried over anhydrous $MgSO_4$, filtered and concentrated under reduced pressure to afford the product as a cream solid (0.11 g, 76% yield) that was sufficiently pure to carry through to the next reaction. Mp 176–178 °C (neat); R_f = 0.24 (DCM:MeOH, 9:1); IR (ATR): 3444 (m), 2803 (m), 1538 (m), 1454 (m), 1153 (s) cm^{-1}; ^{1}H NMR (DMSO–D_6, 300 MHz): δ = 8.64 (s, 1H, CH), 8.17 (d, *J* = 8.5 Hz, 2H, CH), 8.01 (d, *J* = 8.5 Hz, 2H, CH), 7.74

(s, 1H, CH), 6.82 (br s, 2H, NH_2), 2.94–2.86 (m, 4H, CH_2), 2.40–2.32 (m, 4H, CH_2), 2.12 (s, 3H, CH_3); ^{13}C NMR (DMSO–D_6, 75.5 MHz): δ = 155.6 (1C, CNH_2), 141.6 (1C, CH), 140.2 (1C, C), 137.0 (1C, C), 133.1 (2C, CH), 132.0 (1C, C), 128.2 (2C, CH), 125.1 (1C, CH), 53.5 (2C, CH_2), 45.8 (2C, CH_2), 45.3 (1C, CH_3); HRMS–ES+: *m/z* $[M+H]^+$ calcd for $C_{15}H_{20}N_5O_2S$: 334.1338; found: 334.1332.

1,1'-*Bis*(diphenylphosphino)ferrocene (253)

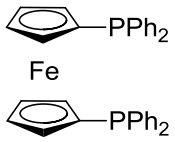

n-BuLi (0.88 M, 7.6 mL, 6.7 mmol) was added dropwise to a solution of ferrocene (0.50 g, 2.7 mmol), TMEDA (1.0 mL, 6.7 mmol) and hexane (5 mL) at 0 °C. The orange slurry was then stirred overnight at room temperature followed by cooling to –78 °C and chlorodiphenylphosphine (1.5 mL, 8.1 mmol) was then added dropwise. The orange-brown slurry was gradually warmed to room temperature and stirred further for two hours before being quenched with H_2O (10 mL) and extracted with DCM (25 mL). The organic layer was dried over anhydrous $MgSO_4$, filtered and concentrated under reduced pressure. Purification was done using column chromatography with 9:1 Hex:DCM as eluent to afford the product as orange crystals (0.47 g, 32% yield). The product was used directly to the next step.

Dichloro[1,1'-*Bis*(diphenylphosphino)-ferrocene]palladium(II) (255)

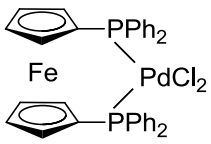

1,1'-*Bis*(diphenylphosphino)ferrocene **253** (0.77 g, 1.4 mmol) was added to dichloro*bis*(acetonitrile)palladium(II) (0.36 g, 1.4 mmol) dissolved in benzene (15 mL). The dark orange solution was stirred at room temperature overnight. The resulting orange precipitate was collected by filtration and the residue was washed with benzene (2 × 10 mL). The solid was then dried under reduced pressure to afford the product as an orange solid (1.0 g, 88% yield). ^{1}H NMR ($CDCl_3$, 300 MHz): δ =7.92–7.88 (m, 8H, CH), 7.51–7.47 (m, 4H, CH), 7.41–7.36 (m, 8H, CH), 4.41–4.37 (m, 4H, CH), 4.22–4.17 (m, 4H, CH); ^{31}P NMR ($CDCl_3$, 162 MHz): δ = 34.4. The spectroscopic data were in agreement with the reported data.[6]

5-Iodopyrazin-2-amine (264)

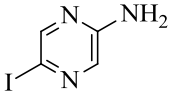

Aminopyrazine (0.15 g, 1.6 mmol) was dissolved in DMF (5 mL) and cooled to 0 °C. *N*-iodosuccinamide (NIS) (0.53 g, 2.4 mmol), dissolved in DMF (3 mL), was added dropwise slowly. The resulting yellow solution was then stirred at room temperature overnight and quenched with a saturated solution of $Na_2S_2O_3$ (5 mL). The mixture was then poured into ice water (15 mL). The dark yellow-orange solution was washed with EtOAc (3 × 25 mL) and the organic layers were combined, followed by washing with brine (30 mL). The organic layer was dried over anhydrous $MgSO_4$, filtered and concentrated under reduced pressure. Purification was done using column chromatography with 7:3 EtOAc:Hex as eluent to afford the product as a yellow-cream solid (0.16 g, 46% yield). R_f = 0.40 (EtOAc:Hex, 1:1); ^{1}H NMR ($CDCl_3$, 300 MHz): δ = 8.21 (d, *J* = 1.4 Hz, 1H, CH), 7.83 (d, *J* = 1.4 Hz, 1H, CH), 4.69–4.52 (br s, 2H, NH_2). The spectroscopic data were in agreement with the reported data.[7]

3-Bromo-5-{4-[(4-methylpiperazin-1-yl)sulfonyl]phenyl}pyrazine-2-amine (241)

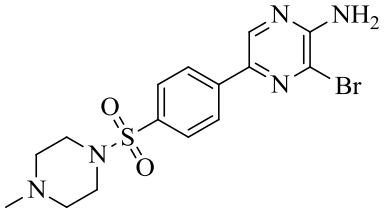

Compound **251** (0.060 g, 0.18 mmol) was dissolved in DCM (1 mL) and NBS (0.040 g, 0.22 mmol) was added portion wise at 0 °C. The reaction was stirred at room temperature for two hours followed by the addition of H_2O (5 mL) and the product was extracted with DCM (2 × 10 mL). The organic layer was acidified with 2 M HCl (10 mL). The layers were separated and the aqueous layer was then basified with a saturated solution of $NaHCO_3$ (20 mL) and washed with DCM (2 × 15 mL). The organic layer was dried over anhydrous $MgSO_4$, filtered and concentrated under reduced pressure to afford the product as a cream solid (0.035 g, 47% yield) that was sufficiently pure to carry through to the next reaction. Mp 184–186 °C (neat); R_f = 0.50 (DCM:MeOH, 9:1); IR (ATR): 3199 (br), 1674 (w), 1145 (m), 1065 (s), 611 (m) cm^{-1}; ^{1}H NMR ($CDCl_3$, 300 MHz): δ = 8.45 (s, 1H, CH), 8.03 (d, *J* = 8.6 Hz, 2H, CH), 7.81 (d, *J* = 8.6 Hz, 2H, CH), 5.21 (br s, 2H, NH_2), 3.15–2.96 (m, 4H, CH_2), 2.54–2.42 (m, 4H, CH_2), 2.27 (s, 3H, CH_3); ^{13}C NMR ($CDCl_3$, 75.5 MHz): δ = 151.9 (1C, CNH_2), 147.6 (1C, C), 140.1 (1C, C), 138.6 (1C, CH), 133.4 (1C, C), 129.6 (1C, CBr), 128.5 (2C, CH_2), 126.1 (2C, CH), 54.1 (2C, CH_2), 45.9 (2C, CH_2), 45.7 (1C, CH_3); HRMS–ES+: *m/z* $[M+H]^+$ calcd for $C_{15}H_{19}N_5O_2SBr$: 412.0443; found: 412.0436.

5-Bromo-3-iodopyrazin-2-amine (265)

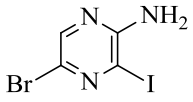

5-Bromopyrazin-2-amine (0.15 g, 0.86 mmol) was dissolved in DMSO (1.5 mL) at room temperature. Iodine (0.13 g, 0.52 mmol) was added in one portion followed by H_5IO_6 (0.12 g, 0.52 mmol). The reaction was stirred overnight at 60 °C and then quenched slowly with a saturated solution of $Na_2S_2O_3$ (5 mL). The mixture was washed with EtOAc (3 × 15 mL) and the organic layers were then collected and washed with brine (20 mL). The organic layer was dried over anhydrous $MgSO_4$, filtered and concentrated under reduced pressure. Purification was done using column chromatography with 7:3 EtOAc:Hex as eluent to afford the product as a bright yellow solid (0.13 g, 51% yield). R_f = 0.78 (EtOAc:Hex, 7:3); ^{1}H NMR (DMSO–D_6, 300 MHz): δ = 8.05 (s, 1H, CH), 6.75 (br s, 2H, NH_2); ^{13}C NMR (DMSO–D_6, 75.5 MHz): δ = 155.8 (1C, CH), 142.7 (1C, CH), 121.3 (1C, CH), 102.7 (1C, CH). The spectroscopic data were in agreement with the reported data.[8]

1-(Piperidin-1-yl)prop-2-en-1-one (275)

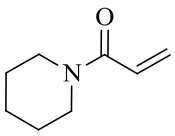

Piperidine (0.63 mL, 6.5 mmol) and Et_3N (1.8 mL, 13 mmol) were dissolved in DCM (7 mL). Acryloyl chloride (1.0 mL, 13 mmol) was dissolved in DCM (3 mL) and added dropwise to the solution at 0 °C via a dropping funnel. The reaction was then stirred at room temperature for two hours, followed by dilution with DCM (20 mL) and washing with brine (2 × 15 mL). The organic layer was dried over anhydrous $MgSO_4$, filtered and concentrated under reduced pressure. Purification was done using column chromatography with EtOAc as eluent to afford the product as a yellow oil (0.6 g, 67% yield). R_f = 0.50 (EtOAc); ^{1}H NMR ($CDCl_3$, 300 MHz): δ = 6.56 (dd, *J* = 16.9, 10.6 Hz, 1H, CH), 6.22 (dd, *J* = 16.9, 2.0 Hz, 1H, CH), 5.63 (dd, *J* = 10.6, 2.0 Hz, 1H, CH), 3.59–3.47 (m, 4H, CH_2), 1.67–1.54 (m, 6H, CH_2); ^{13}C NMR ($CDCl_3$, 75.5 MHz): δ = 165.5 (1C, CO), 128.2 (1C, CH), 127.1 (1C, CH), 47.1 (1C, CH_2), 43.2 (1C, CH_2), 26.7 (1C, CH_2), 25.6 (1C, CH_2), 24.7 (1C, CH_2). The spectroscopic data were in agreement with the reported data.[9]

1-Morpholinoprop-2-en-1-one (276)

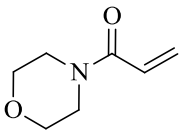

Morpholine (0.56 mL, 6.4 mmol) and Et_3N (1.8 mL, 13 mmol) were dissolved in DCM (7 mL). Acryloyl chloride (1.0 mL, 13 mmol) was dissolved in DCM (3 mL) and added dropwise to the solution at 0 °C via a dropping funnel. The reaction was stirred at room temperature for two hours, followed by dilution with DCM (20 mL) and washing with brine (2 × 15 mL). The organic layer was dried over anhydrous $MgSO_4$, filtered and concentrated under reduced pressure. Purification was done using column chromatography with EtOAc as eluent to afford the product as a yellow oil (0.75 g, 83% yield). R_f = 0.40 (EtOAc); ^{1}H NMR ($CDCl_3$, 300 MHz): δ = 6.53 (dd, *J* = 16.8, 10.4 Hz, 1H, CH), 6.31 (dd, *J* = 16.8, 2.0 Hz, 1H, CH), 5.71 (dd, *J* = 10.4, 2.0 Hz, 1H, CH), 3.69–3.56 (m, 8H, CH_2); ^{13}C NMR ($CDCl_3$, 75.5 MHz): δ = 165.6 (1C, CO), 128.4 (1C, CH), 127.2 (1C, CH), 66.9 (2C, CH_2), 46.3 (1C, CH_2), 42.4 (1C, CH_2). The spectroscopic data were in agreement with the reported data.[9]

1-(Pyrrolidin-1-yl)prop-2-en-1-one (277)

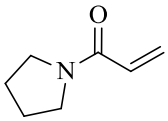

Pyrrolidine (0.60 mL, 7.2 mmol) and Et_3N (2.0 mL, 14 mmol) were dissolved in DCM (7 mL). Acryloyl chloride (1.2 mL, 14 mmol) was dissolved in DCM (3 mL) and added dropwise to the solution at 0 °C via a dropping funnel. The reaction was then stirred at room temperature for two hours, followed by dilution with DCM (20 mL) and washing with brine (2 × 15 mL). The organic layer was dried over anhydrous $MgSO_4$, filtered and concentrated under reduced pressure. Purification was done using column chromatography with EtOAc as eluent to afford the product as a dark yellow oil (0.70 g, 77% yield). R_f = 0.27 (EtOAc); ^{1}H NMR ($CDCl_3$, 300 MHz): δ = 6.45 (dd, *J* = 16.8, 9.6 Hz, 1H, CH), 6.35 (dd, *J* = 16.8, 2.8 Hz, 1H, CH), 5.65 (dd, *J* = 9.6, 2.8 Hz, 1H, CH), 3.56–3.51 (m, 4H, CH_2), 2.01–1.82 (m, 4H, CH_2); ^{13}C NMR ($CDCl_3$, 75.5 MHz): δ = 164.6 (1C, CO), 129.0 (1C, CH), 127.4 (1C, CH), 46.7 (1C, CH_2), 46.0 (1C, CH_2), 26.3 (1C, CH_2), 24.4 (1C, CH_2). The spectroscopic data were in agreement with the reported data.[9]

_N,N_-Diethylacrylamide (278)

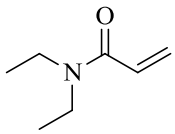

Diethylamine (0.81 mL, 7.9 mmol) and Et_3N (2.2 mL, 16 mmol) were dissolved in DCM (7 mL). Acryloyl chloride (1.3 mL, 16 mmol) was dissolved in DCM (3 mL) and added dropwise to the solution at 0 °C via a dropping funnel. The reaction was then stirred at room temperature for two hours, followed by dilution with DCM (20 mL) and washing with brine (2 × 15 mL). The organic layer was dried over anhydrous $MgSO_4$, filtered and concentrated under reduced pressure. Purification was done using column chromatography with 1:1 Hex:EtOAc as eluent to afford the product as a yellow oil (0.73 g, 73% yield). R_f = 0.43 (Hex:EtOAc, 1:1); ^{1}H NMR ($CDCl_3$, 300 MHz): δ = 6.50 (dd, *J* = 16.7, 10.4 Hz, 1H, CH), 6.29 (dd, *J* = 16.7, 2.3 Hz, 1H, CH), 5.61 (dd, *J* = 10.4, 2.3 Hz, 1H, CH), 3.43–3.30 (m, 4H, CH_2), 1.18–1.09 (m, 6H, CH_3); ^{13}C NMR ($CDCl_3$, 75.5 MHz): δ = 165.6 (1C, CO), 128.0 (1C, CH), 127.5 (1C, CH), 42.2 (1C, CH_2), 40.8 (1C, CH_2), 14.9 (1C, CH_3), 13.1 (1C, CH_3). The spectroscopic data were in agreement with the reported data.[10]

_N_-Phenylacrylamide (284)

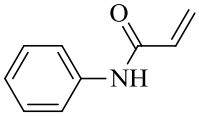

Aniline (0.43 mL, 4.8 mmol) was dissolved in DCM (10 mL) and Et_3N (0.74 mL, 5.2 mmol) was added. The solution was cooled to 0 °C followed by the dropwise addition of acryloyl chloride (0.42 mL, 5.2 mmol, dissolved in 5 mL DCM). The reaction was stirred at 0 °C for three hours and then diluted with DCM (15 mL). The solution was washed with brine (15 mL) and the organic layer was dried over anhydrous $MgSO_4$, filtered and concentrated under reduced pressure. Purification was done using column chromatography with 1:1 Hex:EtOAc as eluent to afford the product as a white solid (0.63 g, 89% yield). R_f = 0.63 (Hex:EtOAc, 1:1); ^{1}H NMR ($CDCl_3$, 300 MHz): δ = 7.76 (br s, 1H, NH),7.60–7.58 (m, 2H, CH), 7.34–7.29 (m, 2H, CH), 7.14–7.09 (m, 1H, CH), 6.43 (dd, *J* = 16.9, 1.6 Hz, 1H, CH), 6.28 (dd, *J* = 16.9, 10.0, Hz, 1H, CH), 5.74 (dd, *J* = 10.0, 1.6 Hz, 1H, CH). The spectroscopic data were in agreement with the reported data.[11]

_N_-(Pyridin-3-yl)acrylamide (283)

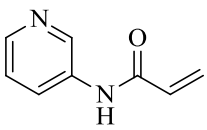

3-Aminopyridine (0.50 g, 5.3 mmol) was dissolved in DCM (30 mL) and Et_3N (1.2 mL, 8.5 mmol) was added. The solution was cooled to –78 °C followed by slow dropwise addition of acryloyl chloride (0.50 mL, 6.4 mmol).

The reaction was gradually warmed to room temperature over four hours. The black-brown solution was concentrated and purified using column chromatography with EtOAc as eluent to afford the product as a cream solid (0.43 g, 54% yield). Mp 112–116 °C (neat); R_f = 0.3 (EtOAc); IR (ATR): 3455 (w), 3015 (br), 2970 (s), 1739 (br), 1552 (m), 1371 (s), 1229 (s) cm^{-1}; ^1H NMR ($CDCl_3$, 300 MHz): δ = 8.61 (dd, *J* = 2.6, 0.4 Hz, 1H, NH), 8.36 (dd, *J* = 4.8, 1.5 Hz, 1H, CH), 8.32–8.23 (m, 1H, CH), 8.17–8.09 (m, 1H, CH), 7.29 (dd, *J* = 8.4, 4.8 Hz, 1H, CH), 6.47 (dd, *J* = 16.9, 1.5 Hz, 1H, CH), 6.30 (dd, *J* = 16.9, 10.1 Hz, 1H, CH), 5.81 (dd, *J* = 10.1,1.5 Hz, 1H). The spectroscopic data were in agreement with the reported data.[12]

_N_-Cyclohexylacrylamide (282)

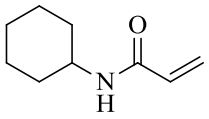

Cyclohexylamine (1.1 mL, 9.8 mmol) and Et_3N (5.5 mL, 39 mmol) were dissolved in DCM (18 mL) and precooled to –78 °C. Acryloyl chloride (3.2 mL, 39 mmol) was dissolved in DCM (3 mL) and added dropwise over five minutes. The reaction was stirred overnight at room temperature and then quenched with H_2O (20 mL). The organic layer was then dried over anhydrous $MgSO_4$, filtered and concentrated under reduced pressure. After purification using column chromatography with 1:1 Hex:EtOAc as eluent, the product was obtained as an off-white solid (0.64 g, 43% yield). R_f = 0.43 (Hex:EtOAc, 1:1); ^1H NMR ($CDCl_3$, 300 MHz): δ = 6.26 (dd, *J* = 16.9, 1.6 Hz, 1H, CH), 6.05 (dd, *J* = 16.9, 10.2 Hz, 1H, CH), 5.61 (dd, *J* = 16.9, 1.6 Hz, 1H, CH), 5.44–5.33 (br s, 1H, NH), 3.92–3.79 (m, 1H, CH), 1.98–1.93 (m, 2H, CH), 1.75–1.60 (m, 3H, CH), 1.46–1.32 (m, 2H, CH), 1.26–1.09 (m, 3H, CH); ^{13}C NMR ($CDCl_3$, 75.5 MHz): δ = 172.3 (1C, CO), 131.4 (1C, CH), 126.2 (1C, CH_2), 48.4 (1C, CH), 33.3 (2C, CH_2), 25.7 (1C, CH_2), 25.0 (2C, CH_2). The spectroscopic data were in agreement with the reported data.[13]

Nicotinaldehyde (286)

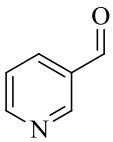

2-Pyridinemethanol (0.30 mL, 3.0 mmol) was added to THF (15 mL) at 0 °C. Manganese dioxide (1.3 g, 15 mmol) was added portion-wise and the reaction was stirred at room temperature overnight. The black mixture was filtered through celite and washed with brine (10 mL). The organic layer was dried over anhydrous $MgSO_4$, filtered and concentrated under reduced pressure. The crude solution was purified using column chromatography with EtOAc to 93:7 EtOAc:MeOH as eluent to afford the product as a

colourless oil (0.20 g, 60% yield). R_f = 0.67 (EtOAc:MeOH, 9:1); ^{1}H NMR ($CDCl_3$, 300 MHz): δ = 10.13 (s, 1H, CH), 9.09 (dd, *J* = 2.1, 0.7, Hz, 1H, CH), 8.85 (dd, *J* = 4.9, 1.8 Hz, 1H, CH), 8.19 (app. dt, ddd, *J* = 5.9, 2.1, 2.1 Hz, 1H, CH), 7.52–7.48 (m, 1H, CH). The spectroscopic data were in agreement with the reported data.[14]

1-(Pyridin-3-yl)prop-2-en-1-ol (287)

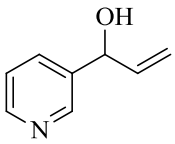

Nicotinaldehyde (0.050 g, 0.46 mmol) was added to THF (2 mL) at 0 °C. Vinyl MgBr (1.0 M, 0.90 mL, 0.93 mmol) was added dropwise. The reaction was gradually warmed to room temperature in three hours, followed by quenching with a saturated solution of NH_4Cl (2 mL). The yellow mixture was extracted with EtOAc (2 × 10 mL) and the organic layers were collected and washed with brine (10 mL). The organic layer was dried over anhydrous $MgSO_4$, filtered and concentrated under reduced pressure. The crude oil was purified using column chromatography with EtOAc as eluent to afford the product as a yellow oil in 98% yield. R_f = 0.2 (EtOAc:Hex, 7:3); ^{1}H NMR ($CDCl_3$, 300 MHz): δ = 8.60 (d, *J* = 2.2 Hz, 1H, CH), 8.53 (dd, *J* = 4.8, 1.8 Hz, 1H, CH), 7.72 (app. dt, ddd, *J* = 6.0, 1.8, 1.8 Hz, 1H, CH), 7.29 (ddd, *J* = 7.9, 4.8, 0.8 Hz, 1H, CH), 6.04 (ddd, *J* = 17.0, 10.3, 6.0 Hz, 1H, CH), 5.42–5.36 (m, 1H, CH), 5.29–5.24 (m, 2H, CH). The spectroscopic data were in agreement with the reported data.[15]

General procedure for the Heck reaction:

Aminopyrazine **265** (1.0 eq.), propenone (1.2 eq.), Et_3N (4.0 eq.), $Pd(OAc)_2$ (0.1 eq.) and DMF (1 mL) were charged to a Schlenk tube. The solution was degassed, filled with N_2 and then stirred at 70 °C overnight. The black-brown solution was diluted with EtOAc and filtered through celite. The organic layer was then washed with brine (2 × 20 mL), dried over anhydrous $MgSO_4$, filtered and concentrated under reduced pressure. Purification was done using column chromatography with an appropriate solvent system as eluent to afford the corresponding product.

(*E*)-3-(3-Amino-6-bromopyrazin-2-yl)-1-(piperidine-1-yl)prop-2-en-1-one (289)

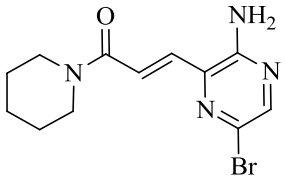

Solvent system: 7:3 EtOAc:Hex. Yellow solid (0.040 g, 56% yield). Mp 128–130 °C (neat); R_f = 0.25 (EtOAc:Hex, 7:3); IR (ATR): 3319 (m), 3174 (m), 2937 (m), 2851 (m), 1629 (m), 1588 (s), 1437 (s) cm^{-1}; ^1H NMR ($CDCl_3$, 300 MHz): δ = 8.04 (s, 1H, CH), 7.61 (d, *J* = 14.5 Hz, 1H, CH), 7.51 (d, *J* = 14.5 Hz, 1H, CH), 5.10 (br s, 2H, NH_2), 3.67–3.60 (m, 4H, CH_2), 1.63–1.58 (m, 6H, CH_2); ^{13}C NMR ($CDCl_3$, 75.5 MHz): δ = 164.6 (1C, CO), 152.0 (1C, CNH_2), 145.0 (1C, CH), 134.8 (1C, C), 133.0 (1C, CH), 127.2 (1C, CBr), 124.2 (1C, CH), 47.3 (1C, CH_2), 43.7 (1C, CH_2), 27.0 (1C, CH_2), 25.8 (1C, CH_2), 24.7 (1C, CH_2); HRMS–ES+: *m/z* $[M+H]^+$ calcd for $C_{12}H_{16}N_4OBr$: 311.0507; found: 311.0502.

(*E*)-3-(3-Amino-6-bromopyrazin-2-yl)-1-morpholinoprop-2-en-1-one (290)

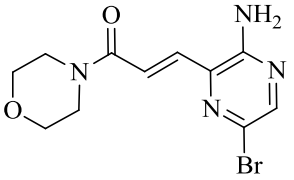

Solvent system: 7:3 EtOAc:Hex. Bright yellow solid (0.038 g, 53% yield). Mp 174–176 °C (neat); R_f = 0.26 (EtOAc:Hex, 7:3); IR (ATR): 3371 (m), 3333 (m), 3208 (m), 1438 (s), 1112 (s), 1041 (m) cm^{-1}; ^1H NMR ($CDCl_3$, 300 MHz): δ = 8.07 (s, 1H, CH), 7.63 (d, *J* = 14.5 Hz, 1H, CH), 7.47 (d, *J* = 14.5 Hz, 1H, CH), 5.04 (br s, 2H, NH_2), 3.73 (m, 8H, CH_2); ^{13}C NMR ($CDCl_3$, 75.5 MHz): δ = 164.8 (1C, CO), 152.0 (1C, CNH_2), 145.5 (1C, CH), 134.2 (1C, C), 133.7 (1C, CH), 127.3 (1C, CBr), 123.0 (1C, CH), 67.0 (2C, CH_2), 46.5 (1C, CH_2), 42.8 (1C, CH_2); HRMS–ES+: *m/z* $[M+H]^+$ calcd for $C_{11}H_{14}N_4O_2Br$: 313.0300; found: 313.0301.

(*E*)-3-(3-Amino-6-bromopyrazin-2-yl)-1-(pyrrolidin-1-yl)prop-2-en-1-one (291)

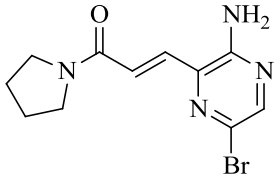

Solvent system: 95:5 DCM:MeOH. Yellow solid (0.037 g, 38% yield). Mp 126–128 °C (neat); R_f = 0.32 (DCM:MeOH, 9:1); IR (ATR): 3457 (m), 3308 (m), 3197 (m), 2922 (m), 2850 (m), 1633 (m), 1582 (s), 1426 (s), 1380 (s), 1114 (m) cm^{-1}; ^1H NMR ($CDCl_3$, 300 MHz): δ = 8.02 (s, 1H, CH), 7.79 (d, *J* = 14.7 Hz, 1H, CH), 7.31 (d, *J* = 14.7 Hz, 1H, CH), 5.46 (br s, 2H, NH_2), 3.73–3.66 (m, 2H, CH_2), 3.57–3.53 (m, 2H, CH_2), 2.02–1.87 (m, 4H, CH_2); ^{13}C NMR ($CDCl_3$, 75.5 MHz): δ = 164.2 (1C, CO), 152.3 (1C, CNH_2), 145.1 (1C, CH), 134.6 (1C, C), 132.8 (1C, CH), 126.8 (1C, CBr), 125.1 (1C, CH), 47.0 (1C, CH_2), 46.4 (1C, CH_2), 26.2

(1C, CH_2), 24.4 (1C, CH_2); HRMS–ES+: *m/z* $[M+H]^+$ calcd for $C_{11}H_{14}N_4OBr$: 297.0351; found: 297.0362.

(*E*)-3-(3-Amino-6-bromopyrazin-2-yl)-*N*,*N*-diethylacrylamide (292)

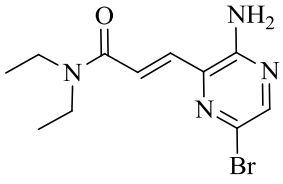

Solvent system: 1:1 Hex:EtOAc. Yellow solid (0.074 g, 75% yield). Mp 126–128 °C (neat); R_f = 0.75 (EtOAc:MeOH, 95:5); IR (ATR): 3345 (s), 3187 (s), 2970 (s), 1736 (s), 1599 (s), 1442 (s), 1214 (s), 1126 (s) cm^{-1}; ^1H NMR ($CDCl_3$, 300 MHz): δ = 8.02 (s, 1H), 7.69 (d, *J* = 14.5 Hz, 1H), 7.39 (d, *J* = 14.5 Hz, 1H), 5.32 (s, 2H), 3.53–3.43 (m, 4H), 1.20 (dt, *J* = 28.8, 7.14 Hz, 6H); ^{13}C NMR ($CDCl_3$, 75.5 MHz): δ = 165.3 (1C, CO), 152.2 (1C, CNH_2), 145.0 (1C, CH), 134.7 (1C, C), 133.3 (1C, CH), 127.0 (1C, CBr), 124.2 (1C, CH), 42.6 (1C, CH_2), 41.3 (1C, CH_2), 15.3 (1C, CH_3), 13.2 (1C, CH_3); HRMS–ES+: *m/z* $[M+H]^+$ calcd for $C_{11}H_{16}N_4OBr$: 299.0507; found: 299.0501.

(*E*)-3-(3-Amino-6-bromopyrazin-2-yl)-*N*-cyclohexylacrylamide (293)

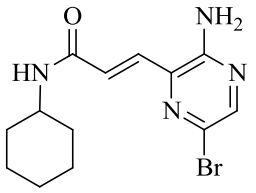

Solvent system: 7:3 EtOAc:Hex. Bright yellow solid (0.038 g, 53% yield). Mp 169–171 °C (neat); R_f = 0.5 (EtOAc:Hex, 7:3); IR (ATR): 3415 (w), 3269 (m), 3169 (m), 1646 (m), 1544 (s), 1445 (s), 1341 (m), 958 (m) cm^{-1}; ^1H NMR ($CDCl_3$, 300 MHz): δ = 8.05 (s, 1H, CH), 7.58 (d, *J* = 14.6 Hz, 1H, CH), 6.96 (d, *J* = 14.6 Hz, 1H, CH), 5.67 (br s, 1H, NH), 5.06 (br s, 2H, NH_2), 3.94–3.82 (m, 1H, CH), 1.98–1.93 (m, 2H, CH_2), 1.79–1.59 (m, 4H, CH_2), 1.46–1.32 (m, 2H, CH_2), 1.28–1.12 (m, 2H, CH_2); ^{13}C NMR ($CDCl_3$, 75.5 MHz): δ = 164.1 (1C, CO), 152.0 (1C, CNH_2), 145.2 (1C, CH), 134.3 (1C, C), 131.5 (1C, CH), 127.8 (1C, CBr), 127.3 (1C, CH), 48.7 (1C, CH), 33.2 (2C, CH_2), 25.6 (2C, CH_2), 24.9 (1C, CH_2); HRMS–ES+: *m/z* $[M+H]^+$ calcd for $C_{13}H_{18}N_4OBr$: 325.0664; found: 325.0651.

(*E*)-3-(3-Amino-6-bromopyrazine-2-yl)-*N*-(pyridin-3-yl)acrylamide (294)

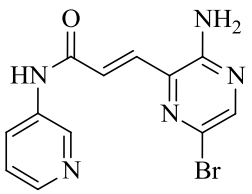

Solvent system: EtOAc. Yellow solid (0.033 g, 33% yield). Mp 208 °C (neat); R_f = 0.5 (EtOAc); IR (ATR): 3647 (w), 3337 (m), 3186 (s), 2858 (w), 1428 (s), 1119 (m) cm^{-1}; ^1H NMR (DMSO–D_6, 300 MHz): δ = 10.6 (s, 1H, NH), 8.86 (s, 1H, CH), 8.29–8.14 (m, 3H, CH), 7.81 (d, *J* = 14.8

Hz, 1H, CH), 7.40–7.35 (m, 1H, CH), 7.22 (d, *J* = 14.8 Hz, 1H, CH), 7.05 (s, 2H, NH_2); ^{13}C NMR (DMSO–D_6, 75.5 MHz): δ = 163.5 (1C, CO), 153.5 (1C, CNH_2), 145.6 (1C, CH), 144.4 (1C, C), 140.8 (1C, CH), 136.0 (1C, C), 133.2 (1C, CH), 132.6 (1C, CH), 126.3 (1C, CBr), 126.0 (1C, CH), 124.1 (1C, CH), 123.8 (1C, CH) ; HRMS–ES+: *m/z* $[M+H]^+$ calcd for $C_{12}H_{11}N_5OBr$: 320.0147; found: 320.0144.

General method for the Suzuki coupling:

The heteroaryl Br (1.0 eq.), boronic acid **243** (1.5 eq.), Cs_2CO_3 (4.0 eq.) and the solvent system Tol:EtOH:H_2O (1.5 mL, 4:1:0.05) were added to a Schlenk tube. The reaction content was degassed using the freeze-pump-thaw technique. Pd(dppf)Cl_2 (0.1 eq.) was then added to the Schlenk tube under argon and the solution was stirred at 70 °C overnight. Silica was added to the black mixture and transferred to the column. Purification was done using column chromatography with EtOAc to 9:1 EtOAc:MeOH as eluent to afford the corresponding product as a solid.

(*E*)-3-{3-Amino-6-[4-({4-methylpiperazin-1-yl}sulfonyl)phenyl]pyrazin-2-yl}-1-(piperidin-1-yl)prop-2-en-1-one (216)

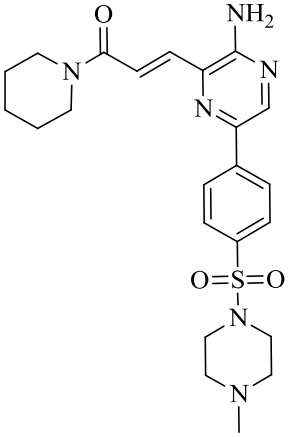

Yellow solid (0.056 g, 73% yield). Mp 134–136 °C (neat); R_f = 0.13 (EtOAc:MeOH, 9:1); IR (ATR): 3367 (br), 2939 (m), 2856 (m), 2803 (m), 1738 (m), 1638 (m), 1590 (s), 1444 (s), 1347 (s), 1284 (s) cm^{-1}; ^1H NMR ($CDCl_3$, 300 MHz): δ = 8.48 (s, 1H, CH), 8.07 (d, *J* = 8.6 Hz, 2H, CH), 7.83 (d, *J* = 8.6 Hz, 2H, CH), 7.77 (d, *J* = 14.7 Hz, 1H, CH), 7.63 (d, *J* = 14.7 Hz, 1H, CH), 5.30 (br s, 2H, NH_2), 3.73–3.62 (m, 4H, CH_2), 3.17–3.03 (m, 4H, CH_2), 2.53–2.42 (m, 4H, CH_2), 2.26 (s, 3H, CH_3), 1.75–1.57 (m, 6H, CH_2); ^{13}C NMR ($CDCl_3$, 75.5 MHz): δ = 164.9 (1C, CO), 152.5 (1C, CNH_2), 141.5 (1C, C), 140.8 (1C, CH), 140.7 (1C, C), 134.7 (1C, C), 134.0 (1C, CH), 133.9 (1C, C), 128.5 (2C, CH), 126.2 (2C, CH), 123.9 (1C, CH), 54.2 (2C, CH_2), 47.3 (1C, CH_2), 46.1 (2C, CH_2), 45.8 (1C, CH_3), 43.7 (1C, CH_2), 27.0 (1C, CH_2), 25.8 (1C, CH_2), 24.7 (1C, CH_2); HRMS–ES+: *m/z* $[M+H]^+$ calcd for $C_{23}H_{31}N_6O_3S$: 471.2178; found: 471.2177.

(*E*)-3-{3-Amino-6-[4-({4-methylpiperazin-1-yl}sulfonyl)phenyl]pyrazin-2-yl}-1-morpholinoprop-2-en-1-one (217)

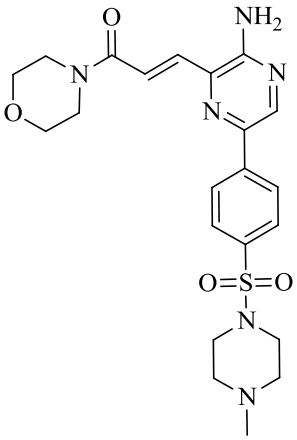

Dark yellow solid (0.052 g, 69% yield). Mp 136–140 °C (neat); R_f = 0.15 (EtOAc:MeOH, 9:1); IR (ATR): 3391 (br), 1638 (m), 1608 (m), 1434 (m), 1344 (s), 1280 (s), 1214 (m), 1156 (s), 956 (m) cm^{-1}; ^1H NMR ($CDCl_3$, 300 MHz): δ = 8.49 (s, 1H, CH), 8.05 (d, *J* = 8.4 Hz, 2H, CH), 7.82 (d, *J* = 8.4 Hz, 2H, CH), 7.78 (d, *J* = 14.5 Hz, 1H, CH), 7.59 (d, *J* = 14.5 Hz, 1H, CH), 5.18 (br s, 2H, NH_2), 3.76 (m, 8H, CH_2), 3.07 (m, 4H, CH_2), 2.49 (m, 4H, CH_2), 2.26 (s, 3H, CH_3); ^{13}C NMR ($CDCl_3$, 75.5 MHz): δ = 165.1 (1C, CO), 152.5 (1C, CNH_2), 141.4 (1C, C), 141.2 (1C, CH), 141.0 (1C, C), 134.9 (1C, C), 134.8 (1C, CH), 133.4 (1C, C), 128.5 (2C, CH), 126.3 (2C, CH), 122.6 (1C, CH), 67.0 (2C, CH_2), 54.2 (2C, CH_2), 46.5 (1C, CH_2), 46.1 (2C, CH_2), 45.8 (1C, CH_3), 42.8 (1C, CH_2); HRMS–ES+: *m/z* $[M+H]^+$ calcd for $C_{22}H_{29}N_6O_4S$: 473.1971; found: 473.1974.

(*E*)-3-{3-Amino-6-[4-({4-methylpiperazin-1-yl}sulfonyl)phenyl]pyrazin-2-yl}-1-(pyrrolidin-1-yl)prop-2-en-1-one (218)

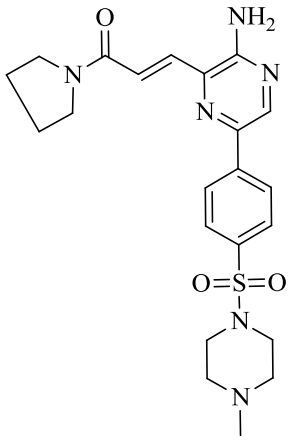

Dark cream solid (0.032 g, 70% yield). Mp 131–132 °C (neat); R_f = 0.22 (EtOAc:MeOH, 9:1); IR (ATR): 3354 (br), 2919 (m), 2802 (m), 1643 (m), 1593 (s), 1437 (s), 1172 (s), 1154 (s) cm^{-1}; ^1H NMR ($CDCl_3$, 300 MHz): δ = 8.51 (s, 1H, CH), 8.09 (d, *J* = 8.6 Hz, 2H, CH), 7.86–7.80 (m, 3H, CH), 7.48 (d, *J* = 14.6 Hz, 1H, CH), 5.27 (s, 2H, NH_2), 3.76 (t, *J* = 6.7 Hz, 2H, CH_2), 3.64 (t, *J* = 6.7 Hz, 2H, CH_2), 3.14–3.05 (m, 4H, CH_2), 2.53–2.49 (m, 4H, CH_2), 2.28 (s, 3H, CH_3), 2.11–1.91 (m, 4H, CH_2); ^{13}C NMR ($CDCl_3$, 75.5 MHz): δ = 164.3 (1C, CO), 152.6 (1C, CNH_2), 141.5 (1C, C), 140.9 (1C, CH), 140.7 (1C, C), 134.7 (1C, C), 133.7 (1C, CH), 133.5 (1C, C), 128.5 (2C, CH), 126.2 (2C, CH), 125.0 (1C, CH), 54.2 (2C, CH_2), 47.0 (1C, CH_2), 46.4 (1C, CH_2), 46.1 (2C, CH_2), 45.9 (1C, CH_3), 26.2 (1C, CH_2), 24.5 (1C, CH_2); HRMS–ES+: *m/z* $[M+H]^+$ calcd for $C_{22}H_{29}N_6O_3S$: 457.2022; found: 457.2019.

(*E*)-3-{3-Amino-6-[4-({4-methylpiperazin-1-yl}sulfonyl)phenyl]pyrazin-2-yl}-*N*,*N*-diethylacrylamide (219)

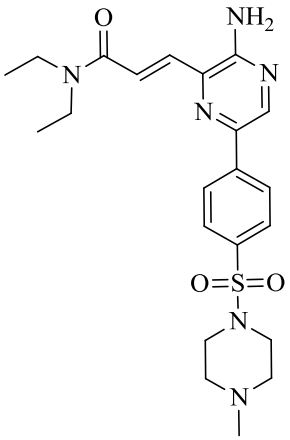

Dark cream solid (0.048 g, 78% yield). Mp 126–128 °C (neat); R_f = 0.30 (EtOAc:MeOH, 9:1); IR (ATR): 3336 (br), 2927 (m), 1639 (m), 1594 (s), 1456 (s), 1286 (s), 1169 (s), 947 (m) cm^{-1}; ^1H NMR ($CDCl_3$, 300 MHz): δ = 8.47 (s, 1H), 8.06 (d, *J* = 8.5 Hz, 2H), 7.87–7.80 (m, 3H), 7.55 (d, *J* = 14.6 Hz, 1H), 5.35 (br s, 2H), 3.57–3.49 (m, 4H), 3.13–3.00 (m, 4H), 2.51–2.47 (m, 4H), 2.26 (s, 3H), 1.30 (t, *J* = 7.1 Hz, 3H), 1.20 (t, *J* = 7.1 Hz, 3H); ^{13}C NMR ($CDCl_3$, 75.5 MHz): δ = 165.4 (1C, CO), 152.6 (1C, CNH_2), 141.5 (1C, C), 140.8 (1C, CH), 140.5 (1C, C), 134.6 (1C, C), 134.3 (1C, CH), 133.8 (1C, C), 128.5 (2C, CH), 126.1 (2C, CH), 123.9 (1C, CH), 54.2 (2C, CH_2), 46.1 (2C, CH_2), 45.8 (1C, CH_3), 42.7 (1C, CH_2), 41.4 (1C, CH_2), 15.3 (1C, CH_3), 13.3 (1C, CH_3); HRMS–ES++: *m/z* $[M+H]^+$ calcd for $C_{22}H_{31}N_6O_3S$: 459.2178; found: 459.2174.

(*E*)-3-{3-Amino-6-[4-({4-methylpiperazin-1-yl}sulfonyl)phenyl]pyrazin-2-yl}-*N*-cyclohexylacrylamide (220)

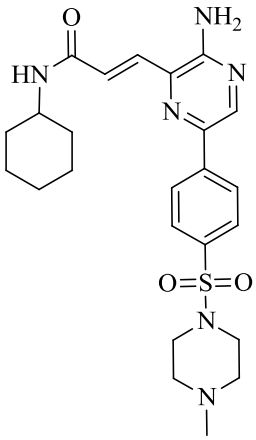

Yellow solid (0.045 g, 75% yield). Mp 160–163 °C (neat); R_f = 0.26 (EtOAc:MeOH, 9:1); IR (ATR): 3336 (br), 3207 (br), 2923 (s), 2851 (s), 1654 (m), 1456 (s), 1345 (m), 1166 (s), 942 (m) cm^{-1}; ^1H NMR ($CDCl_3$, 300 MHz): δ = 8.45 (s, 1H, CH), 8.04 (d, *J* = 8.4 Hz, 2H, CH), 7.80–7.73 (m, 3H, CH), 7.13 (d, *J* = 14.7 Hz, 1H, CH), 6.00 (d, *J* = 8.4 Hz, 1H, NH), 5.32 (br s, 2H, NH_2), 3.98–3.84 (m, 1H, CH), 3.12–3.01 (m, 4H, CH_2), 2.49–2.45 (m, 4H, CH_2), 2.25 (s, 3H, CH_3), 2.03–1.93 (m, 2H, CH_2), 1.80–1.69 (m, 2H, CH_2), 1.67–1.59 (m, 1H, CH_2), 1.47–1.13 (m, 5H, CH_2); ^{13}C NMR ($CDCl_3$, 75.5 MHz): δ = 164.5 (1C, CO), 152.6 (1C, CNH_2), 141.4 (1C, C), 140.8 (1C, CH), 140.5 (1C, C), 134.6 (1C, C), 133.4 (1C, CH), 132.6 (1C, C), 128.4 (2C, CH), 127.4 (1C, CH), 126.1 (2C, CH), 54.1 (2C, CH_2), 48.8 (1C, CH), 46.0 (2C, CH_2), 45.8 (1C, CH_3), 32.2 (2C, CH_2), 25.6 (2C, CH_2), 25.0 (1C, CH_2); HRMS–ES+: *m/z* $[M+H]^+$ calcd for $C_{24}H_{33}N_6O_3S$: 485.2335; found: 485.2336.

8.3 Chapter 4

3-Amino-6-bromopyrazine-2-carboxylic acid (300)

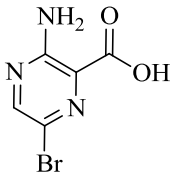

LiOH (0.35 g, 14 mmol) dissolved in H_2O (6 mL) was added slowly to a solution of bromine ester **305** (0.63 g, 2.7 mmol) and MeOH (6 mL) at room temperature. The dark orange solution was heated to 90 °C for two hours before the reaction was quenched with concentrated HCl (pH<2) at 0 °C. The white slurry was basified with a saturated solution of $NaHCO_3$ and extracted with EtOAc (20 mL). The aqueous layer was concentrated to about 15 mL and left to crystallise at room temperature to afford the product as yellow needles (0.39 g, 66% yield). R_f = 0.1 (DCM:MeOH, 95:5); ^{1}H NMR (DMSO–D_6, 600 MHz): δ = 8.05 (s, 1H, CH); ^{13}C NMR (DMSO–D_6, 150 MHz): δ = 167.2 (1C, CO), 155.2 (1C, CNH_2), 144.9 (1C, CH), 134.2 (1C, C), 121.9 (1C, CBr). The spectroscopic data were in agreement with the reported data.[16]

Methyl-3-aminopyrazine-2-carboxylate (301)

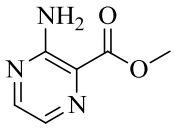

Concentrated H_2SO_4 (0.70 mL, 13 mmol) was added dropwise to a solution of 3-aminopyrazine-2-carboxylic acid (0.70 g, 5.0 mmol) and MeOH (7 mL) at 0 °C. The white slurry was left to stir at room temperature for three days and the dark brown solution was neutralised with a saturated solution of $NaHCO_3$ at 0 °C. The product was extracted with DCM (3 × 30 mL) and the combined organic layers were washed with brine, dried over anhydrous $MgSO_4$, filtered and then concentrated under reduced pressure. The crude material was recrystallised using H_2O to afford the product as an orange solid (0.56 g, 72% yield). R_f = 0.7 (DCM:MeOH, 9:1); ^{1}H NMR (DMSO–D_6, 600 MHz): δ = 8.25 (d, *J* = 2.2 Hz, 2H, CH), 7.90 (d, *J* = 2.2 Hz, 2H, CH), 7.31 (br s, 2H, NH_2), 3.85 (s, 3H, CH_3); ^{13}C NMR (DMSO–D_6, 150 MHz): δ = 166.4 (1C, CO), 155.8 (1C, CNH_2), 147.7 (1C, CH), 132.5 (1C, CH), 123.2 (1C, C), 52.0 (1C, CH_3O). The spectroscopic data were in agreement with the reported data.[17]

Methyl-3-amino-6-bromopyrazine-2-carboxylate (302)

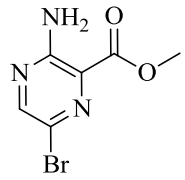

Aminopyrazine ester **301** (0.47 g, 3.1 mmol) was dissolved in CH_3CN (6 mL) and cooled to 0 °C. NBS (0.60 g, 3.4 mmol), dissolved in DMF (1 mL), was then added dropwise to the solution and the reaction was allowed to stir overnight at room temperature. The dark brown solution was concentrated, diluted with EtOAc (20 mL) and washed with ice water (50 mL). The aqueous layer was washed with EtOAc (2 × 30 mL) and the combined organic layers were then washed with brine (20 mL). The organic layer was dried over anhydrous $MgSO_4$, filtered and concentrated under reduced pressure. Purification using column chromatography with DCM as eluent afforded the product as a light orange solid (0.52 g, 73% yield). R_f = 0.20 (DCM); ^{1}H NMR ($CDCl_3$, 300 MHz): δ = 8.42 (s, 1H, CH), 7.54 (br s, 2H, NH_2), 3.85 (s, 3H, CH_3); ^{13}C NMR ($CDCl_3$, 75.5 MHz): δ = 166.2 (1C, CO), 154.9 (1C, CNH_2), 150.4 (1C, CH), 125.0 (1C, C), 123.6 (1C, CBr), 53.1 (1C, CH_3). The spectroscopic data were in agreement with the reported data.[18]

3-Amino-6-bromo-*N*-butylpyrazine-2-carboxamide (306)

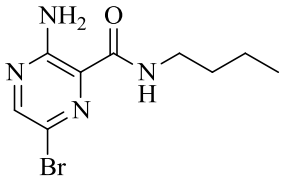

3-Amino-6-bromopyrazine-2-carboxylic acid **300** (0.025 g, 0.11 mmol) was added to DCM (1.5 mL) at room temperature under argon. Thionyl chloride (0.030 mL, 0.41 mmol) was added dropwise and the suspension was heated at 50 °C for two hours. The dark yellow suspension was evaporated under argon and DCM (1 mL) was added. A mixture of butylamine (0.015 mL, 0.14 mmol) and Et_3N (0.030 mL, 0.22 mmol) was added dropwise at 0 °C and the suspension was stirred overnight at room temperature. The suspension cleared over time and the orange solution was concentrated under reduced pressure and diluted with EtOAc (10 mL) and water (10 mL). The aqueous layer was extracted with EtOAc (2 × 10 mL) and the combined organic layers were dried over anhydrous $MgSO_4$, filtered and concentrated under reduced pressure. Purification using column chromatography with DCM as eluent afforded the product as a cream solid in 45% yield. R_f = 0.17 (DCM); ^{1}H NMR ($CDCl_3$, 600 MHz): δ = 8.20 (s, 1H), 7.66 (s, 1H), 3.43–3.39 (m, 2H), 1.63–1.57 (m, 2H), 1.43–1.37 (m, 2H), 0.96 (t, *J* = 7.4 Hz, 3H). No further spectroscopic analysis was carried out.

3-Amino-*N*-methoxy-*N*-methylpyrazine-2-carboxamide (310)

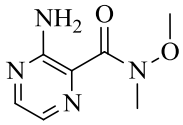

3-Aminopyrazine-2-carboxylic acid **299** (0.50 g, 3.6 mmol) was dissolved in DMF (5 mL) at 60 °C. Carbonyldiimidazole (0.70 g, 4.3 mmol) was added to the solution in one portion and the reaction was left to stir at 60 °C for three hours. *N*,*O*-Dimethylhydroxylamine (0.42 g, 4.3 mmol) was then added in one portion and the dark orange solution was left to stir further for 16 hours. The reaction mixture was concentrated by heating the solution overnight at 60 °C in open air. The dark brown slurry was transferred to the column and purified using DCM as eluent to remove impurities before eluting the product with 95:5 DCM:MeOH. The product was obtained as a white-yellow solid (0.62 g, 94% yield). Mp 91–92 °C (neat); R_f = 0.33 (DCM:MeOH, 95:5); IR (ATR): 3466 (m), 3292 (m), 3157 (m), 2920 (m), 1606 (s), 1463 (m), 1434 (m), 1385 (m), 983 (m), 830 (m) cm^{-1}; ^1H NMR ($CDCl_3$, 300 MHz): δ = 8.03 (d, *J* = 2.5 Hz, 1H, CH), 7.84 (d, *J* = 2.5 Hz, 1H, CH), 5.94 (br s, 2H, NH_2), 3.79 (s, 3H, CH_3), 3.41 (s, 3H, CH_3); ^{13}C NMR ($CDCl_3$, 75.5 MHz): δ = 154.6 (1C, CO), 144.8 (1C, CH), 132.0 (1C, CH), 61.5 (1C, CH_3). The spectroscopic data were in agreement with the reported data.[19]

3-Amino-6-bromo-*N*-methoxy-*N*-methylpyrazine-2-carboxamide (311)

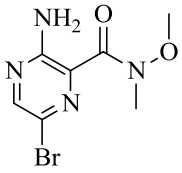

Weinreb ester **310** (0.20 g, 1.1 mmol) was dissolved in $CHCl_3$ (5 mL) at 0 °C. NBS (0.22 g, 1.2 mmol) was then added portion wise and the yellow solution was left to stir at 40 °C overnight. The brown solution was concentrated and purified using column chromatography with 7:3 Hex:EtOAc as eluent to afford the product as a white yellow solid (0.26 g, 90% yield). Mp 78–80 °C (neat); R_f = 0.5 (1:1, Hex:EtOAc); IR (ATR): 3401 (s), 3313 (m), 3174 (s), 2976 (m), 1622 (vs), 1449 (s), 1373 (m), 1199 (m), 983 (m) cm^{-1}; ^1H NMR ($CDCl_3$, 300 MHz): δ = 8.14 (s, 1H, CH), 6.03 (br s, 2H, NH_2), 3.85 (s, 3H, CH_3), 3.40 (s, 3H, CH_3); ^{13}C NMR ($CDCl_3$, 75.5 MHz): δ = 153.9 (1C, CO), 147.3 (1C, CH), 123.3 (1C, C), 61.8 (1C, CH_3); HRMS–ES+: *m/z* $[M+H]^+$ calcd for $C_7H_{10}N_4O_2Br$: 260.9987; found: 260.9992.

1-(3-Amino-6-bromopyrazin-2-yl)prop-2-yn-1-one (297)

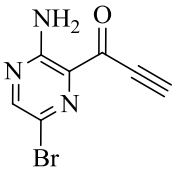

Weinreb **311** (0.10 g, 0.38 mmol) was dissolved in THF (3 mL) at 0 °C and ethynyl MgBr (0.50 M, 2.3 mL, 1.1 mmol,) was then added dropwise. The dark orange-yellow solution was stirred for one hour at 0 °C, followed by one

hour at room temperature. The orange suspension was cooled to –10 °C, quenched with 2 M HCl (4 mL) and then extracted with EtOAc (3 × 10 mL). The combined organic layers were dried over anhydrous $MgSO_4$, filtered and concentrated under reduced pressure. Purification was done using column chromatography with 8:2 Hex:EtOAc as eluent to afford the fluorescent product as a bright orange solid (0.075 g, 86% yield). Mp 144 °C (neat); R_f = 0.71 (Hex:EtOAc, 1:1); IR (ATR): 3396 (s), 3265 (m), 3140 (br), 2100 (m), 1616 (s), 1126 (s), 999 (s) cm^{-1}; ^1H NMR ($CDCl_3$, 300 MHz): δ = 8.32 (s, 1H, CH), 5.76 (br s, 2H, NH_2), 3.62 (s, 1H, CH); ^{13}C NMR ($CDCl_3$, 75.5 MHz): δ = 178.0 (1C, CO), 154.0 (1C, CNH_2), 151.6 (1C, CH), 129.7 (1C, C), 125.6 (1C, CBr), 84.7 (1C, CH), 80.3 (1C, C); HRMS–ES+: *m/z* $[M+H]^+$ calcd for $C_7H_5N_3OBr$: 225.9616; found: 225.9615.

1-(3-Amino-6-bromopyrazin-2-yl)ethanone (298)

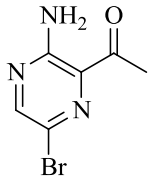

Weinreb **311** (0.50 g, 1.9 mmol) was dissolved in THF (6 mL) at 0 °C and methyl MgBr (3.0 M, 1.9 mL, 5.7 mmol,) was then added dropwise. The red-brown solution was stirred for one hour at 0 °C, followed by one hour at room temperature. The brown solution was cooled to –10 °C, quenched with 2M HCl (5 mL) and then extracted with EtOAc (3 × 15 mL). The combined organic layers were dried over anhydrous $MgSO_4$, filtered and concentrated under reduced pressure. Purification was done using column chromatography with 9:1 Hex:EtOAc as eluent to afford the product as a bright yellow solid in 83% yield. Mp 149–151 °C (neat); R_f = 0.74 (Hex:EtOAc, 7:3); IR (ATR): 3410 (s), 3306 (s), 3190 (m), 1656 (s), 1613 (m), 1595 (m), 1131 (m) cm^{-1}; ^1H NMR ($CDCl_3$, 300 MHz): δ = 8.26 (s, 1H, CH), 2.66 (s, 3H, CH_3); ^{13}C NMR ($CDCl_3$, 75.5 MHz): δ = 201.7 (1C, CO), 153.4 (1C, CNH_2), 150.6 (1C, CH), 129.6 (1C, C), 124.2 (1C, CBr), 26.4 (1C, CH_3); HRMS–ES+: *m/z* $[M+H]^+$ calcd for $C_6H_7N_3OBr$: 215.9772; found: 215.9765.

General method for the Michael addition:

Ethynyl pyrazine **297** (1.0 eq.) was dissolved in DCM at 0 °C and the required secondary amine (1.3 eq.) was added dropwise. The deep orange solution was left to stir for two hours at room temperature and then directly transferred to a column. Purification was done with a suitable solvent system to afford the corresponding product.

(*E*)-1-(3-Amino-6-bromopyrazin-2-yl)-3-morpholinoprop-2-en-1-one (312)

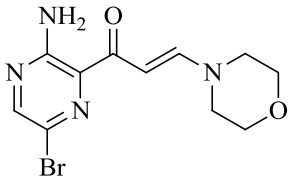

Solvent system: DCM to 95:5 DCM:MeOH. Yellow solid (0.13 g, 93% yield). Mp 160–161 °C (neat); R_f = 0.47 (DCM:MeOH, 95:5); IR (ATR): 3353 (m), 3258 (m), 3163 (m), 2919 (m), 2851 (m), 1604 (m), 1559 (s), 1109 (m), 815 (m) cm^{-1}; ^1H NMR ($CDCl_3$, 300 MHz): δ = 8.15 (s, 1H, CH), 7.71 (d, *J* = 12.9 Hz, 1H, CH), 6.55 (d, *J* = 12.9 Hz, 1H, CH), 3.78–3.75 (m, 4H, CH_2), 3.48–3.45 (m, 4H, CH_2); ^{13}C NMR ($CDCl_3$, 75.5 MHz): δ = 188.3 (1C, CO), 154.1 (1C, CNH_2), 152.7 (1C, CH), 148.2 (1C, CH), 131.8 (1C, C), 123.7 (1C, CBr), 91.8 (1C, CH), 66.5 (2C, CH_2), 53.0 (1C, CH_2), 46.3 (1C, CH_2); HRMS–ES+: *m/z* $[M+H]^+$ calcd for $C_{11}H_{14}N_2O_2Br$: 313.0300; found: 315.0295.

(*E*)-1-(3-Amino-6-bromopyrazin-2-yl)-3-(piperidin-1-yl)prop-2-en-1-one (317)

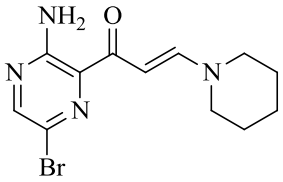

Solvent system: EtOAc. Deep orange solid (0.085 g, 89% yield). Mp 156–158 °C (neat); R_f = 0.64 (EtOAc); IR (ATR): 3343 (m), 2925 (m), 2853 (m), 1620 (m), 1550 (m), 1139 (m), 811 (m) cm^{-1}; ^1H NMR ($CDCl_3$, 300 MHz): δ = 8.12 (s, 1H, CH), 7.76 (d, *J* = 12.8 Hz, 1H, CH), 6.48 (d, *J* = 12.8 Hz, 1H, CH), 3.47–3.38 (m, 4H, CH_2), 1.75–1.63 (m, 6H, CH_2); ^{13}C NMR ($CDCl_3$, 75.5 MHz): δ = 187.8 (1C, CO), 154.1 (1C, CNH_2), 153.1 (1C, CH), 147.7 (1C, CH), 132.4 (1C, C), 123.6 (1C, CBr), 90.7 (1C, CH), 55.5 (1C, CH_2), 46.8 (1C, CH_2), 26.7 (1C, CH_2), 25.2 (1C, CH_2), 24.1 (1C, CH_2); HRMS–ES+: *m/z* $[M+H]^+$ calcd for $C_{12}H_{16}N_4OBr$: 311.0507; found: 311.0502.

(*E*)-1-(3-Amino-6-bromopyrazin-2-yl)-3-(pyrrolidin-1-yl)prop-2-en-1-one (318)

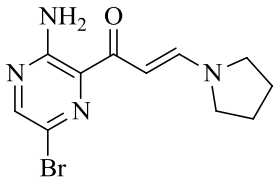

Solvent system: 7:3 EtOAc:Hex. Orange-yellow solid (0.080 g, 85% yield). Mp 168–171 °C (neat); R_f = 0.53 (EtOAc:Hex, 7:3); IR (ATR): 3347 (m), 3251 (m), 3161 (m), 2968 (m), 2864 (m), 1545 (s), 1508 (m), 1452 (m), 1255 (m), 1028 (m) cm^{-1}; ^1H NMR ($CDCl_3$, 300 MHz): δ = 8.12 (s, 1H, CH), 7.99 (d, *J* = 12.7 Hz, 1H, CH), 6.34 (d, *J* = 12.7 Hz, 1H, CH), 3.58 (t, *J* = 6.6 Hz, 2H, CH_2), 3.37 (t, *J* = 6.9 Hz, 2H, CH_2), 2.09–1.88 (m, 4H, CH_2); ^{13}C NMR ($CDCl_3$, 75.5 MHz): δ = 187.3 (1C, CO), 154.1 (1C, CNH_2), 150.1 (1C, CH), 147.7 (1C, CH),

132.4 (1C, C), 123.6 (1C, CBr), 92.8 (1C, CH), 52.7 (1C, CH_2), 47.5 (1C, CH_2), 25.4 (1C. CH_2), 25.3 (1C, CH_2); HRMS–ES+: *m/z* $[M+H]^+$ calcd for $C_{11}H_{14}N_4OBr$: 297.0351; found: 297.0357.

(*E*)-1-(3-Amino-6-bromopyrazin-2-yl)-3-(diethylamino)prop-2-en-1-one (319)

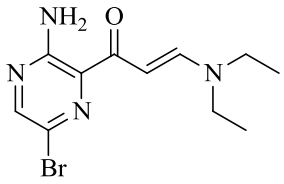

Solvent system: 1:1 EtOAc:Hex. Light orange solid (0.090 g, 95% yield). Mp 146–148 °C (neat); R_f = 0.63 (EtOAc:Hex, 7:3); IR (ATR): 3395 (m), 3284 (s), 2974 (m), 1623 (m), 1544 (s), 1509 (m), 1260 (m), 1046 (m) cm^{-1}; ^1H NMR ($CDCl_3$, 300 MHz): δ = 8.12 (s, 1H, CH), 7.80 (d, *J* = 12.8 Hz, 1H, CH), 6.44 (d, *J* = 12.8 Hz, 1H, CH), 3.37 (q, *J* = 7.2 Hz, 4H, CH_2), 1.25 (t, *J* = 7.2 Hz, 6H, CH_3); ^{13}C NMR ($CDCl_3$, 75.5 MHz): δ = 187.6 (1C, CO), 154.2 (1C, CNH_2), 152.7 (1C, CH), 147.7 (1C, CH), 132.5 (1C, C), 123.6 (1C, CBr), 91.4 (1C, CH), 50.7 (1C, CH_2), 43.2 (1C, CH_2), 14.9 (1C, CH_3), 12.0 (1C, CH_3); HRMS–ES+: *m/z* $[M+H]^+$ calcd for $C_{11}H_{16}N_4OBr$: 299.0507; found: 299.0514.

(*E*)-1-(3-Amino-6-bromopyrazin-2-yl)-3-(1*H*-imidazol-1-yl)prop-2-en-1-one (320)

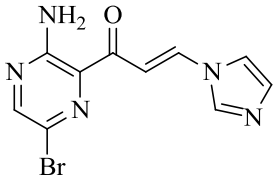

Solvent system: EtOAc. Orange-white solid (0.050 g, 71% yield). Mp 188 °C (neat); R_f = 0.44 (EtOAc); IR (ATR): 3450 (m), 3385 (m), 3250 (m), 3121 (s), 1663 (s), 1490 (vs) cm^{-1}; ^1H NMR ($CDCl_3$, 300 MHz): δ = 8.31 (s, 1H, CH), 8.02 (d, *J* = 14.2 Hz, 1H, CH), 7.88 (br s, 1H, CH), 7.80 (d, *J* = 14.2 Hz, 1H, CH), 7.46–7.42 (m, 1H, CH), 7.22–7.19 (m, 1H, CH); ^{13}C NMR ($CDCl_3$, 75.5 MHz): δ = 189.3 (1C, CO), 154.4 (1C, CNH_2), 151.0 (1C, CH), 138.7 (1C, CH), 136.2 (1C, C), 132.1 (1C, CH), 129.3 (1C, CH), 124.4 (1C, CBr), 116.8 (1C, CH), 109.5 (1C, CH); HRMS–ES+: *m/z* $[M+H]^+$ calcd for $C_{10}H_9N_5OBr$: 293.9990; found: 293.9983.

(*Z*)-1-(3-Amino-6-bromopyrazin-2-yl)-3-(cyclohexylamino)prop-2-en-1-one (322)

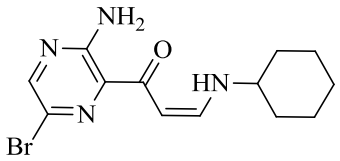

Ethynyl pyrazine **301** (0.040 g, 0.18 mmol) was dissolved in DCM (2 mL) at 0 °C and cyclohexylamine (0.022 mL, 0.19 mmol) was added dropwise. The deep orange solution was left to stir for two hours at room temperature and then directly transferred to a column. Purification was done with 1:1 Hex:EtOAc as solvent system to afford the product as a cream solid (0.054 g, 93% yield). R_f = 0.65 (Hex:EtOAc, 7:3); ^1H NMR ($CDCl_3$, 300 MHz): δ = 10.19

(br s, 1H, NH), 8.11 (s, 1H, CH), 7.06 (dd, *J* = 13.2, 7.6, Hz, 1H, CH), 6.31 (d, *J* = 7.6 Hz, 1H, CH), 3.23–3.09 (m, 1H, CH), 2.03–1.92 (m, 2H, CH_2), 1.85–1.74 (m, 2H, CH_2), 1.66–1.55 (m, 2H, CH_2), 1.48–1.29 (m, 4H, CH_2); ^{13}C NMR ($CDCl_3$, 75.5MHz): δ = 188.4 (1C, CO), 153.8 (1C, CNH_2), 153.0 (1C, CH), 147.5 (1C, CH), 132.3 (1C, C), 124.0 (1C, CBr), 90.4 (1C, CH), 57.8 (1C, CH), 34.2 (2C, CH_2), 25.5 (2C, CH_2), 24.7 (1C, CH_2); HRMS–ES+: *m/z* $[M+H]^+$ calcd for $C_{13}H_{18}N_4OBr$: 325.0664; found: 325.0657.

General method for the aldol condensation:

Methyl ketone **298** (1.0 eq.) and a suitable aldehyde (1.1 eq.) were dissolved in dioxane and water (15:1 ratio) at room temperature. LiOH (1.6 eq.) was added and the solution was stirred overnight at room temperature. The resulting suspension was diluted with brine (30 mL) and extracted with EtOAc (10 × 10 mL). The combined organic layers were dried over anhydrous $MgSO_4$, filtered and concentrated under reduced pressure. The crude material was purified using column chromatography with an appropriate solvent system to afford the corresponding product.

(*E*)-1-(3-Amino-6-bromopyrazin-2-yl)-3-(pyridin-3-yl)prop-2-en-1-one (325)

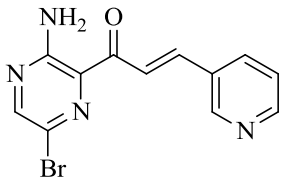

Solvent system: 7:3 EtOAc:Hex. Bright yellow solid (0.15 g, quantitative yield). Mp 179 °C (dec) (neat); R_f = 0.36 (Hex:EtOAc, 7:3); IR (ATR): 3392 (s), 3243 (s), 3119 (s), 1652 (s), 1599 (vs), 1519 (m), 1413 (m), 994 (m) cm^{-1}; ^{1}H NMR ($CDCl_3$ with 10 drops of MeOH, 300 MHz): δ = 8.77 (d, *J* = 1.8 Hz, 1H, CH), 8.52 (dd, *J* = 4.9, 1.8 Hz, 1H, CH), 8.25–8.20 (m, 2H, CH), 8.03 (app. dt, ddd, *J* = 8.0, 8.0, 1.8 Hz, 1H, CH), 7.74 (d, *J* = 16.1 Hz, 1H, CH), 7.38–7.33 (dd, *J* = 8.0, 4.9 Hz, 1H, CH); ^{13}C NMR ($CDCl_3$, 75.5 MHz): δ = 189.3 (1C, CO), 154.6 (1C, CNH_2), 150.7 (1C, CH), 150.6 (1C, CH), 150.1 (1C, CH), 140.0 (1C, CH), 135.3 (1C, CH), 131.1 (1C, C), 129.5 (1C, C), 124.1 (1C, CH), 123.9 (1C, CBr), 123.0 (1C, CH); HRMS–ES+: *m/z* $[M+H]^+$ calcd for $C_{12}H_{10}N_4OBr$: 305.0038; found: 305.0034.

(*E*)-1-(3-Amino-6-bromopyrazin-2-yl)-3-(pyridin-2-yl)prop-2-en-1-one (327)

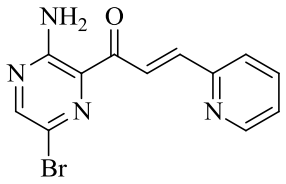

Solvent system: 7:3 EtOAc:Hex. Bright yellow solid (0.15 g, quantitative yield). Mp 172–175 °C (neat); R_f = 0.27 (Hex:EtOAc, 7:3); IR (ATR): 3371 (vs), 3250 (m), 3123 (m), 3028 (m), 1738 (m), 1604 (s), 1463 (m), 1378 (m), 982 (m) cm^{-1}; ^1H NMR ($CDCl_3$, 300 MHz): δ = 8.72 (d, *J* = 7.2 Hz, 1H, CH), 8.59 (d, *J* = 15.8 Hz, 1H, CH), 8.29 (s, 1H, CH), 7.84 (d, *J* = 15.8 Hz, 1H, CH), 7.75 (app. dt, ddd, *J* = 7.7, 7.7, 1.8 Hz, 1H, CH), 7.61 (d, *J* = 7.7 Hz, CH), 7.30 (ddd, *J* = 7.7, 4.8, 1.8 Hz, 1H, CH); ^{13}C NMR ($CDCl_3$, 75.5 MHz): δ = 190.3 (1C, CO), 154.5 (1C, C), 153.7 (1C, CNH_2), 150.7 (1C, CH), 150.4 (1C, CH), 143.1 (1C, CH), 136.9 (1C, CH), 130.0 (1C, C), 124.9 (1C, CH), 124.7 (1C, CH), 124.5 (1C, CH), 124.4 (1C, CBr); HRMS–ES+: *m/z* $[M+H]^+$ calcd for $C_{12}H_{10}N_4OBr$: 305.0038; found: 305.003.

(*E*)-1-(3-Amino-6-bromopyrazin-2-yl)-3-(pyridin-4-yl)prop-2-en-1-one (329)

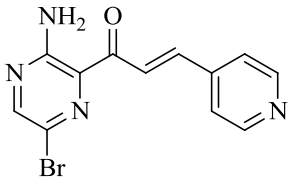

Solvent system: EtOAc. Bright yellow solid (0.15 g, quantitative yield). Mp 172 °C (dec) (neat); R_f = 0.13 (EtOAc); IR (ATR): 3369 (m), 2918 (m), 1653 (m), 1593 (vs), 1317 (m), 1007 (m) cm^{-1}. ^1H NMR (DMSO–D_6, 300MHz): δ = 8.67 (d, *J* = 5.9 Hz, 2H, CH), 8.52 (s, 1H, CH), 8.25 (d, *J* = 16.1 Hz, 1H, CH), 7.74–7.68 (m, 3H, CH); ^{13}C NMR (DMSO–D_6, 75.5MHz): δ = 188.6 (1C, CO), 154.7 (1C, CNH_2), 151.4 (1C, CH), 150.5 (2C, CH), 141.6 (1C, CH), 140.1 (1C, CH), 128.2 (1C, C), 125.1 (1C, C), 122.4 (1C, CBr), 122.3 (2C, CH); HRMS–ES+: *m/z* $[M+H]^+$ calcd for $C_{12}H_{10}N_4OBr$: 305.0038; found: 305.0034.

General method for the Suzuki coupling:

The suitable heteroaryl Br (1.0 eq.), boronic acid **243** (1.5 eq.), Cs_2CO_3 (4.0 eq.) and the solvent system Tol:EtOH:H_2O (1.5 mL, 4:1:0.05) were added to a Schlenk tube. The reaction content was degassed using the freeze-pump-thaw technique. Pd(dppf)Cl_2 (0.1 eq.) was then added to the Schlenk tube under argon and the solution was stirred at 70 °C overnight. Silica was added to the black mixture and transferred to the column. Purification using column chromatography was done using EtOAc to 9:1 EtOAc:MeOH as eluent to afford the corresponding product as a solid.

(*E*)-1-{3-Amino-6-[4-({4-methylpiperazin-1-yl}sulfonyl)phenyl]pyrazin-2-yl}-3-(piperidin-1-yl)prop-2-en-1-one (228)

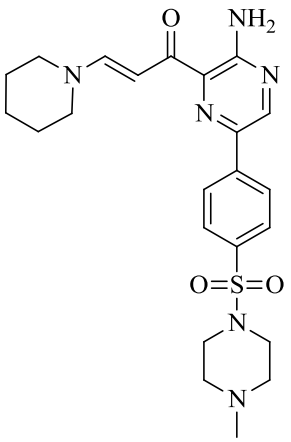

Yellow solid (73% yield). Mp 190–191 °C (neat); R_f = 0.33 (EtOAc:MeOH, 9:1); IR (ATR): 3570 (m), 3343 (m), 2933 (m), 2851 (m), 2793 (m), 1627 (m), 1565 (s), 1550 (m), 1149 (m) cm^{-1}; ^1H NMR ($CDCl_3$, 300 MHz): δ = 8.59 (s, 1H, CH), 8.08 (d, *J* = 8.6 Hz, 2H, CH), 7.84–7.80 (m, 3H, CH), 6.71 (d, *J* = 12.8 Hz, 1H, CH), 3.50–3.42 (m, 4H, CH_2), 3.13–3.05 (m, 4H, CH_2), 2.53–2.48 (m, 4H, CH_2), 2.27 (s, 3H, CH_3), 1.75–1.68 (m, 6H, CH_2); ^{13}C NMR ($CDCl_3$, 75.5 MHz): δ = 189.0 (1C, CO), 154.6 (1C, CNH_2), 153.1 (1C, CH), 143.2 (1C, CH), 141.7 (1C, C), 138.1 (1C, C), 134.3 (1C, C), 132.0 (1C, C), 128.5 (2C, CH), 126.0 (2C, CH), 90.7 (1C, CH), 55.5 (1C, CH_2), 54.2 (2C, CH_2), 46.8 (1C, CH_2), 46.1 (2C, CH_2), 45.8 (1C, CH_3), 26.7 (1C, CH_2), 25.2 (1C, CH_2), 24.2 (1C, CH_2); HRMS–ES+: *m/z* $[M+H]^+$ calcd for $C_{23}H_{31}N_6O_3S$: 471.2178; found: 471.2181.

(*E*)-1-{3-Amino-6-[4-({4-methylpiperazin-1-yl}sulfonyl)phenyl]pyrazin-2-yl}-3-morpholinoprop-2-en-1-one (229)

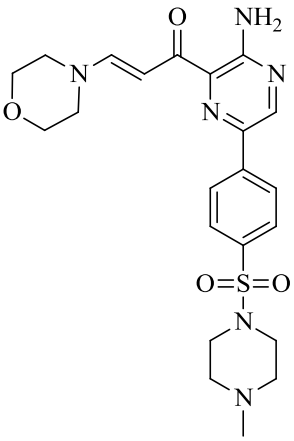

Dark yellow solid (69% yield). Mp 194–196 °C (neat); R_f = 0.17 (EtOAc:MeOH, 9:1); IR (ATR): 3608 (w), 3353 (m), 2919 (m), 2800 (m), 1630 (m), 1563 (s), 1154 (m), 937 (m) cm^{-1}; ^1H NMR ($CDCl_3$, 300 MHz): δ = 8.61 (s, 1H, CH), 8.06 (d, *J* = 8.6 Hz, 2H, CH), 7.83 (d, *J* = 7.8 Hz, 2H, CH), 7.78 (d, *J* = 7.8 Hz, 1H, CH), 6.78 (d, *J* = 8.6 Hz, 1H, CH), 3.82–3.78 (m, 4H, CH_2), 3.51–3.48 (m, 4H, CH_2), 3.12–3.05 (m, 4H, CH_2), 2.51–2.48 (m, 4H, CH_2), 2.27 (s, 3H, CH_3); ^{13}C NMR ($CDCl_3$, 75.5 MHz): δ = 189.4 (1C, CO), 154.6 (1C, CNH_2), 152.6 (1C, CH), 143.6 (1C, CH), 141.6 (1C, C), 138.3 (1C, C), 134.4 (1C, C), 131.3 (1C, C), 128.5 (2C, CH), 126.0 (2C, CH), 91.8 (1C, CH), 66.5 (2C, CH_2), 54.2 (2C, CH_2), 46.1 (2C, CH_2), 45.8 (1C, CH_3); HRMS–ES+: *m/z* $[M+H]^+$ calcd for $C_{22}H_{29}N_6O_4S$: 473.1971; found: 473.1974.

(*E*)-1-{3-Amino-6-[4-({4-methylpiperazin-1-yl}sulfonyl)phenyl]pyrazin-2-yl}-3-(pyrrolidin-1-yl)prop-2-en-1-one (230)

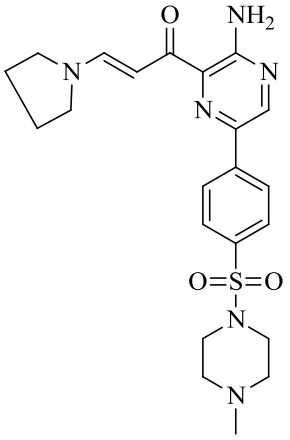

Yellow solid (76% yield). Mp 190–192 °C (neat); R_f = 0.36 (EtOAc:MeOH, 9:1); IR (ATR): 3346 (m), 2938 (m), 2800 (m), 1630 (m), 1593 (m), 1561 (s), 1537 (m), 1154 (m), 944 (m) cm^{-1}; ^1H NMR ($CDCl_3$, 300 MHz): δ = 8.59 (s, 1H, CH), 8.09–8.03 (m, 3H, CH), 7.82 (d, *J* = 8.9 Hz, 2H, CH), 6.57 (d, *J* = 12.7 Hz, 1H, CH), 3.76 (t, *J* = 6.8 Hz, 2H, CH_2), 3.64 (t, *J* = 6.8 Hz, 2H, CH_2) 3.12–3.04 (m, 4H, CH_2), 2.50–2.47 (m, 4H, CH_2), 2.26 (s, 3H, CH_3), 2.13–1.96 (m, 4H, CH_2); ^{13}C NMR ($CDCl_3$, 75.5 MHz): δ = 188.4 (1C, CO), 154.6 (1C, CNH_2), 150.0 (1C, CH), 143.1 (1C, CH), 141.8 (1C, C), 138.1 (1C, C), 134.3 (1C, C), 132.0 (1C, C), 128.5 (2C, CH), 125.9 (2C, CH), 92.8 (1C, CH), 54.2 (2C, CH_2), 52.7 (1C, CH_2), 47.4 (1C, CH_2), 46.1 (2C, CH_2), 45.9 (1C, CH_3), 25.4 (1C, CH_2), 25.3 (1C, CH_2); HRMS–ES+: *m/z* $[M+H]^+$ calcd for $C_{22}H_{29}N_6O_3S$: 457.2022; found: 457.2023.

(*E*)-1-{3-Amino-6-[4-({4-methylpiperazin-1-yl}sulfonyl)phenyl]pyrazin-2-yl}-3-(diethylamino)prop-2-en-1-one (231)

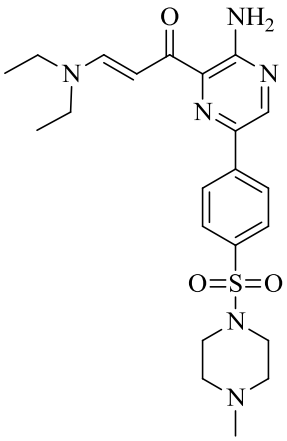

Yellow solid (86% yield). Mp 176–177 °C (neat); R_f = 0.5 (EtOAc:MeOH, 9:1); IR (ATR): 3351 (m), 2972 (m), 2802 (m), 1630 (m), 1561 (s), 1538 (m), 1344 (m), 1046 (m), 952 (m) cm^{-1}; ^1H NMR ($CDCl_3$, 300 MHz): δ = 8.59 (s, 1H), 8.08 (d, *J* = 8.7 Hz, 2H), 7.88–7.81 (m, 3H), 6.69 (d, *J* = 12.9 Hz, 1H), 3.41 (q, *J* = 7.2 Hz, 4H), 3.13–3.04 (m, 4H), 2.51–2.47 (m, 4H), 2.26 (s, 3H), 1.29 (t, *J* = 7.2 Hz, 6H); ^{13}C NMR ($CDCl_3$, 75.5 MHz): δ = 188.7 (1C, CO), 154.6 (1C, CNH_2), 152.4 (1C, CH), 143.1 (1C, CH), 141.7 (1C, C), 138.0 (1C, C), 134.3 (1C, C), 132.0 (1C, C), 128.5 (2C, CH), 125.8 (2C, CH), 91.6 (1C, CH), 54.2 (2C, CH_2), 50.9 (1C, CH_2), 46.1 (2C, CH_2), 45.9 (1C, CH_3), 43.3 (1C, CH_2), 15.0 (1C, CH_3), 11.9 (1C, CH_3); HRMS–ES+: *m/z* $[M+H]^+$ calcd for $C_{22}H_{31}N_6O_3S$: 459.2178; found: 459.2172.

(*E*)-1-{3-Amino-6-[4-({4-methylpiperazin-1-yl}sulfonyl)phenyl]pyrazin-2-yl}-3-(pyridin-2-yl)prop-2-en-1-one (236)

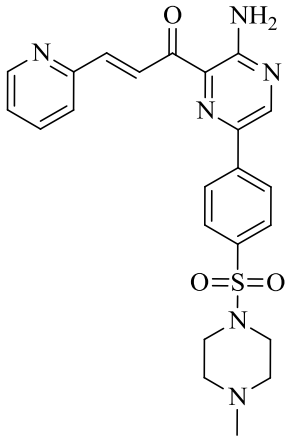

Dark yellow solid (40% yield). Mp 196–200 °C (neat); R_f = 0.27 (EtOAc:MeOH, 9:1); IR (ATR): 3340 (m), 2929 (m), 2815 (m), 1652 (m), 1601 (s), 1580 (s), 1342 (s), 1151 (s), 952 (s) cm^{-1}; ^1H NMR ($CDCl_3$, 300 MHz): δ = 8.81 (d, *J* = 15.8 Hz, 1H, CH), 8.74–8.72 (m, 2H, CH), 8.16 (d, *J* = 8.4 Hz, 2H, CH), 7.89–7.84 (m, 3H, CH), 7.76 (app. td, ddd, *J* = 7.7, 7.7, 1.7 Hz, 1H, CH), 7.59 (d, *J* = 7.7 Hz, 1H, CH), 7.31 (d, *J* = 7.7, 5.1 Hz, 1H, CH), 3.16–3.04 (m, 4H, CH_2), 2.52–2.48 (m, 4H, CH_2), 2.26 (s, 3H, CH_3); ^{13}C NMR ($CDCl_3$, 75.5 MHz): δ = 191.3 (1C, CO), 154.9 (1C, C), 153.7 (1C, CNH_2), 150.4 (1C, CH), 145.7 (1C, CH), 142.8 (1C, CH), 140.7 (1C, C), 139.2 (1C, C), 136.9 (1C, CH), 135.0 (1C, C), 129.6 (1C, C), 128.6 (2C, CH), 126.2 (2C, CH), 125.0 (1C, CH), 124.9 (1C, CH), 124.5 (1C, CH), 54.2 (2C, CH_2), 46.1 (2C, CH_2), 45.8 (1C, CH_3); HRMS–ES+: *m/z* $[M+H]^+$ calcd for $C_{23}H_{25}N_6O_3S$: 465.1709; found: 465.1707.

(*E*)-1-{3-Amino-6-[4-({4-methylpiperazin-1-yl}sulfonyl)phenyl]pyrazin-2-yl}-3-(pyridin-3-yl)prop-2-en-1-one (237)

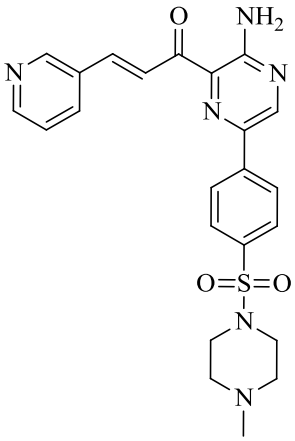

Yellow solid. (43% yield). Mp 170–172 °C (neat); R_f = 0.21 (EtOAc:MeOH, 9:1); IR (ATR): 3404 (m), 3122 (m), 2806 (m), 1655 (m), 1595 (s), 1415 (m), 1343 (m), 1171 (m), 1006 (m) cm^{-1}; ^1H NMR ($CDCl_3$, 300 MHz): δ = 8.98–8.90 (m, 1H, CH), 8.75 (s, 1H, CH), 8.65–8.64 (m, 1H, CH), 8.51 (d, *J* = 16.1 Hz, 1H, CH), 8.11 (d, *J* = 8.4 Hz, 1H, CH), 8.03–8.00 (m, 1H, CH), 7.89–7.83 (m, 3H, CH), 7.41–7.37 (m, 1H, CH), 3.18–3.04 (m, 4H, CH_2), 2.56–2.45 (m, 4H, CH_2), 2.26 (s, 3H, CH_3); ^{13}C NMR ($CDCl_3$, 75.5 MHz): δ = 190.4 (1C, CO), 154.9 (1C, CNH_2), 151.3 (1C, CH), 150.4 (1C, CH), 145.9 (1C, CH), 140.7 (1C, C), 140.2 (1C, CH), 139.3 (1C, C), 135.1 (1C, C), 135.0 (1C, CH), 131.0 (1C, C), 129.3 (1C, C), 128.7 (2C, CH), 126.1 (2C, CH), 124.0 (1C, CH), 122.9 (1C, CH), 54.2 (2C, CH_2), 46.2 (2C, CH_2), 45.8 (1C, CH_3); HRMS–ES+: *m/z* $[M+H]^+$ calcd for $C_{23}H_{25}N_6O_3S$: 465.1709; found: 465.1696.

8.4 Chapter 6

1-(3-Amino-6-bromopyrazin-2-yl)prop-2-en-1-one (336)

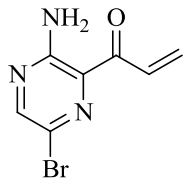

Weinreb **311** (0.10 g, 0.38 mmol) was dissolved in THF (3 mL) at 0 °C and vinyl MgBr (1.0 M, 1.2 mL, 1.2 mmol,) was then added dropwise. The red-brown solution was stirred for one hour at 0 °C, followed by one hour at room temperature. The brown solution was cooled to –10 °C, quenched with 2M HCl (2 mL) and then extracted with EtOAc (3 × 15 mL). The combined organic layers were dried over anhydrous $MgSO_4$, filtered and concentrated under reduced pressure. Purification was done using column chromatography with 9:1 Hex:EtOAc as eluent to afford the product as a yellow solid in 62% yield. Mp 118–120 °C (neat); R_f = 0.71 (Hex:EtOAc, 7:3); IR (ATR): 3378 (m), 3245 (m), 3176 (m), 2970 (m), 2922 (m), 1738 (m), 1659 (m), 1601 (s), 1373 (m), 999 (m) cm^{-1}; ^1H NMR ($CDCl_3$, 300 MHz): δ = 8.28 (s, 1H, CH), 7.85 (dd, *J* = 17.3, 10.5 Hz, 1H, CH), 6.54 (dd, *J* = 17.3, 2.0 Hz, 1H, CH), 5.90 (dd, *J* = 10.5, 2.0 Hz, 1H, CH); ^{13}C NMR ($CDCl_3$, 75.5 MHz): δ = 190.4 (1C, CO), 154.5 (1C, CNH_2), 150.6 (1C, CH), 130.8 (1C, CH), 130.0 (1C, CH), 129.4 (1C, C), 124.3 (1C, CBr); HRMS–ES+: *m/z* $[M+H]^+$ calcd for $C_7H_7N_3OBr$: 227.9772; found: 227.9780.

3-Amino-*N*-methoxy-*N*-methyl-6-(4-((4-methylpiperazine-1-yl)sulfonyl)phenyl)pyrazine-2-carboxamide (337)

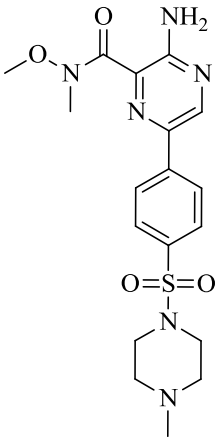

Weinreb amide **311** (0.10 g, 0.38 mmol), boronic acid **243** (0.25 g, 0.57 mmol), Cs_2CO_3 (0.50 g, 1.5 mmol) and the solvent system Tol:EtOH:H_2O (3.5 mL, 4:1:0.05) were added to a Schlenk tube. The reaction content was degassed using the freeze-pump-thaw technique. $Pd(dppf)Cl_2$ (0.030 g, 0.040 mmol) was then added to the Schlenk tube under argon and the solution was stirred at 70 °C overnight. Silica was added to the black mixture and transferred to the column. Purification was done using EtOAc to 9:1 EtOAc:MeOH as eluent to afford the product as a dark cream solid in 81% yield. Mp 116–120 °C (neat); R_f = 0.21 (EtOAc:MeOH, 9:1); IR (ATR): 3347 (m), 2798 (m), 1591 (s), 1454 (m), 1328 (m), 1167 (m), 941 (m) cm^{-1}; ^1H NMR ($CDCl_3$, 300 MHz): δ = 8.58 (s, 1H, CH), 8.00 (d, *J* = 8.6 Hz, 2H, CH), 7.81 (d, *J* = 8.6 Hz, 2H, CH), 6.09 (br s, 2H, NH_2), 3.87 (s, 3H, CH_3), 3.52 (br s, 3H, CH_3), 3.13–3.03 (m, 4H, CH_2),

2.55–2.44 (m, 4H, CH_2), 2.26 (s, 3H, CH_3); ^{13}C NMR ($CDCl_3$, 75.5 MHz): δ = 153.9 (1C, CNH_2), 142.4 (1C, CH), 140.9 (1C, C), 138.1 (1C, C), 134.6 (1C, C), 128.5 (1C, CH_3), 125.8 (2C, CH_2), 45.8 (2C, CH_2), 61.6 (1C, CH_3), 60.4 (1C, CH_3), 54.0 (2C, CH_3), 46.0 (2C, CH_2), 45.7 (1C, CH_3); HRMS–ES+: *m/z* $[M+H]^+$ calcd for $C_{18}H_{25}N_6O_4S$: 421.1658; found: 421.1649.

1-(3-Amino-6-(4-((4-methylpiperazin-1-yl)sulfonyl)phenyl)pyrazin-2-yl)ethanone (340)

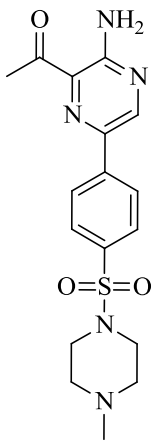

Weinreb amide **311** (0.075 g, 0.35 mmol), boronic acid **243** (0.15 g, 0.52 mmol), Cs_2CO_3 (0.46 g, 1.4 mmol) and the solvent system Tol:EtOH:H_2O (2.5 mL, 4:1:0.05) were added to a Schlenk tube. The reaction content was degassed using the freeze-pump-thaw technique. Pd(dppf)Cl_2 (0.026 g, 0.040 mmol) was then added to the Schlenk tube under argon and the solution was stirred at 70 °C overnight. Silica was added to the black mixture and transferred to the column. Purification was done using EtOAc to 95:5 EtOAc:MeOH as eluent to afford the product as a yellow solid in 90% yield. Mp 177 °C (neat); R_f = 0.33 (EtOAc:MeOH, 95:5); IR (ATR): 3413 (m), 3259 (m), 2800 (m), 1671 (s), 1592 (vs), 1169 (vs), 1153 (vs), 943 (m) cm^{-1}; ^1H NMR ($CDCl_3$, 300 MHz): δ = 8.73 (s, 1H, CH), 8.10 (d, *J* = 8.7 Hz, 2H, CH), 7.85 (d, *J* = 8.7 Hz, 2H, CH), 3.14–3.04 (m, 4H, CH_2), 2.80 (s, 3H, CH_3), 2.51–2.48 (m, 4H, CH_2), 2.27 (s, 3H, CH_3); ^{13}C NMR ($CDCl_3$, 75.5 MHz): δ = 202.7 (1C, CO), 153.8 (1C, CNH_2), 145.5 (1C, CH), 140.7 (1C, C), 139.0 (1C, C), 135.0 (1C, C), 129.2 (1C, C), 128.6 (2C, CH), 125.9 (2C, CH), 54.1 (2C, CH_2), 46.1 (2C, CH_2), 45.8 (1C, CH_3), 26.4 (1C, CH_3); HRMS–ES+: *m/z* $[M+H]^+$ calcd for $C_{17}H_{22}N_5O_3S$: 376.1443; found: 376.1440.

8.5 Biological testing

8.5.1 Inhibition of GSK-3 (Radiometric Assay)

GSK-3β biological testings were carried out at the Centro de Investigaciones Biológicas, Madrid, Spain

GSK-3β enzyme (Sigma) was incubated with 15 μM of ATP, 0.2 μCi of [γ-32P]ATP, GS-1 substrate, and different concentrations of test compound. GSK-3β activity was assayed in 50 mM Tris, pH 7.5, 10 mM $MgCl_2$, 1 mM EGTA, and 1 mMEDTA buffer at 37 °C, in the presence of 15 mM GS-1 (substrate), 15 μM of ATP, 0.2 μCi of [γ-32P] ATP in a final volume of 12 μL.

After 20 min of incubation at 37 °C, 4 μL aliquots of the supernatant were spotted onto 2 × 2 pieces of Whatman P81 phosphocellulose paper, and the filter was washed four times (at least 10 min each time) in 1% phosphoric acid. The dried filters were transferred into scintillation vials, and the radioactivity was measured in a liquid scintillation counter. Blank values were subtracted, and the GSK-3β activity was expressed in percentage of maximal activity. The IC_{50} value is defined as the concentration of each compound that reduces enzyme activity by 50% with respect to that without inhibitor present.

8.5.2 Inhibition of GSK-3 (Luminescent Assay).

Human recombinant GSK-3β was purchased from Millipore (Millipore Iberica S.A.U.) The prephosphorylated polypeptide substrate was purchased from Millipore (Millipore Iberica S.A.U.). Kinase-Glo Luminescent Kinase Assay was obtained from Promega (Promega Biotech Iberica, SL). ATP and all other reagents were from Sigma-Aldrich (St. Louis, MO). Assay buffer contained 50 mM HEPES (pH 7.5), 1 mM EDTA, 1 mM EGTA, and 15 mM magnesium acetate. The method of Baki *et al.*[20] was followed for the inhibition of GSK-3β. Kinase-Glo assays were performed in assay buffer using black 96-well plates. In a typical assay, 10 μL (10 μM) of test compound (dissolved in dimethyl sulfoxide [DMSO] at 1 mM concentration and diluted in advance in assay buffer to the desired concentration) and 10 μL (20 ng) of enzyme were added to each well followed by 20 μL of assay buffer containing 25 μM substrate and 1 μM ATP. The final DMSO concentration in the reaction mixture did not exceed 1%. After a 30 min incubation at 30 °C, the enzymatic reaction was stopped with 40 μL of Kinase-Glo reagent. Glow-type luminescence was recorded after 10 min using a FLUOstar Optima (BMG Lab technologies GmbH, Offenburg, Germany) multimode reader. The activity is proportional to the difference of the total and consumed ATP. The inhibitory activities were calculated on the basis of maximal activities measured in the absence of inhibitor. The IC_{50} value was defined as the concentration of each compound that reduces a 50% the enzymatic activity with respect to that without inhibitors.

GSK-3β reversibility studies:

To study the type of enzymatic inhibition for the compounds, assays were performed to determine the activity of the enzyme after several times of incubation of the enzyme with the

inhibitor. A reversible inhibitor does not increase the inhibition of the enzyme with the time of incubation, while an irreversible inhibitor increases the inhibition percentage as it increases the time of incubation with the enzyme.

8.6 References

1. W. L. F. Armarego and C. L. L. Chai, in *Purification of Laboratory Chemicals (Sixth Edition)*, Butterworth-Heinemann, Oxford, 2009.
2. M. R. Winkle, J. M. Lansinger and R. C. Ronald, *Journal of the Chemical Society, Chemical Communications*, 1980, 87-88.
3. S. Zhou, Z. Liao, J. Yuan, C. Qian and X. Chen, *Research on Chemical Intermediates*, 2013, **39**, 4121-4125.
4. W. Devine, J. L. Woodring, U. Swaminathan, E. Amata, G. Patel, J. Erath, N. E. Roncal, P. J. Lee, S. E. Leed, A. Rodriguez, K. Mensa-Wilmot, R. J. Sciotti and M. P. Pollastri, *Journal of Medicinal Chemistry*, 2015, **58**, 5522-5537.
5. C. B. Aakeroy, P. D. Chopade, C. Ganser and J. Desper, *Chemical Communications*, 2011, **47**, 4688-4690.
6. T. Hayashi, M. Konishi, Y. Kobori, M. Kumada, T. Higuchi and K. Hirotsu, *Journal of the American Chemical Society*, 1984, **106**, 158-163.
7. C.-M. Chou, Y.-W. Tung, M.-I. Ling, D. Chan, W. Phakhodee and M. Isobe, *Heterocycles*, 2012, **86**, 1323-1339.
8. Y. Younis, F. Douelle, D. González Cabrera, C. Le Manach, A. T. Nchinda, T. Paquet, L. J. Street, K. L. White, K. M. Zabiulla, J. T. Joseph, S. Bashyam, D. Waterson, M. J. Witty, S. Wittlin, S. A. Charman and K. Chibale, *Journal of Medicinal Chemistry*, 2013, **56**, 8860-8871.
9. R. N. Shakhmaev, A. U. Ishbaeva and V. V. Zorin, *Russian Journal of Organic Chemistry*, 2012, **48**, 908-913.
10. M. Fu, L. Chen, Y. Jiang, Z.-X. Jiang and Z. Yang, *Organic Letters*, 2016, **18**, 348-351.
11. F. Wang, H. Yang, H. Fu and Z. Pei, *Chemical Communications*, 2013, **49**, 517-519.
12. J. Eriksson, O. Åberg and B. Långström, *European Journal of Organic Chemistry*, 2007, **2007**, 455-461.

13. A. F. Tominey, J. Liese, S. Wei, K. Kowski, T. Schrader and A. Kraft, *Beilstein Journal of Organic Chemistry*, 2010, **6**, 66.
14. E. Quesada and R. J. K. Taylor, *Tetrahedron Letters*, 2005, **46**, 6473-6476.
15. G. Zhang, T. Kumamoto, T. Heima and T. Ishikawa, *Tetrahedron Letters*, 2010, **51**, 3927-3930.
16. X. Dai, H. Liu, A. Palani, S. He, R. Nargund, D. Xiao, N. Zorn, Q. Dang, C. C. Mccomas, X. Peng, P. Li, R. Soll, Patent WO2014/209727 A1, 2014.
17. H. Duan, M. Ning, X. Chen, Q. Zou, L. Zhang, Y. Feng, L. Zhang, Y. Leng and J. Shen, *Journal of Medicinal Chemistry*, 2012, **55**, 10475-10489.
18. C. Delvare, C. S. Harris, L. Hennequin, P. Koza, C. Lambert-van der Brempt, J. Pelleter and O. Willerval, *ACS Combinatorial Science*, 2011, **13**, 449-452.
19. I. Bruce, E. Budd, L. Edwards, C. Howsham, Patent US20090239847 A1, 2009.
20. A. Baki, A. Bielik, L. Molnár, G. Szendrei and G. M. Keserü, *ASSAY and Drug Development Technologies*, 2007, **5**, 75-84.

Appendix

Additional biological testing on the chloroquine sensitive *Plasmodium falciparum* strain, NF54

1.1 Overview

This section discusses the additional biological testing that was carried out on the sensitive *P. falciparum* malaria strain, NK54. Our research group also develops novel anti-malarial inhibitors[1-5] and our colleagues at the University of Cape Town, Chibale and co-workers,[6, 7] have reported potent biological activities for the amino-pyridine and -pyrazine series against two *Plasmodium falciparum* strains (K1 and NF54). We envisaged that the synthesised aminopyrazine series reported in this thesis could potentially inhibit *P. falciparum*. Therefore, the biological activities of the synthesised compounds were determined *in vitro* against the chloroquine sensitive strain of *P. falciparum*, NF54.

1.2 Brief background

Each year malaria affects in the region of 300 – 500 million people and is responsible for the death of roughly 2.5 million people.[8] Since the 1940s, the development of anti-malarial drugs has played an important role in the control and treatment of malaria. However, the widespread use of antimalarials has caused the development of resistance in *P. falciparum* parasites, which has resulted in an increased malaria mortality.[9] This has necessitated the need for the development of new molecules with novel mechanisms of action.[10]

Chibale and co-workers,[7] developed a series of aminopyrazine inhibitors (see Fig. 1.1 for representative examples **330** – **333**) that showed low nanomolar potency against both the sensitive and resistant strains of *P. falciparum*. In addition, these inhibitors demonstrated good *in vivo* efficacy using the *Plasmodium berghei* mouse model[11] and also metabolic stability in human microsomes.

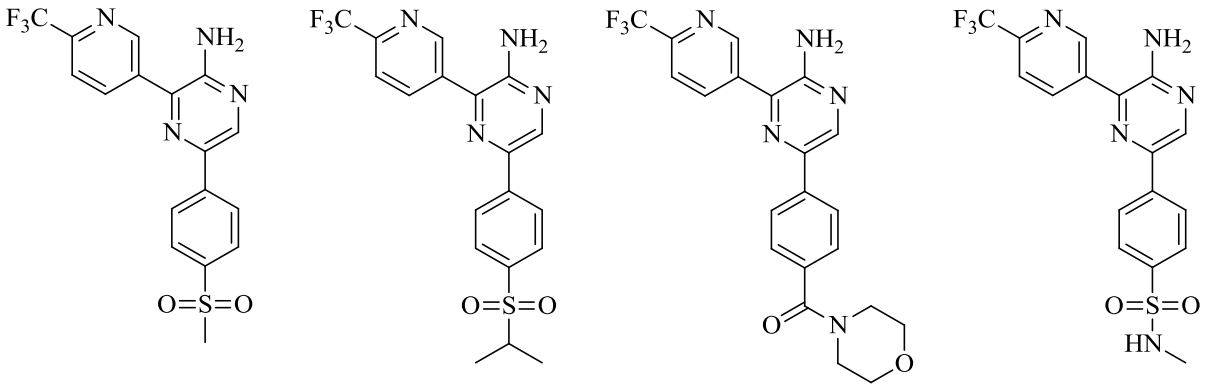

330
NF54 : 10 nM
K1 : 8.4 nM

331
NF54 : 20 nM
K1 : 17 nM

332
NF54 : 9.0 nM
K1 : 10 nM

333
NF54 : 23 nM
K1 : 21 nM

Figure 1.1. Some of the potent aminopyrazine inhibitors against the *P. falciparum* strains reported by Chibale and co-workers[7]

The inhibitors that were developed by Chibale and co-workers[7] consisted of a similar aminopyrazine core that was described in this thesis. Therefore, the synthesised Michael acceptor derivatives discussed in chapter three and four were subjected to *in vitro* testing on the sensitive *P. falciparum* strain, NF54, and will be discussed in the next section.

1.3 Biological results

The synthesised compounds **216** – **220** and **228** – **231** were tested for their *in vitro* activity (whole cell assay) using the modified method of Trager[12] and Makler[13] against the sensitive *P. falciparum* strain, NF54. A full dose-response analysis was performed on all compounds to determine the concentration inhibiting 50% of parasite growth (IC_{50}) and the values are shown in Table 1.1. Chloroquine, a known antiplasmodial inhibitor, was used as a reference standard.[14]

Table 1.1. NF54 IC_{50} values of compounds **216** – **220** and **228** – **231**

#	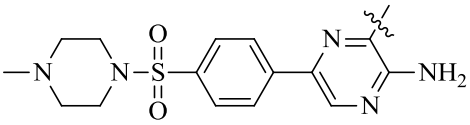	**IC_{50} (µM)**
216	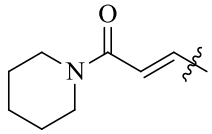	2.38
217	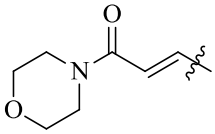	0.776
218	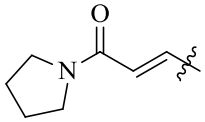	4.85
219	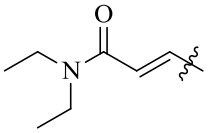	0.201
220	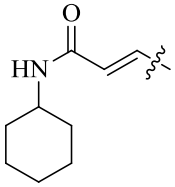	15.6
228	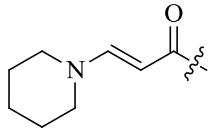	2.70
229	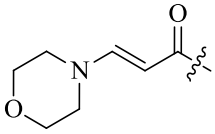	10.0
230	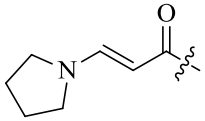	4.85
231	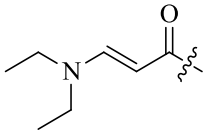	0.106
Chloroquine		0.007

The *in vitro* assay against the chloroquine-sensitive strain delivered mixed results. The small diethylamine side chain-containing compounds, **219** and **231**, were the most potent with IC_{50} values in the nanomolar range, while the bulky cyclohexylamine **220** perform the poorest (15.6 μM).

Regardless of the position of the Michael acceptor, the biological activities were similar for the piperidine (**216** and **228**), pyrrolidine (**218** and **230**) and diethylamine (**219** and **231**) derivatives. However, for the morpholine derivatives (**217** and **229**), a large difference in potency was observed, which suggests that the shape of the molecule could result in a possible hydrogen-bonding interaction with the oxygen atom of the morpholine ring (**217**) or a repulsive interaction for compound **229**. The diethylamine derivatives (**219** and **231**) are the only molecules tested that do not have a ring structure and this could play a role in the potency difference between the pyrrolidine (**218** and **231**) and diethylamine (**219** and **231**) derivatives. This could suggest that one of the diethyl groups is lost to form the NH atoms which could enhance the potency of the molecule. In addition, it has been confirmed that molecules that consist of a diethylamine fragment, as seen in chloroquine, exhibited enhanced potency.[15, 16] The relative inactivity of cyclohexylamine **220** (which does possess the NH atoms) suggests that there is no tolerance for bulky groups at this position.

1.4 The search for the pharmacophore

The aforementioned antiplasmodial results prompted the search for the active fragment that could serve as a pharmacophore for the second generation of antiplasmodial inhibitors. The fragments of the most potent compounds, **219** and **231**, were tested for their *in vitro* activity (whole cell assay) by using the same procedure as mentioned in section 1.3. The results are tabulated in Table 1.2. All three fragments, **292**, **319** and **251**, were deemed inactive, with IC_{50} values in the high micromolar range. For this reason, the fragment that was essential for biological activity could not be determined.

Table 1.2. NF54 IC_{50} values of compounds **292**, **319** and **251**

#	Fragment	IC_{50} (µM)
292	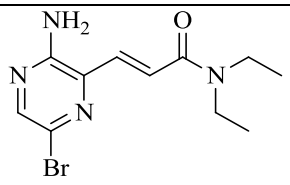	>10.0
319	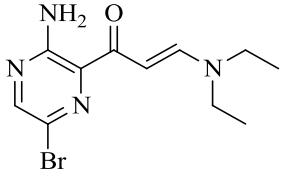	>10.0
251	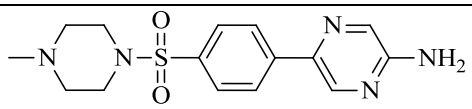	8.86
Chloroquine		0.007

These results have thus necessitated the need for further exploration to determine the active pharmacophore. A second round of biological testing could include different fragments of compounds **219** and **231** or modifications to the tested fragments **251**, **292** and **319**. This will be discussed as future work in the next section.

1.5 Future antiplasmodial biological testing to determine the pharmacophore

Antiplasmodial biological testing revealed that the most active compound from each series was, in both cases, the diethyl derivative (**219** and **231**) with IC_{50} values of 0.201 and 0.106 µM respectively. Fragments of **219** and **131** were then tested for their antiplasmodial activity to identify the pharmacophore. However, all fragments exhibited activity in the high micromolar range. This concluded that the pharmacophore must be a fragment that consisted of combined moieties of **292**/**319** and **251**. Therefore, a phenotypic screening would be required to identify the fragment that is essential for antiplasmodial activity. Using diethyl **292** as an example, three fragments could be constructed (Fig. 1.2). Compounds **351** and **352** consist of a side chain and a partial sulfonamide core, while compound **353** contains the scaffold that is attached to a portion of the side chain.

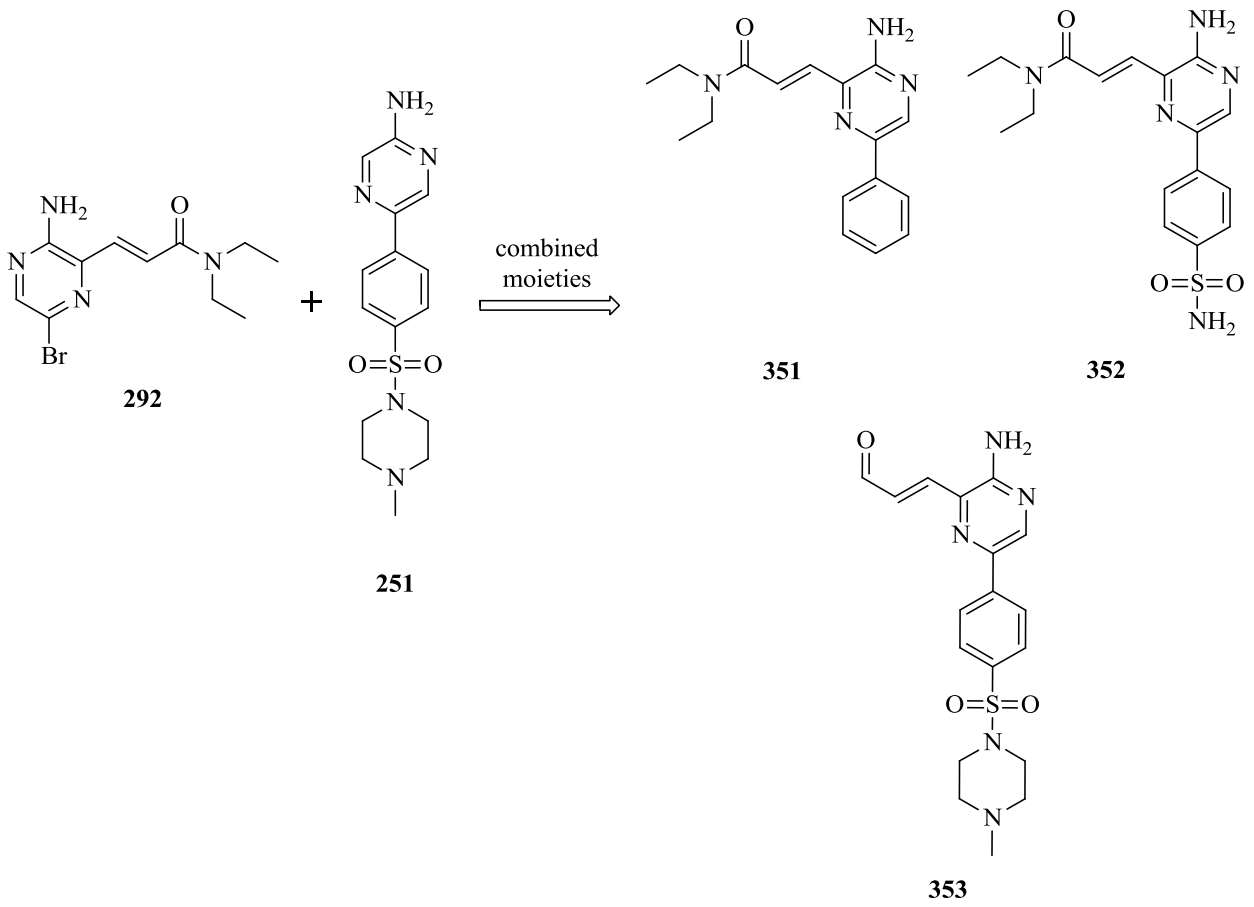

Figure 1.2. Combined moieties of **292** and **251** to construct new fragments

The diethyl derivatives **219** and **231** could also be slightly modified to determine which fragment of the molecule is essential for antiplasmodial activity. Using diethyl **219** again as the example, this molecule could potentially be modified at six different positions (Figure 1.3). The amino group on the pyrazine core could be removed (compound **354**) to determine whether this functional group is necessary for activity. The pyrazine ring could also be replaced by a pyridine ring (compound **355** and **356**) to determine whether the position of the nitrogen plays a role in the potency of this compound. The sulfonamide core could be modified to replace the sulfone with a carbonyl (compound **357**) and the methylpiperazine to piperidine (compound **358**). Lastly, the Michael acceptor could be converted into a simple alkene (compound **359**).

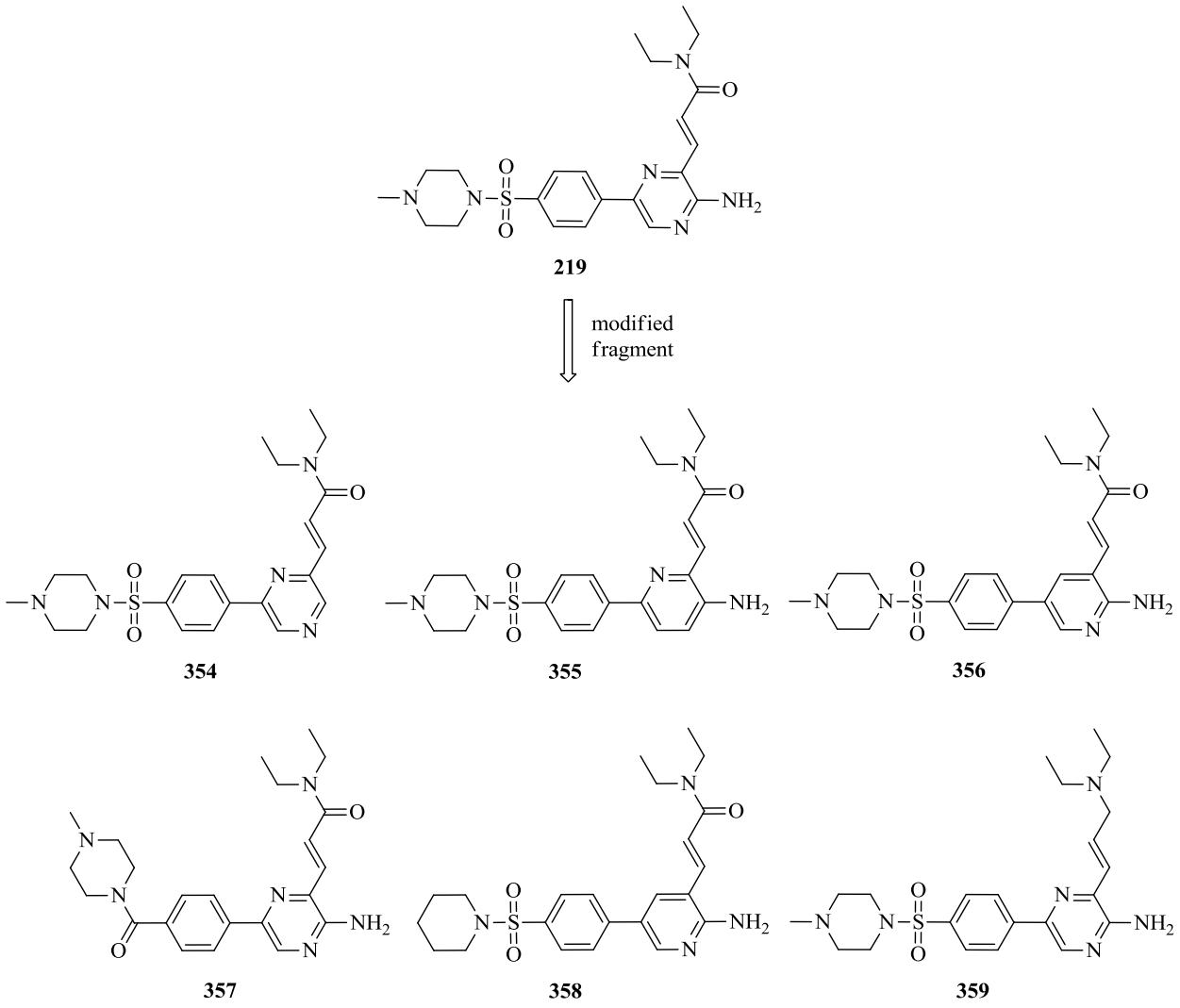

Figure 1.3. Modified fragments of diethyl **219** to identify the fragment that is essential for antiplasmodial activity

Ultimately, this dissertation describes the synthesis of some interesting new compounds. With the aid of molecular modelling, two different approaches to drug development have been used. The main focus was a target-based approach attempting to develop an inhibitor for GSK-3β with the possibility of forming a covalent interaction with Cys199 inside the ATP-binding site. The results were moderate but raise some useful points of departure for further exploration. In addition, the minor foray into the phenotypic screen against *P. falciparum* is a good reminder to keep one's mind open to interesting possibilities. The unexpectedly good efficacy of the two diethyl compounds could open the door to studies that focus on determining the active

pharmacophore of these compounds as well as structure-activity relationships to develop novel antiplasmodial agents.

1.6 Experimental section

1.6.1 Inhibition of NF54

Biological testings were carried out at the University of Cape Town, Department of Pharmacology, Cape Town, South Africa.

The samples were tested in triplicate on one or two separate occasions against a chloroquine sensitive (CQS) strain of *Plasmodium falciparum* (NF54). Continuous *in vitro* cultures of asexual erythrocyte stages of *P. falciparum* were maintained using a modified method of Trager and Jensen.[12] Quantitative assessment of anti-plasmodial activity *in vitro* was determined via the parasite lactate dehydrogenase assay using a modified method described by Makler.[13] The samples were prepared to a 20 mg/mL stock solution in 100% DMSO and sonicated to enhance solubility. Samples were tested as a suspension if not completely dissolved. Stock solutions were stored at –20 ºC. Further dilutions were prepared on the day of the experiment. Chloroquine (CQ) was used as the reference drug in all experiments. A full dose-response analysis was performed for all compounds to determine the concentration inhibiting 50% of parasite growth (IC_{50} value). Samples were tested at a starting concentration of 100 µg/mL, which was then serially diluted 2-fold in complete medium to give 10 concentrations; with the lowest concentration being 0.2 µg/mL. The same dilution technique was used for all samples. The highest concentration of solvent to which the parasites were exposed had no measurable effect on the parasite viability (data not shown). The IC_{50} values were obtained using a non-linear dose-response curve fitting analysis via Graph Pad Prism v.4.0 software.

1.7 References

1. A. R. Hamann, W. A. L. Van Otterlo, M. A. L. Blackie, C. De Kock and P. J. Smith, *South African Journal of Chemistry*, 2013, **66**, 231-236.
2. A. R. Hamann, C. de Kock, P. J. Smith, W. A. L. van Otterlo and M. A. L. Blackie, *Bioorganic & Medicinal Chemistry Letters*, 2014, **24**, 5466-5469.

3. L. Taleli, C. de Kock, P. J. Smith, S. C. Pelly, M. A. L. Blackie and W. A. L. van Otterlo, *Bioorganic & Medicinal Chemistry*, 2015, **23**, 4163-4171.
4. L. Jacobs, C. de Kock, K. A. de Villiers, P. J. Smith, V. J. Smith, W. A. L. van Otterlo and M. A. L. Blackie, *ChemMedChem*, 2015, **10**, 2099-2110.
5. M. Clements, T. le Roex and M. Blackie, *ChemMedChem*, 2015, **10**, 1786-1792.
6. Y. Younis, F. Douelle, T.-S. Feng, D. G. Cabrera, C. L. Manach, A. T. Nchinda, S. Duffy, K. L. White, D. M. Shackleford, J. Morizzi, J. Mannila, K. Katneni, R. Bhamidipati, K. M. Zabiulla, J. T. Joseph, S. Bashyam, D. Waterson, M. J. Witty, D. Hardick, S. Wittlin, V. Avery, S. A. Charman and K. Chibale, *Journal of Medicinal Chemistry*, 2012, **55**, 3479-3487.
7. Y. Younis, F. Douelle, D. González Cabrera, C. Le Manach, A. T. Nchinda, T. Paquet, L. J. Street, K. L. White, K. M. Zabiulla, J. T. Joseph, S. Bashyam, D. Waterson, M. J. Witty, S. Wittlin, S. A. Charman and K. Chibale, *Journal of Medicinal Chemistry*, 2013, **56**, 8860-8871.
8. M. A. L. Blackie, P. Beagley, S. L. Croft, H. Kendrick, J. R. Moss and K. Chibale, *Bioorg. Med. Chem.*, 2007, **15**, 6510-6516.
9. T.Mita, K. Tanabe and K. Kita, *Parasitology International*, 2009, **58**, 201-209.
10. Y. Kabri, N. Azas, A. Dumètre, S. Hutter, M. Laget, P. Verhaeghe, A. Gellis and P. Vanelle, *Eur. J. Med. Chem.*, 2010, **45**, 616-622.
11. S. A. Charman, S. Arbe-Barnes, I. C. Bathurst, R. Brun, M. Campbell, W. N. Charman, F. C. K. Chiu, J. Chollet, J. C. Craft, D. J. Creek, Y. Dong, H. Matile, M. Maurer, J. Morizzi, T. Nguyen, P. Papastogiannidis, C. Scheurer, D. M. Shackleford, K. Sriraghavan, L. Stingelin, Y. Tang, H. Urwyler, X. Wang, K. L. White, S. Wittlin, L. Zhou and J. L. Vennerstrom, *Proceedings of the National Academy of Sciences*, 2011, **108**, 4400-4405.
12. W. Trager and J. B. Jensen, *Science*, 1976, **193**, 673-675.
13. M. T. Makler, J. M. Ries, J. A. Williams, J. E. Bancroft, R. C. Piper, B. L. Gibbins and D. J. Hinrichs, *Am J Trop Med Hyg*, 1993, **48**, 739-741.
14. A. B. S. Sidhu, D. Verdier-Pinard and D. A. Fidock, *Science*, 2002, **298**, 210-213.
15. K. Singh, H. Kaur, P. Smith, C. de Kock, K. Chibale and J. Balzarini, *Journal of Medicinal Chemistry*, 2014, **57**, 435-448.

16. M. Sinha, V. R. Dola, A. Soni, P. Agarwal, K. Srivastava, W. Haq, S. K. Puri and S. B. Katti, *Bioorganic & Medicinal Chemistry*, 2014, **22**, 5950-5960.